CHAPTER 1
INTRODUCTION

1.1. Non-alcoholic fatty liver disease (NAFLD) & Non-alcoholic Steatohepatitis (NASH)

Non-alcoholic fatty liver disease (NAFLD) is a pathological condition where the triglycerides accumulate in hepatocytes, which is also known as hepatic steatosis. This condition can lead to steatohepatitis and develop further to fibrosis and cirrhosis progressively, which is a hallmark characteristic of non-alcoholic steatohepatitis (NASH) (Neushwander & Caldwell, 2003). NAFLD is a common but often silent chronic liver disease which shows resemblance to alcoholic liver disease, clinically and histologically, but which occurs in people who consume little or no alcohol (Bacon et al., 1994).

NAFLD is strongly correlated to obesity and insulin resistance, where it is recognised to represent as hepatic manifestation of metabolic syndrome (Dowman et al., 2011). The prevalence of NAFLD increased with patient exhibit one or more features of the metabolic syndrome which are insulin resistance (IR), obesity, glucose intolerance or diabetes, dyslipidemia and hypertension (Dowman et al., 2011). Marchesini et al. (1999) have reported that NAFLD patients who had IR assessed using the homeostasis model assessment (HOMA) index have a higher value of body mass index (BMI) (>30kg/m^2), visceral fat distribution and glucose intolerance. These findings further support that NAFLD is strongly correlated with other features of the metabolic syndrome, which suggests NAFLD as another component of this syndrome (Cortez et al., 1999). The pathophysiology of metabolic syndrome (MS) and NAFLD maybe due, at least in part to polymorphisms of genes involved in insulin resistance, lipid metabolism and inflammation causing the metabolic abnormalities (Day, 2004).

There are also drugs that are capable of inducing steatosis such as glucocorticoids, amiodarone, synthetic oestrogens and highly active antiretroviral drugs (HAART) (Preiss et al., 2008; Stefan et al., 2008; Neushwander et al., 2003). Endocrine disorders such as Polycystic ovary

syndrome (PCOS) (Setji et al., 2006), hypopituitarism (Adams et al., 2004) and hypothyroidism (Loria et al., 2009) also lead to fat accumulation in the liver.

The prevalence of NAFLD was estimated about 30% in adults and 3.5-5% of adults have NASH (Dowman et al., 2011; Browning et al., 2004). Recent study have reported that NAFLD is affecting both genders, all ethnicities, prominently in all age segments including 53% of obese children (Dowman et al., 2011; Clark et al., 2003; McCullough et al., 2005). Approximately 20% of NASH patients are at risk of developing cirrhosis and dying from end stage liver disease or liver cancer in short or medium term follow-up studies. 90% of morbidly obese individual may have NAFLD and 20% have NASH. However, the pathological changes may be progressive through this spectrum such that up to one third of patients with NASH will develop cirrhosis over longer-term follow up (Dowman et al., 2011; Clark et al., 2003).

1.2. Clinical Manifestation and Laboratory findings

A previous study reported that 48-100% of NASH patients are asymptomatic, despite their abnormal liver function test (LFT) (Bacon et al., 1994). Based on physical examination, 75% of NASH patients have hepatomegaly and 25% have splenomegaly (Ludwig et al., 1980; Lee et al., 1989). The serum alanine aminotransferase (ALT) was found to be increased up to 3 fold more than serum aspartate aminotransferase (AST) in 65-95 % of NASH patients, which is in contrast to alcoholic hepatitis (Powell et al., 1990; Bacon et al., 1994). In addition, the alkaline phosphatase (ALP) and gamma glutaryl transferase (γ-GT) are elevated in up to one third of these patients (Neushwander et al., 2003). The liver synthetic and excretory functions, as determined by levels of clotting factors, albumin and bilirubin are usually within the normal range. (De Knegt, 2001)

Plasma glucose is elevated due to impaired glucose tolerance or diabetes mellitus (Reid et al., 2001; Chitturi et al., 2002). 51% of NASH patients were hyperinsulinemic, and this was further supported by an increase in C-peptide levels which is an indicator of insulin hyper secretion. Dyslipidemia can be observed in NASH where there is an elevation of serum triglycerides (TG) and, serum low density lipoprotein (LDL) cholesterol followed by low levels of serum high density lipoprotein (HDL) cholesterol. (Chitturi et al., 2002)

1.3. Histological Findings

Liver biopsy was set as the gold standard to determine the presence of NASH and its severity by evaluating the grade and stage of the disease (Bravo et al., 2001). Liver biopsy is crucial because there is no relationship between the degree of abnormal LFT and the severity of the histopathological findings of this disease (Sonsuz et al., 2000; Mofrad et al., 2003). The recently developed grading system of Brunt is used to determine the severity of steatohepatitis (Brunt & Tiniakos, 2010; Brunt et al., 1999). There is also other non-invasive method other than liver biopsy for NASH diagnosis conformation. Serum keratin 18 (K18) fragments is a marker of hepatocyte apoptosis, has been reported as promising biomarker for NASH, with sensitivity and specificity of up to 77% and 92% respectively (Feldstein et al., 2009).

Hepatic steatosis is characterized by accumulation of fat droplets in hepatocytes also known as ballooning degeneration of hepatocytes (Figure 1.1). Steatohepatitis is described by a macro vesicular or large droplet steatosis (2mm), associated with a necro-inflammatory reaction, which is situated in the lobular parenchyma. It consists of a mixed infiltrate of mononuclear cells and neutrophils, causing liver injury with ballooning of the hepatocytes. The degree of necro-inflammation is also based on the extent of hepatocellular steatosis and the ballooning together with the disarray of hepatocytes (Figure 1.2). (Brunt et al., 2005)

A recent study by National Institute of Diabetes and Digestive and Kidney Diseases (NIDDK) have suggested a common set of minimal criteria in order to diagnose NASH which include lobular inflammation, ballooning degeneration, fibrosis and steatosis (Kleiner et al., 2005). NASH is associated with a pericellular, perisinusoidal fibrosis in the perivenular area or a periportal fibrosis, in which the localization of the fibrosis will vary with the stage of the disease. Liver fibrosis is present in 37-84% of the liver biopsies and may result in cirrhosis, the prevalence of which varies from 7- 30% of biopsies. (De Knegt, 2001; Reid, 2001; Angulo, 2002; Clark et al., 2002)

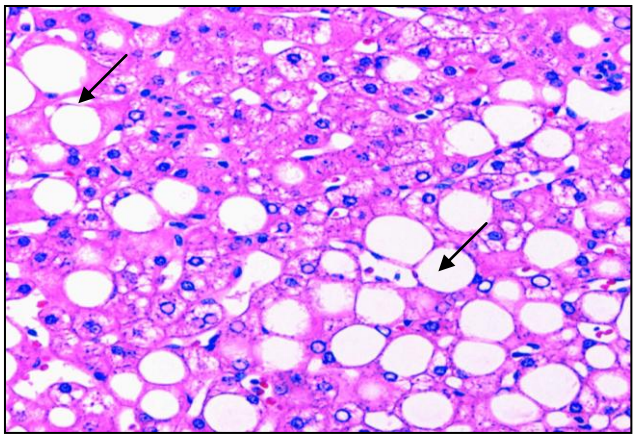

Figure 1.1: Hepatic steatosis, ballooning degeneration of hepatocytes with glycogenated nuclei (as shown in arrow) (H&E, x 200)
(Adapted from Brunt et al., 2005)

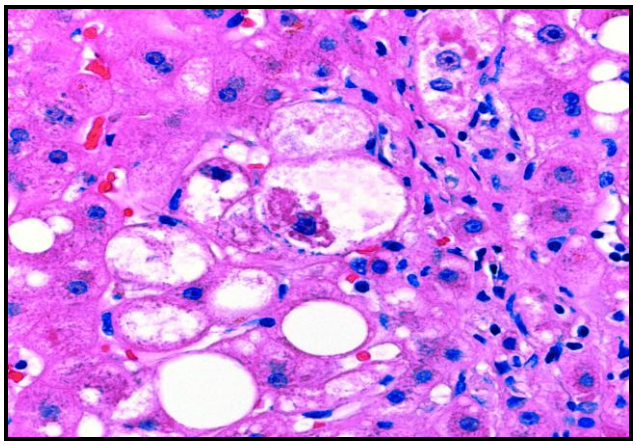

Figure 1.2: Steatohepatitis, with several hepatocytes showing ballooning degeneration intermixed with steatosis and foci of inflammatory cells in hepatic lobules. Mallory hyaline showing eosinophilic and ropy inclusions in cytoplasm (H&E, x 400) (Adapted from Brunt et al., 2005).

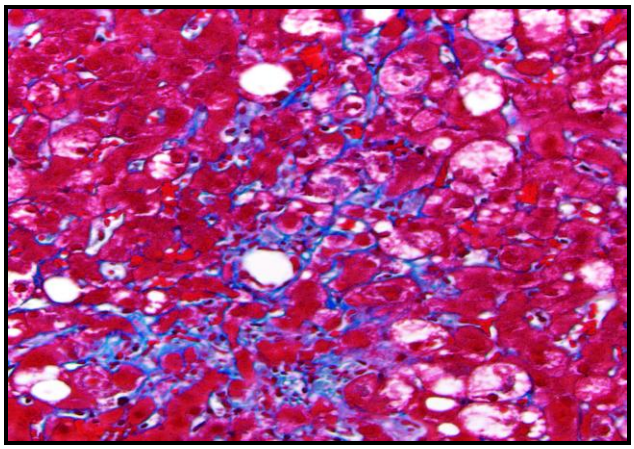

Figure 1.3: Perivenular/ pericellular fibrosis in zone 3
(Masson trichrome x 200) (Adapted from Brunt et al., 2005)

1.4. Pathogenesis of Non-alcoholic Steatohepatitis (NASH)

A ‘multi- hit’ hypothesis has been suggested for NAFLD progression to NASH (Estep et al. 2009; Malhi and Gores, 2008; Miele et al. 2003; Charlton et al. 2002). The first hit was described as the development of hepatic steatosis due to insulin resistance (IR). Insulin resistance condition leads to increased serum levels of non esterified or free fatty acids (FFAs). Subsequently, increased FFA transport into hepatocytes would increased the hepatic de novo lipogenesis that exceed both the hepatic FFA β-oxidation and very low-density lipoprotein (VLDL) export, leading to increased hepatic steatosis (Malhi and Gores, 2008). Miele et al. (2003) & Charlton et al. (2002) suggest that hepatic steatosis occurrence is largely due to the increase in lipogenesis and decreases in lipid export out from the liver.

Accumulation FFAs in hepatocytes promote apoptosis through a number of pathways, including increased stress of membrane bound organelles such as mitochondria, endoplasmic reticulum (ER), and lysosomes (Malhi and Gores, 2008). FFAs activate a number of complex intracellular pathways, including induction of activation of c-jun N-terminal kinase, the pro-apoptotic protein Bax and Toll-like receptor 4 to induce lipotoxicity. All these activation pathways lead to lysozomal and mitochondrial permeabilization leading to increase in oxidative stress, pro-inflammatory cytokines gene expression, ER stress, and hepatocyte apoptosis (Malhi and Gores, 2008). All these factors will lead to fibrosis and cirrhosis. In some patients it develops progressively to hepatocellular carcinoma (Day, 2002).

However recent evidence suggests that both steps may occur simultaneously. It’s widely accepted that oxidative stress plays a pivotal role in the liver injury progression (McClain et al., 2007). There are various factors that cause oxidative stress which are; severity of IR, rate of β-oxidation, disturbance in type of fat accumulated within hepatocytes, overproduction of cytokines and adipokines associated with inflammatory process that accompany fat accumulation both systemically and within the liver and finally endoplasmic reticulum (ER) stress that arises because of accumulation of mis-folded protein. One or more of these mechanisms may be involved in different

proportions in any given individual leading to a final common pathway of progressive liver injury and advanced fibrosis. (Marra et al., 2008; McClain et al., 2007)

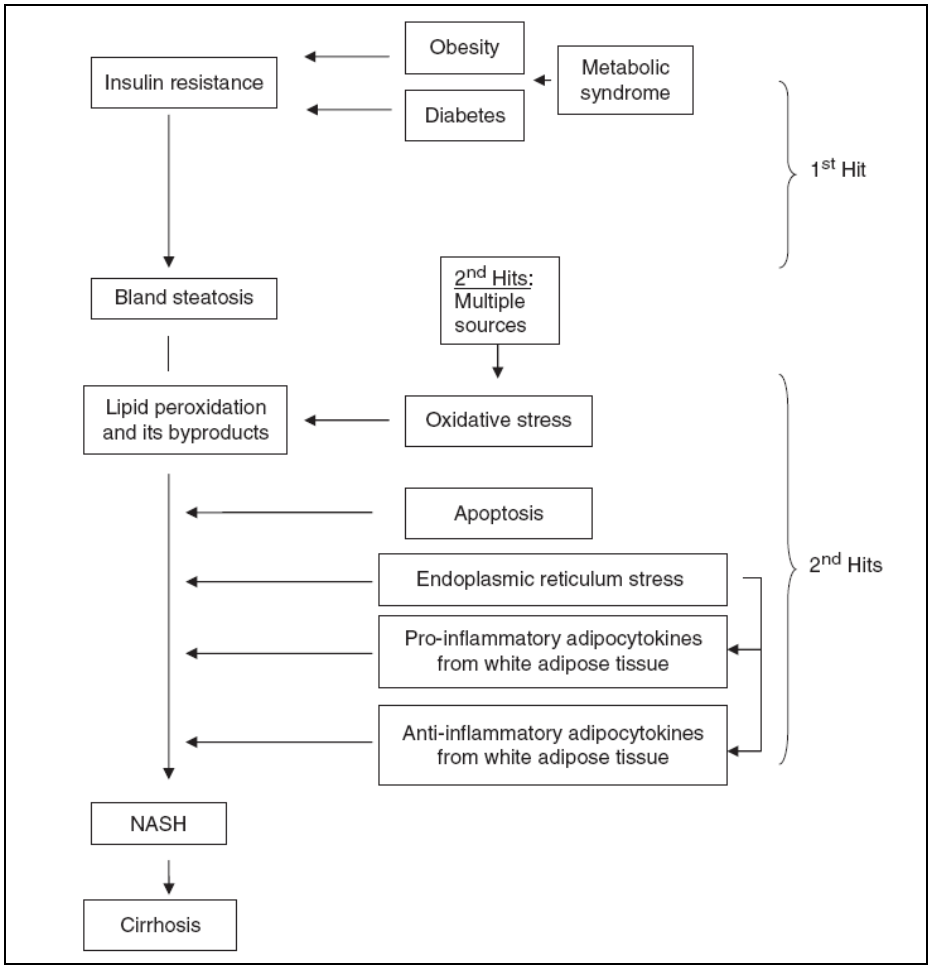

Figure 1.4: Non-alcoholic steatohepatitis pathogenesis (Adapted from Lam & Younossi, 2011).

IR and visceral obesity are characterized as the risk factors involved in NASH (Wanless & Lentz, 1990). The basal rate of whole body lipolysis depends on the total body fat mass, when there is an expansion of adipose tissue it would lead to an increase in plasma free fatty acid (FFA) concentrations due to lipolysis of adipose tissue. An increased in FFAs level leads to up regulation of TNFα expression. TNFα inhibits the insulin-stimulated tyrosine phosphorylation of insulin receptor and insulin receptor substrate (IRS-1) in adipocytes, thus interfering the insulin signalling. This condition would disrupt the insulin mediated suppression of lipolysis in adipose tissue leading insulin resistance in adipose tissue (Fruhbeck et al.,

2001; Hube et al., 1999; Mohamed-Ali, et al., 1998; Peraldi et al., 1996; Hotamisligil et al., 1995).

Previous studies have described that NASH has a stronger correlation with visceral obesity rather than peripheral obesity (Chitturi et al., 2002). This is because the visceral adipocytes tend to be more prone to lipolysis than those from the peripheral adipose tissue (Arner. P, 1998). Visceral adipose tissue appears to be less mature than the subcutaneous adipose tissue and produces more FFA, tumour necrosis factor (TNF)-α and resistin followed by lower amounts of adiponectin. Resistin is an amino acid protein expressed in white adipose tissue that plays a role in insulin resistance (Steppan et al., 2001). Upregulation of resistin level in mice lead to increase in plasma glucose and insulin level (Banerjee et al., 2004). Resistin expression is down regulated by Thiazolidinediones (Troglitazone, Rosiglitazone & Piolgitazone) and fasting condition in mice model (Steppan et al., 2001). Over expression of Resistin in a mouse model caused dyslipidemia which is characterized by increased in serum total cholesterol and triglyceride levels, and decreased in high density lipoprotein cholesterol concentration (Sato et al., 2005).

Whereas adiponectin is an adipocyte-derived hormone that is expressed in adipose tissue (Maeda et al., 1996). Adiponectin exerts its function by augmenting insulin sensitivity and also acts as an anti-inflammatory agent. Adiponectin down regulates SREBP-1C expression, which is a master regulator of fatty acid synthesis (Shklyaev et al., 2003). In addition, adiponectin also increased β-oxidation of free fatty acids and decreases de novo free fatty acids production within hepatocytes. These effects will protect hepatocytes against triglyceride accumulation. (Wang et al., 2006; Xu et al., 2003)

Visceral adiposity is an immediate source of FFA that is delivered directly to the liver via the portal vein. An elevation of plasma FFA and TNF-α concentration caused activation of inhibitor kappa kinase beta (IKKβ) in adipocytes and hepatocytes. IKKβ activation decreases the tyrosine phosphorylation of insulin receptor substrate (IRS) 1 and 2 followed by inactivation of phosphatidylinositol 3-kinase (PI3-K) and down regulates other

insulin signalling events (Shulman, 2000). Thus, insulin cannot activate the glucose transport mechanism-4 (GLUT-4), so the glucose is not transported into the cells (Shulman, 2000; Day, 2002). The anti-lipolysis effect of insulin in adipose tissue is also impaired in this condition, which leads to further elevation of FFA concentration contributing to obesity related IR. FFA impairs the ability of insulin to suppress hepatic glucose output. Steatosis occurs when the liver is overloaded by FFAs and is unable to secrete them into the circulation. (Diez et al., 2003; Musso et al., 2003)

FFA and their metabolites are ligands for the transcription factor, peroxisome proliferator-activated receptor-α (PPAR-α). PPAR-α plays an important role in fat oxidation where it regulates the transcription of enzymes involved in mitochondrial and peroxisomal β-oxidation and also cytochrome P450 enzymes which involved in ω-oxidation. Leptin concentrations were found higher in hepatic insulin resistance, where it helps to ease the entry of FFAs into mitochondrial through carnitine palmitoyl-tranferase-1 (CPT-1) activation. This process is known mitochondrial β-oxidation. Therefore, both of these processes caused an increased fatty acid oxidation. (Day, 2002)

Conversely, FFA metabolism augments the production of reactive oxygen species (ROS) such as singlet oxygen, super oxide anion, hydrogen peroxide (H_2O_2), hydroxyl radical and up regulates uncoupling protein-2 (UCP-2) expression. The ROS extract the hydrogen atoms from fatty acids and create a destructive chain reaction known as lipid peroxidation (Benzie, 1996). Lipid peroxidation causes disruption of membranes and produces reactive metabolites like malondialdehyde (MDA), 4-hydroxynonenal (HNE), which affect cellular dysfunction (Day, 2002). Loguercio et al. (2001) reported that MDA and HNE levels are increased about 90% in NASH patients compared to patients with steatosis, illustrating the augmentation of oxidative stress.

TNF-α and lipid peroxidation products (Day, 2002) have been reported to restrict the electron-transport chain of the mitochondria, damage the mitochondrial DNA, and deplete the mitochondrial protein, worsening the mitochondrial dysfunction and increasing the production of ROS.

Mitochondrial damage further restricts β-oxidation of lipid and increasing the steatosis. (Day, 2002)

Mitochondrial β-oxidation produces energy, but it causes leakage in electron that creates ROS (Day, 2002). Peroxisomal β-oxidation is an intracellular process that metabolizes FFA to Acetyl-CoA. Acetyl-CoA is then transported into the mitochondria for further degradation. Peroxisomes can oxidize long-chain FFA more rapidly than mitochondria and boost the capacity of cells to metabolize FFA. During β-oxidation, peroxisomes produce H_2O_2, promoting oxidative stress. (Benzie, 1996)

ROS and lipid peroxidation end products cause direct damage to the hepatocytes causing disruption of the membranes, proteins and DNA (De Knegt, 2001; Day, 2002). They also induce an inflammatory response by up-regulating the pro-inflammatory cytokines [TNF-α and transforming growth factor (TGF-β)], infiltration of polymorph nuclear and mononuclear leukocytes, activation of kupffer cells, and expression of Fas-ligand. This can lead to necrosis, apoptosis and Fas-ligand-mediated cell death. (Angulo et al., 2001)

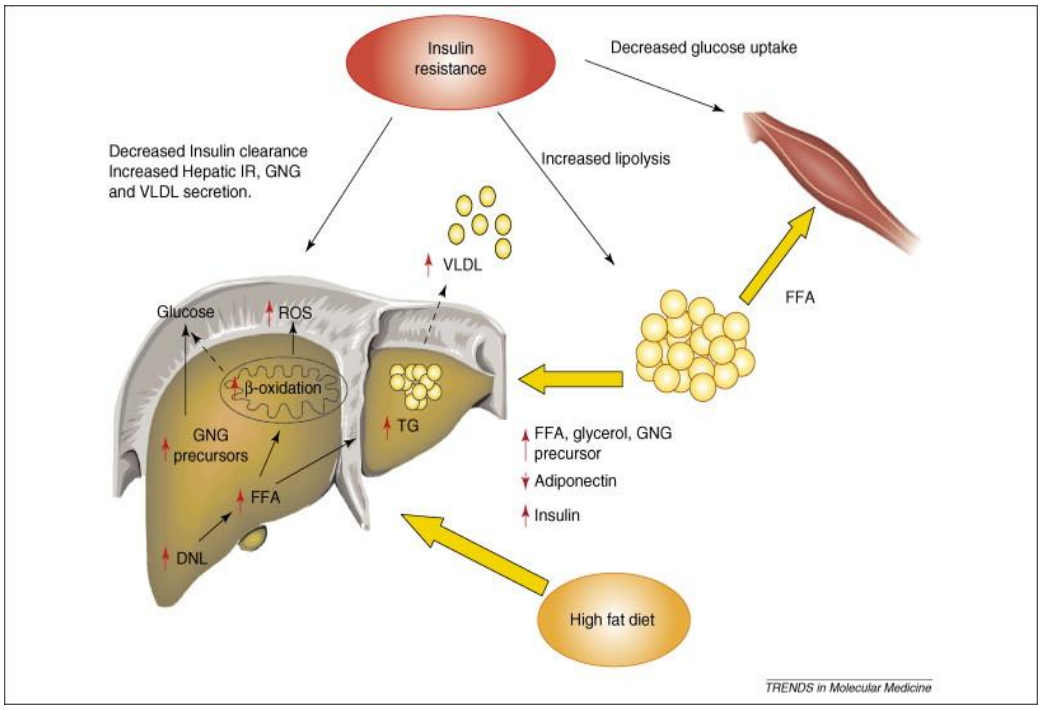

Figure 1.5: Mechanisms of fat accumulation in non-alcoholic steatohepatitis. Insulin resistance causes an influx of FFAs to the liver, owing to increased lipolysis, especially in the visceral adipose tissue. Increased de novo lipogenesis and fat from the diet also contribute to the fatty-acid pool. Both VLDL generation and FFA oxidation are increased and are sufficient to prevent intrahepatic lipid accumulation. (DNL: de novo lipogenesis; GNG: gluconeogenesis; ROS: reactive oxygen species; TG: triglycerides; VLDL: very low-density lipoproteins) (Adapted from Marra et al., 2008).

Hepatic stellate cells (HSCs) are known as lipocytes, fat-storing cells or Ito cells. This cell is one of the non-parenchemal cells (NPCs) that are responsible for fibrosis development. The role of leptin and its receptor (Ob-R) were investigated in fibrosis condition using Zucker (fa/fa) rats, where the rats were induced with thioacetamide (TAA) resulting in HSCs activation. These HSCs produce excess of extracellular matrix components and transformed into myofibroblast-like cells (Ikejima et al., 2002). TNF-α, TGF-β, MDA and HNE were capable to activate the HSCs, resulting in the production of connective tissue growth factor (CTGF) and other extracellular matrix proteins needed for fibrosis (Galli et al., 2002). CTGF is expressed excessively and in parallel with the amount of liver fibrosis in NASH patients. It is also up-regulated by hyperinsulinemia and hyperglycemia. (Paradis et al., 2001)

Leptin is the product of the obese gene (ob) that regulates food intake and body weight. Homozygus mutation of the leptin gene is associated with obesity. Hyperleptinemia is present in NASH, obese patients with Hepatitis C virus (HCV) and also chronic alcoholic hepatitis patients who have increased predisposition of cirrhosis (Ikejima et al., 2002). Marra, F. (2002) has reported that leptin may play a crucial role in developing fibrosis in NASH by stimulating HSCs via their surface receptor (Marra, F. 2002). Leptin also caused an increase in phagocytosis and proinflammatory cytokine levels and T-cell mediated immune responses in the liver. Hence, leptin may be involved in the pathogenesis of the inflammatory response and fibrosis observed in variety of liver disease associated with obesity. (Ikejima et al., 2002)

Kupffer cells activation up regulates the proinflammatory cytokine secretion (PDGF and TGFβ) to activate the stellate cells during liver injury (Cai et al., 2005). Endothelin 1 (ET1) is a potent vasoconstrictor produced by sinusoidal endothelial cells that exert a paracrine effect particularly on stellate cells rather than hepatocytes and kupffer cells. ET1 regulates stellate cells contractility that increases intrahepatic portal hypertension. ET1 also exert proliferative effects on activated stellate cells (Rockey, 1997). Transforming growth factor-β1 (TGFβ1) is a growth inhibitor that inhibits cell proliferation particularly epithelial cells, promotes transdifferentiation of HSC to myofibroblast and ECM accumulation. TGFβ1 promotes αSMA production in activated stellate cells during liver injury. (Gressner & Weiskirchen, 2006)

Cytokine secretion due to fat accumulation (TNFα, TGFβ, IL-6), oxidative stress, ER stress triggers hepatic damage and further promotes inflammation and insulin resistance (Marciniak & Ron, 2006). NF-kB activation exacerbates liver injury and is involved in maintenance of the cell survival by exerting anti-apoptotic effect (Schwabe & Brenner, 2007). TNFα mediates JNK (c-Jun N-terminal kinase) signalling pathway, whereas both inflammation and insulin resistance activate the pathway. JNK signalling pathway is activated in obesity and insulin resistance condition (Sethi & Hotamisligil, 1999; Boden, 1997). Genetic deletion of JNK1 in lean and obese

mice decreased adiposity, improved insulin sensitivity and enhanced insulin receptor signalling capacity (Hirosumi et al., 2002).

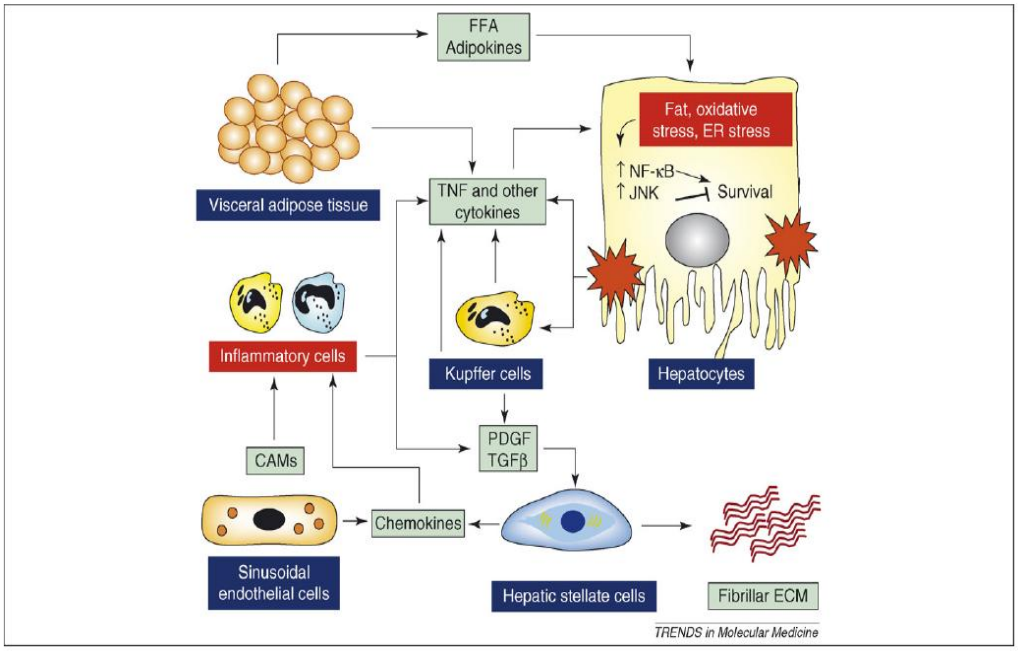

Figure 1.6: Mechanisms of inflammation in NASH. Damage to hepatocytes caused by fat loading and resulting lipotoxicity leads to the activation of intracellular signalling pathways, which leads to the expression of several cytokines that are responsible for the recruitment of inflammatory cells. Hepatic damage also affects the biology of other liver cells, such as Kupffer cells, which become activated and contribute to cytokine secretion. Recruitment of inflammatory cells is also conditioned by factors produced by activated hepatic stellate cells and sinusoidal endothelial cells. Most liver-resident cells are targeted by adipokines secreted by visceral adipose tissue. These events lead to a vicious circle that causes worsening of liver damage, further inflammation, maintenance of steatosis, disease progression and insulin resistance. (CAM: cell adhesion molecule; ECM: extracellular matrix; ER: endoplasmic reticulum; JNK: c-Jun N-terminal kinase, PDGF: platelet-derived growth factor; TGF-β: transforming growth factor-β). (Adapted from Marra et al., 2008).

1.5. Treatment of NASH

At the present moment there is no generally accepted treatment for NASH. Regular exercise and diet control are the alternative therapy to drugs, and they effectively improved the liver function test (Marchesini et al., 2001) and histological changes (Dixon et al., 2004). But, in some studies the histological changes worsened with drastic weight loss (Andersen et al., 1991).

There are two classes of insulin sensitizing agents, metformin and thiazolidinediones (TZDs) that are used to treat insulin resistance (IR). Metformin was effective in improving the insulin sensitivity, reducing ALT and glucose levels (Marchesini et al., 2001), but did not produce any improvement in fibrosis in patients with NASH. (Nair et al., 2004)

TZD are the new class of antidiabetic drugs which consist of 3 compounds that are clinically used, Troglitazone (Rezulin ®), Rosiglitazone (Avandia ®) and Pioglitazone (Actos ®). In 1997, Troglitazone was the first TZD to gain approval from the Food and Drug Administration (FDA) and was used clinically in obese and diabetic patients. Troglitazone enhances insulin sensitivity and promote adipocytes differentiation. Unfortunately, Troglitazone caused severe hepatotoxicity that leads to death in over 500 cases. Finally, Troglitazone was withdrawn from the market in 2000 (Caldwell et al., 2001). The second generation of TZDs are Rosiglitazone and Pioglitazone have proven to have low rates of hepatotoxicity (Neuschwander-Tetri et al., 2003).

Neuschwander-Tetri et al. (2003) have reported that Rosiglitazone given to NASH patients (4mg daily for 48 weeks) caused a significant improvement in insulin sensitivity (the ability to suppress endogenous glucose production) and mean serum ALT. Rosiglitazone also showed a significant improvement in hepatocytes ballooning, numbers of kupffer cells and the global necroinflammatory grade. The characteristic of zone 3 fibrosis of NASH was also improved. Therefore, Rosiglitazone changes the pattern of inflammation from lobular to portal predominance. (Neuchwander et al., 2003)

Pioglitazone given to 55 randomised NASH patients (45mg daily plus hypocaloric diet) significantly enhanced insulin sensitivity, normalised serum ALT level, and reduced serum AST levels. Histological findings showed that Pioglitazone improved steatosis, necrosis ballooning and inflammation, but did not show a significant change in fibrosis compared to a placebo group. (Belfort et al., 2006)

Both Rosiglitazone (Neuchwander et al., 2003) and Pioglitazone (Lutchman et al., 2007) caused peripheral weight gain. Fatigue or mild lower-extremities edema were reported with Rosiglitazone (Neuchwander et al., 2003) and Pioglitazone (Belfort et al., 2006), but these side effects were only observed in few patients. Pioglitazone has been reported to be more effective than Rosiglitazone in reducing low density lipoprotein (LDL) cholesterol and triglycerides in type 2 diabetes patients (Miyazaki et al., 2001). This is because Pioglitazone is not only a full PPARγ agonist but also a partial PPARα agonist, unlike Rosiglitazone that only exhibits PPARγ agonist effects (Sakamoto et al., 2000).

TZDs exert their anti-diabetic effect through by acting as ligands for the peroxisome proliferator-activated receptor-γ (PPAR-γ). When activated, PPAR-γ will heterodimerize with retinoid X receptor (RXR) and form a PPAR-γ-RXR complex, then this complex will bind to a specific DNA sequence in the promoter of a target gene to induce the transcription via PPAR-response elements (PPREs) (Kliewer et al., 1992; Keller et al., 1993). The binding of ligand to PPARγ will result in changes in the expression levels of PPAR target genes.

TZDs act as insulin sensitizers by increasing the glucose uptake in adipose tissue and skeletal muscle. A study conducted in Type 2 DM animal models proved that TZDs can reduce plasma glucose levels and triglycerides to normal values. Similar findings were observed when TZDs were given to type 2 diabetes patients, where they reduced plasma glucose, insulin, triglycerides and FFAs (Gastaldelli et al., 2007).

Obesity is strongly associated with adipocyte hypertrophy, and leads to hepatic and peripheral IR as well as overproduction of FFAs, TNF-α, and leptin (Kadowaki, 2000). When PPAR-γ is activated by a ligand, an elevation in the level of adipocyte differentiation is observed leading to the production of more numerous, smaller adipocytes. These small adipocytes are more insulin-sensitive, producing less FFA, TNF-α, and leptin. Therefore, insulin is more effective and there is less need for the pancreatic β-cells to elevate their insulin secretion (Figure 1.7 Right Panel). This improvement in glucose and lipid metabolism is accompanied by weight gain and an increase in subcutaneous fat (Miyazaki et al., 2002).

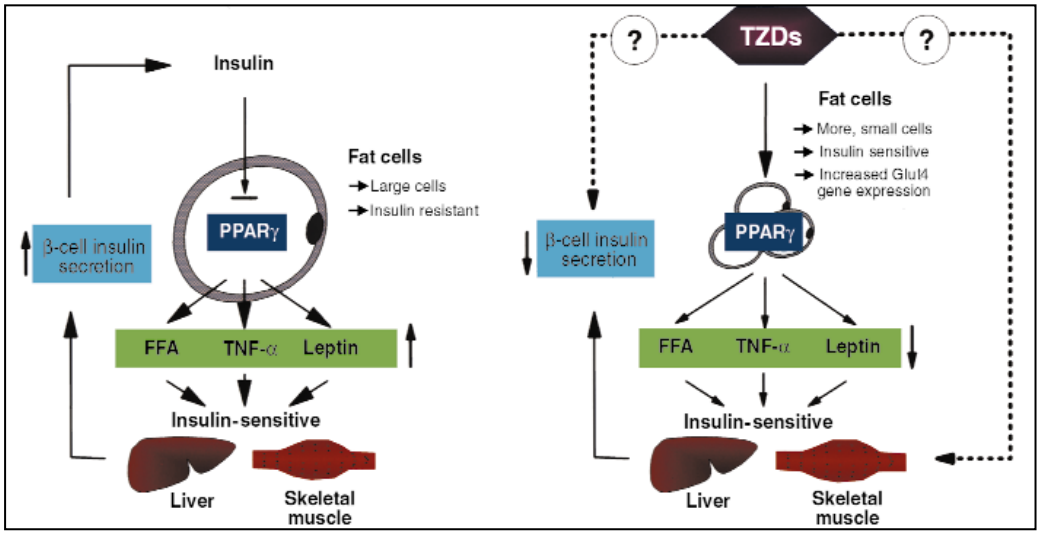

Figure 1.7: **Left Panel:** Insulin resistance condition affect the fat cells caused increased in FFAs, TNF-α and Leptin. **Right Panel:** Mechanism of TZDs action on PPAR-γ caused improved insulin sensitivity, adipocytes differentiation and increased glucose uptake (Adapted from Kahn et al., 2000).

Pioglitazone used in type 2 diabetes treatment, caused an elevation in adiponectin levels improving insulin resistance and reduced hepatic fat content (Bajaj et al., 2004). Both rosiglitazone and pioglitazone reduced plasma resistin (Bajaj et al., 2004; Jung et al., 2005) and impaired TNF-α activation (Iwata et al., 2001; Hernandez et al., 2004) in both type 2 diabetes patients and animal models. A previous study has reported that, both pioglitazone and rosiglitazone retarded the liver fibrosis in rats via PPAR-γ receptor stimulation leading to the reduction of activation of HSCs and subsequent collagen synthesis (Galli et al., 2002).

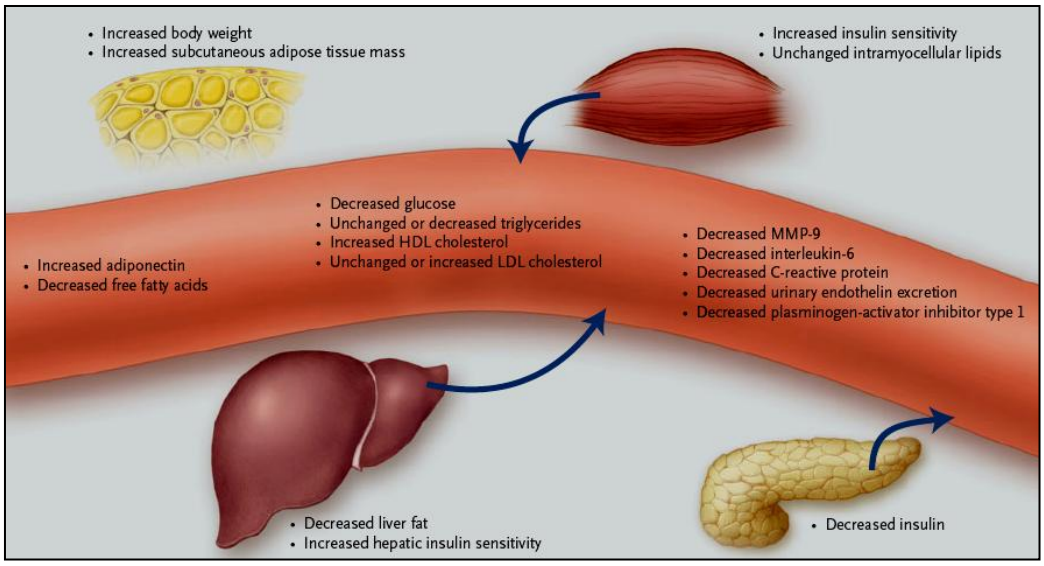

Figure 1.8: Mechanism of action of TZDs in vivo in humans. TZDs increased lipogenesis and increased subcutaneous adipose tissue mass and body weight. TZDs decrease circulating or urinary markers of cardiovascular risk and vascular inflammation such as plasminogen-activator inhibitor type 1, C-reactive protein, matrix metalloproteinase 9 (MMP-9), and urinary endothelin excretion. (Adapted from Yki-Jarvinen, 2004)

Yki-Jarvinen (2004) has reported that both Pioglitazone and Rosiglitazone reduced the risk of cardiovascular disease by improving the glucose and lipid metabolism. Rosiglitazone given to diabetes patients with coronary artery disease caused reduction MMP-9, interleukin-6 (IL-6), C-reactive protein and plasminogen-activator inhibitor type-1 which are cardiovascular risk markers (Marx et al., 2003).

Other than that, the effects of PPAR γ ligand were also observed in stellate cells and kupffer cells. PPAR γ ligands, 15-deoxy-protaglandin J_2 (15d-PGJ_2) and ciglitazone both inhibit PDGF induced stellate proliferation and αSMA expressions in human (Galli et al., 2000). The PPAR γ agonist AD4833 (Pioglitazone hydrochloride) was also reported to decrease both lipopolysaccharide (LPS) induced nitric oxide (NO) and TNFα levels in a rat kupffer cells culture model (Uchimura et al., 2001).

Aithal et al. (2008) have reported that (30mg/day) Pioglitazone (PGZ) was given to non-diabetic NASH patients for 12 months, this dose induced an increased in body weight, followed by reduction in plasma glucose, HbA1c, insulin C peptide, alanine aminotransferase (ALT), γ-glutamyltransferase (GGT) and ferritin compared to placebo treated group. Histological scoring with PGZ treatment also have shown some improvement in hepatocellular injury, Mallory–Denk bodies, and fibrosis scoring but no change in steatosis scoring compared to placebo treated group.

Currently there are no data on the underlying molecular mechanism either on NAFLD progression or Pioglitazone mechanism of action in non-diabetic NASH patients. Therefore the aims of this study were to further investigate the aforementioned molecular mechanism. This study was a follow-up study from Aithal et al. (2008), where the liver biopsy and liver paraffin blocks taken from both placebo and pioglitazone were used to study genes, protein and immunohistochemistry expression of stellate cell markers and hepatocyte markers expression in order to achieve the study objectives.

1.6. Research Objectives

- To investigate the molecular mechanism underlying the progression of NAFLD from normal liver as well as how it leads to the progression of NASH.
- To investigate the molecular mechanisms underlying the effects of Pioglitazone and placebo treatment in non-diabetic NASH patients.
- To investigate the behaviour and molecular expression of human hepatic stellate cells in culture plated on different culture surface mimic the *in vivo* condition of Space of Disse.
- To determine the expression of adipogenic, nuclear receptors and stellate cells activation markers in the *in vitro* culture model of human hepatic stellate cell over time.
- To determine the effects of nuclear receptor ligands upon activation and proliferation upon PDGF-BB incubation in a human hepatic stellate cells *in vitro* culture model.

CHAPTER 2

Methods & Materials

2.1. Subjects and study design

Patients were recruited for the randomised double-blind placebo trial from the Queen's Medical Centre in Nottingham and Derby City General Hospital. Patients between the ages of 18 and 70 years who were able to give consent were initially screened by medical history and physical examination. Patients with weekly alcohol consumption >210g for men and >140g for women were excluded from this study. Patients with disease including hepatitis B and C, heart failure, renal impairment and hepatic steatosis were also excluded, as subjects taking medication for fatty liver disease. Each patient had an ultrasound examination of the liver and liver biopsy was performed according to a standard protocol. Diagnosis of NASH was confirmed on histology by the presence of fat and evidence of hepatocyte injury, inflammation or fibrosis. (Aithal et al., 2008)

All NASH patients entered a 3 month run in period prior to randomisation and were instructed by a dietician to reduce their calorie intake by 500 Kcal per day as well as performing modest exercise (such as walking, swimming or gardening etc) regularly for 30-40 minutes per day at least 5 days per week. Sixty one patients were randomised to receive either 30 mg/day of Pioglitazone (30 patients) (Takeda Pharmaceuticals UK) or placebo (31 patients) for 12 months. (Aithal et al., 2008)

Anthropometric data (height, weight, and waist:hip ratio), blood count, standard liver function test and fasting blood samples for determination of glucose, insulin, HbA1c and lipid profile were collected at baseline and the end of Pioglitazone treatment. At each 4 monthly visit, brief examination was carried out in particular to look for adverse side effects. The compliance was also monitored during this visit using tablet counts. Liver biopsies were collected at the end of 1-year treatment from both Pioglitazone and placebo group. (Aithal et al., 2008)

All materials used in this work were of the highest available quality and were purchased from Sigma, UK or BDH unless otherwise stated.

2.2. RNA isolation and purification

2.2. 1. Materials for RNA isolation and purification

Tri Reagent (Ambion Inc, USA); 1-Bromo-3-Chloro-propane (BCP), (Sigma, UK); Sodium Acetate (NaAc) 2M pH 4.0; Isopropanol (Sigma, UK); 70% Ethanol; RNAse free water (Qiagen, UK); RNAse free DNAse (Qiagen, UK); RNAse Cleanup Mini Kit (Qiagen, UK)

2.2. 2. Method for RNA isolation and purification

50mg of the frozen tissue was transferred into a polypropylene snap-cap tube containing 2ml of ice-cold monophasic lysis reagent (TRI reagent), followed by 15-30 seconds homogenization at room temperature using tissue homogenizer (Ultra-turrax,T25, IKA®-Labortechnik). Then, the homogenates was left for 5 minutes at room temperature to permit complete dissociation of nucleoprotein complexes; 0.4 ml of BCP was added per ml of monophasic lysis reagent, followed by vortexing of the sample. The sample was then centrifuged at 10,000g for 15 minutes at 4° C. The upper aqueous phase was transferred into a fresh tube, and the supernatant bottom phase kept for protein extraction. 0.25ml NaAc (2M, pH 4) and 0.7ml Isopropanol were added per ml of aqueous phase, and the sample was then stored overnight at -20°C. The precipitated RNA was collected by centrifugation at 13,000rpm for 15 minutes at 4°C in a microfuge. The pellet was washed twice with 70% ethanol followed by 10 minutes centrifugation 13,000rpm at 4°C. The ethanol was removed with a disposable pipette tip, and the open tube left on the bench for 5 minutes to allow the ethanol to evaporate. The pellet was then dissolved in 30-50µl of RNAse-free H_2O. Total RNA was purified after DNase treatment using the RNAeasy Mini Kit according to the manufacturer's instructions**.** The total RNA concentration was measured at the absorbance of 260 nm using Nanodrop-1000 Spectrophotometer (Thermo Scientific, USA) and the integrity of RNA was checked using an Agilent 2100 Bioanalyzer (Agilent Techonologies, USA).

2.3. cDNA synthesis & Taqman Real time-PCR validations

2.3.1. Materials for cDNA synthesis & Taqman Real time-PCR validations

SuperScript™ III Reverse Transcriptase (200U/µl) (Invitrogen, UK); 5X First strand buffer (Invitrogen, UK); 0.1M DTT (Invitrogen, UK); 100ng/µl Random Primer (Promega, UK); 10mM dNTP mix (Promega, UK); RNaseOUT™ Recombinant Ribonuclease Inhibitor (40 U/µl) (Invitrogen, UK).

2.3. 2. Method for cDNA synthesis & Taqman Real time -PCR Validations

A total of 200ng of RNA was reverse transcribed into cDNA using Superscript III Reverse Transcriptase (RT) (Invitrogen, UK) according to manufacturer's instructions. The mRNA concentrations of selected genes were quantified using ABI Prism 7700 sequence detection system instrument and software (Applied Biosystems, USA). cDNA was diluted in 1:8 dilution and 3µl of synthesized cDNA was mixed with Taqman Universal PCR master mix (Applied Biosystem, USA) and gene specific primer and probe mixture (Eurofins MWG Operon, Germany) in a final volume of 13µl and all samples were run in triplicates Relative expression levels were determined using five-point serial dilution standard curve, generated from human liver cDNA.

Assays were deemed acceptable if there was no more than 0.5 cycle threshold (Ct) difference between the values of a triplicate, the slope of the standard curve was between -3.2 to -3.6 and the r^2 was between 0.95-0.99 (Figure 2.1). The mRNA expression levels of specific genes were normalized to the geometric mean of the mRNA expression level of β-actin and HMBS which were used as the reference genes for the liver biopsy samples and β-actin for human stellate cell samples.

The primers and probes used in this study are designed using Primer Express III software shown in Appendix 1.

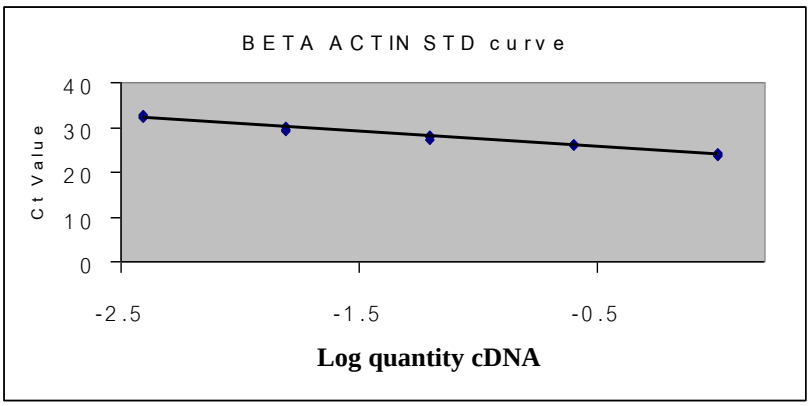

Figure 2.1: Taqman Real-time PCR standard curve showing the slope value (-3.43) and correlation co-officient (r^2) value (0.99).

2.4. Method for Custom Taqman Low Density Array

The selected probe ID genes were sent to Applied Biosystem (USA) to design 384 wells micro fluidic card with 4 samples per card. A total of 400ng of RNA was reverse transcribed into cDNA using Superscript III Reverse Transcriptase (RT) (Invitrogen,UK) according to manufacturer's instructions. 60µl of synthesized cDNA was mixed with 50µl of HPLC water and 110µl of Taqman® Universal PCR master mix, No AmpErase® UNG (Applied Biosystem, USA).

The mRNA concentrations of selected genes in the samples were quantified using ABI PRISM® 7900HT sequence detection system instrument (Applied Biosystems, USA). The gene expression was later quantified using SDS RQ Manager Software, Applied Biosystem (USA).

2.5. Pre-Amplification technique for stellate cells cDNA

The aim of this technique is to amplify the lower expression of target genes in human hepatic stellate cells to quantify the gene expressions.

2.5.1. Materials for Pre-amplification technique for stellate cells cDNA

TaqMan PreAmp Master Mix (2X) or Taqman® Fast Master Mix; Reverse and Forward primers of target genes; Tris-EDTA (TE) Buffer (1X) ; cDNA samples.

2.5.2. Method for Pre-amplification technique for stellate cells cDNA

20µl of each reverse and forward primer were pooled in 2ml eppendorf tube. In this study there were 18 target genes (as shown in table 5.1 in chapter 5) and 1 reference gene (β-actin) which were amplified (19 pairs of primers). The pooled assay mix must be diluted 50 times. The calculation of pooled assay mix is as shown as below:

Pooled Assay Mix dilution: 20µl X 38 (19 pairs of primers)

: 760µl of pooled primers mix.

From the above calculation these pooled primers mix has been diluted 38 times. The final dilution is 50 times. Therefore, the pooled primers mix was diluted 12 times with TE buffer to reach final dilution of 50 times. Therefore, 240µl of TE buffer (20µl X 12) was added to the pooled primers mix to become Pooled Assay Mix. Then all the samples were prepared for PCR Preamplification reaction. 25µl of TaqMan PreAmp Master Mix (2X) was added into a PCR reaction tube, followed by 12.5µl of Pooled Assay Mix and 12.5µl of 400ng cDNA sample. The final volume for the PCR reaction is 50µl. The PCR Preamplification reaction was performed as shown in Table below:

Table 2.1: PCR Preamplification reactions

	Hold	10 cycles	
Temperature	95°C	95°C	60°C
Time	10 minutes	15 seconds	4 minutes

The PCR product is diluted in 1:5 dilutions with 1X TE buffer after the PCR reaction. Then these samples were used for the Taqman Real time PCR for target gene quantification and analysis for the human hepatic stellate cells experiments.

2.6. Protein expression analysis

2.6. 1. Materials for Protein expression analysis

Solutions

5X SDS Urea Buffer

90mM Tris HCl, 4% (w/v) SDS, 5 % (v/v) β-mercaptoethanol (β-ME), 7M Urea (Urea was dissolved in deionised water first using Amberlite Monobed resin for 30 minutes), 0.1% (w/v) Bromophenol blue. (Sigma Chemicals, UK)

4X Separation gel buffer

1.5M Tris Base; 0.4% (w/v) SDS pH 8.8 with concentrated HCl

4X Stacking gel buffer

0.5M Tris Base; 0.4% (w/v) SDS pH 6.8 with concentrated HCl

12% Separation gel (for 4 mini gels)

18.6ml 30% (w/v) **Acrylamide;** 11.4ml HPLC water; 10ml 4X separation buffer pH 8.8, 400µl 10% (w/v) Ammonium persulfate (APS); 40µl TEMED.

4X Stacking gel (for 4 mini gels)

4ml 30% (w/v) **Acrylamide;** 26ml HPLC water; 10ml 4X Stacking buffer pH6.8; 200µl 10% (w/v) Ammonium persulfate (APS); 20µl TEMED.

10X Running Buffer (1000ml)

144g Glycine; 30Tris Base; 100ml 10% (w/v) SDS, made up to 1litre with HPLC water

10X Transfer Buffer (SDS free) (1000ml)

30g Tris Base; 144g Glycine, made up to 1litre with HPLC water

Transfer Buffer working solution

80ml 10X Transfer Buffer; 160ml Methanol, made up to 800ml with HPLC water

10X Tris Buffered Saline (TBS) (1000ml)

24.23g Tris Base; 80.06g Sodium Chloride (NaCl) pH 7.6 with concentrated HCl

1X Tris Buffered Saline-Tween 20 (TBS-T)

100ml 10X TBS with 1ml of Tween 20, made up to 1litre with HPLC water

Coomassie Blue R350 solution

0.4g of Coomassie blue R350 was dissolved in 200mL of 40% (v/v) methanol in HPLC water with stirring as needed. The solution was filtered to remove any insoluble material and 200ml of 20% (v/v) acetic acid was added in the solution.

Coomassie Gel fixing solution

500mL of USP-grade 95% (v/v) ethanol was added to 300ml of HPLC water, 100ml of glacial acetic acid and the total volume was adjusted to 1litre with HPLC water.

Coomassie Gel destaining solution

500mL of HPLC-grade methanol was added to 300ml of water, 100ml of glacial acetic acid and the total volume adjusted to 1litre with HPLC water.

Coomassie Gel Storage solution

25ml of glacial acetic acid made up to a final volume of 500ml of HPLC water.

2.6. 2. Method for Protein Extraction

The remaining supernatant bottom phase from the RNA extraction (as described in section 2.2.2) was used for protein extraction. After removing the aqueous phase, 1.9ml of Isopropanol (Sigma, UK) was added per ml of supernatant, and the mixture was left at room temperature for 10 minutes. Then the samples were centrifuged at 5000rpm for 10 minutes at 4°C. The supernatant was removed and the pellet washed 3 times with 0.3M Guanidium-HCl in 95% alcohol. Finally, 2ml of ethanol was added and the solution was incubated for 20 minutes at room temperature followed by centrifugation at 7500rpm for 5 minutes at 4°C. The, supernatant was discarded and the protein pellet was dissolved in SDS Urea buffer by sonication (1 time for 10 seconds) and boiled for 5 minutes. The protein sample was then centrifuged at 13000rpm for 10 minutes.

2.6. 3. Western blotting gel electrophoresis

The gel electrophoresis was run at 120 Volt for 2 hours followed by transferring the protein from the gel on to nitrocellulose membrane at 105volt for 1 hour according the manufacturer’s description (Bio-Rad, USA).

2.6. 4. Immunodetection following western blotting

The nitrocellulose membrane was blocked with 5% (w/v) Marvel 1X TBS-T washing solution for one hour on a shaker. The blocking solution was discarded, followed by addition of primary antibody in 5% (w/v) Marvel 1X TBS-T and the membrane was incubated overnight at 4°C. Following primary antibody incubation, the membrane was washed with 3X 10 sec washes and 3 times 5 minutes washes with TBS-T.

The secondary antibody (1:10000 dilution) in 5% (w/v) Marvel 1X TBS-T solution was then added and the membrane was incubated for one hour at room temperature. The membrane was then washed 3X 10sec washes and 1X 5 minutes with 1X TBS-T. Finally the membrane was immersed in distilled water for 5 minutes prior to scanning of the membrane using the Odyssey® Infrared Image system (LICOR Biosystem, USA) using 700nm (red channel) and 800nm (green channel) with the focus offset to membrane imaging. Densitometry was performed using Odyssey® Imaging System Software (LICOR Biosystem, USA).

Table 2.2: List of antibody used for western blotting protein expressions in this study.

Primary Antibody	**Dilution used**
β-actin, (A5441) Sigma-Aldrich USA	1:5000
Proliferating cell nuclear antigen (PCNA) (SC-7907), Santa Cruz, USA	1:200
Peroxisome proliferator activator receptor (PPAR)-γ (SC-7273),Santa Cruz, USA	1:100
α-smooth muscle actin (αSMA) (A5228), Sigma-Aldrich, USA	1:200
Secondary Antibody	**Dilution Used**
IRDye® 700CW Conjugated Goat Anti-Rabbit IgG, (926-32221) Licor Bioscience, USA	1:10000
IRDye® 800CW Conjugated Goat Anti-Mouse IgG, (92632210) Licor Bioscience, USA	1:10000

2.7. Immunohistochemistry

2.7.1. Materials for immunohistochemistry

Solutions

Xylene, Industrial Methylated Spirit (IMS) from Fisher Scientific, UK

Citrate saline buffer

21g Citric acid; 250ml of 1M Sodium Hydroxide (NaOH), pH 6.0, made up to 10litres with distilled water

TRIS/HCl Buffered saline (TBS)

81g Sodium Chloride (NaCl); 6g TRIS (hydroxymethyl methylamine); 42ml Hydrochloric acid (HCl) 1M, pH 7.6. pH was adjusted to 7.6 with 1M NaOH and made up to a volume of 10litres.

1% acid alcohol

30ml Concentrated HCl; 2.1ltres Industrial methylated spirit (IMS), 900ml of deionised water

Scott's Tap Water

10.5g Sodium Hydrogen Carbonate ($NaHCO_3$); 60g Magnesium sulphate ($MgSO_4$), 3litres of deionised water

Mayer's Haematoxylin

50g aluminium potassium sulphate (alum) dissolved in 1000 ml distilled water. 1g of haematoxylin was then added followed by addition of 0.2g sodium iodide and 20ml acetic acid. The solution was boiled, allowed to cool to room temperature and filtered through Whatman 3M filter paper before use.

Harris's Haematoxylin (without acetic acid)

HD Supplies, UK

Methlygreen stain

DAKO, Denmark

2.7.2. Method for rehydrating the immuno sample slide

The sample slide was immersed in 2 Xylene bath for 5minutes and 2 minutes. Then the slide was immersed in 3 bath of IMS for 30 sec each bath. The slide was rinsed in distilled water for 5 minutes.

2.7.3. Method for antigen retrieval of immuno sample slide

The slide was placed onto a plastic rack followed by an immersion in 850ml of citrate saline buffer in a plastic container. The container was then moved into the microwave with the lid was placed onto the container. The sample was then irradiated at 'MEDHIGH' for 23minutes for antigen retrieval purpose. After that the sample was taken out from the solution, was left in running cold tap water for 15minutes. The sample immunostained using specific kits and the protocol was followed as described by the manufacturer. List of immunostaining kits used in this study is as shown below:

Table 2.3: List of immunostaining kit used in this study

Immunostaining Kit
Single Immunohistochemistry using Dako Real™ Detection System, Peroxidase/DAB+, Rabbit/ Mouse Kit, Dako (K5001)
Dual immunohistochemistry staining using the EnVision™ G|2 Doublestain System, Rabbit/Mouse (DAB+/Permanent Red Kit, Dako (K5362)
TUNEL immunohistochemistry using ApopTag® Peroxidase *In situ* Apoptosis Detection Kit (S7100) Chemicon International (USA)
TUNEL - *In situ* cell death detection kit, fluorescein (11684795910), Roche, Germany

2.7.4. Method for counterstaining the immuno slide sample

The slide was washed in running tap water for 15minutes, and then followed by incubation in Mayer's haematoxylin for 2 minutes. If using Harris Haematoxylin incubate the slide for 6 minutes. After that, the slides was rinsed in running cold water followed by 5 seconds dip in 1% acid alcohol and then rinsed in running cold water. The slide was incubated in Scott's tap water for 30 seconds followed by rinsed in running cold water. The slide was dehydrated in 3 IMS bath for 30 seconds each and 2 bath of Xylene followed by mounting with DPX (BDH Supplies, UK) of the section with coverslip.

2.8. TUNEL assay

2.8. 1. Material for positive control tissue for TUNEL assay

DN buffer Solution

3ml of 1M Tris Base, pH 7.2, 400µl of 1M Magnesium Chloride ($MgCl_2$); 1.54mg Dithiothreitol (DTT) made up to 100ml of distilled water.

2.8. 2. Method for positive control tissue for TUNEL assay

Section was pre-treated with DN Buffer at room temperature for 5 minutes after performing both DEPC treatment and antigen retrieval with Proteinase K (as described by the manufacturer's kit). DNase 1 enzyme (Qiagen, UK) dissolved in DN Buffer with final concentration of 1µg/ml, was incubated on the section for 10 minutes at room temperature. Finally the section was rinsed with distilled water for 3minutes each 5 times.

2.9. Double immunoflourescence staining

2.9.1 Materials for double immunoflourescence staining

Buffer 1 (Washing buffer for immunoflourescence)

2 tablet of Phosphate buffer saline (PBS) (Dulbecco A); 2g Bovine serum albumin (BSA); 200µl Tween-20 made up to 200ml of distilled water.

DABCO Fluorescent mounting medium

200mg DABCO (1-4-Diazabicyclo-2-2-2-octane), Sigma-Aldrich, UK; 10ml 1X PBS (Dulbecco A); 90ml Glycerol (ICN Biomedical Inc, USA). Solution was mixed together and stored at 4°C.

DAPI (4'6-diamino-2-phentl-indole, dehydrochloride) stock solution

10mg DAPI (Invitrogen, UK) was dissolved in 10ml of distilled water to make 1mg/ml stock solution. For working solution used 1:500 dilutions on to the section for 10 minutes.

2.9.2. Method for double immunoflourescence staining

The sample slide was rehydrated and antigen retrieved as describes previous in section 2.6.2 and 2.6.3. The section was blocked with peroxidase blocking solution (S2023, Dako) for 15 minutes followed by washed with deionised water. Then the section was incubated with first blocking serum (10% serum from the species that the secondary antibody was raised in) for 30 minutes to block unspecific binding of the antibodies in Buffer 1. The serum was decanted followed by **first primary antibody** in Buffer 1 incubation in a humidified chamber for overnight at 4°C. The **first primary antibody** solution was decanted and washed the section 3 times in Buffer 1 for 5 minutes each wash. The **first secondary antibody (labelled with Fluorochrome-1)** in Buffer1 was incubated on the section for 1 hour at 4°C in dark. Finally the first secondary antibody solution was decanted and the section was washed 3 times in Buffer 1 for 5 minutes each in dark. The similar process of blocking and incubation of **second primary antibody** and **second secondary antibody** were repeated as described previously. Then the section was washed quickly and incubated on DAPI (1:500) dilution for 10 minutes and followed by quick washed once again. The section was then mounted with DABCO mounting medium and sealed the coverslip with nail polish and store in the dark -20°C or 4°C**.**

Table 2.4: List of sources and dilution of primary antibody used for these study.

Primary Antibody	**Dilution**	**Incubation period**
α SMA (M0851) Dako, Denmark	1:250	1hour at room temperature
Desmin (M0760) Dako, Demark	1:50	1hour at room temperature
CRBP1 (SC-30106), Santa Cruz, USA	1:200	1hour at room temperature
GFAP (Z0334) Dako, Denmark	1:100	1hour at room temperature
GFAP Ab-1 (MS-280-P1), Thermo Scientific, USA	1:100	Overnight at 4°C
Caspase 3, (G748A) Promega, UK	1:500	3 hours at room temperature
M30 (12140322001), Roche Germany	1:50	3hours at room temperature
PPAR α (P0869), Sigma-Aldrich, UK	1:200	1 hour at room temperature
PPAR β (SC-7197), Santa Cruz, USA	1:100	3hours at room temperature
PPAR γ (SC-7273), Santa Cruz, USA	1:100	1 hour at room temperature
Ki67 (PA0118) Vision Biosystems Bond™, UK (Ready to use for immunohistochemistry)	-	1 hour at room temperature
Secondary Antibody	**Dilution**	**Incubation period**
Alexa Fluor® 488 Goat anti-rabbit IgG (H+L), (A11008) Invitrogen, UK	1:500	1 hour at 4°C in the dark
Rhodamine Red™-X Goat anti-rabbit IgG (H+L), (R6394) Invitrogen, UK	1:500	1 hour at 4°C in the dark
Alexa Fluor® 488 Goat anti-mouse IgG (H+L), (A11001) Invitrogen, UK	1:500	1 hour at 4°C in the dark
Rhodamine Red™-X Goat anti-mouse IgG (H+L), (R6393) Invitrogen, UK	1:500	1 hour at 4°C in the dark

2.10. Stereology Count of hepatic stellate cells

The dissector method was used for stereology count (Mayhew, 1996). It was done randomly and blindly in order to prevent biasness. The number and diameter of HSCs and hepatocytes are taken from 25 frames using the 40X objective magnification, only positive cell bodies containing nucleus in the box and the ones that touches the dotted lines were counted. The cell that touches the straight lines must not be counted.

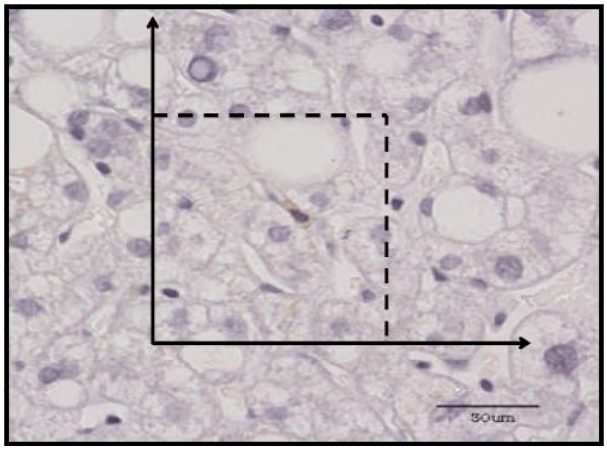

Then the % Cell / %Total cell volume were calculated in the formula stated below:

$$N_V = \frac{N_N}{[D \times (4 / \pi)] + T}$$

N_v = Number of cell per unit volume

N_N = Number of nucleus per frame

D = Diameter (μm); $\pi = 3.142$

T = Thickness of the section (μm)

2.11. Liver Perfusion

2.11.1. Materials for liver perfusion

Solutions

10x Hanks-Hepes (HH) buffer pH 7.4

80g NaCl; 4.0g KCl; 0.6g KH_2PO_4; 1.2g Na_2HPO_4 $12H_20$; 47.6g HEPES; 0.1g Phenol red; 4.0g NaOH

All components were dissolved in 1litre of Steripak water, sterilised by autoclaving or vacuum filtration and store at 4°C in glass bottle.

Soltran solution for transport and flushing of tissue

Soltran buffer from Baxter was diluted to 300mOsmol/l (500ml Soltran + 300ml sterile water)

EGTA, 25mM

4.8g EGTA (Sigma E3889) dissolved in 250ml 1X HH, 25ml 1M NaOH. Made up to 500ml with 1X HH, autoclaved and stored at 4°C.

Calcium chloride, 250mM

9.2g of calcium chloride (dihydrate) in 250ml of Steripak water. Autoclaved and stored at 4°C.

MBG solution (HH^+)

31g sodium bicarbonate (Sigma S6297), 25g glucose (Sigma G7021) and 7.5g methionine (Sigma M9500) were dissolved in 500ml Steripak water, Filter sterilised (use filter unit for Duran bottle), and stored at -20°C in 50ml aliquots.

Percoll/HBSS:

Percoll (Amersham 17-0891-01, density 1.131 g/ml) was diluted in 9:1 with 10x HBSS and stored in 10ml aliquots at 4°C.

2.11.2. Preparation for liver perfusion

The water bath was heated to 43°C followed by thawing 50ml of MBG solution. Both the tissue culture hood was sterilised and then the sterilised perfusion tubing was recirculated with 70% IMS followed sterilised water (1litre). The perfusion buffer was made up with 1X HH supplemented with 20ml of MBG in 1litre solution.

The following solutions were prepared in Duran bottles:

a) 1X HH buffer + 10mL MBG + 10mL EGTA in 500ml solution
b) 1X HH buffer + 20mL MBG + 20mL EGTA in 1litre solution
c) 1X HH buffer + 10mL MBG (without EGTA) in 1litre solution (100ml of solution was removed for mincing the tissue after digestion/perfusion)
d) 1X HH buffer + 10mL MBG + 10mL calcium chloride + 65 U collagenase + 80mg trypsin inhibitor in 500ml solution

All these solutions were warmed up in the water bath and aerated with 95% oxygen, 5% CO_2 before used.

2.11.3. Method for liver perfusion

1. The tissue was collected from theatre in cold Soltran buffer from Baxter then the tissue was weighed for the record. Then the tissue was flushed with diluted cold Soltran using a syringe. Tissue was cannulated and perfused with 1500ml perfusion buffer with EGTA, using Watson-Marlow 323 pump set at 45rpm 20 minutes. This solution was not recirculated.

2. The tissue was then flushed with perfusion buffer without EGTA prior to collagenase digestion for 6 minutes and this solution was not recirculated. Then, changed to the perfusion buffer with collagenase solution and was recirculated for approx. 20 minutes until the lobe is soft and blanched.

3. The tissue was carefully removed and placed into perfusion buffer without EGTA and minced gently with blunt-ended scissors and then filtered through a 250-µm and then a 100-µm nylon mesh. The filter was flushed with HBSS solution.

4. The filtered solution was divided into 50ml tubes and collected by centrifugation at 50g for 4min at room temperature using Heraeus Biofuge Primo centrifuge. There were 2 layers observed, where the supernatant was

used for the non-parenchemal cells (NPCs) isolation and cell pellet contains hepatocytes.

2.12. Non-parenchemal cells isolation

2.12.1. Materials for Non-parenchemal cells isolation

Solutions

Phosphate buffer solution (PBS), Dulbecco A

1 tablet of PBS in 100ml of deionised water.

PBS with 0.3% Bovine Serum Albumin (BSA), Sigma-Aldrich

1 tablet of PBS in 100ml of deionised water; 0.3g BSA

10X PBS

10 tablet of PBS in 100ml of deionised water.

100% Percoll solution

Take 9 parts of Percoll add 1 part of 10X PBS

Histodenz 27.6% (w/v), Sigma-Aldrich, USA

27.6g dissolved in 100 ml of distilled water. Please cover the tube with aluminium foil, because Histodenz is light sensitive.

2.12.2. Method for non-parenchemal cells (NPC) isolation

1. The supernatant obtained from the liver perfusion (as described in section 2.10.3) containing NPCs was spun down at 300g for 10mins at 4°C.
2. Then the pellet was gently resuspended in 20ml PBS containing 0.3% BSA solution followed by 16ml of 27.6% (w/v) of Histodenz, which gave a final concentration of 13% (w/v) and centrifuged at 900g for 30 minutes at 4°C.
3. The supernatant was transferred into a new tube, and diluted up to a volume of 40ml in PBS with 0.3% BSA, and then shaken at 150 rpm for 30 minutes at 4°C. After that, the solution was centrifuged at 300g for 10 minutes at 4°C
4. Following centrifugation, the cell pellet was collected by gently resuspended in 6ml of PBS and with 6.6ml of 100% Percoll solution, made up 52% Percoll with NPCs.

5. 2ml of 52% Percoll with NPCs was pipetted in 50ml tubes followed by 4ml of 50% Percoll, 4ml of 35% Percoll and 1ml of PBS with 0.3% followed by centrifugation at 900Xg for 30 minutes at 4°C.
6. Three different cell bands were obtained with the one at the top of layer was enriched in hepatic stellate cells (HSCs) (Fraction 1), the one at the interface between the two Percoll gradient cushions mainly enriched in liver endothelial cells (LECs) (fraction 2) and one near the bottom of the centrifugation tube enriched in Kupffer cells (KCs) (fraction 3) (See Figure 2.2).
7. The HSCs was collected and washed with PBS at 1000rpm for 5 minutes and cell pellet was resuspended in RPMI-1640 media containing 10% heat-inactivated foetal calf serum (FCS), 4mmol L-glutamine, 100µg/ml Penicillin, 100µg/ml Streptomycin and transfer to humidified chamber at 37°C with 5% CO_2 in separate flask. Culture media was changed every 48 hour thereafter.

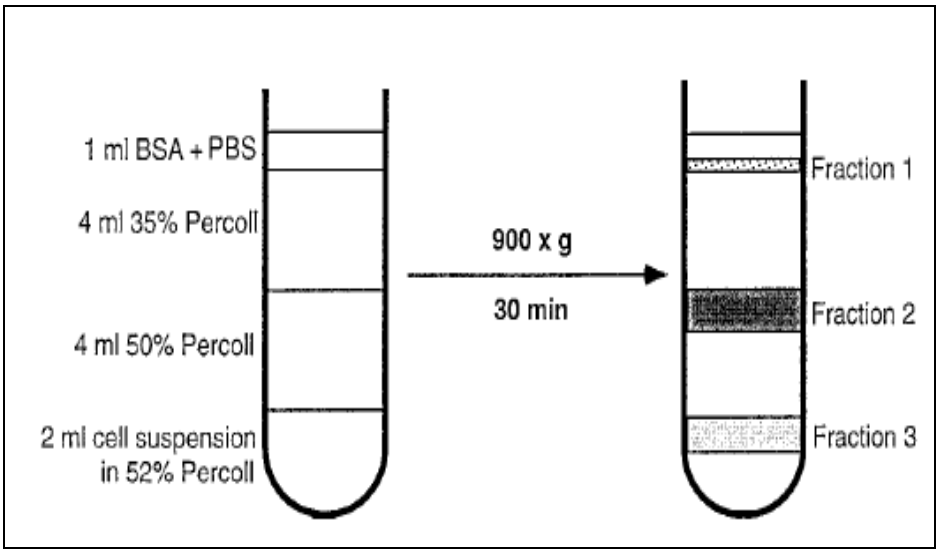

Figure 2.2: Schematic description of separated liver NPC band after Percoll centrifugation. Fraction 1 (hepatic stellate cells); Fraction 2 (liver endothelial cells); Fraction 3 (Kupffer cells).

2.13. Method for thin layer Matrigel (B&D Biosciences) coating

Matrigel was thawed overnight at 4°C. The pre-cooled pipette was used to mix the matrigel basement membrane matrix for homogeneity on ice. Dilute Matrigel basement membrane was diluted in 1:2 dilutions using the cold Roswell Park Memorial Institute (RPMI) serum free medium on ice. 400µl of diluted matrigel basement membrane matrix was added onto each well (12 well plates) on ice. Then, incubate at 40ºC for an hour with lid closed. Then, the unbound material was aspirated and followed by rinsed gently using the serum free media before the plate was used.

2.14. Collagen coating on cell culture plates

2.14.1. Materials for collagen coating on cell culture plates

100mg of collagen (Sigma, UK) was dissolved in 100ml 0.1M acetic acid, to give a final concentration of 1mg/ml. The collagen solution was filtered through a sterile Falcon 0.45µm cellulose acetate membrane filter into a sterile 100ml Duran bottle. This solution was stored for up to 3 months at 4°C until use or longer.

2.14.2. Method for collagen coating for 12-well plate

Calf skin collagen solution (1 mg/ml) was diluted 1:10 dilution with sterile water to obtain a working concentration of 100 µg/ml. The plastic dish was coated with 10 µg/cm^2 (use 1200 µl/well with 12.0 cm^2/well) and incubated overnight in a class II culture cabinet with lid being removed. The excess fluid was removed from the coated surface followed by one wash with cold sterile PBS (2 ml/well) and another wash with sterile water (again 2ml/well).

The plate was dried in tissue culture cabinet or non-humidified incubator at 37ºC), once dried; the plate was stored at room temperature or for longer term in a fridge.

2.15. Sub-culturing the human hepatic stellate cells (HSCs)

2.15.1. Materials for sub culturing the human hepatic stellate cells (HSCs)

1X Phosphate Buffered Saline (PBS), Dulbecco A

1 tablet of PBS in 100ml of deionised water and followed by autoclaved for sterilization

10X Trypsin EDTA solution (Sigma, UK)

Dilute 1:10 with sterile PBS, aliquot into universal containers and stored at -20°C.

2.15.2. Methods for sub culturing human hepatic stellate cells (HSCs)

When cells were confluent, the media was aspirated and replaced and rinsed with 1X PBS. 5ml of trypsin EDTA solution was added in 75cm2 size flask and incubated for 10 minutes 37°C in tissue culture non-humidified chamber. The trypsin solution was swirled around the flask to detach the cells from the flask. Then 15ml of RPMI medium was added and mixed. The cell mixture was pipetted out from the flask into a 50ml tube, followed by centrifugation at 1000rpm for 5 min. The supernatant was aspirated and the pellet was resuspended in fresh media. The cells were diluted and were plated accordingly depending on the required number of cells needed to perform the experiment.

2.16. MTT assay

MTT assay is a colorimetric assay for measuring the mitochondrial reductase activity in proliferating cells. It measures the cleavage of yellow tetrazolium salt MTT to purple formazan crystals by metabolic active cells.

2.16.1. Materials MTT assay (11465007001) Roche, Germany

Solutions

MTT labelling reagent

5ml MTT (3-[4, 5-dimethylthiazol-2-yl]-2, 5-dipheyltetrazolium bromide) with 5mg/ml concentration. Keep it away from light.

Solubilization solution (1X, ready to use)

10% SDS in 0.01M HCl. Keep it away from light

2.16.2. Method for MTT cell proliferation assay

The MTT assay was performed as described by the manufacturer. The wavelength of the measure absorbance of the formazan product is read 550nm (test fliter) with reference absorbance set as 650nm (reference filter) using Dynex Technologies MRX II.

2.17. Statistical Analysis

Data are presented as mean ± SEM. Descriptive, Levene test, One-way ANOVA and Bonferroni post hoc test were used to analyze all the data. A p value < 0.05 was considered as statistically significant.

CHAPTER 3

Immunohistochemistry & Protein Expression in human liver: Assessment of the effects of Pioglitazone therapy in NASH patients.

3.1. Introduction

Pioglitazone (PGZ) is PPAR γ agonist that mainly acts on adipose tissue by promoting adipocyte differentiation and proliferation and decreasing lipolysis (Miyazaki et al., 2002). In type 2 diabetic patients treated with Pioglitazone, glucose uptake, fatty acid oxidation and improved insulin sensitivity in skeletal muscle are all observed (Coletta et al., 2009). Meanwhile in the liver of type 2 diabetic patients, hepatic fat content and endogenous glucose production (gluconeogenesis) are reduced and hepatic insulin sensitivity is increased with PGZ treatment (Ravikumar et al., 2008; Bajaj et al., 2003). Thus the effects of pioglitazone upon liver fat content and insulin resistance may reflect the effects of whole body glucose and fat metabolism.

Aithal et al. (2008) described that non-diabetic NASH patients treated with Pioglitazone had reduced hepatocellular injury and fibrosis compared to placebo treated patients whereas there was no significant change in liver fat content between these two groups. This suggests that pioglitazone therapy may target other processes in addition to lipid metabolism which are of relevance in NASH. In human liver PPAR γ is primarily expressed in the non parenchemal cell fraction – in particular stellate cells. It has been reported that treatment of stellate cells with PPAR γ agonists inhibits stellate cell activation and progression to the activated myofibroblastic phenotype. The possibility that Pioglitazone exerts its effects directly upon hepatic stellate cells in terms of regulation of cellular activation, proliferation and gene expression was therefore investigated by immunohistochemistry of hepatocyte and hepatic stellate cell (HSC) markers involved injury, apoptosis and proliferation (as shown in Table 3.1) were studied in human tissue sections. Single immunohistochemistry method was used followed by counter staining with Mayer‘s or Harris’s Haematoxylin as described in Chapter 2 (Materials and Methods). This analysis was then complemented by mRNA and protein analysis of core liver biopsy samples taken from the same group of patients.

Table 3.1: List of antibodies used in this study.

Antibody	Function	Cell type stained
α SMA	actin family of proteins and a marker of activated HSCs (Safadi et al.,2002)	Vascular portal area (arterioles and veins) in normal liver, activated HSCs (Van Rossen et al., 2009)
CRBP1	mediates retinol esterification to retinyl esters and retinol oxidation to retinal and retinoic acid (Blomhoff et al., 1991)	both quiescent and activated HSCs, very low levels in hepatocytes, billiary epithelial cells (Van Rossen et al., 2009)
Desmin	Muscle-specific class III intermediate filament and quiescent marker of HSCs (Van Rossen et al., 2009)	quiescent HSCs in rats (Geerts et al., 2001) and vascular smooth muscle cells in arterioles in humans (Van Rossen et al., 2009)
GFAP	Involved in vascular remodelling in hepatic damaged tissue where there is an increase in neovascularisation during liver fibrosis (Corpechot et al., 2002)	quiescent HSCs located in the lobule near portal tracts in normal liver, early stage of HSCs activation throughout the lobule (Carotti et al., 2008)
PPAR γ	Marker of quiescent HSC, controls adipogenic gene expressions (She et al., 2005)	Not clearly shown in the both human and animal liver
PPAR β	Regulates pro-proliferation and involved in activation of HSCs (Hellemans et al., 2003)	hepatocytes and HSCs
PPAR α	Regulates mitochondrial & peroxisomal fatty acid β-oxidation (Van Raalte et al., 2004)	hepatocytes
Caspase 3	plays a key role in the execution of apoptotic cell both by extrinsic (death ligand) and intrinsic (mitochondrial) pathways (Feldstein et al., 2005)	apoptotic hepatocytes (Feldstein et al., 2003)
TUNEL	labelling DNA fragments utilizing terminal deoxynucleotidyl transferase (TdT) for detection of apoptotic cells (www.chemicon.com)	Apoptotic cells
M30	Determine early epithelial cell apoptosis by recognizing specific caspase cleavage sites (Caulin et al., 1997)	apoptotic hepatocytes (Feldstein et al., 2009)
Ki67	Promotes cell proliferation associated with ribosomal RNA transcription. Inhibition of Ki-67 leads to inhibition of ribosomal RNA synthesis. (Bullwinkel et al., 2006)	Only expressed in mitotic cells

RESULTS

3.2. HSCs marker single immunohistochemistry

Cellular retinol binding protein 1 (CRBP1) is a carrier protein involved in retinol transportation and it is expressed in both quiescent and activated stellate cells but the expression was lesser in other hepatic cell types (Van Rossen et al., 2009). In liver injury, quiescent stellate cells are transformed into myofibroblast-like cells that express α smooth muscle actin (αSMA) which is a marker of activated stellate cell phenotype (Safadi et al., 2002). Immunohistochemistry was performed on human NASH liver formalin-fixed, paraffin-embedded (FFPE) samples to confirm both CRBP1 and αSMA expression as shown in Figure 3.1 below.

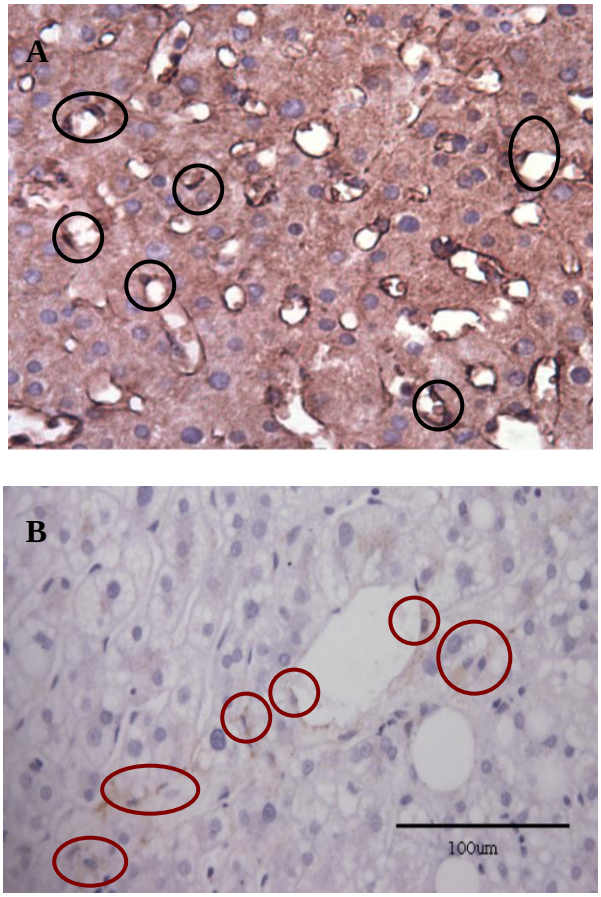

Figure 3.1: CRBP1 and αSMA immunohistochemistry staining in NASH patients. FFPE sections from human liver biopsies taken from NASH patients were deparaffinised and subjected to immunohistochemistry as described in section 3.2. CRBP1 (A) was used as a marker of total stellate cells number and αSMA (B) was used as a marker of activated stellate cells (myofibroblast). Photographs are representative of 7 sections each taken from 7 patients. Black circles show stellate cells positively staining with CRBP1 and red circles show positive staining of activated stellate cells with αSMA.

3.2.1. αSMA & CRBP1 double immunostaining

In an attempt to identify the total stellate cell number and the proportion of activated stellate cells in this population, double immunoflourescence was carried out using anti-CRBP1 and anti-αSMA antibodies.

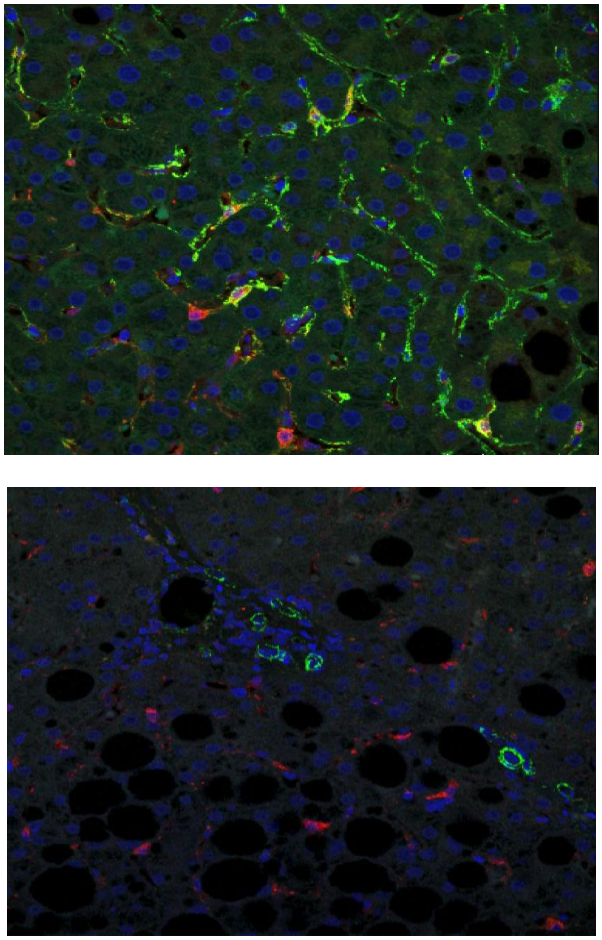

Figure 3.2: CRBP1 and αSMA double immunoflourescence staining in NASH patients. FFPE sections from human liver biopsies taken from NASH patients were deparaffinised and subjected to double immunoflourescence as described in section 3.2.1. CRBP1 was used as a marker of total stellate cells number and αSMA was used as a marker of activated stellate cells (myofibroblast). Photographs are representative of 7 sections each taken from 7 patients. Green staining shows activated stellate cells positively staining with αSMA; red staining shows stellate cells positively staining with CRBP1; yellow staining show the co-localisation of αSMA & CRBP1 staining; blue staining shows DAPI staining of nuclei.

Double immunoflourescence of CRBP1 and αSMA showed evidence of co-localization; this further indicated that CRBP1 is a marker for total stellate cell number rather than quiescent cells as has been previously suggested. There is a problem with double immunoflourescence staining in that whilst the expression is clear, it is hard to count the cell numbers making stereology counting unreliable.

3.2.2. αSMA & CRBP1 double immunohistochemistry

Double immunohistochemistry was performed in order to achieve objectives as mentioned previously.

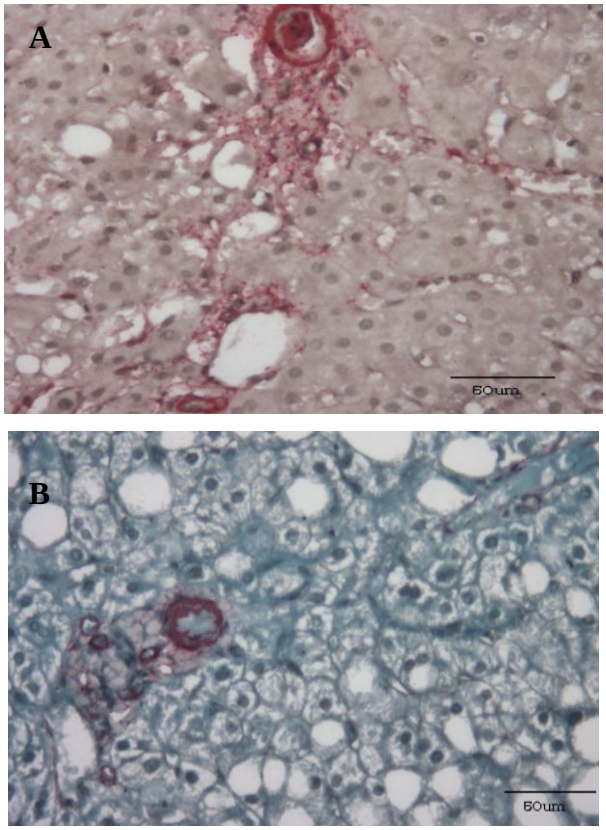

Figure 3.3: CRBP1 and αSMA double immunohistochemistry staining in NASH patients. FFPE sections from human liver biopsies taken from NASH patients were deparaffinised and subjected to double immunohistochemistry without methylgreen counterstaining (A) and with methlygreen counterstaining (B) as described in section 3.2.2. CRBP1 was used as a marker of total stellate cells number and αSMA was used as a marker of activated stellate cell). Photographs are representative of 7 sections each taken from 7 patients. Red staining shows activated stellate cells positively staining with αSMA. Black staining shows stellate cells positively staining with CRBP1.

Double immunohistochemistry leads to false positive staining, where the initial staining (anti-CRBP1) need to be over stained to prevent a loss of signal following application of the second antibody (anti-αSMA). Counter-staining with methlygreen as described in the method for dual immunohistochemistry kit, reduced the ability to verify positively stained cells. Since, double immunostaining is unsuitable to achieve the determination of HSC number; single immunohistochemistry staining was identified as the preferred method for stereology counting. All the immunostaining was independently verified by a consultant histopathologist (Dr Philip V. Kaye).

3.2.3. α-smooth muscle actin (α-SMA) immunohistochemistry

3.2.3.1. α-SMA immunohistochemistry in normal liver, NAFLD & NASH patients

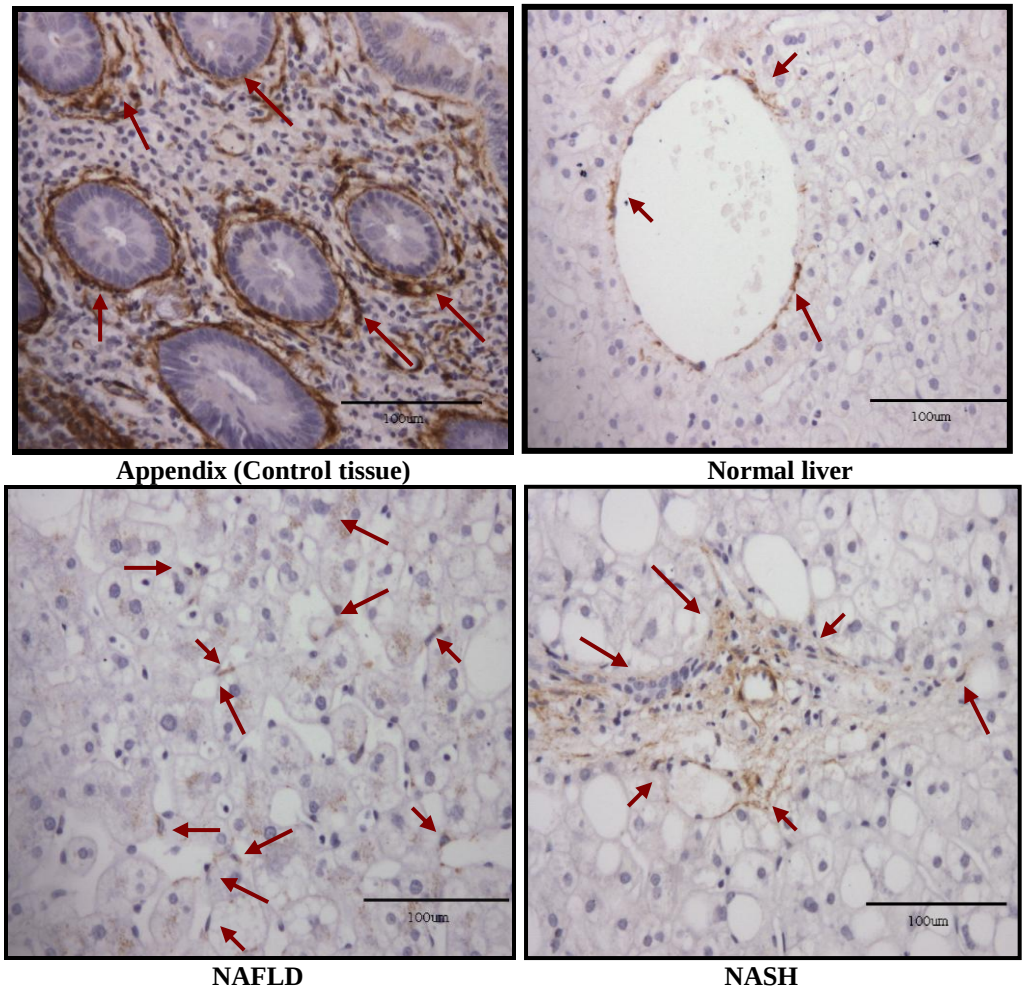

Appendix (Control tissue) **Normal liver**

NAFLD **NASH**

Figure 3.4.1: αSMA immunohistochemistry staining in human liver. FFPE sections from human liver biopsies taken from normal liver, NAFLD and NASH patients were deparaffinised and subjected to single immunohistochemistry as described in section 3.2.3. αSMA was used as a marker of activated stellate cells. Photographs are representative of 34 sections each taken from 34 patients. Brown staining shows activated stellate cells; vascular smooth muscle also positively stained with αSMA around the sinusoidal edge.

αSMA staining was evident around blood vessels in normal liver. Meanwhile in NAFLD and NASH; there was a clear increase in αSMA staining in stellate cells.

Stereology counting was performed on αSMA stained sections as shown in Table 3.2.1 below:

Table 3.2.1: Stereology counting of αSMA positive hepatic stellate cells in normal liver, NAFLD and NASH patients. Data is presented as % of cell/ % total cell volume.

Groups/ Markers	**Normal liver (n = 7)**	**NAFLD (n = 7)**	**NASH (n = 20)**	**P value**
α-SMA	**22.60 ± 1.71[a,b]**	**41.57 ± 3.10[a]**	**43.73 ± 2.71[b]**	**0.004[a]; 0.000[b]**

(a: Normal liver Vs NAFLD; b: Normal liver Vs NASH; c: NAFLD Vs NASH) (n = number of patients) Stereology counting was performed as described in method section 2.10. Data are presented as mean ± S.E.M.

αSMA the most reliable marker of activated stellate cell number showed a significant increase in both steatosis and NASH patients as compared to normal liver.

3.2.3.2. α-SMA immunohistochemistry in Pioglitazone & Placebo treated NASH patients

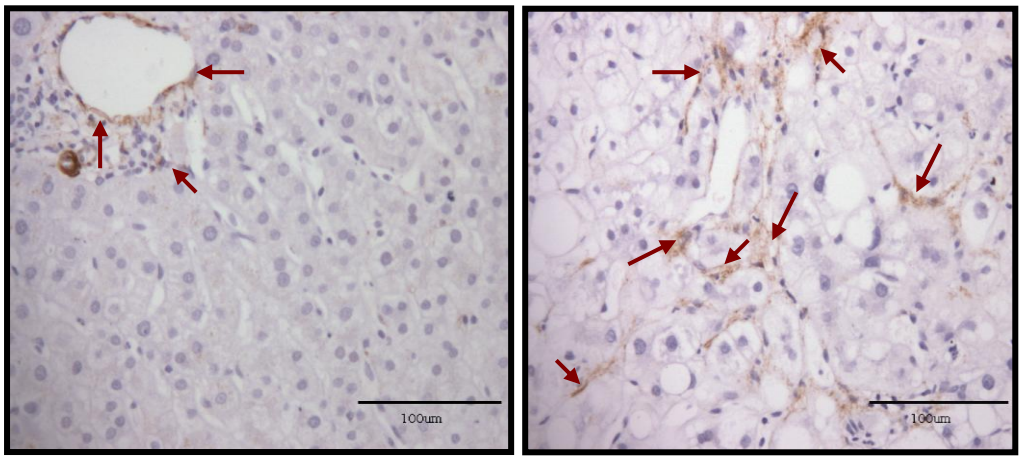

Pioglitazone **Placebo**

Figure 3.4.2: αSMA immunohistochemistry staining in human NASH treated liver. FFPE sections from human liver biopsies taken from Piogliltazone and placebo treated NASH patients were deparaffinised and subjected to single immunohistochemistry as described in section 3.2.3. αSMA was used as a marker of activated stellate cells. Photographs are representative of 21 sections each taken from 21 patients. Brown staining shows activated stellate cells; vascular smooth muscle also positively stained with αSMA around the sinusoidal edge.

αSMA staining was evident around blood vessels in PGZ treated liver. Meanwhile in placebo treated NASH patients; there was a clear increase in αSMA staining in stellate cells. Stereology counting was performed on αSMA stained sections as shown in Table 3.2.2 below:

Table 3.2.2: Stereology counting of αSMA positive hepatic stellate cells in NASH/Pre-trial, Pioglitazone and Placebo treated NASH patients. Data is presented as % of cell/ % total cell volume.

Groups/ Markers	NASH/ Pre-trial (n = 20)	Pioglitazone (n =9)	Placebo (n = 12)	P value
α-SMA	**43.73 ± 2.71[a]**	**35.57 ± 2.36[a,c]**	**44.97 ± 1.44[c]**	**0.034[a]; 0.006[c]**

(a: NASH/Pretrial Vs Pioglitazone; b: NASH/Pretrial Vs Placebo; c: Pioglitazone Vs Placebo) (n= number of patients) Stereology counting was performed as described in method section 2.10. Data are presented as mean ± S.E.M.

In the samples taken from the study, Pioglitazone treated patients showed a significant reduction in αSMA positive stellate cells as compared to pre-trial and placebo groups.

3.2.4. CRBP1 immunohistochemistry

3.2.4.1. CRBP1 immunohistochemistry in normal liver, NAFLD & NASH patients

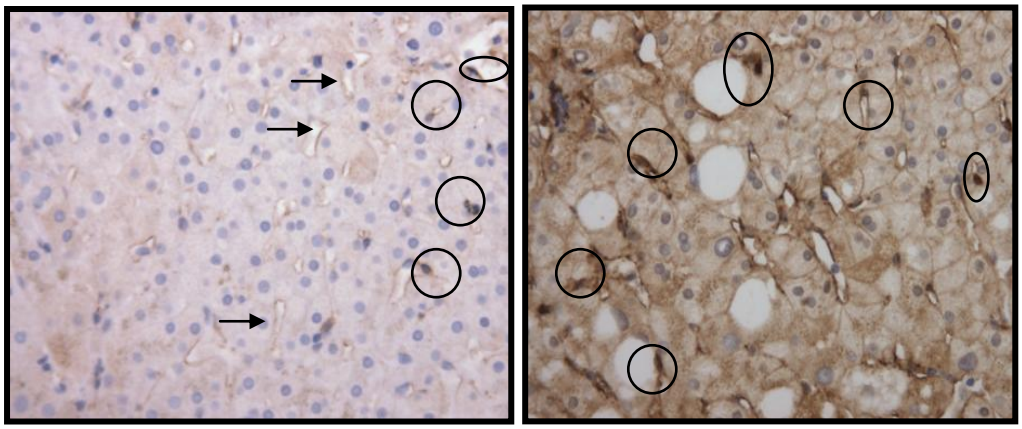

Normal liver **NAFLD**

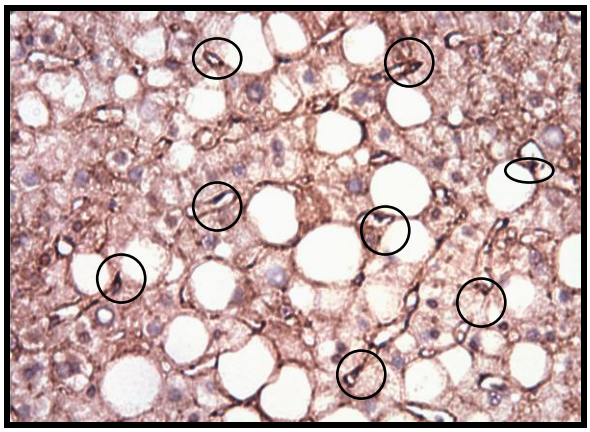

NASH

Figure 3.5.1: CRBP1 immunohistochemistry in human liver. FFPE sections from human liver biopsies taken from normal liver, NAFLD and NASH patients were deparaffinised and subjected to single immunohistochemistry as described in section 3.2.4. CRBP1 was used as a marker of total stellate cell number. Photographs are representative of 34 sections each taken from 34 patients. Black circles show stellate cells positively staining with CRBP1. Black arrows show sinusoidal areas positively staining with CRBP1.

In normal liver, CRBP1 stained stellate cells and around the sinusoidal lining. CRBP1 staining was similar in terms of indicating total cell number in the sample groups. Stereology counting was performed on CRBP1 stained sections as shown in Table 3.3.1 below:

Table 3.3.1: Stereology counting of CRBP1 positive hepatic stellate cells in normal liver, NAFLD and NASH patients. Data is presented as % of cell/ % total cell volume.

Groups/ Markers	Normal liver (n = 7)	NAFLD (n = 7)	NASH (n = 20)	P value
CRBP1	45.70 ± 3.21	48.74 ± 2.63	52.17 ± 1.95	NS

(a: Normal liver Vs NAFLD; b: Normal liver Vs NASH; c: NAFLD Vs NASH) (n = number of patients) Stereology counting was performed as described in method section 2.10. Data are presented as mean ± S.E.M.

3.2.4.2. CRBP1 immunohistochemistry in Pioglitazone & Placebo treated NASH patients

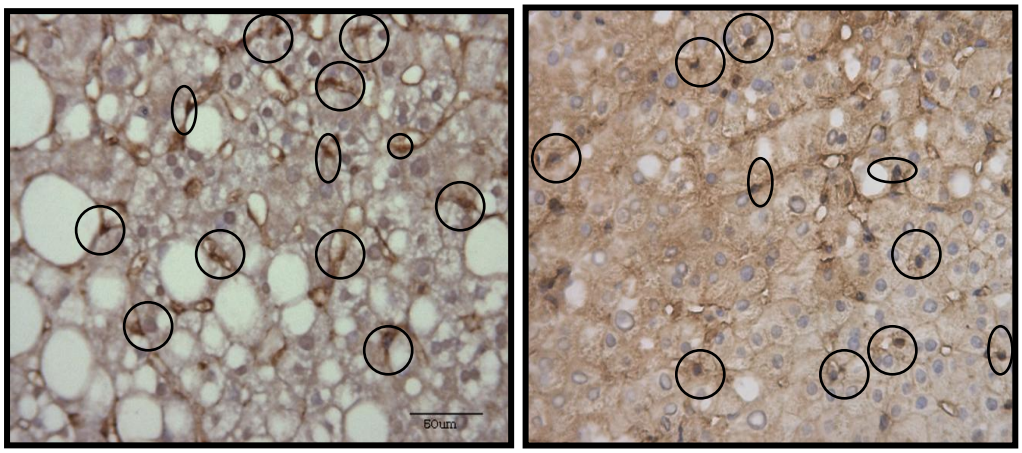

Pioglitazone **Placebo**

Figure 3.5.2: CRBP1 immunohistochemistry in human NASH treated liver. FFPE sections from human liver biopsies taken from Pioglitazone and placebo treated patients were deparaffinised and subjected to single immunohistochemistry as described in section 3.2.4. CRBP1 was used as a marker of total stellate cell number. Photographs are representative of 21 sections each taken from 21 patients. Black circles show stellate cells positively staining with CRBP1. Black arrows show sinusoidal areas positively staining with CRBP1.

Stereology counting was performed on CRBP1 stained sections as shown in Table 3.3.2 below:

Table 3.3.2: Stereology counting of CRBP1 positive hepatic stellate cells in NASH/Pre-trial, Pioglitazone and Placebo treated NASH patients. Data is presented as % of cell/ % total cell volume.

Groups/ Markers	NASH/ Pre-trial (n = 20)	Pioglitazone (n =9)	Placebo (n = 12)	P value
CRBP1	52.17 ± 1.95	46.78 ± 2.51[c]	53.75 ± 2.93[c]	0.075[c]

(a: NASH/Pretrial Vs Pioglitazone; b: NASH/Pretrial Vs Placebo; c: Pioglitazone Vs Placebo) (n= number of patients) Stereology counting was performed as described in method section 2.10. Data are presented as mean ± S.E.M.

In the samples taken from the study, Pioglitazone treated patients showed a reduction in CRBP1 positive stellate cells as compared to placebo group with a trend.

3.3. Quiescent stellate cells markers

The data presented thus far indicate that CRBP1 is a marker for stellate cells regardless of activation state. It was considered desirable to attempt to quantify quiescent stellate cell number in order to compare with the activated and total cell numbers. There are several other markers of stellate cells that have been described. Desmin (Geerts et al., 2001) and GFAP (Gard & Dutton, 1985) have been described as marker of quiescent stellate cells in animal models. Nuclear receptor (PPARγ) plays a role in maintaining the quiescent phenotype of stellate cells and expression of PPARγ has been reported to decrease markedly upon stellate cell activation. (She et al., 2005), and Pioglitazone is an agonist of PPARγ (Yki-Jarvinen, 2004). Therefore antibodies to Desmin, GFAP and PPARγ were used in attempt to identify quiescent, adipogenic stellate cells.

3.3.1. Desmin immunohistochemistry

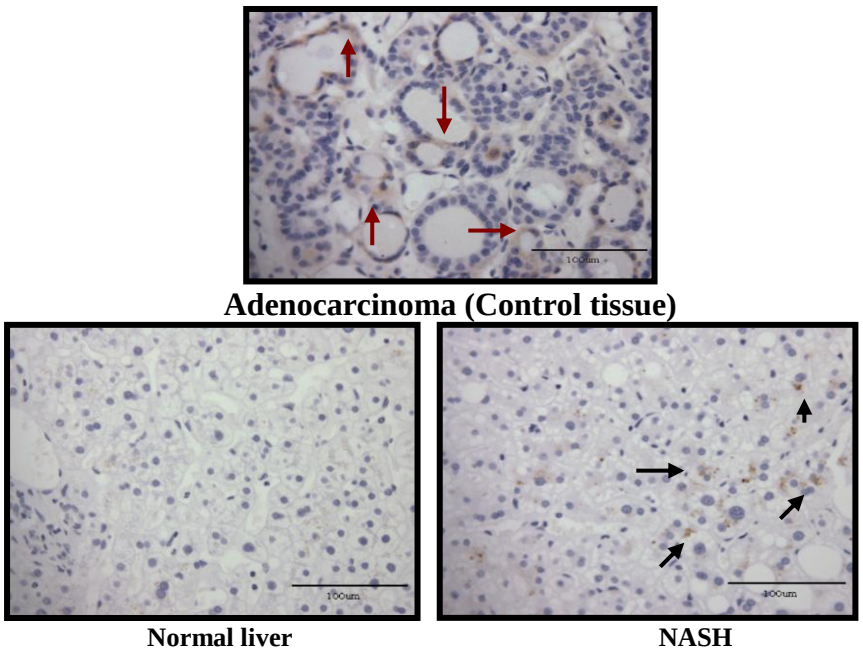

Figure 3.6: Desmin immunohistochemistry in human liver. FFPE sections from human liver biopsies taken from normal liver and NASH patients were deparaffinised and subjected to single immunohistochemistry as described in section 3.3.1. Desmin was assessed as a marker of quiescent stellate cells. Photographs are representative of 55 sections each taken from 55 patients. Red arrows show cells positively desmin stained on the control tissue. Black arrows show non-specific lipofuscan, which is a yellow-brown pigment granule.

No evidence of Desmin staining suggested that human hepatic stellate cells may differ in their expression of quiescent markers as compared to rodents.

3.3.2. GFAP immunohistochemistry (Z0334, DAKO)

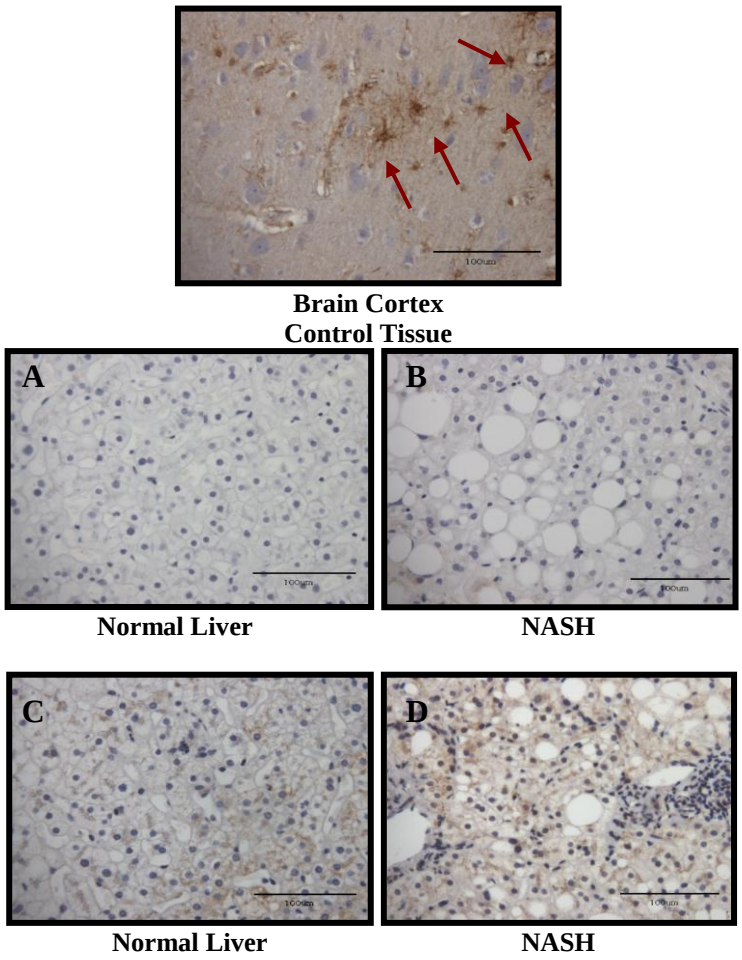

Figure 3.7: GFAP immunohistochemistry in human liver using antibody from DAKO. FFPE sections from human liver biopsies taken from normal liver and NASH patients were deparaffinised and subjected to single immunohistochemistry as described in section 3.3.2. GFAP has been described as an early marker of stellate cell activation. Photographs are representative of 55 sections each taken from 55 patients. Red arrows show astrocytes positively stained with GFAP. No expression was observed in study samples with GFAP (1:4000) antibody dilution as shown in normal liver (A) and NASH (B) patients. The staining was repeated with this antibody using a 1:100 dilution as shown in normal liver (C) and NASH (D) patients.

GFAP expression is not detected in human liver when immunostained using Z0334 from DAKO using neither a 1:4000 nor 1:100 dilution. Carotti et al. (2008) reported that GFAP was expressed in human hepatitis C patients, particularly staining the hepatic stellate cells. Therefore, the GFAP immunostaining was repeated again in this study using an alternative antibody as described.

3.3.3. GFAP immunohistochemistry (GA-5, Thermo Scientific)

3.3.3.1. GFAP immunohistochemistry in normal liver, NAFLD & NASH patients

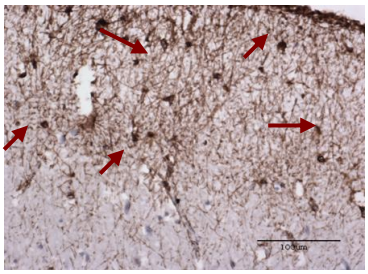

Brain Cortex (Control tissue)

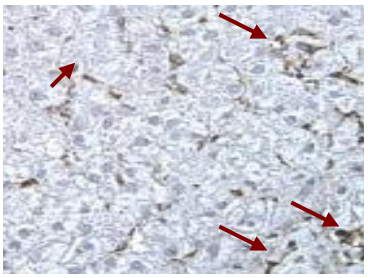

Acute hepatitis C patient (Carotti et al (2008)

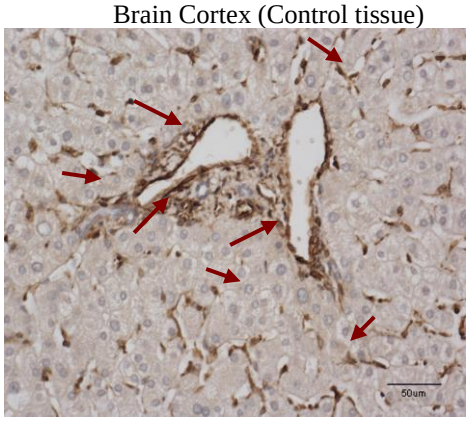

Normal liver

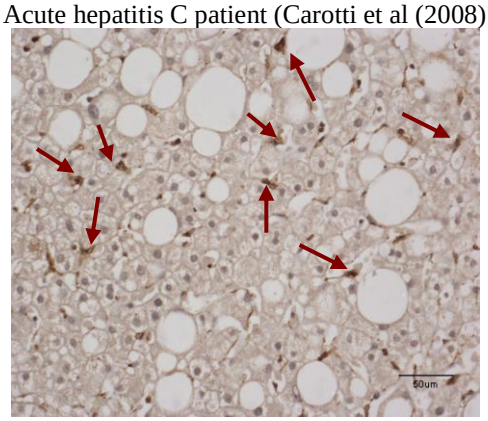

NAFLD

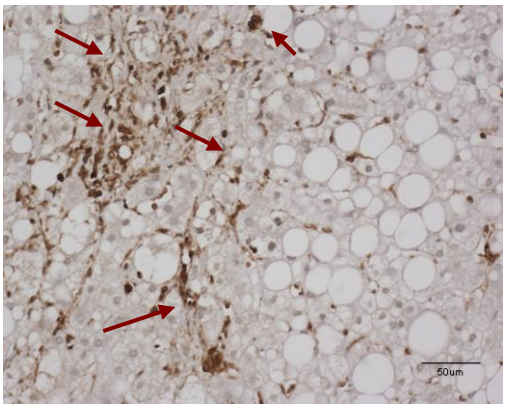

NASH

Figure 3.8.1: GFAP immunohistochemistry in human liver using antibody from Thermo Scientific. FFPE sections from human liver biopsies taken from control tissue, normal liver, NAFLD and NASH were deparaffinised and subjected to single immunohistochemistry as described in section 3.3.3. Photographs are representative of 34 sections each taken from 34 patients. Red arrows show both astrocytes and stellate cells positively stained with GFAP.

The GFAP antibody stained HSCs and vascular smooth muscle tissue throughout the study group.

Stereology counting was performed for stellate cells that are positively stained with GFAP as shown in Table 3.4.1 below:

Table 3.4.1: Stereology counting of GFAP positive hepatic stellate cells in normal liver, NAFLD and NASH patients. Data is presented as % of cell/ % total cell volume.

Groups/ Markers	Normal liver (n = 7)	NAFLD (n = 7)	NASH (n = 20)	P value
GFAP	**46.06 ± 2.82[b]**	**43.58 ± 2.47[c]**	**53.91 ± 1.02[b,c]**	**0.003[b]; 0.000[c]**

(a: Normal liver Vs NAFLD; b: Normal liver Vs NASH; c: NAFLD Vs NASH) (n = number of patients) Stereology counting was performed as described in methods section 2.10. Data are presented as mean ± S.E.M.

GFAP expression in stellate cells was increased significantly in NASH patients as compared to normal liver and steatosis.

3.3.3.2. GFAP immunohistochemistry in Pioglitazone & Placebo treated NASH patients

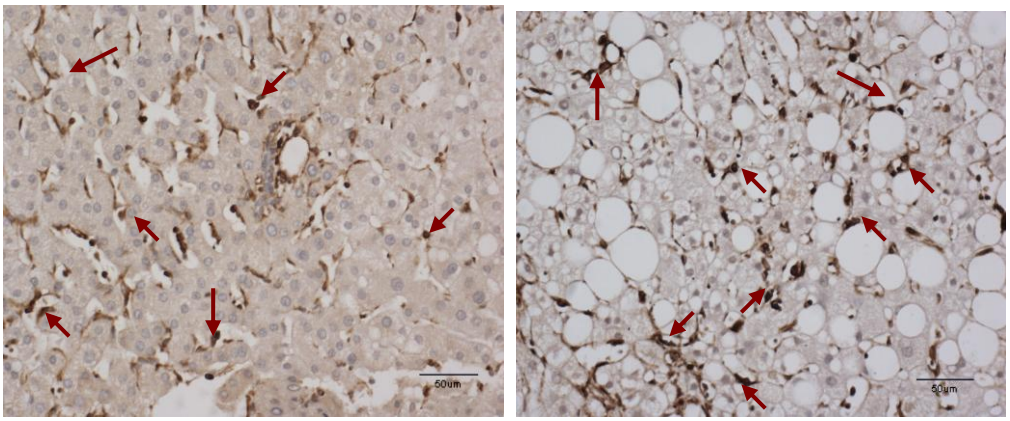

Pioglitazone Placebo

Figure 3.8.2: GFAP immunohistochemistry in human NASH treated liver using antibody from Thermo Scientific. FFPE sections from human liver biopsies taken from Pioglitazone and placebo treated NASH patients were deparaffinised and subjected to single immunohistochemistry as described in section 3.3.3. Photographs are representative of 21 sections each taken from 21 patients. Red arrows show both astrocytes and stellate cells positively stained with GFAP.

The GFAP antibody stained HSCs and vascular smooth muscle tissue. Stereology counting was performed for stellate cells that are positively stained with GFAP as shown in Table 3.4.2 below:

Table 3.4.2: Stereology counting of GFAP positive hepatic stellate cells in NASH/Pre-trial, Pioglitazone and Placebo treated patients. Data is presented as % of cell/ % total cell volume.

Groups/ Markers	NASH (n = 20)	Pioglitazone (n =9)	Placebo (n = 12)	P value
GFAP	53.91 ± 1.02	50.42 ± 3.18	53.14 ± 2.11	NS

(a: NASH/Pretrial Vs Pioglitazone; b: NASH/Pretrial Vs Placebo; c: Pioglitazone Vs Placebo) (n = number of patients) Stereology counting was performed as described in methods section 2.10. Data are presented as mean ± S.E.M.

GFAP expression did not show any significant difference throughout the study groups as shown above.

3.3.4. PPAR γ immunohistochemistry

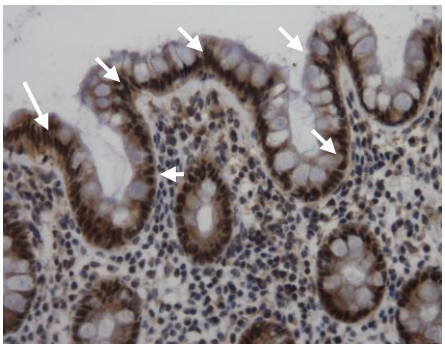

Colon tissue (Control tissue)

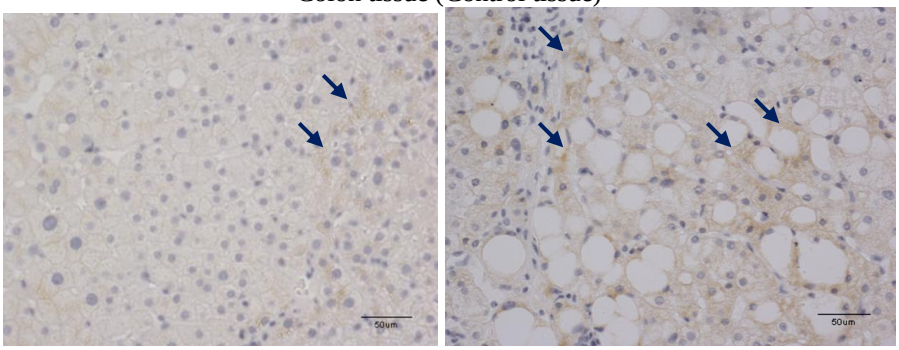

Normal liver NASH

Figure 3.9: PPAR γ immunohistochemistry in human liver. FFPE sections from human liver biopsies taken from normal liver, NASH patients and control tissue were deparaffinised and subjected to single immunohistochemistry as described in section 3.3.4. PPAR γ is a marker of quiescent stellate cells. Photographs are representative of 7 sections each taken from 7 patients. White arrows show colonic epithelial cells positively stained with PPAR γ, Blue arrows show back ground staining and lipofuscan in human normal liver and NASH patients.

No evidence of PPAR γ expression was observed in human liver, which was surprising given the clear positive staining seen in the control colonic epithelial tissue. Hepatic stellate cells are known to express PPAR γ (She et al., 2005), thus it is unclear why this antibody stained the colonic epithelial cells but not the stellate cells. There is very little immunohistochemistry data for PPAR γ in the literature with very few of the commercially available antibodies having been shown to be compatible with immunohistochemistry as distinct from western blotting (Wang & Cheng, 2008). PPAR γ protein expression in stellate cells was not determined in this study group.

3.4.Nuclear receptors

PPAR β was reported to be involved in stellate cell proliferation and activation (Hellemans et al., 2003). When the stellate cells become activated, PPAR γ expression is diminished followed by an increase in PPAR β expression (She et al., 2005; Hellemans et al., 2003). PPARβ is also highly expressed in hepatocytes. PPAR α modulates the activities of mitochondrial and peroxisomal β-oxidation as well as microsomal ω-oxidation, and thus plays a key role in energy expenditure in hepatocytes but is not described as being expressed in stellate cells (Pyper et al., 2010).

3.4.1. PPAR β immunohistochemistry

3.4.1.1. PPAR β immunohistochemistry in normal liver, NAFLD & NASH patients

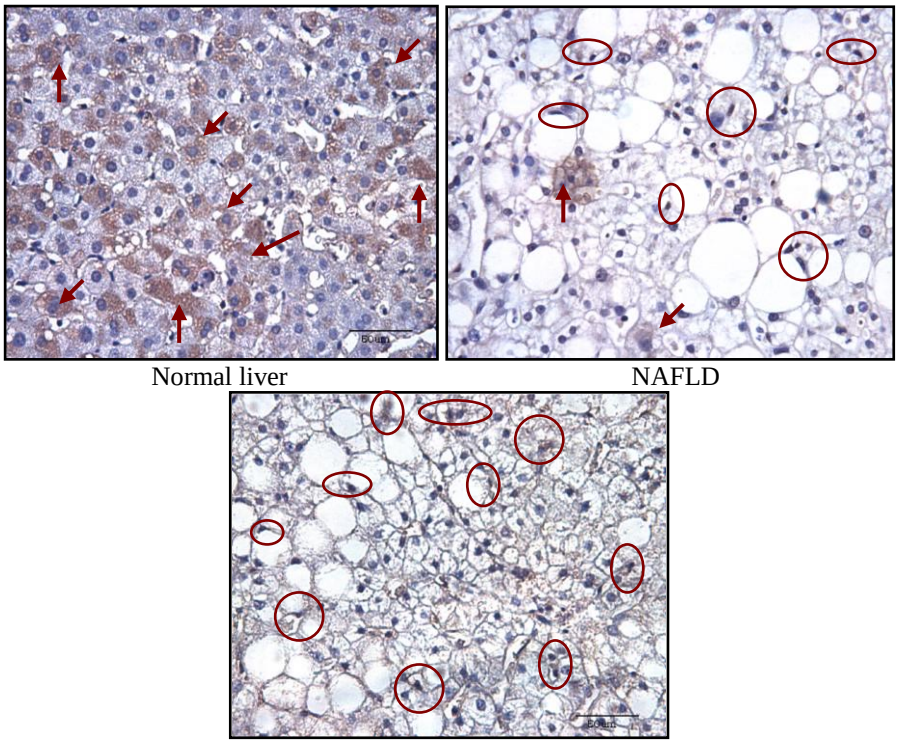

Figure 3.10.1: PPARβ immunohistochemistry in human liver. FFPE sections from human liver biopsies taken from normal liver, NAFLD and NASH patients were deparaffinised and subjected to single immunohistochemistry as described in section 3.4. PPAR β is a marker of stellate cells activation and proliferation. Photographs are representative of 34 sections each taken from 34 patients. Red arrows show hepatocytes and red circles show HSCs positively stained with PPAR β.

In normal liver, PPAR β expression was seen in hepatocytes and stellate cells, meanwhile in steatosis and NASH expression in hepatic stellate cells was clearly more evident.

Stereology counting was performed on PPAR β stained cells as shown in Table 3.5.1 below:

Table 3.5.1: Stereology counting of hepatic stellate cells and hepatocytes positively stained with PPAR β in normal liver, NAFLD and NASH patients. Data is presented as % of cell/ % total cell volume.

Groups/ Markers	**Normal liver (n = 7)**	**NAFLD (n = 7)**	**NASH (n = 20)**	**P value**
PPAR β Hepatocytes	18.01 ± 2.22	13.08 ± 1.41	15.77 ± 1.44	NS
PPAR β HSCs	**15.46 ± 3.14[b]**	**28.18 ± 1.26[c]**	**15.40 ± 1.65[b,c]**	**0.003[b]; 0.000[c]**

(a: Normal liver Vs NAFLD; b: Normal liver Vs NASH; c: NAFLD Vs NASH) (n = number of patients) Stereology counting was performed as described in methods section 2.10. Data are presented as mean ± S.E.M.

PPAR β expression was elevated in the stellate cells of the steatosis group as compared to others.

3.4.1.2. PPAR β immunohistochemistry in Pioglitazone & Placebo treated NASH patients

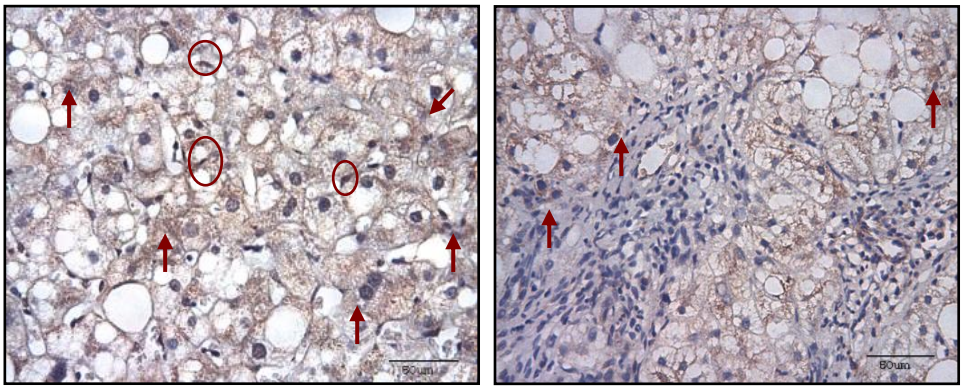

Pioglitazone Placebo

Figure 3.10.2: PPAR β immunohistochemistry in human NASH treated liver. FFPE sections from human liver biopsies taken from Pioglitazone and placebo treated NASH patients were deparaffinised and subjected to single immunohistochemistry as described in section 3.4. PPAR β is a marker of stellate cells activation and proliferation. Photographs are representative of 21 sections each taken from 21 patients. Red arrows show hepatocytes and red circles show HSCs positively stained with PPAR β.

Stereology counting was performed on both PPAR β stained cells as shown in Table 3.5.2 below:

Table 3.5.2: Stereology counting of hepatic stellate cells and hepatocytes positively stained with PPAR β in NASH/Pre-trial, Pioglitazone and Placebo treated NASH patients. Data is presented as % of cell/ % total cell volume.

Groups/ Markers	NASH (n = 20)	Pioglitazone (n =9)	Placebo (n = 12)	P value
PPAR β Hepatocytes	**15.77 ± 1.44[b]**	**15.90 ± 2.06[c]**	**8.94 ± 0.96[b,c]**	**0.001[b] ; 0.010[c]**
PPAR β HSCs	15.40 ± 1.65	11.81 ± 1.46[c]	15.54 ± 2.62[c]	0.075[c]

(a: NASH/Pretrial Vs Pioglitazone; b: NASH/Pretrial Vs Placebo; c: Pioglitazone Vs Placebo) (n = number of patients) Stereology counting was performed as described in methods section 2.10. Data are presented as mean ± S.E.M.

PPAR β hepatocytes expression was decreased significantly in placebo treated group compared to Pre-trial and Pioglitazone group. Pioglitazone treated patients showed a reduction in PPAR β HSCs expression with a trend compared to placebo treated group.

3.4.2. PPAR α immunohistochemistry

Potential effects of Pioglitazone acting via PPAR α, where it has been described as being a weak agonist of PPAR α (Sakamoto et al., 2000) make this an important target to study.

3.4.2.1. PPAR α immunohistochemistry in normal liver, NAFLD & NASH patients

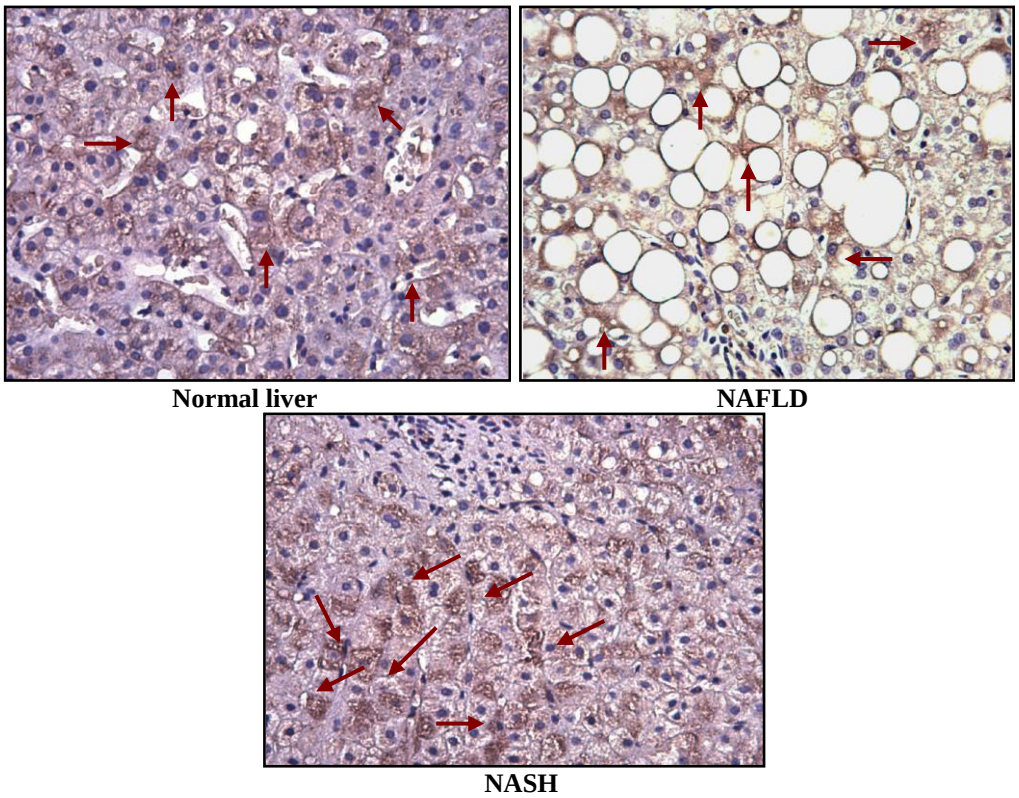

Figure 3.11.1: PPARα immunohistochemistry in human liver. FFPE sections from human liver biopsies taken from normal liver, NAFLD and NASH patients were deparaffinised and subjected to single immunohistochemistry as described in section 3.4.2. Photographs are representative of 34 sections each taken from 34 patients. Red arrows show hepatocytes positively stained with PPAR α.

PPAR α expression was only found in hepatocytes as expected.

Stereology counting was performed on PPAR α stained cells as shown in Table 3.6.1 below:

Table 3.6.1: Stereology counting of hepatocytes positively stained with PPAR α in normal liver, NAFLD and NASH patients. Data is presented as % of cell/ % total cell volume.

Groups/ Markers	Normal liver (n = 7)	NAFLD (n = 7)	NASH (n = 20)	P value
PPAR α Hepatocytes	18.86 ± 2.22	17.11 ± 2.01	21.17 ± 2.07	NS

(a: Normal liver Vs NAFLD; b: Normal liver Vs NASH; c: NAFLD Vs NASH) (n = number of patients) Stereology counting was performed as described in methods section 2.10. Data are presented as mean ± S.E.M.

No significant difference was observed in PPAR α expression throughout the study group.

3.4.2.2. PPAR α immunohistochemistry in Pioglitazone & Placebo treated NASH patients

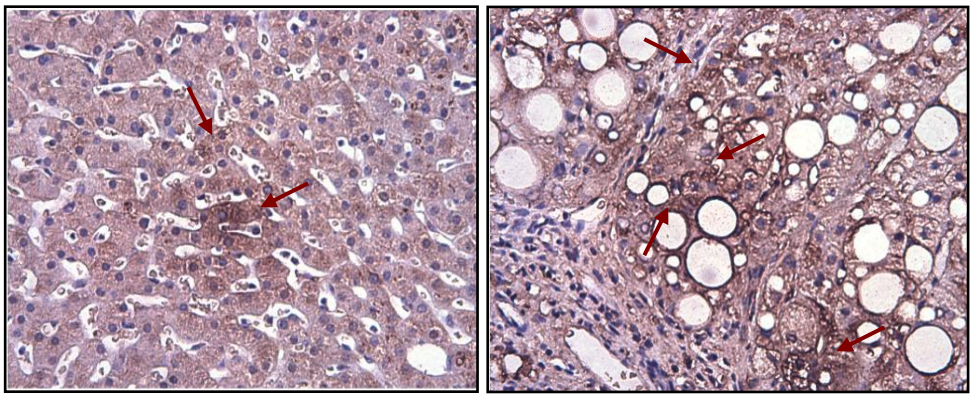

Pioglitazone **Placebo**

Figure 3.11.2: PPAR α immunohistochemistry in human NASH treated liver. FFPE sections from human liver biopsies taken from Pioglitazone and placebo treated NASH patients were deparaffinised and subjected to single immunohistochemistry as described in section 3.4.2. Photographs are representative of 21 sections each taken from 21 patients. Red arrows show hepatocytes positively stained with PPAR α.

Stereology counting was performed on PPAR α stained cells as shown in Table 3.6.2 below:

Table 3.6.2: Stereology counting of hepatocytes positively stained with PPAR α in NASH/Pre-trial, Pioglitazone and Placebo treated NASH patients. Data is presented as % of cell/ % total cell volume.

Groups/ Markers	NASH (n = 20)	Pioglitazone (n =9)	Placebo (n = 12)	P value
PPAR α Hepatocytes	**21.17 ± 2.07[a]**	**13.53 ± 1.47[a, c]**	**22.26 ± 1.70[c]**	**0.020[a] ; 0.012[c]**

(a: NASH/Pretrial Vs Pioglitazone; b: NASH/Pretrial Vs Placebo; c: Pioglitazone Vs Placebo) (n = number of patients) Stereology counting was performed as described in methods section 2.10. Data are presented as mean ± S.E.M.

PPAR α expression was decreased significantly with PGZ treatment compared to placebo and pre-trial group.

3.5. Apoptotic and cell proliferation markers

Pioglitazone reduced the number of αSMA and PPAR β positive HSCs suggesting that the activated stellate cell number and cell proliferation are reduced. Markers of apoptosis and cell proliferation were studied to determine the fate of the stellate cell. Caspase 3, M30 and TUNEL assay were used as markers of apoptosis and Ki67 was used as a marker for cell proliferation.

3.5.1. Caspase 3 immunohistochemistry

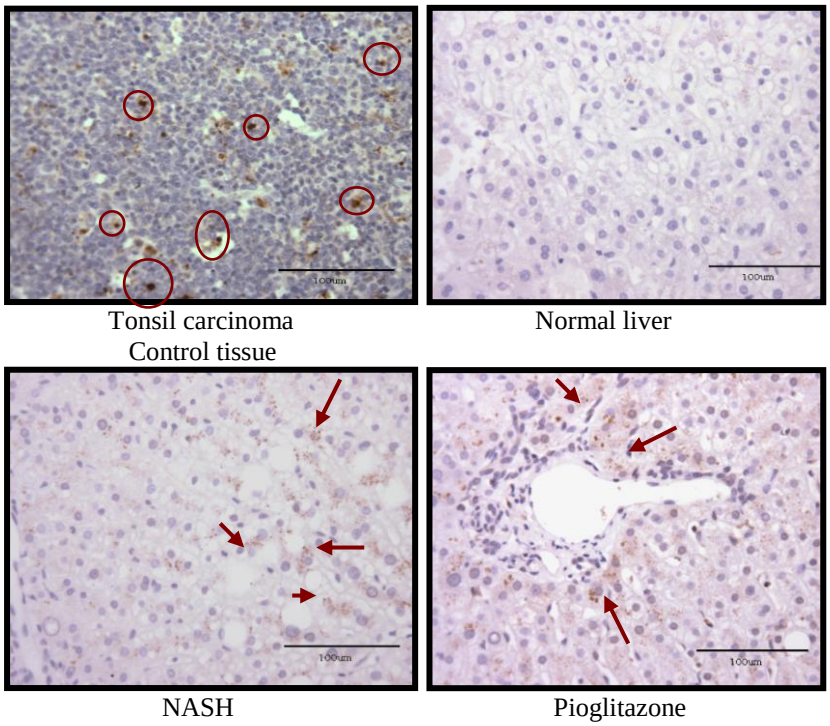

Figure 3.12: Caspase 3 immunohistochemistry in human liver. FFPE sections from human liver biopsies taken from normal liver, NASH, Pioglitazone treated NASH patients were deparaffinised and subjected to single immunohistochemistry as described in section 3.5.1. Caspase 3 is a marker of apoptosis. Photographs are representative of 55 sections each taken from 55 patients. Red arrows show cells positively stained with Caspase 3.

Caspase 3 expressions were diffused and granulated in all samples tested, and was difficult to distinguish from lipofuscan in the liver samples. Therefore, TUNEL assay was used to determine apoptotic cell numbers.

3.5.2. TUNEL assay immunoflourescence

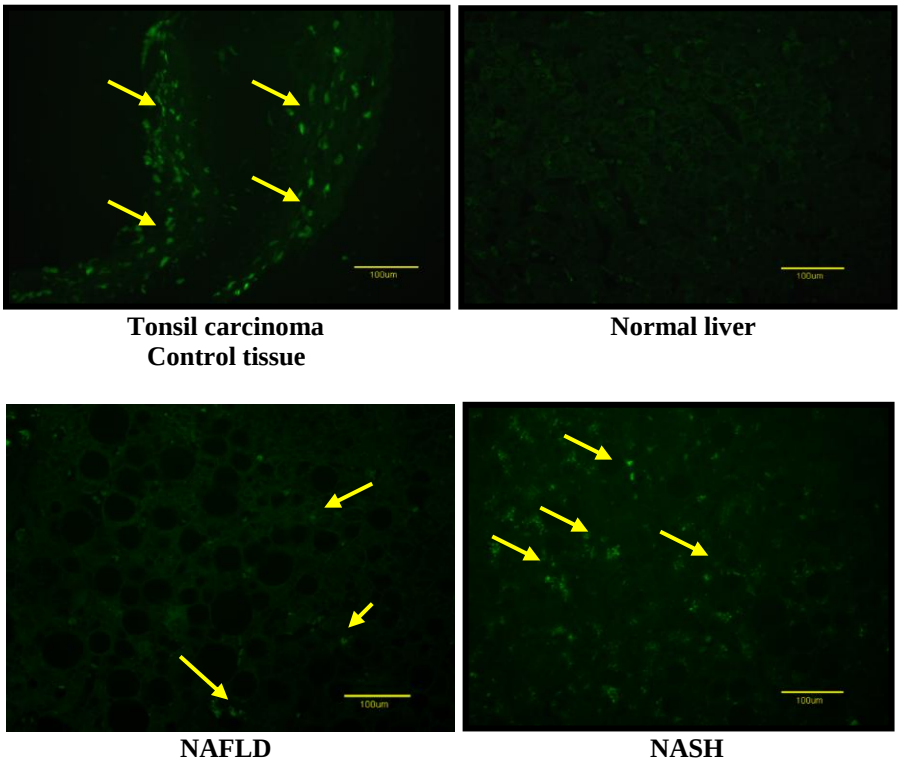

Figure 3.13: TUNEL assay immunoflourescence in human liver. FFPE sections from human liver biopsies taken from normal liver, NAFLD and NASH patients were deparaffinised and subjected to single immunoflourescence as described in section 3.5.2. TUNEL assay is a marker of apoptosis. Photographs are representative of 55 sections each taken from 55 patients. Yellow arrows show cells positively stained with TUNEL assay.

TUNEL assay immunoflourescence was evident in the positive control tissue as well as in the study group samples. Very little staining was evident in normal liver sections. It was not possible to identify the cell type by TUNEL assay immunoflourescence. Thus, as it was desirable to determine the level of apoptosis in stellate cells and hepatocytes separately, immunohistochemical analysis was attempted.

3.5.3. TUNEL assay immunohistochemistry

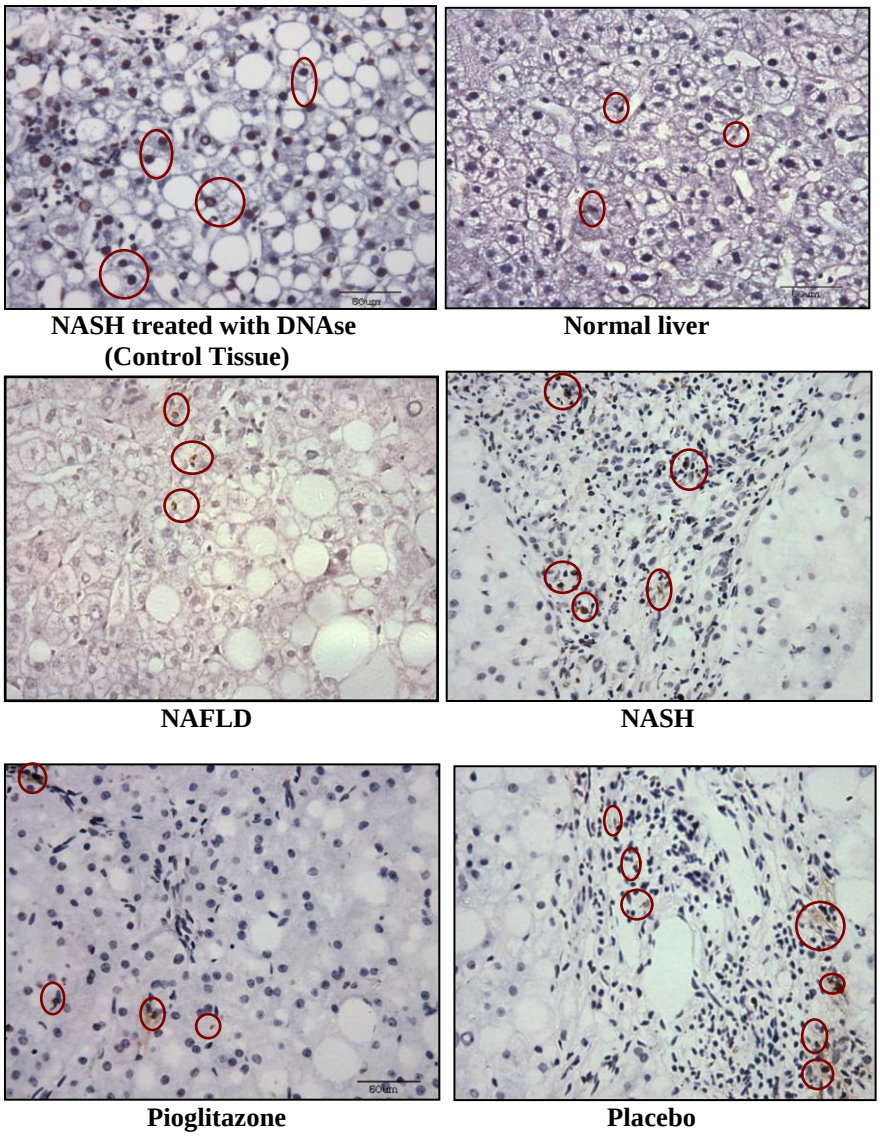

Figure 3.14: TUNEL assay immunohistochemistry in human liver. FFPE sections from human liver biopsies taken from normal liver, NAFLD, NASH, Pioglitazone and placebo treated NASH patients were deparaffinised and subjected to single immunohistochemistry as described in section 3.5.3. Photographs are representative of 55 sections each taken from 55 patients. Red circles show positive cells stained with TUNEL assay.

NASH liver sections treated with DNAse were used as the control tissue as described in method section 2.8.2. TUNEL assay showed apoptotic cells, clearly identifiable as stellate cells by their morphology. Apoptotic epithelial cells were not evident using the TUNEL assay; therefore Cytokeratin-18 (M30), which has been reported to be a reproducible and specific marker of epithelial cell apoptosis was assayed to determine the number of apoptotic epithelial cell particularly in hepatocytes.

3.5.4. Cytokeratin-18 (M30) immunohistochemistry

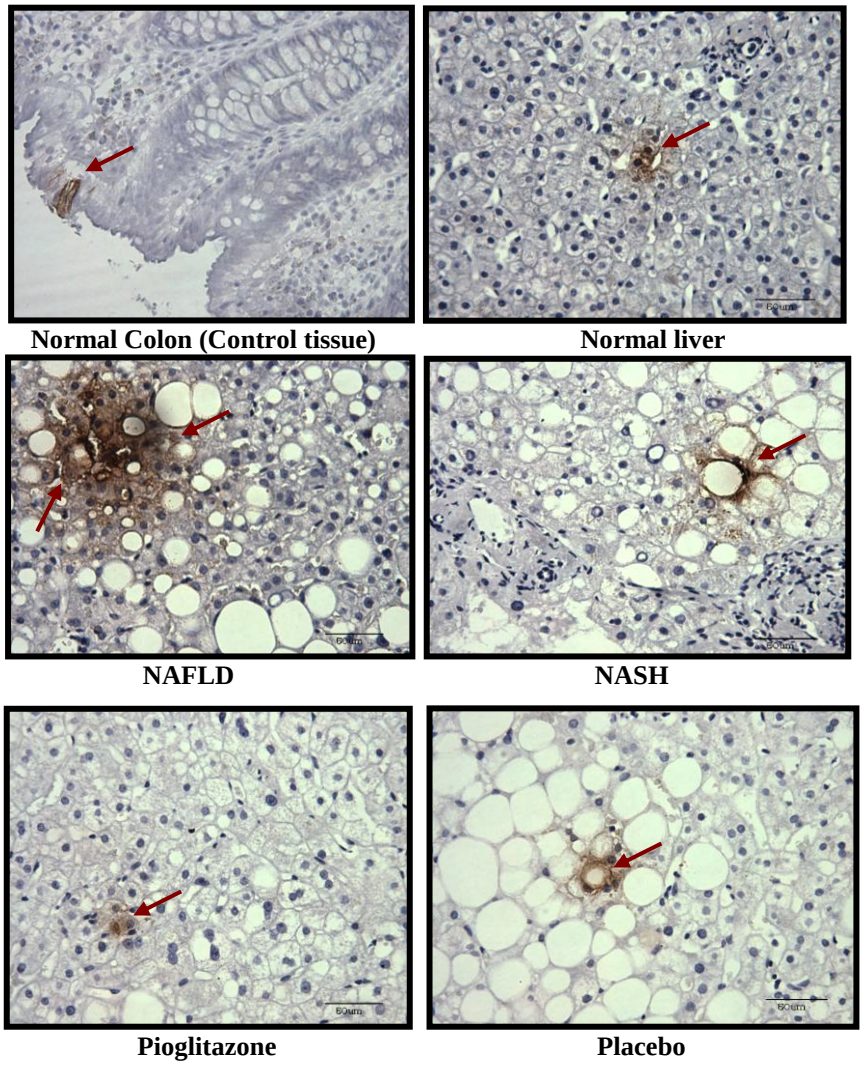

Figure 3.15: M30 immunohistochemistry in human liver. FFPE sections from human liver biopsies taken from normal liver, NAFLD, NASH, Pioglitazone and placebo treated NASH patients were deparaffinised and subjected to single immunohistochemistry as described in section 3.5.4. M30 is a marker of epithelial cell apoptosis. Photographs are representative of 55 sections each taken from 55 patients. Red arrows show hepatocytes positively stained with M30.

M30 expression was evident in both control and the study samples. Hepatocyte M30 expression was clearly elevated in steatosis as compared to other groups.

Stereology counting was performed on both M30 and TUNEL assay stained as shown in Table 3.7.1 and Table 3.7.2 below:

Table 3.7.1: Stereology counting of hepatic stellate cell and hepatocyte apoptosis markers in normal liver, NAFLD and NASH patients. Data is presented as % of cell/ % total cell volume.

Groups/ Markers	Normal liver (n = 7)	NAFLD (n = 7)	NASH (n = 20)	P value
M30	1.73 ± 0.50	4.01 ± 1.64	2.38 ± 0.47	NS
TUNEL	16.96 ± 4.78	22.17 ± 8.33	27.85 ± 2.41	NS

(a: Normal liver Vs NAFLD; b: Normal liver Vs NASH; c: NAFLD Vs NASH) (n = number of patients) Stereology counting was performed as described in method section 2.10. Data are presented as mean ± S.E.M.

Table 3.7.2: Stereology counting of hepatic stellate cell and hepatocyte apoptosis markers in NASH/Pre-trial, Pioglitazone and Placebo treated NASH patients. Data is presented as % of cell/ % total cell volume.

Groups/ Markers	NASH (n = 20)	Pioglitazone (n =9)	Placebo (n = 12)	P value
M30	2.38 ± 0.47	1.84 ± 0.22	1.94 ± 0.52	NS
TUNEL	27.85 ± 2.41	24.32 ± 4.03	31.05 ± 3.13	NS

(a: NASH/Pretrial Vs Pioglitazone; b: NASH/Pretrial Vs Placebo; c: Pioglitazone Vs Placebo) (n = number of patients) Stereology counting was performed as described in method section 2.10. Data are presented as mean ± S.E.M.

No significant differences were observed in terms of apoptotic cell number between groups.

3.5.5. Ki67 immunohistochemistry

As stellate cell numbers (as determined by GFAP and αSMA but not CRBP1) may increase, a proliferation cell marker was used to determine whether stellate cells showed a different rate of proliferation between groups. Thus, the rate of cell proliferation was another important parameter to investigate using the anti-Ki67 antibody.

3.5.5.1. Ki67 immunohistochemistry in normal liver, NAFLD & NASH patients

Control (Colon Tumor)

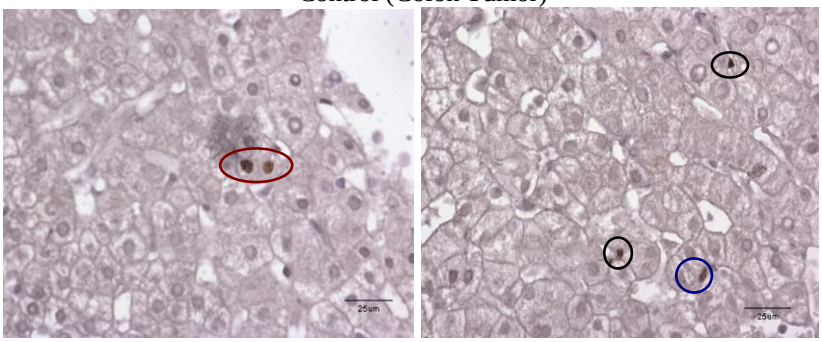

Normal liver (40X)

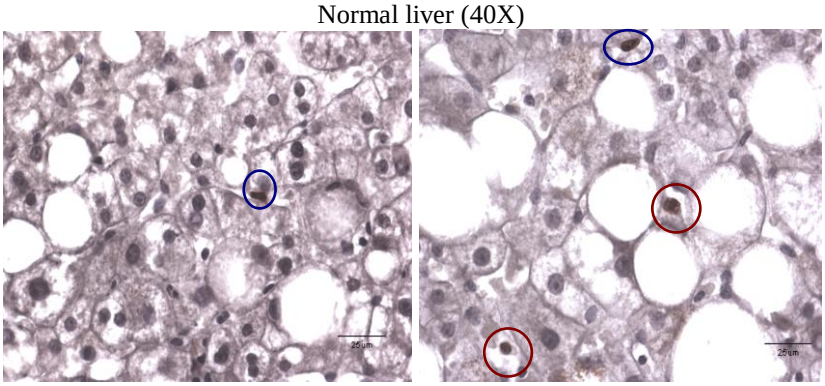

NAFLD (40X)

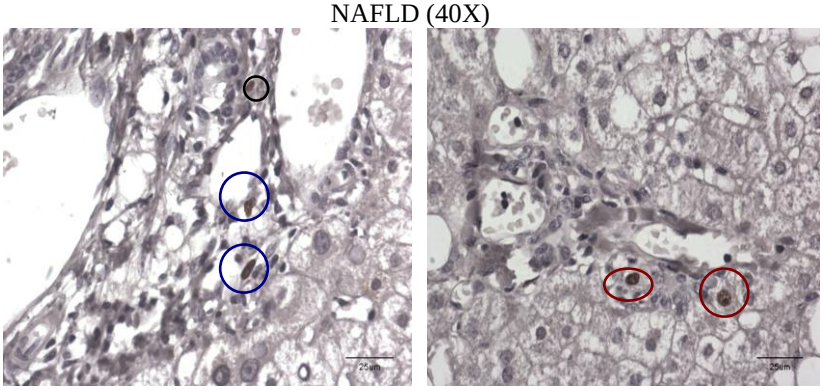

NASH (40X)

Figure 3.16.1: Ki67 immunohistochemistry in human liver. FFPE sections from human liver biopsies taken from normal liver, NAFLD and NASH patients were deparaffinised and subjected to single immunohistochemistry as described in section 3.5.5. Photographs are representative of 19 sections each taken from 19 patients. Red circles show hepatocytes, Blue circles show non-parenchemal cells, Black circles show immune cells positively stained with positive Ki67.

There are 3 types of cells stained in Ki67 immunohistochemistry; hepatocytes, non-parenchemal cells and immune cells. Non-parenchemal cells were identified by their longitudinal shape while immune cells were identified as small round cells. Hepatocytes were identified as double or single nucleated cells positively stained with Ki67. All results were independently verified by histopathology consultant Dr Philip V. Kaye.

It's not possible for all cases to differentiate whether Ki67 stains kupffer cells, stellate cells or endothelial cells; therefore all the non-parenchemal cells were included as a single category. Stereology counting was performed on Ki67 stained cells as shown in Table 3.8.1 below:

Table 3.8.1: Stereology counting of Ki67 stained cells in normal liver, NAFLD and NASH patients. Data is presented as % of cell/ % total cell volume.

Group	**Normal liver (N=5)**	**NAFLD (N=6)**	**NASH/ Pretrial (N=8)**	**P value**
% Hepatocyte	11.11 ± 10.62	23.41 ± 0.15	16.41 ± 0.15	NS
% Non-parenchemal cell	9.74 ± 13.97	13.34 ± 0.01	11.32 ± 0.11	NS
% Immune cell	2.82 ± 6.30	7.29 ± 0.12	9.00 ± 0.08	NS
% Total cell	23.67 ± 12.42	44.04 ± 10.50	36.73 ± 7.38	NS

(a: Normal liver Vs NAFLD; b: Normal liver Vs NASH; c: NAFLD Vs NASH) (n = number of patients) Stereology counting was performed as described in method section 2.10. Data are presented as mean ± S.E.M.

3.5.5.2. Ki67 immunohistochemistry in Pioglitazone & Placebo treated NASH patients

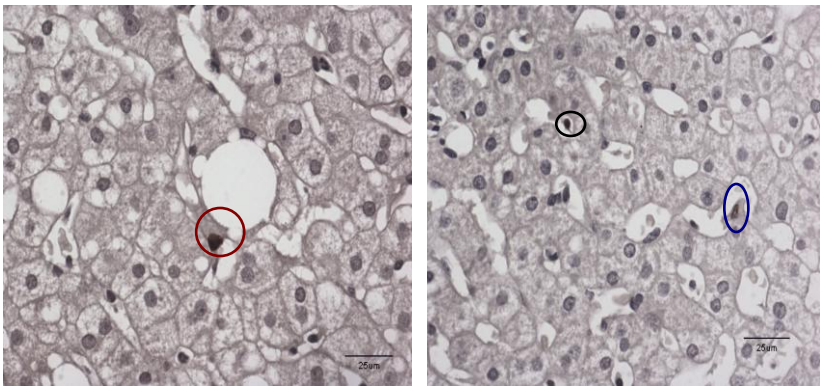

Pioglitazone treated NASH patients (40X)

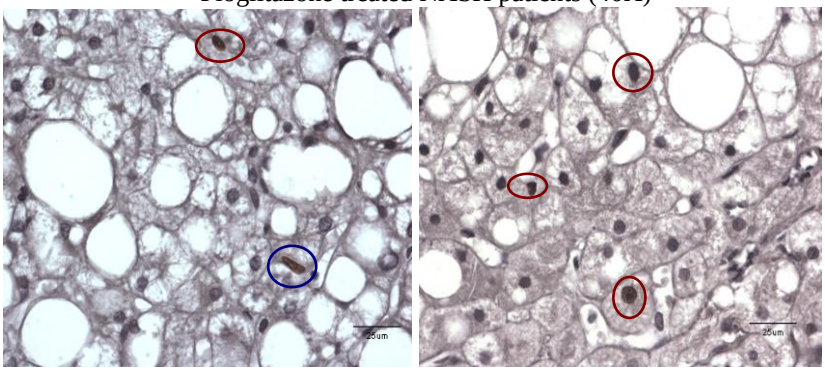

Placebo treated NASH patients (40X)

Figure 3.16.2: Ki67 immunohistochemistry in human NASH treated liver. FFPE sections from human liver biopsies taken from Pioglitazone and placebo treated NASH patients were deparaffinised and subjected to single immunohistochemistry as described in section 3.5.5. Photographs are representative of 13 sections each taken from 13 patients. Red circles show hepatocytes, Blue circles show non-parenchemal cells, Black circles show immune cells positively stained with positive Ki67.

Table 3.8.2: Stereology counting of Ki67 stained cells in NASH/Pre-trial, Pioglitazone and Placebo treated NASH patients. Data is presented as % of cell/ % total cell volume.

Group	**NASH/ Pretrial (N=8)**	**Pioglitazone (N=6)**	**Placebo (N=7)**	**P value**
% Hepatocyte	16.41 ± 0.15	11.44 ± 11.20	25.15 ± 0.09	NS
% Non-parenchemal cell	11.32 ± 0.11	9.21 ± 10.23	19.37 ± 0.08	NS
% Immune cell	9.00 ± 0.08	7.98 ± 7.82	13.59 ± 0.12	NS
% Total cell	**36.73 ± 7.38[b]**	**22.53 ± 7.77[c]**	**58.11 ± 2.95[b,c]**	**0.022[b]; 0.002[c]**

(a: NASH/Pretrial Vs Pioglitazone; b: NASH/Pretrial Vs Placebo; c: Pioglitazone Vs Placebo) (N = number of patients) Stereology counting was performed as described in method section 2.9. Data are presented as mean ± S.E.M.

There were no discernable differences between the cell types examined, but Pioglitazone appeared to decrease overall cell proliferation regardless of cell type.

3.6. Protein expression of PCNA in human liver samples

Western blotting was used to determine Proliferating cell nuclear antigen (PCNA) levels in total liver protein extracts as an alternative marker of cell proliferation.

3.6.1. PCNA protein expression in human liver samples

a.Normal liver (n=7)

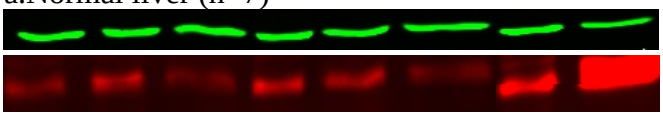

Beta actin (42 KDa)

PCNA (36 KDa)

Hela cell

b.NAFLD (n=7)

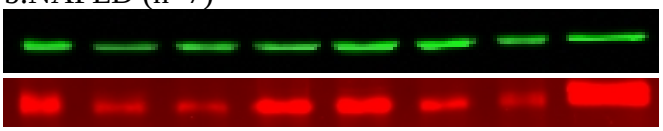

Beta actin (42 KDa)

PCNA (36 KDa)

Hela cell

c. NASH/Pretrial (n=8)

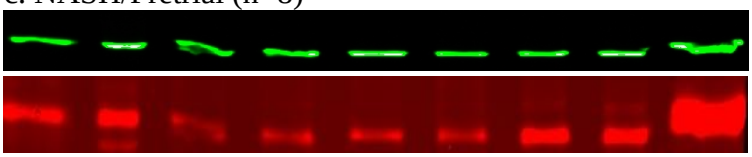

Beta actin (42kDa)

PCNA (36kDa)

Hela cell

d. Pioglitazone treated NASH patients (n=7)

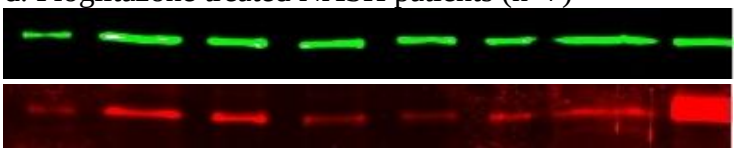

Beta actin (42KDa)

PCNA (36 KDa)

Hela cell

e. Placebo treated NASH patients (n=6)

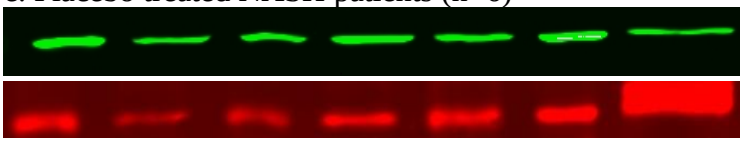

Beta actin (42KDa)

PCNA (36KDa)

Hela cell

Figure 3.17: Beta actin and PCNA protein expressions in normal liver, NAFLD, NASH, Pioglitazone and placebo treated NASH patients. (n = number of patients)

PCNA protein expression was studied in parallel with the Ki67 stereology counting. HeLa cell protein was used as a positive control. Densitometry results of PCNA immunoblotting are as shown in Figure 3.18.1 and 3.18.2 over leaf.

3.6.2. PCNA protein expressions quantification

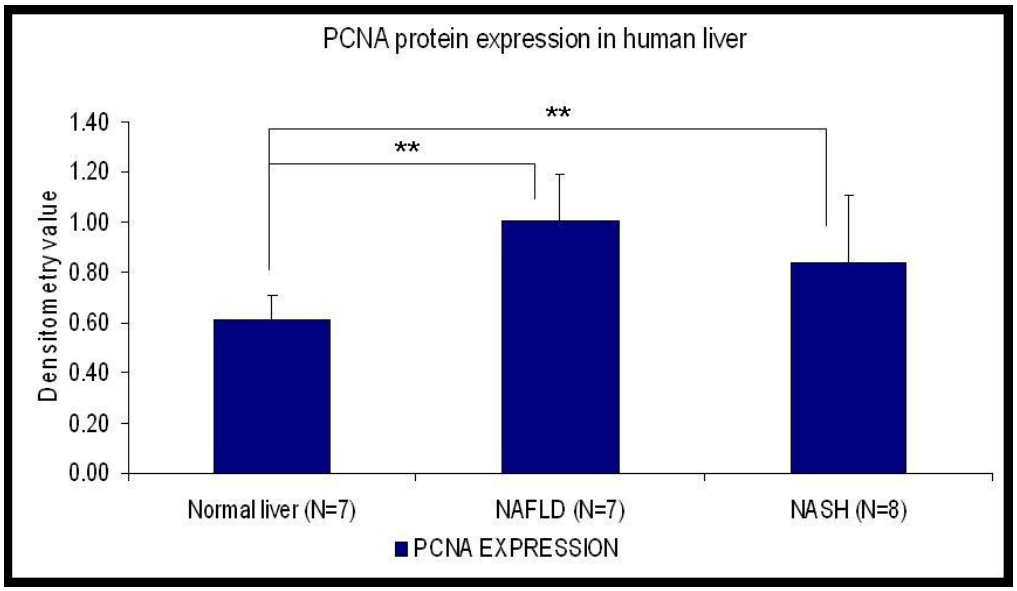

Figure 3.18.1: PCNA protein expression in normal liver, NAFLD and NASH. (N= number of patients; ****** p <0.05; ******* p <0.001). PCNA protein expression was normalised with β-actin. Data are presented as mean ± S.E.M.

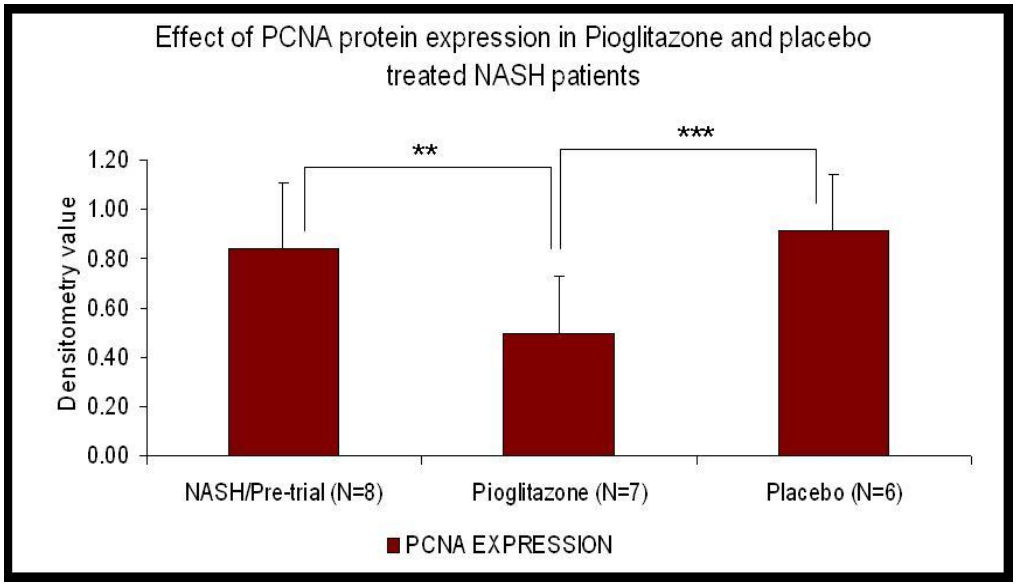

Figure 3.18.2: PCNA protein expression in Pre-trial, Pioglitazone & Placebo treated NASH patients. (N= number of patients; ****** p <0.05; *******p <0.001). PCNA protein expression was normalised with β-actin. Data are presented as mean ± S.E.M.

PCNA expression was higher in steatosis and NASH compared to normal liver. PGZ treated patients showed a reduction in PCNA expression as compared to pre-trial and placebo groups.

3.7. Discussion

During liver injury, stellate cells lose their vitamin A storing capacity and transformed into activated myofibroblast-like cells which express α smooth muscle actin (αSMA) (Friedman, 1993). These cells then produce extracellular matrix (ECM) which can lead to fibrosis followed by cirrhosis (Carroti et al., 2008; Friedman, 2000). αSMA is marker of activated HSCs in humans (Schmitt-Graff et al.,1991) and in normal liver it can be seen around the vascular area of portal tract veins & arteries (Van Rossen et al., 2009). The data from this study showed that, αSMA levels are increased in both steatosis and NASH patients compared to normal liver and αSMA expression was reduced significantly by PGZ treatment.

Cellular retinol binding protein 1 (CRBP1) is reported to be a quiescent marker for HSCs where it is involved in mediating both retinol esterification to retinyl esters and retinol oxidation to retinal and retinoic acid (Blomhoff et al., 1985). Based on dual immunohistochemistry and double immunoflourescence of α-SMA and CRBP1, there was clear co-localization of both markers but also some cells only stain with one marker. Since CRBP1 stained both quiescent and activated stellate cells, stereology counting of this staining is an indicator of total stellate cell number. There were no significant differences in CRBP1 expression between the groups studied.

Glial fibrillary acidic protein (GFAP) is a neuronal marker that is not only expressed in both astrocytes and non-myelinating Schwann cells (Lim et al., 2007), but has also been reported as being expressed in quiescent hepatic stellate cells (Buniatian et al., 1996), pancreatic stellate cells (Apte et al., 1998) and in kidney podocytes (Buniatian et al., 1998). GFAP expression has been shown to increase in acute inflammation but is decreased in chronic inflammation in the livers of rats treated with carbon tetrachloride (CCl_4) (Nikki et al., 1996).

GFAP was found to be expressed in stellate cells, and around the vascular portal area. Stereology counting indicated that in NASH patients, GFAP expression was increased as compared to normal liver and steatosis. A previous study has reported that GFAP is a marker for early injury in the liver, where the expression was increased in both recurrent post-transplant hepatitis C virus (HCV) and chronic HCV patients and decreased expression was observed in cirrhotic-HCV patients (Carroti et al., 2008). In this study, no significant differences were observed between PGZ and placebo treated patients.

In conclusion, αSMA expression which denotes an increase in stellate cell activation, is elevated in NAFLD and NASH, and is reduced following pioglitazone treatment. Whether the increased in GFAP expression is a marker of liver injury and its significance in terms of stellate cell phenotype is not clear. Using dual immunoflourescence for CRPB1 and GFAP and also a-SMA and GFAP would be informative in terms of understanding the sub-population of stellate cells that express GFAP. CRBP1 expression data suggest no change in overall number of stellate cells during the progression from normal liver to NAFLD and NASH.

Peroxisome proliferator activated receptors (PPARs) are nuclear receptors of which there are three isotypes: PPAR-α, β, and γ. PPAR α is highly expressed in hepatocytes and plays a major role in lipid metabolism (Peters et al., 2005). Meanwhile PPAR γ regulates adipogenesis and it is highly expressed in adipose tissue (Tontonoz et al., 1994). PPAR β is expressed in many cell types is an important regulator of high density lipoprotein (HDL) cholesterol level, skeletal muscle fatty acid catabolism and glucose homeostasis (Leibowitz et al., 2000; Oliver et al., 2001; Grimaldi et al., 2005; Lee et al., 2006), but the role of PPAR β in liver is not clear.

PPAR β expression was observed in both hepatocytes and stellate cells. In NAFLD, PPAR β expression was increased significantly in stellate cells, meanwhile in placebo treated patient, hepatocytes PPAR β expression was reduced significantly as compared to both pre-trial and PGZ treated patients.

PPAR β is a marker of activated and or proliferation stellate cells. It was highest in NAFLD, with no further increased in NASH. The number of cells stained far less than other markers including αSMA, suggests that PPAR β expressed in a sub-population of stellate cell. PPARγ expression could not be detected using the available antibodies in the liver. A previous study suggests that upon activation PPAR γ expression is decreased (She et al., 2005), and PPAR β expression is subsequently increased in stellate cells in culture (Hellemans et al., 2003) but we are unable to confirm this *in vivo* due to the inability to detect PPAR γ at the protein level**.** PPARs are generally seen as anti-proliferative (Gizard et al., 2005; Harman et al., 2004; Han et al., 2007) and anti-inflammatory (Michalik & Wahli, 2006) but the β isotype has been implicated in the proliferative phase of wound healing via interaction with the TGFβ/SMAD pathway (Michalik & Wahli, 2006). The role of PPAR β in stellate cells should still be a matter for debate.

M30 or cytokeratin-18 (CK-18) is a marker of hepatocyte cell death and is a marker of early apoptosis caspase activity. Furthermore, plasma CK-18 levels were higher in NASH patients when compared to NAFLD (Feldstein et al., 2009). TUNEL assay is an alternative of measuring the levels of apoptosis is cells or tissues where DNA defragmentation occurs and apoptotic bodies are stained. Feldstein et al. (2003) reported that, using the TUNEL assay, in conjunction with caspase 3 and 7 staining, hepatocyte apoptosis was greater in NASH as compared to simple steatosis. Indeed, increased apoptosis in NASH has been widely reported. In this current study, both M30 and TUNEL stereology counting did not reveal any significant difference between the groups examined. The reason for the differences observed in terms of apoptosis between this and previous studies is difficult to ascertain. Both M30 and TUNEL assays in this study indicated higher levels of apoptosis in NAFLD and NASH patients as compared to histologically normal control tissue, but the data failed to reach significance. It is possible that either a lack of sensitivity and/or background levels of staining masked the differences in apoptotic cell number in this study.

Ki67 is a marker of cell proliferation which is widely used for cancer prognosis (Scholzen and Gerdes, 2000). Ki67 is expressed in G_1, S, G_2 and M phases but not during G_0 phase of the cell cycle (Gerdes et al., 1991; Bullwinkle et al., 2006). PCNA is another marker widely used in the analysis of proliferation in normal and neoplastic tissue (Demeter at al., 1994). It is expressed in the nucleus of cells during DNA synthesis (Essers et al., 2005) and is expressed during G_0, G_1, and further induced in S phase of the cell cycle (Celis et al., 1987).

The current study showed that PGZ decreased both hepatic PCNA and Ki67 expression compared to pre-trial and placebo treated groups. For Ki67 no changes in proliferation of a particular cell type were observed, thus it is unclear whether PGZ influences hepatocyte, immune cell or non-parenchymal cell proliferation or whether all cell types are equally affected. PGZ has previously been shown to reduce cell proliferation in partial hepatectomy rat (Yamamoto et al., 2008) as well as in cancer (Takano et al., 2008). The relationship between the effect of PGZ upon cell proliferation and the beneficial therapeutic effect seen in NASH patients is not clear. If PGZ inhibits stellate cell proliferation then it is possible that this may be influential in reducing fibrosis, but this effect would be hard to dissect out from the potential anti-inflammatory actions of PGZ.

Overall these data suggest that PGZ exerts its effects at least in part by reducing the numbers of activated stellate cells in the livers of NASH patients. It is also possible that inhibition of stellate cell proliferation is also a beneficial effect of PGZ therapy. Whether these effects are mediated via changes in whole body metabolism or are due to the direct action of PGZ upon stellate cells is a matter for conjecture.

.

CHAPTER 4

Gene Expression in human liver: Assessment of the effects of Pioglitazone therapy in NASH patients.

4.1. Taqman RT-PCR Principle and gene expression analysis

RNA samples from liver biopsies were analyzed using the Agilent Bioanalyser 2100 to determine the RNA integrity and RNA integrity number (RIN). Some of these samples partially degraded with sample having RIN value of ≤2.0. Taqman Real-time Polymerase chain reaction (RT-PCR) was used to quantify the gene expression in this study. Taqman RT-PCR is an absolute quantitation method that generates copy numbers for each test sample by relating test sample cycle threshold (Ct) values, back to a standard curve of Ct values based on a dilution series of cDNA samples containing the target species of interest (Hughes & Moody, 2007).

TaqMan probes are hydrolysis probes that are designed to increase the specificity of real-time PCR assays. TaqMan probes consist of a fluorophore covalently attached to the 5'-end of the oligonucleotide probe and a quencher at the 3'-end (Figure 4.1). TaqMan probe annealed within a DNA region amplified by a specific set of primers. As the Taq polymerase extends the primer and synthesizes the nascent strand, the 5' to 3' exonuclease activity of the polymerase degrades the probe that has annealed to the template. Degradation of the probe releases the fluorophore from it and breaks the close proximity to the quencher, thus relieving the quenching effect and allowing fluorescence of the fluorophore. The quencher molecule quenches the fluorescence emitted by the reporter (fluorophore) when excited by the cycler's light source via FRET (Fluorescence Resonance Energy Transfer). As long as the reporter (fluorophore) and the quencher are in proximity, quenching inhibits any fluorescence signals (Figure 4.1). (Applied Biosystem)

Hence, fluorescence detected in the real-time PCR thermal cycler is directly proportional to the fluorophore released and the amount of DNA template present in the PCR and displayed as an amplification plot (Figure 4.2). (Applied Biosystem)

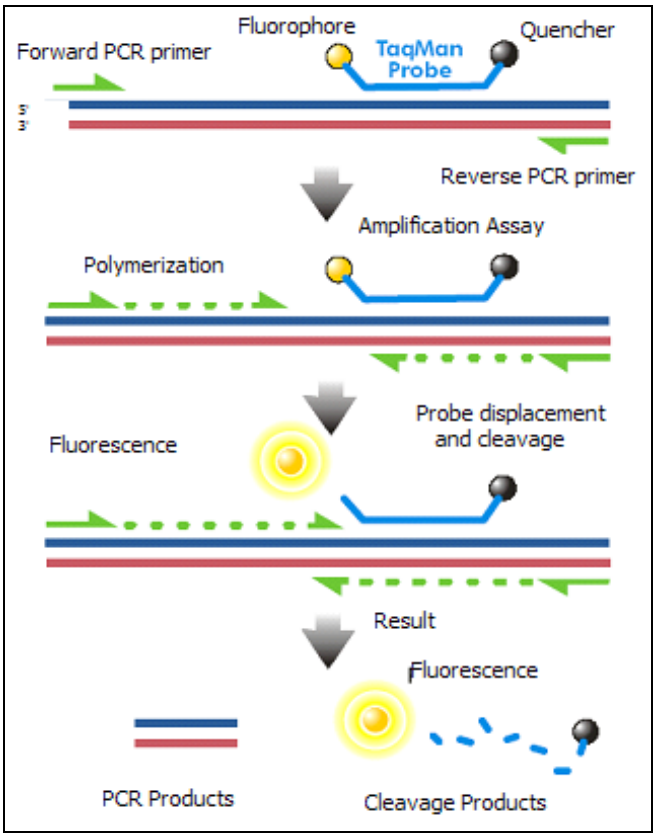

Figure 4.1: Taqman Probe chemistry mechanism (Applied Biosystem)

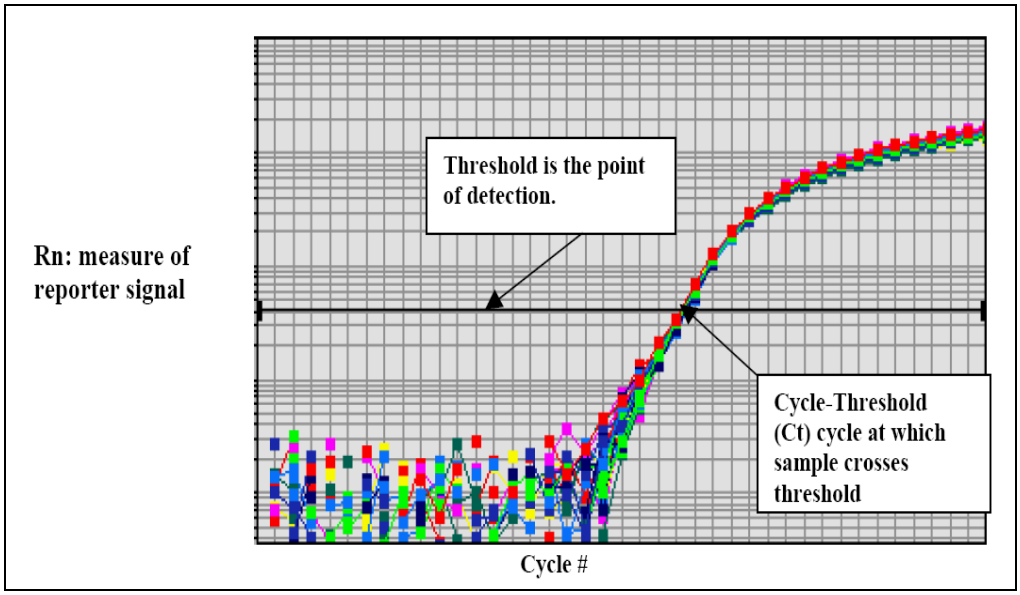

Figure 4.2: Amplification curve of Taqman Real-time PCR. (Applied Biosystem)

The reference gene (β-actin) was studied first using Taqman Real-time PCR to asses whether or not these samples were of sufficient quality to produce reliable gene expression data for the analysis. The Taqman Real-time PCR slope should be within the range (-3.2 to -3.6) and correlation coefficient (r^2) also should be from 0.95 to 0.99 (Hughes & Moody, 2007) as shown in Figure 4.3 below:

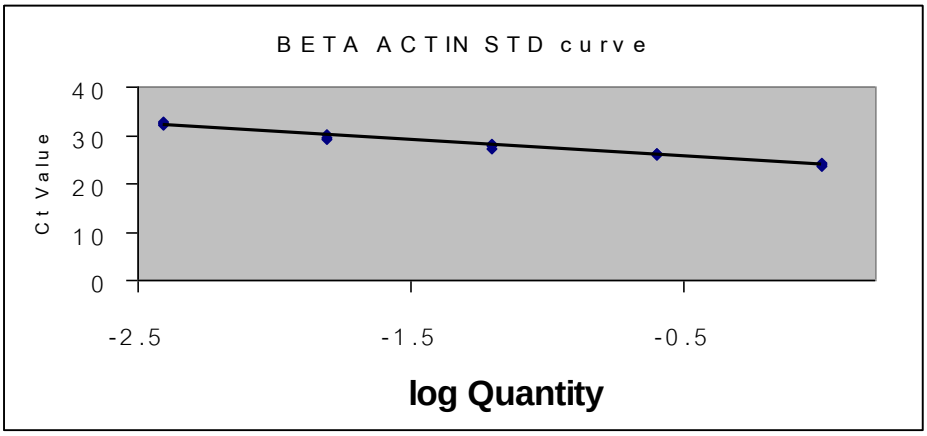

slope	-3.430398149
intercept	23.81719783
r2	-0.989169953

Figure 4.3 Taqman Real-time PCR of reference gene (β-actin) gene expression standard curve using serial dilution of human liver cDNA.

The reference gene expression results were acceptable for all samples. Target gene expression of genes involved in carbohydrate and lipid metabolism gene were studied initially. Target gene expression was normalised using the geometric mean of 2 reference genes [β-actin & hydroxymethylbilane synthase (HMBS)] and the results are shown in Table 4.1.

Results

4.2. Taqman Real-time PCR gene expression in Pre-trial, Pioglitazone and placebo treated NASH patients.

Table 4.1: Effects of 12 months of Pioglitazone treatment on gene expression in NASH patients.

Target gene	Pre-trial (n = 22)	Pioglitazone (n = 12)	Placebo (n = 12)	P VALUE
ChREBP	**2.156 ± 0.435 B**	**3.971 ± 1.049 B**	2.117 ± 0.520	**0.049 B**
SREBP1C	**1.478 ± 0.258 A**	**2.150 ± 0.610 C**	**0.310 ± 0.062 A,C**	**0.022 A 0.002 C**
CPT1	0.492 ± 0.156	0.793 ± 0.275	0.476 ± 0.136	NS
PDK4	1.679 ± 0.369	2.137 ± 0.481	0.842 ± 0.295	NS
PK2	1.549 ± 0.363	1.317 ± 0.377	1.227 ± 0.337	NS
GCK	0.658 ± 0.284	0.794 ± 0.374	1.401 ± 0.725	NS

Gene expression values are normalised using the geometric mean of the reference genes [β- actin and HMBS]. Data are presented as mean ± SEM. Carbohydrate regulatory element binding protein (ChREBP), Sterol regulatory element binding protein-1C (SREBP-1C), Carnitine palmitoyl transferase-1 (CPT-1), Pyruvate dehydrogenase kinase 4 (PDK4), Pyruvate kinase 2 (PK2) and Glucokinase (GCK)
(A: Pre-trial Vs Placebo; B: Pre-trial Vs Pioglitazone; C: Pioglitazone Vs Placebo)

No significant differences between groups in terms of reference gene expression were observed. Taqman real-time PCR results indicated that PGZ increased both ChREBP and SREBP1C gene expression as compared to placebo. SREBP1C levels decreased in placebo group as compared to the pre-trial group. No significant differences in β-oxidation and glucose metabolism genes were observed in these samples. These results were surprising in that the two master regulators of lipogenesis were elevated in PGZ treated patients.

PGZ increases lipogenesis in adipose tissue via activation of PPAR γ2 (Miyazaki et al., 2000), however, the whole-body insulin sensitizing effects of PGZ might be expected to reduce lipogenesis in the liver. Conversely both ChREBP and SREBP1C expression/activity are increased by glucose and insulin, thus increased lipogenesis by up regulation of these genes. As the target gene for SREBP1C (GCK) (Foretz et al., 1999; Kim et al., 2004) and ChREBP (PK2) (Iizuka & Horikawa, 2008) were unaltered the overall picture of the effects of PGZ on gene expression in NASH patients was unclear.

4.3. Taqman Low density array gene expression in human liver

Microarray gene expression analysis followed by pathway-based interpretation of the subsequent data sets would provide a much more comprehensive picture of the transcriptional changes induced by PGZ. The relative poor quality of the RNA samples precluded this. It was decided that low density Taqman array would be used. Taqman Low density array is a relative quantitation method that uses the ΔΔCt method that compares target species mRNA levels between different samples by correcting for a reference gene and relating expression levels to a reference control for examples an untreated sample (Hughes & Moody, 2007).

Target genes thought to be involved in the pathogenesis of NAFLD/NASH were selected. The official symbol, abbreviation and function of the gene selected for low density array analysis are listed in Table 4.2 and all the information was obtained from Ref Seq (NCBI) over leaf.

Table 4.2: List of gene categories, symbol, abbreviation and gene functions used in this study.

Symbol	Gene	Function
Reference genes		
18sRNA	18s ribosomal nucleic acid	Ribosomal RNA subunit
ABL1	c-abl oncogene 1, receptor tyrosine kinase	cell differentiation, cell division, cell adhesion, and stress response.
HPRT1	hypoxanthine phosphoribosyltransferase1	catalyzes conversion of hypoxanthine to inosine monophosphate and guanine to guanosine monophosphate for energy production
MRPL19	mitochondrial ribosomal protein L19	protein synthesis within the mitochondrion
Glycolysis genes		
ALDOB	aldolase B, fructose-bisphosphate	catalyzes the reversible conversion of fructose-1,6-bisphosphate to glyceraldehyde 3-phosphate & Dehydroxyacetone phosphate.
LDHA	Lactate Dehydrogenase B	catalyzes lactate & NAD to pyruvate and NADH in the final step of glycolysis
PFKL	Phosphofructokinase, liver	catalyzes fructose 6-phosphate to fructose 1,6-bisphosphate a key step in glycolysis
Gluconeogenesis genes		
ATF3	Activating transcription factor 3	Represses gluconeogenic enzymes in liver & increased in liver regeneration (Younossi, 2005).
G6PC	Glucose 6-phosphatase, catalytic subunit	catalyzes the hydrolysis of glc 6-phosphate to glucose and orthophosphate
PCK2	Phosphoenolpyruvate carboxykinase 2	catalyzes the formation of phosphoenolpyruvate from oxaloacetate, with the release of carbon dioxide and GDP.
Pentose phosphate pathway genes		
G6PD	Glucose 6-phosphate dehydrogenase	produce NADPH, a key electron donor in the defense against oxidizing agents and in reductive biosynthetic reactions.
TALDO1	Transaldolase 1	key enzyme of the nonoxidative pentose phosphate pathway providing ribose-5-phosphate for nucleic acid synthesis and NADPH for lipid biosynthesis.
TKT	Transketolase	catalyzes the reverse reaction, the conversion of sedoheptulose-7-P and glyceraldehyde-3-P to pentose
Glycogen metabolism genes		
GSK3B	glycogen synthase kinase 3 beta	phosphorylating and inactivating glycogen synthase. GSK3B is involved in energy metabolism, neuronal cell development, and body pattern formation
PGM1	phosphoglucomutase 1	converted to glucose 6-phosphate by cytosolic phosphoglucomutase I.
PYGL	Phosphorylase Glycogen Liver	catalyzes the removal of glucose residues, as glucose 1-phosphate, from the ends of glycogen branches

Symbol	Gene	Function
Kreb cycle genes		
CA5A	carbonic anhydrase 5A,	catalyze the reversible hydration of carbon dioxide
FH	Fumarate hydratase	catalyzes the formation of L-malate from fumarate
MDH2	Malate dehydrogenase 2	catalyzes the reversible oxidation of malate to oxaloacetate, utilizing the NAD/NADH cofactor system in the citric acid cycle
PDK2	Pyruvate dehydrogenase kinase 2	Phosphorylate PDC inhibiting glycolysis
UCP2	Uncoupling protein 2	reduce the mitochondrial membrane potential in mammalian cells.
Glucose transporter gene		
GLUT2	glucose transporter 2	mediates facilitated bidirectional glucose transport
Fatty acid synthesis genes		
ACC2	acetyl-Coenzyme A carboxylase beta	catalyzes the carboxylation of acetyl-CoA to malonyl- CoA, the rate-limiting step in fatty acid synthesis.
ACLY	ATP citrate lyase	catalyzes the formation of acetylCoA and oxaloacetate from citrate and CoA with a concomitant hydrolysis of ATP to ADP and phosphate
ChREBP	Carbohyrate response element binding protein	Promotes fatty acid synthesis genes
FASN	Fatty acid synthase	catalyze the synthesis of palmitate from acetyl-CoA and malonyl-CoA, in the presence of NADPH, into long-chain saturated fatty acids
ME1	Malic enzyme 1	catalyzes the oxidative decarboxylation of malate to pyruvate
SCD	Stearoyl CoA desaturase	catalyzes a rate-limiting step in the synthesis of unsaturated fatty acids.
SREBP-1C	Sterol regulatory element binding transcription factor 1	Promotes genes involved in sterol biosynthesis
Triacylglycerol biosynthesis genes		
DGAT2	Diacylglycerol O-acyltransferase 2	utilizes diacylglycerol and fatty acyl CoA as substrates in order to catalyze the final stage of triacylglycerol synthesis
GPD1	Glycerol-3-phosphate dehydrogenase 1	catalyzes the unidirectional conversion of glycerol-3-phosphate to dihydroxyacetone phosphate with concomitant reduction of the enzyme-bound FAD
Triacylglycerol biosynthesis genes		
MTTP	Mitochodrial triglyceride transfer protein	play a central role in lipoprotein assembly
PPAP2C	Phosphatidic acid phosphatase type 2C	convert phosphatidic acid to diacylglycerol, and promotes synthesis of glycerolipids & also in receptor-activated signal transduction mediated by phospholipase D
THRSP	Thyroid hormone responsive (SPOT14)	This gene is rapidly up-regulated by signals that induce lipogenesis such as enhanced glucose metabolism and thyroid hormone administration. (LaFave et al., 2006)

Symbol	Gene	Function
Lipid Metabolism genes		
ACADL	acyl-Coenzyme A dehydrogenase, long chain	catalyze the initial step of mitochondrial beta-oxidation of straight-chain fatty acid.
ACADVL	Acyl-Coenzyme A dehydrogenase, very long chain	catalyzes the first step of the mitochondrial fatty acid beta-oxidation pathway. This acyl-Coenzyme A dehydrogenase is specific to long-chain and very-long-chain fatty acids
ACOX1	acyl-Coenzyme A oxidase 1	first enzyme of the fatty acid beta-oxidation pathway, which catalyzes the desaturation of acyl-CoAs to 2-trans-enoyl-CoAs. It donates electrons directly to molecular oxygen, thereby producing hydrogen peroxide.
ACSL4	Acyl-CoA synthetase long-chain family member 4	controls the level of free arachidonic acid (AA) regulating eicosanoid production
ADIPOR1	Adiponectin receptor 1	Mediate increased AMPK expression
ADIPOR2	Adiponectin receptor 2	Mediate increase PPARα expression
CAT	Catalase	Antioxidant gene shown to be upregulated in the liver in response to CYP2E1-dependent oxidative stress.
CD36	CD36	Promotes fatty acid uptake, transport
ECHS1	enoyl Coenzyme A hydratase, short chain, 1, mitochondrial	catalyzes the hydration of 2-trans-enoyl-coenzyme A (CoA) intermediates to L-3-hydroxyacyl-CoAs.
GSTA4	Glutathione S-transferase A4	Cellular defenses against the oxidative stress. Increased in response to CYP2E1-dependent production of mitochondrial ROS, to TNF-α, IL-6 and EGF. Younossi et al. (2005) reported that CAT and GSTA4 were upregulated in both NASH and obese control compared to non-obese control.
HADHB	hydroxyacyl-Coenzyme A dehydrogenase, beta subunit	catalyzes the last three steps of mitochondrial beta-oxidation of long chain fatty acids.
HMGCS2	3-hydroxy-3-methylglutaryl-Coenzyme A synthase 2	Rate limiting enzyme of the HMG-CoA pathway of fatty acid metabolism (ketogenesis).
LPL	Lipoprotein Lipase	dual functions of triglyceride hydrolase and ligand/bridging factor for receptor-mediated lipoprotein uptake
NRF1	Nuclear respiratory factor 1	protective function against oxidative stress and potentially a function in lipid homeostasis in the liver.
Lipid Metabolism genes		
PHB	Prohibitin	A chaperon involved in the assembly of mitochondrial respiratory chain (Nitjmans et al., 2000).
PLIN	Perilipin	coats lipid storage droplets in adipocytes, thereby protecting them until they can be broken down by hormone-sensitive lipase
Cholesterol metabolism genes		
APOC3	Apolipoprotein C-III	inhibits lipoprotein lipase and hepatic lipase & delay the catabolism of triglyceride-rich particles
APOE	Apolipoprotein E	Catabolises the triglyceride-rich lipoprotein constituents [Chylomicron and very low density lipoprotein (VLDL) remnants]

Symbol	Gene	Function
Nuclear receptors genes		
FXR	Farnesoid X receptor	Suppressed cholesterol 7 alpha-hydroxylase (CYP7A1), the rate-limiting enzyme in bile acid synthesis from cholesterol.
PPARα	Peroxisome proliferator-activated receptor alpha	regulates the expression of genes involved in fatty acid beta-oxidation and is a major regulator of energy homeostasis
PPARβ	Peroxisome proliferator-activated receptor beta	Regulates lipid metabolism, and epidermal cell proliferation
PGC1α	Peroxisome proliferator-activated receptor gamma, coactivator 1 alpha	enhances metabolically relevant pathways, such as gluconeogenesis, fatty acid oxidation, thermogenesis, oxidative phosphorylation and mitochondrial biogenesis
PGC1β	Peroxisome proliferator-activated receptor gamma, coactivator 1 beta	enhances metabolically relevant pathways, such as gluconeogenesis, fatty acid oxidation, thermogenesis, oxidative phosphorylation and mitochondrial biogenesis
PXR	Pregnane X receptor	Regulates of the cytochrome P450 gene CYP3A4, binding to the response element of the CYP3A4 promoter as a heterodimer with the 9-cis retinoic acid receptor RXR.
RXRα	Retinoid X receptor, alpha	mediate the biological effects of retinoids by their involvement in retinoic acid-mediated gene activation.
Adipogenic genes		
CEBPA	CCAAT/enhancer binding protein (C/EBP), alpha	Modulate leptin gene that help regulate body weight homeostasis
CEBPB	CCAAT/enhancer binding protein (C/EBP), beta	regulation of genes involved in immune and inflammatory responses
LXR-α	Liver-X-receptor alpha	regulating the expression of genes involved in hepatic bile and fatty acid synthesis, glucose metabolism as well as sterol efflux
LXR-β	Liver-X-receptor beta	regulating the expression of genes involved in hepatic bile and fatty acid synthesis, glucose metabolism as well as sterol efflux
PPARγ	Peroxisome proliferator-activated receptor gamma	Regulates of adipocyte differentiation.
ADN	Adipsin	role for adipose tissue in immune system biology
FABP4	Fatty acid binding protein 4	Promotes in fatty acid uptake, transport, and metabolism
Insulin signalling genes		
MAP2K4	Mitogen-activated protein kinase kinase 4	Directly activate the MAP kinases in response to various environmental stresses or mitogenic stimuli. Ceramides initiate apoptosis by activating MAP2K4 (Verheij et al., 1996), leading to activation of stress-activated protein kinase (SAPK) (Sanchez et al., 1994).
UGCG	UDP-glucose ceramide glucosyltransferase	catalyzes the first glycosylation step in glycosphingolipid biosynthesis from ceramides (Icikawa et al., 1996).

Symbol	Gene	Function
Inflammatory genes		
BCL2	B-cell CLL/lymphoma 2	Exert an anti-apoptotic effect
CASP3	caspase 3	plays a central role in the execution-phase of cell apoptosis
CCL2	chemokine (C-C motif) ligand 2	regulates immunoregulatory and inflammatory processes
IkBα	nuclear factor of kappa light polypeptide gene enhancer in B-cells inhibitor, alpha	inhibitor of NFKB signalling which prevent nuclear migration of p65:p50 heterodimer
IKKG	inhibitor of kappa light polypeptide gene enhancer in B-cells, kinase gamma	activates NF-kappaB resulting in activation of genes involved in inflammation, immunity, cell survival (Marra et al., 2007)
IL6	interleukin 6	induces a transcriptional inflammatory response through interleukin 6 receptor, alpha
PDGFB	platelet-derived growth factor beta	Regulates cell growth and division.
TGFB1	Transforming growth factor, beta 1	Profibrogenic cytokines that activates action the hepatic stellate cells and caused ECM accumulation (Gressner & Weiskirchen, 2006)
TGFBR1	transforming growth factor, beta receptor 1	TGFB1 binds to TGFBR1 to exert its effect
TGFBR2	transforming growth factor, beta receptor II	regulate the transcription genes related to cell proliferation
TNFRSF1B	tumor necrosis factor receptor superfamily, member 1B	Mediates anti-apoptotic effect.
TNFα	tumor necrosis factor (TNF superfamily, member 2)	Regulates cell proliferation, differentiation, apoptosis, lipid metabolism, and coagulation.
Hepatic stellate cells activation, fibrosis and regeneration genes		
FGF2	fibroblast growth factor 2	Promotes mitogemic, angiogenesis and stellate cells activation
KLF6	Kruppel-like factor 6	tumor suppressor effects
MMP1	Matrix metalloproteinase 1	was expressed in human HSCs when plated on matrigel surface (Znoyko et al., 2006)
MMP2	Matrix metalloproteinase 2	Secreted by activated HSCs and caused ECM breakdown, promotes fibrosis (Preaux et al., 1999)
MMP9	Matrix metalloproteinase 9	Secreted by activated kupffer cells and caused ECM breakdown (Preaux et al., 1999)
MMP13	matrix metalloproteinase 13	Was expressed in human L190 HSC cell line (Migita et al., 2005)
PTGS2	Prostaglandin-endoperoxide synthase 2	Promotes prostaglandin biosynthesis & involved in inflammation and mitogenesis
RBP4	retinol binding protein 4, plasma	translocating retinol from the liver stores to the peripheral tissues

Symbol	Gene	Function
Hepatic stellate cells activation, fibrosis and regeneration genes		
RELN	Reelin	control cell-cell interactions critical for cell positioning and neuronal migration during brain development
SPP1	secreted phosphoprotein 1	Promotes cell-matrix interaction
TIMP1	TIMP metallopeptidase inhibitor 1	inhibitors of the matrix metalloproteinases (MMPs) and prevent cell apoptosis
TIMP2	TIMP metallopeptidase inhibitor 2	inhibitors of the matrix metalloproteinases (MMPs) and prevent cell apoptosis
VEGFA	vascular endothelial growth factor A	mediates vascular permeability, inducing angiogenesis, vasculogenesis and endothelial cell growth, promoting cell migration, and inhibiting apoptosis
Endoplasmic reticulum stress genes		
DDIT3	DNA-damage-inducible transcript 3	Regulator induced by ER stress and a key factor in the ER stress mediated apoptosis pathway.
ERN1	Endoplasmic reticulum to nucleus signalling 1	possesses intrinsic kinase activity and an endo-ribonuclease activity and it is important in altering gene expression as a response to endoplasmic reticulum-based stress signals
XBP1	X-box binding protein 1	regulates the expression of genes important to the proper functioning of the immune system and in the cellular stress response

Table 4.2 above indicates the 92 target gene selected. 4 of these genes showed no amplification in any of the experimental samples (IL6, PDGFB, MMP1 and MMP13) and 56 showed no significant differences between groups. All the target genes were normalised using the geometric mean of the reference genes (ABL1, HPRT1, MRPL19 and 18Srna). Quantitation of gene expression was calculated using the ΔΔCT method (Hughes & Moody, 2007).

The gene expressions were analysed using SPSS 16 software, where One-way ANOVA with a Bonferroni Post Hoc test was used to analyse the results. Gene expression patterns were further analysed using Ingenuity Pathway Analysis (IPA) to identify the molecular pathways involved as shown in Appendix 2.

4.3. Taqman Low density array gene expression in human liver

4.3.1. Taqman low density array gene expression in normal liver, NAFLD & NASH patients

Table 4.3: Comparison of gene expression levels in normal liver, NAFLD & NASH samples measured using Low density Taqman arrays.

Genes/ Group	Normal Liver (N = 7)	NAFLD (N = 7)	NASH (N = 22)	P value
Adipogenic gene				
CEBPα	**1.910 ± 0.367[b]**	**2.465 ± 0.229[c]**	**0.809 ± 0.096[b,c]**	**0.001[b]; 0.000[c]**
Adipsin	**1.361 ± 0.182[b]**	**0.894 ± 0.143[c]**	**0.462 ± 0.059[b,c]**	**0.000[b]; 0.026[c]**
Lipid Metabolism				
ChREBP	1.027 ± 0.197	**0.847 ± 0.145[c]**	**1.575 ± 0.138[c]**	**0.019[c]**
ME1	**0.461 ± 0.047[b]**	0.804 ± 0.161	**1.549 ± 0.228[b]**	**0.016[b]**
THRSP	**0.642 ± 0.085[a]**	**1.416 ± 0.139[a]**	1.137 ± 0.111	**0.018[a]**
Glucose Metabolism				
G6PC	**3.958 ± 0.929[a,b]**	**0.818 ± 0.145[a]**	**0.717 ± 0.171[b]**	**0.000[a,b]**
PGM1	**0.341 ± 0.082[b]**	**0.372 ± 0.031[c]**	**1.355 ± 0.187[b,c]**	**0.007[b]; 0.009[c]**
UCP2	**36.481 ± 4.063[b]**	**25.638 ±10.473[c]**	**1.406 ± 0.419[b,c]**	**0.000[b]; 0.001[c]**
Inflammatory, apoptosis, cell proliferation markers				
TGFβ1	**1.899 ± 0.177[a,b]**	**1.147 ± 0.272[a]**	**0.637 ± 0.082[b]**	**0.022[a]; 0.000[b]**
TGFβR1	**1.369 ± 0.152[b]**	1.021 ± 0.189	**0.752 ± 0.111[b]**	**0.022[b]**

(a: Normal liver Vs NAFLD; b: Normal liver Vs NASH; c: NAFLD Vs NASH) Data are presented as mean ± S.E.M.

In NAFLD patients, CEBPα and THRSP showed a significant increased compared to NASH and normal liver. Meanwhile in NASH patients; ChREBP, ME1 and PGM1 expression were increased whereas there was a significant reduction in CEBPα, Adipsin, G6PC, UCP2, TGFB1 and TGFBR1compared to NAFLD patients. All the other gene expressions were highlighted as shown in figures in over leaf.

4.3.2. Taqman low density array FABP4 and FASN gene expression in normal liver, NAFLD & NASH patients

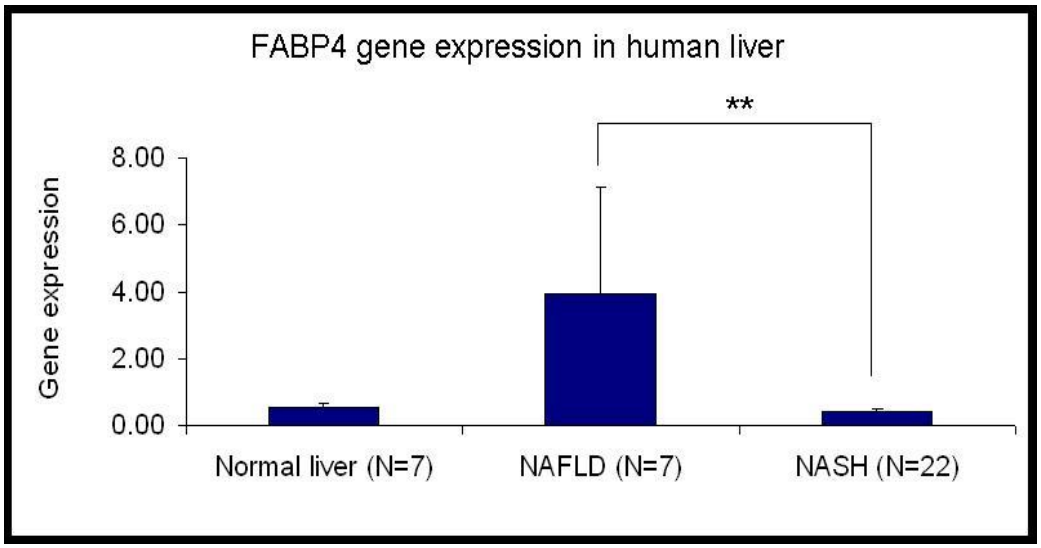

Figure 4.4: FABP4 gene expression in normal liver, NAFLD and NASH. Data are presented as mean ± S.E.M. (N= number of patients; * p<0.05; **p<0.01; ***p<0.000).

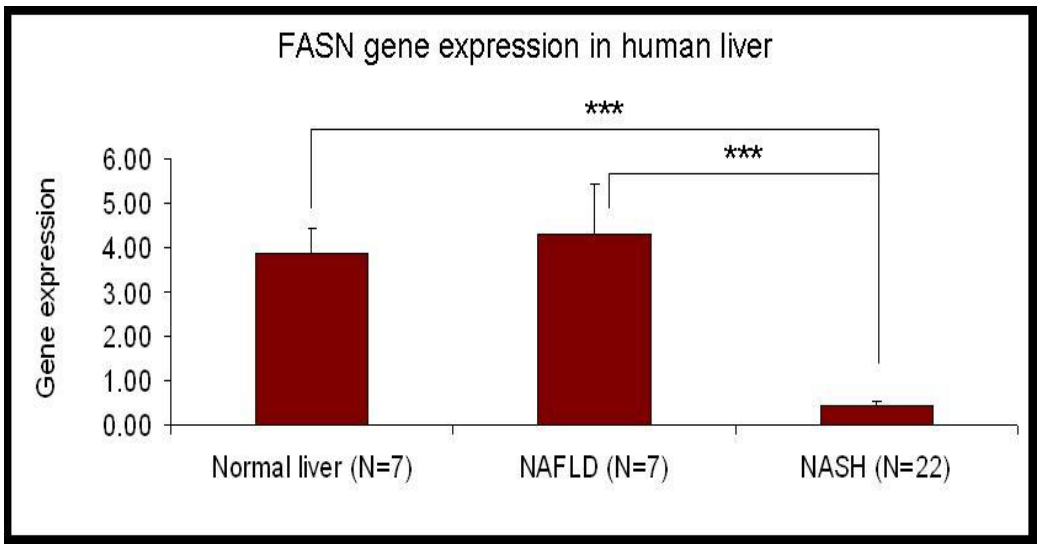

Figure 4.5: FASN gene expression in normal liver, NAFLD and NASH. Data are presented as mean ± S.E.M. (N= number of patients; * p<0.05; **p<0.01; ***p<0.000).

FABP4 gene expression was increased significantly in NAFLD patients compared to NASH patients. Meanwhile in NASH patients, FASN gene expression showed significant reduction compared to normal liver and NAFLD patients.

4.3.3. Taqman low density array ACSL4 and PXR gene expression in normal liver, NAFLD & NASH patients

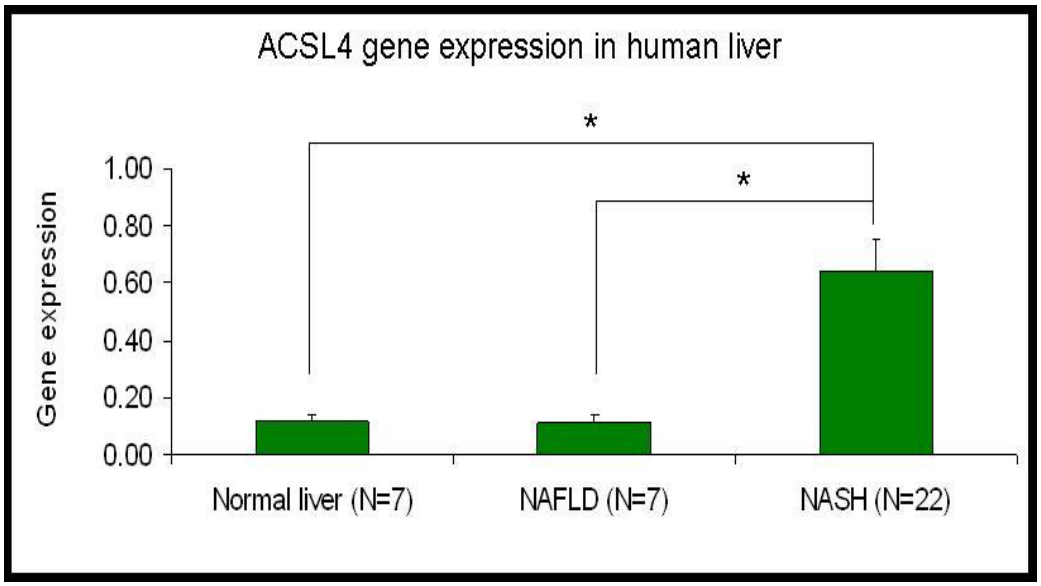

Figure 4.6: ACSL4 gene expression in normal liver, NAFLD and NASH. Data are presented as mean ± S.E.M. (N= number of patients; * p<0.05; **p<0.01; ***p<0.000).

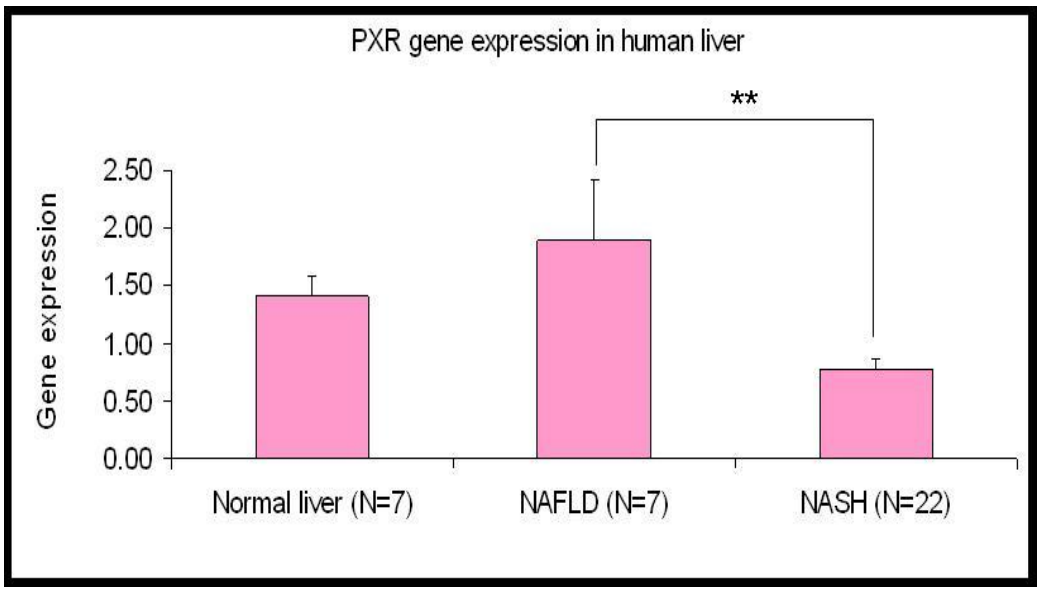

Figure 4.7: PXR gene expression in normal liver, NAFLD and NASH. Data are presented as mean ± S.E.M. (N= number of patients; * p<0.05; **p<0.01; ***p<0.000).

ACSL4 gene expression was elevated in NASH patients compared to normal liver and NAFLD patients. Meanwhile, PXR gene expression was increased in NAFLD compared to NASH patients.

4.3.4. Taqman low density array TNFα and TNFRSF1B gene expression in normal liver, NAFLD & NASH patients

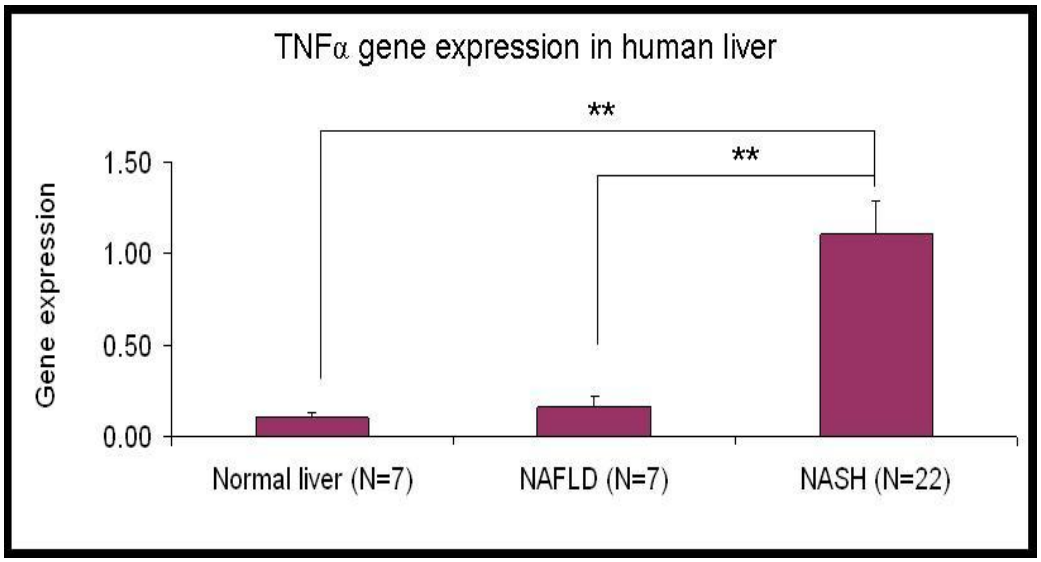

Figure 4.8: TNFα gene expression in normal liver, NAFLD and NASH. Data are presented as mean ± S.E.M. (N= number of patients; * p<0.05; **p<0.01; ***p<0.000).

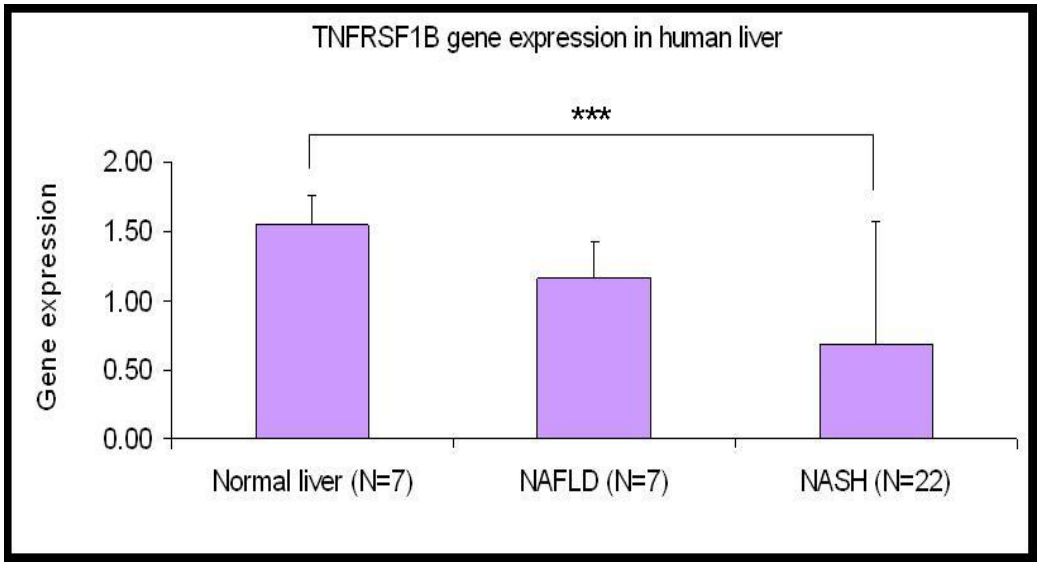

Figure 4.9: TNFRSF1B gene expression in normal liver, NAFLD and NASH. Data are presented as mean ± S.E.M. (N= number of patients; * p<0.05; **p<0.01; ***p<0.000).

TNFα gene expression was elevated in NASH compared to NAFLD and normal liver group. Meanwhile, TNFRSF1B gene expression was reduced in significantly in NASH compared to normal liver group.

4.3.5. Taqman low density array BCL2 and XBP1 gene expression in normal liver, NAFLD & NASH patients

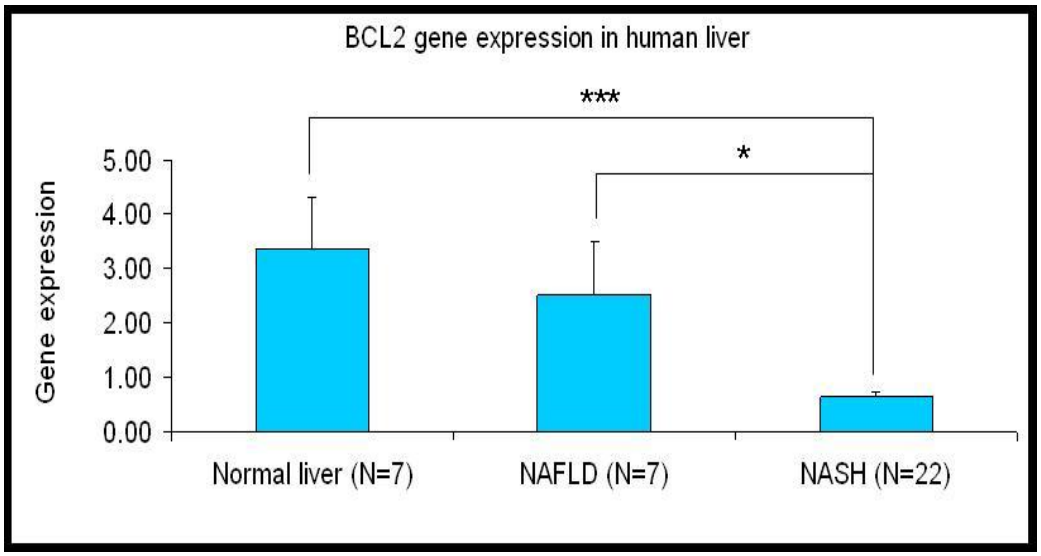

Figure 4.10: BCL2 gene expression in normal liver, NAFLD and NASH. Data are presented as mean ± S.E.M. (N= number of patients; * p<0.05; **p<0.01; ***p<0.000).

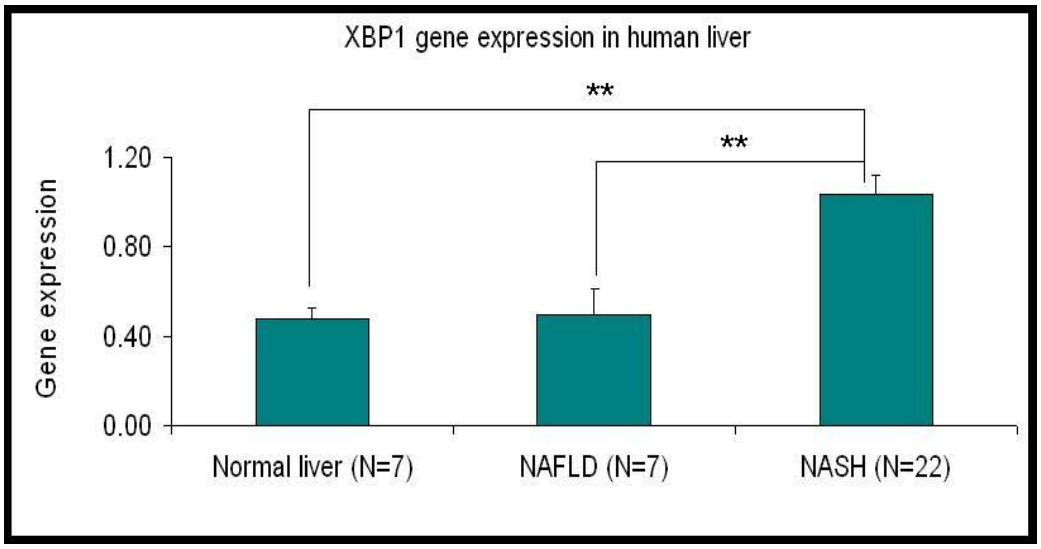

Figure 4.11: XBP1 gene expression in normal liver, NAFLD and NASH. Data are presented as mean ± S.E.M. (N= number of patients; * p<0.05; **p<0.01; ***p<0.000).

BCL2 gene expression was reduced significantly in NASH compared normal liver and NAFLD patients. Meanwhile, XBP1 which is a marker of ER stress was elevated in NASH patients compared to normal liver and NAFLD patients.

4.4. Taqman Low density array gene expression in Pre-trial/NASH treated patients

4.4.1. Taqman low density array gene expression in Pre-trial/NASH, Pioglitazone and placebo treated NASH patients

Table 4.4: Effects of 12 months treatment of Pioglitazone or Placebo on gene expression measured using Taqman low density arrays.

Genes /Group	NASH/Pretrial (N = 22)	Pioglitazone (N = 13)	Placebo (N = 11)	P value
Lipid Metabolism				
ACC2	**1.284 ± 0.150[b]**	1.868 ± 0.241	**0.656 ± 0.085[b]**	**0.045[b]**
ADIPOR2	**0.921 ± 0.171[b]**	0.846 ± 0.140	**0.350 ± 0.060[b]**	**0.048[b]**
HMGCS2	**1.510 ± 0.348[b]**	1.106 ± 0.183	**0.257 ± 0.046[b]**	**0.033[b]**
Glucose Metabolism				
GPD1	**1.063 ± 0.108[b]**	1.148 ± 0.146	**0.637 ± 0.093[b]**	**0.044[b]**
PPAP2C	**0.399 ± 0.099[b]**	0.227 ± 0.036	**1.081 ± 0.344[b]**	**0.024[b]**
Nuclear receptors				
LXRα	**1.251 ± 0.120[a]**	**1.892 ± 0.302[a]**	0.898 ± 0.110	**0.042[a]**
PXR	**0.776 ± 0.101[a]**	**1.453 ± 0.255[a]**	0.657 ± 0.104	**0.010[a]**
PGC1α	**0.747 ± 0.133[a]**	**1.986 ± 0.570[a]**	0.364 ± 0.081	**0.012[a]**
RXRα	**1.191 ± 0.130[a]**	**1.977 ± 0.240[a]**	0.898 ± 0.092	**0.003[a]**
Inflammatory markers				
TNFα	**1.103 ± 0.179[b]**	0.543 ± 0.173	**0.544 ± 0.119[b]**	**0.048[b]**
TNFRSF1B	**0.688 ± 0.088[a]**	**1.310 ± 0.312[a]**	0.614 ± 0.127	**0.037[a]**
IkBα	**1.040 ± 0.103[a]**	**2.082 ± 0.265**[a]	0.654 ± 0.092	**0.000[a]**

(a: Pre-trial Vs Pioglitazone; b: Pre-trial Vs Placebo) Data are presented as mean ± SEM

Pioglitazone treatment induced up-regulation of LXRα, PXR, PPARGC1α, RXRα, TNFRSF1B and IkBα. Meanwhile in the placebo group, up regulation PPAP2C was observed followed by a reduction in ACC2, ADIPOR2, HMGCS2, GPD1 and TNFα as compared to pre-trial samples. There other gene expressions were highlighted in figures showed in over leaf.

4.4.2. Taqman low density array ACADVL and UCP2 gene expression in Pre-trial, Pioglitazone and placebo treated NASH patients

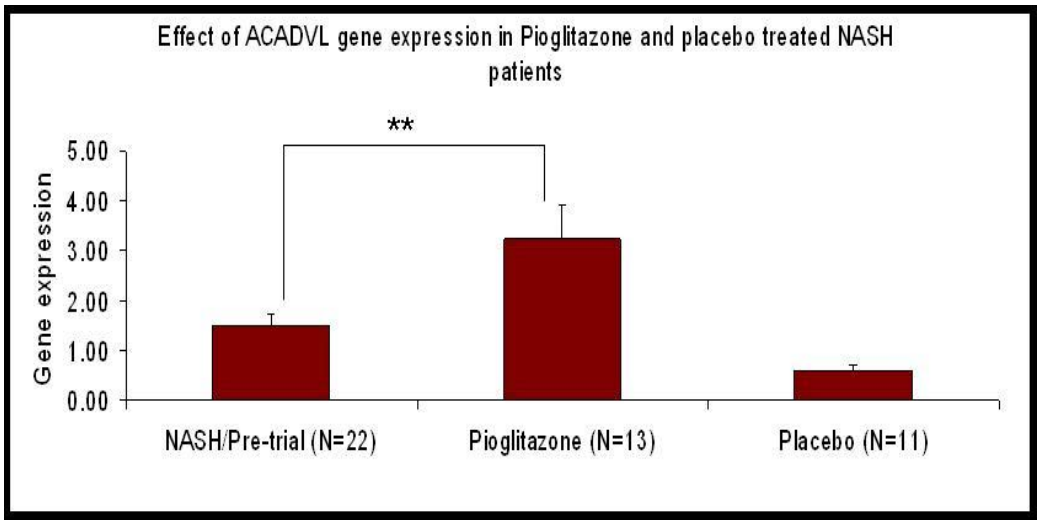

Figure 4.12: ACADVL gene expression in Pre-trial/NASH, Pioglitazone and placebo treated NASH patients. Data are presented as mean ± S.E.M. (N= number of patients; * p<0.05; **p<0.01; ***p<0.000).

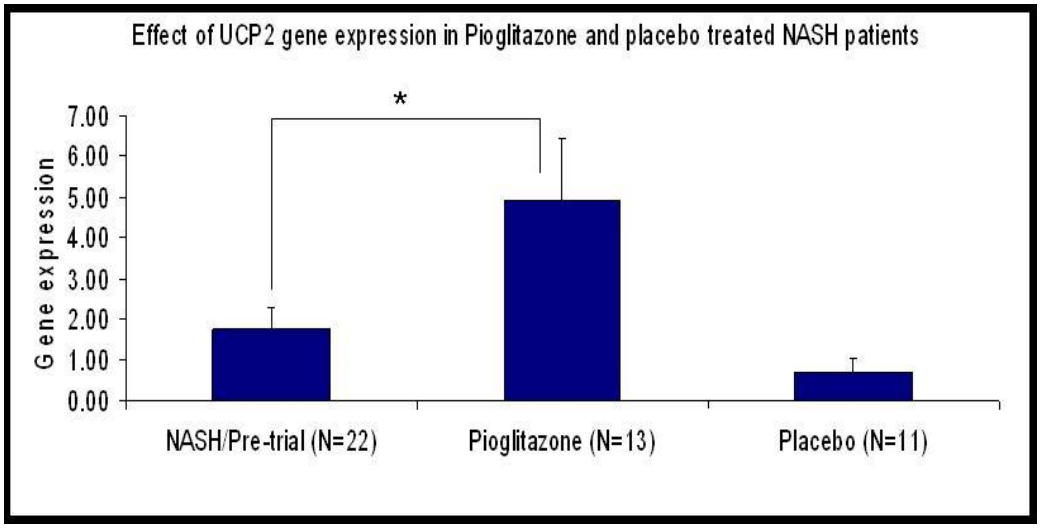

Figure 4.13: UCP2 gene expression in Pre-trial/NASH, Pioglitazone and placebo treated NASH patients. Data are presented as mean ± S.E.M. (N= number of patients; * p<0.05; **p<0.01; ***p<0.000).

ACADVL and UCP2 gene expressions were increased significantly compared pre-trial NASH patients.

4.4.3. Taqman low density array APOE and PPAR β gene expression in Pre-trial, Pioglitazone and placebo treated NASH patients

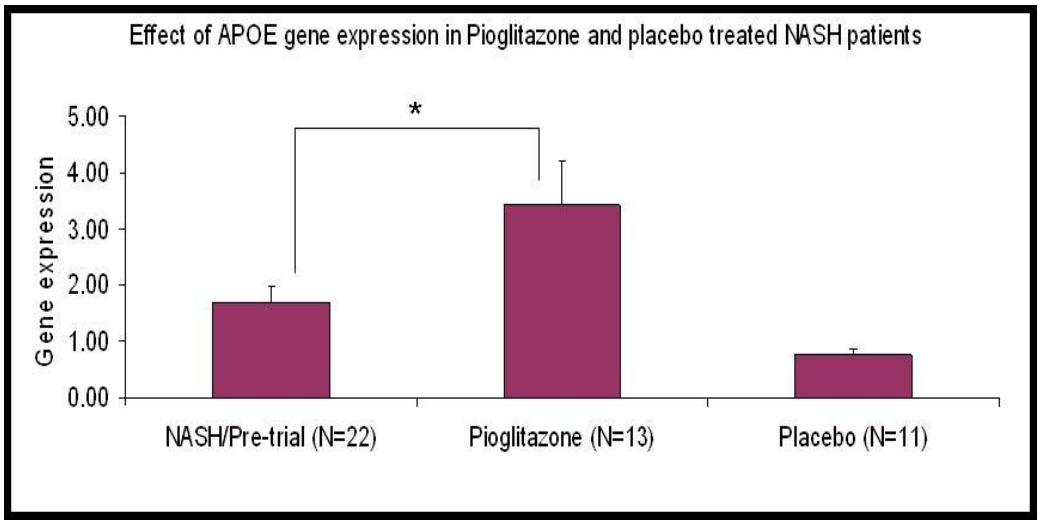

Figure 4.14: APOE gene expression in Pre-trial/NASH, Pioglitazone and placebo treated NASH patients. Data are presented as mean ± S.E.M. (N= number of patients; * p<0.05; **p<0.01; ***p<0.000).

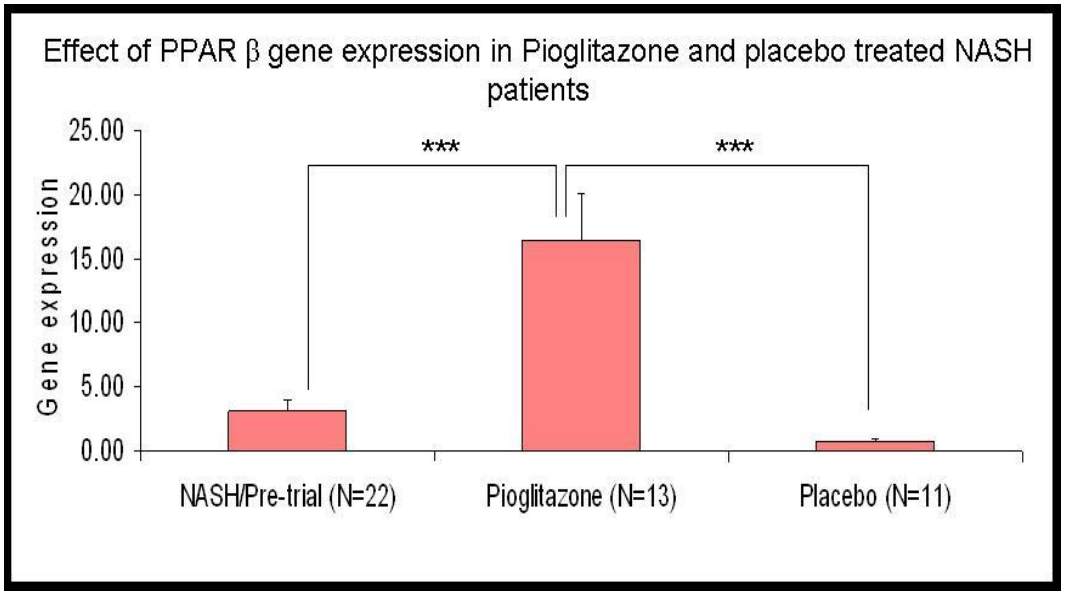

Figure 4.15: PPAR β gene expression in Pre-trial/NASH, Pioglitazone and placebo treated NASH patients. Data are presented as mean ± S.E.M. (N= number of patients; * p<0.05; **p<0.01; ***p<0.000).

APOE and PPAR β gene expressions were increased significantly compared pre-trial NASH patients.

A most striking and unexpected result of this analysis was the increase in PPAR β expression induced by PGZ. Both the size of the fold increase in expression and the relatively large standard error made this result require further investigation. Therefore, the PPAR β expression analysis was repeated using conventional Taqman Real-time PCR using different, custom designed primers and probe (Table 4.5 and Figure 4.16).

Table 4.5: PPAR β gene expression levels in human liver measured using conventional Taqman Real-Time PCR in normal liver, NAFLD and NASH.

Group/ Gene	Normal liver (N=7)	NAFLD (N=7)	NASH (N=22)	P value
PPAR β	0.862 ± 0.196	0.588 ± 0.103	0.718 ± 0.111	NS

Gene expression values are normalised with reference gene (β- actin). Data are presented as mean ± SEM. (a: Normal liver Vs NAFLD; b: Normal liver Vs NASH; c: NAFLD Vs NASH)

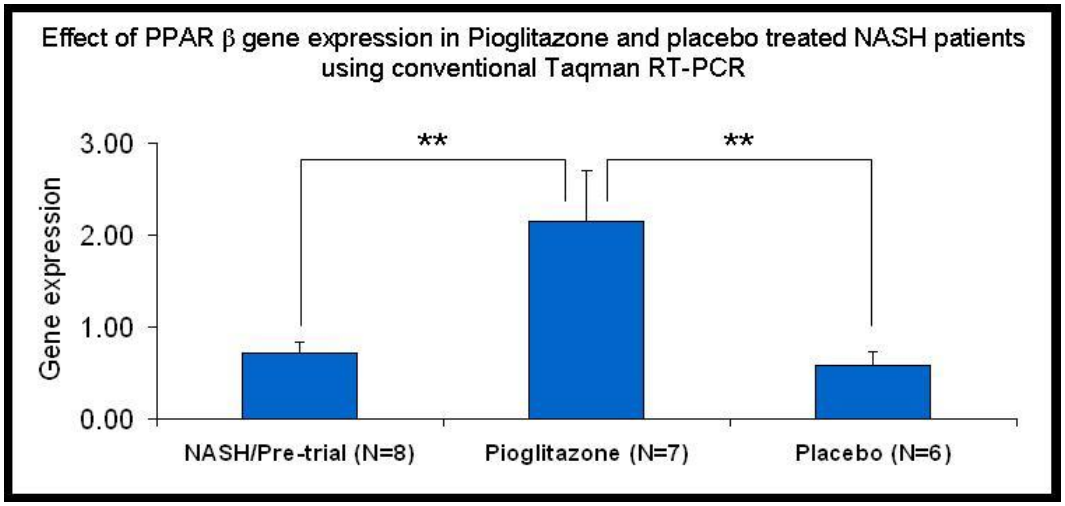

Figure 4.16: PPAR β gene expression in Pre-trial/NASH, Pioglitazone and placebo treated NASH patients. Gene expression values are normalised with reference gene (β-actin). Data are presented as mean ± S.E.M. (N= number of patients; * $p<0.05$; **$p<0.01$; ***$p<0.000$).

There are no differences in PPARβ expression between normal liver, NAFLD and NASH samples. The differences in expression between the Pretrial and PGZ group was smaller (3 fold as compared to 5 fold) using the second Taqman assay. However this second analysis confirms the stimulation effects of PGZ upon PPAR β expression.

4.5. Discussion

Pioglitazone treatment appeared to increase the expression of lipogenic transcriptional factors as determined by Taqman real time PCR but the genes under the control of these transcription factors were not altered. Hence, custom Taqman low density arrays were used to analyse the effects of PGZ. All the target genes were normalised using the geometric mean of the control genes (ABL1, HPRT1, MRPL19 and 18sRNA) using the ΔΔCT quantitation method. Using this technique, several genes did not amplify (MMP1, MMP13, PDGFB and IL6). The reason for the lack of detection of these genes is not clear; it may be due to design faults in the primer/probe set or lack of expression of these genes in human liver.

A previous study has shown that IL6 was expressed in human hepatocellular carcinoma patients (Chew et al., 2010); meanwhile PDGFB was also detected in hepatitis C recurrent transplant patients (Ben-Ari et al., 2006). MMP1 was expressed in human liver myofibroblast cells during fibrosis (Znoyko et al., 2006) and MMP13 in L190 human HSCs line (Migita et al., 2005). Further study is required in order to confirm the current findings of undetermined expression.

4.5.1. Normal liver, NAFLD and NASH

In NAFLD patients, adipogenic gene expression (CEBPα, FABP4, and Adipsin) was found higher compared to NASH patients. All these genes not only promote fat accumulation in the liver but also maintain the adipogenic phenotype of stellate cells reducing inflammation and fibrosis in these patients (Larter et al., 2008). FASN catalyses last step of fatty acid synthesis and was elevated in human NAFLD but not in NASH samples. An increase in FASN expression in both human and animal models of steatosis did not induce inflammation (Dorn et al., 2010). Therefore this current study further supports the notion that that fat accumulation does not directly cause liver injury in NAFLD patients.

ACSL4 is a gene that controls the unesterified arachidonic acid level in cells (Younossi et al., 2005; Hertz et al., 1998). Younossi et al. (2005) reported that both ACSL4 and α-fetoprotein (AFP) gene expression was higher in NASH compared to steatosis patients. AFP is a serum marker of Hepatocellular carcinoma (HCC) diagnosis (Younossi et al., 2005; Magee et al., 1998). ASCL4 is also highly expressed in hepatocellular carcinoma (HCC) (Magee et al., 1998). ACSL4 was also up-regulated in NASH patients compared NAFLD in this study, this indicate that NASH patients maybe at risk of developing HCC, and that NASH is effectively a pre-cancerous state (Hashimoto & Tokushige, 2011).

ChREBP is a transcription factor that regulates lipogenesis in response to increased cellular carbohydrate (Dentin et al., 2004). The Ob/Ob mouse is an animal model of NAFLD, wherein these mice are hyperphagic, hyperinsulinemic, hyperlipidemic and hyperglycemic. Excessive accumulations of fat exacerbate insulin signalling in the liver leading to hepatic steatosis and insulin resistance (Postic et al., 2007). ChREBP expression was increased in Ob/Ob mice (Dentin et al., 2006). Both SCD1 and GPAT gene expression were reduced followed by up regulation of CPT1 gene expression in Ob/Ob mice with ChREBP inhibition. This condition indicates that the inhibition of ChREBP decreased TG synthesis and increased fat oxidation. ChREBP knockdown in Ob/Ob mice, improved insulin signalling by restoration of Akt and Foxo1 phosphorylation by insulin (Dentin et al., 2006). In this study, the ChREBP level was increased in NASH patients compared to NAFLD patients, indicating that increased in ChREBP leads to decreased in insulin sensitivity.

ME1 is cytosolic NADP-dependent enzyme that generates NADPH for fatty acid biosynthesis. ME1 expression has been shown to be up regulated by triiodothyronine (T3) (Yin et al., 2005): in high cholesterol fed mice ME1 is down regulated (Maxwell et al., 2003). SREBP1a and SREBP1c have been reported to activate ME1 expression animal model during lipogenesis (Shimano et al., 1999). In this study, ME1 expression was elevated in NASH

samples compared to normal liver indicating ME1 providing NADPH for fatty acid biosynthesis.

THRSP, otherwise known as S14 expression has been show to be up regulated in the streptozotocin-induced diabetic rat model after insulin and fructose administration. Meanwhile, administration of dibutryl cAMP and theophylline fully blocked the insulin-mediated increase in S14 gene transcription, indicating that hepatic cAMP levels play a negative role in regulating THRSP gene transcription *in vivo* (LaFave et al., 2006; Jump et al., 1990). LaFave et al. (2006) reported that an increased in THRSP expression was associated with an increase in lipogenesis and a concomitant reduction in β-oxidation (LaFave et al., 2006; Perez-Castillo et al., 1987). The elevated level of THRSP in NAFLD patients suggests that fat accumulation in the liver occurs at least in part due to the accumulation of endogenously synthesised triglyceride.

PGM1 expression was elevated in NASH patients compared to NAFLD patients. This enzyme converts glucose 1-phosphate to glucose 6-phosphate at the penultimate step of glycogen breakdown. The elevated levels of PGM1 in NASH would be consistent with increased glucose production by the liver which occurs in insulin resistant states. Whether the development of NASH as distinct from simple lipid accumulation drives hepatic glucose output is not clear. NASH patients have hepatic inflammation and inflammatory states are known to cause insulin resistance. The picture is somewhat complicated by the fact that G6PC expression was found to be lower in NAFLD and NASH as compared to normal liver. G6PC converts glucose-6-phosphate into glucose and is the final step in the breakdown of glycogen and in gluconeogenesis. This observed reduction in G6PC expression is unexpected and given that another key component of the gluconeogenic pathway, PEPCK showed no differences in expression in the samples examined, it is difficult to draw firm conclusions regarding molecular regulation of glucose metabolism in these patients.

UCP2 is a mitochondrial membrane anion carrier that acts as negative regulator of mitochondrial superoxide production (Fleury et al., 1997). In the current study, UCP2 expression was decreased significantly in NASH as compared to normal liver and NAFLD patients. Previous study has reported that mRNA UCP2 expression in the liver was lowered in healthy patients but elevated in NASH patients (Serviddio et al., 2008). Further study need to be done using standard Taqman RT-PCR to confirm the current finding which seem to be in contradiction with previous study.

TNFα expression was up regulated in NASH followed by decreased in TNFRSF1B expression. TNFRSF1B or other wise known as p75 act as an anti-inflammatory cytokine that blocks TNFα regulated inflammatory process (Tilg et al., 2006). TNFRSF1B also mediates an anti-apoptotic effect by forming a heterocomplex with cellular inhibitor of apoptosis (c-IAP) 1 and 2 protein (RefSeq). BCL2 exert an anti-apoptosis effect in normal liver and NAFLD patients, in contrast to NASH patients in this study. Current finding showed that cells are progressing to apoptosis that will further exacerbate the liver injury in NASH as TNFα mediates its action (Rust et al., 2000; Wieckowska et al., 2006).

TGFβ1 inhibit cell proliferation and differentiation in epithelial cell and inhibit extracellular matrix (ECM) synthesis. TGFβ1 exerts its effect by binding on TGFβR1 (Huang & Huang, 2005). In NASH patients, reduction of both TGFβ1 and TGFβR1 promotes cell proliferation of activated cell and increased extracellular matrix synthesis that will further worsen the injury.

PXR is a nuclear receptor that regulates xenobiotic metabolism and has also been shown to have anti-inflammatory and anti fibrotic effects (Mencarelli et al., 2010; Wallace et al., 2010; Wahli, 2008). PXR expression was higher in NAFLD than in NASH. This finding indicates that, NASH patients exhibit inflammation and fibrosis compared to NAFLD patients.

XBP1 is an early marker of endoplasmic reticulum (ER) stress and regulates the unfolded protein response XBP1 has also more recently been shown to be an important regulator in lipogenesis after carbohydrate feeding in

mice. XBP1 deficient mice showed a reduction in ACC2, DGAT2, SCD1 and SREBP2 expression leading to hypocholesterolemia and hypotriglyceridemia (Lee et al., 2008). Rutkowski et al. (2008) have reported that XBP1 activated acute ER stress responses that in turn can lead to hepatic steatosis and disruption of hepatic VLDL secretion (Ota et al., 2008). XBP1 expression was elevated in NASH patients as compared to normal and NAFLD patients. Interestingly other ER stress markers (DDIT3 and ERN1) showed similar expression in all samples. It would be interesting to examine the target genes of the XBP1 transcriptional response to see if they show elevated expression in NASH patients.

Overall in NAFLD patients, fat accumulation exerts a protective effect in the liver from oxidative stress and inflammation as previously shown (Yamaguchi et al., 2007; Listerberger et al., 2003). Meanwhile in NASH patients, upregulation of apoptosis, stellate cell activation and proliferation, followed by oxidative stress and endoplasmic reticulum (ER) stress, exacerbate the liver injury.

4.5.2. Effects of Pioglitazone in non-diabetic NASH patients

Pioglitazone caused elevations of PXR, IkBα and TNFRSF1B expression compared to the pre-trial group. PXR is a xenobiotic activated nuclear receptor that exerts anti-inflammatory and anti fibrotic effects (Mencarelli et al., 2010; Wallace et al., 2010; Wahli, 2008). NFkβ was bound to IkBα and IkBβ in unstimulated cell to prevent nuclear transportation from the cytoplasm (Baldwin, 1996). Specific kinase phosphorylation (viruses, cytokine, and activator of protein kinase C) (Kopp & Gosh, 1995; Siebenlist et al., 1994), causing rapid degradation of IkB subunit by proteosomes (DiDonato et al., 1996; Chen et al., 1996). This action leads NFkB translocation to the nucleus causing activation of proinflammatory cytokine, chemokines (chemotactic cytokine that attract inflammatory cell to site of inflammation) and anti-apoptotic effects (Barnes & Karin, 1997). TNFRSF1B or p75 play a role in blocking TNFα mediates inflammatory response (Tilg et al., 2006). TNFRSF1B has been reported to mediate an anti-apoptotic effect by forming a heterocomplex with cellular inhibitor of apoptosis (c-IAP) 1 and 2 protein

(RefSeq). Overall, PGZ exert an anti-inflammatory and anti-fibrotic effects by up regulating all these markers in non-diabetic NASH patients.

PGC1α is a nuclear receptor co-activator, which increases mitochondrial fat oxidation is skeletal muscle (Miura et al., 2008). PGC1α was reported to activate both PPAR β (Miura et al., 2008) and subsequently ACADVL (Espinoza et al., 2010). ACADVL is a protein that is targeted to the inner mitochondrial membrane where it catalyzes the first step of the mitochondrial fatty acid beta-oxidation pathway. Pioglitazone treatment increased PGC1α, PPAR β and ACADVL suggesting that fatty acid oxidation was increased by pioglitazone treatment. In addition, UCP2 expression was also elevated, which may in turn reduce the ROS production which is associated with increased beta-oxidation.

ChREBP and SREBP1C are transcriptional factors that are regulated by glucose and insulin to promote lipogenesis in the liver (Browning & Horton, 2004). LXR is a ligand activated transcriptional factor that belongs to the nuclear receptor family. LXR regulates cholesterol and bile acid metabolism. The SREBP1C promoter contains an LXR binding site, and SREBP1C expression can be activated in the presence of LXR agonist (Browning & Horton, 2004). ChREBP also has been reported as a direct target of LXR (Cha et al., 2007). PGZ increased the expression of ChREBP, SREBP1C and LXRα in NASH patients, which suggests that de-novo lipogenesis may be increased.

APOE is lipoprotein responsible for VLDL –TG secretion out from the liver to adipose tissue (Mahley & Huang, 1999). APOE deficient mice exhibit higher TG, cholesterol accumulation in the liver (Kuipers et al., 1996). An elevation of APOE in mice liver leads to an increased the VLDL-TG export and also increased the VLDL-APOB production rate. This finding indicates that hepatic APOE influences the number of VLDL particles secreted by the liver (Maugeais et al., 2000). In this study, Pioglitazone treatment up regulates APOE expression indicates that it increased in VLDL-TG secretion out from the liver to the adipose tissue.

Overall, Pioglitazone inhibit both stellate cells activation and cell proliferation. This ligand also exerts an anti-inflammatory effect leading to an improvement liver injury and fibrosis in non-diabetic NASH patients. Pioglitazone treatment also increased β-oxidation, VLDL-TG export out from liver followed by increased lipogenesis, neither of these effects, lead to a change in liver fat content, a finding which is supported by clinical data by Aithal et al. (2008).

4.5.3. Effects observed in placebo treated non-diabetic NASH patients

ACC2 and SREBP1C both regulate lipogenesis in the liver (Browning & Horton, 2004). Meanwhile, ADIPOR2 is an adiponectin receptor that regulates PPARα activity (Welen et al, 2005) and HMGCS2 activates β-oxidation and it also a rate limiting enzyme that control ketogenesis (Younossi et al., 2005). Placebo treated non-diabetic NASH patients shown to reduce both lipogenesis and β-oxidation activity, in regards to down regulation of these genes (ACC2, SREBP1C and HMGCS2). Both conditions also indicate that improve steatosis in placebo treated patients compared to pre-trial group.

Glycerol is produce by lipolysis of adipose tissue; it is also used as substrate in the liver for hepatic gluconeogenesis. GPD1 is responsible for glycerol metabolism (Patsouris et al., 2004). This indicates that gluconeogenesis is decreased in placebo group.

PPAP2C expression was elevated in placebo treated compared to pre-trial group. PPAP2C converts phosphatidic acid into diacylglycerol (DAG) in the liver (Zhang et al., 2000). DAG mediated the activation of protein kinase C (PKCε) in the liver, that may decrease insulin receptor substrate (IRS) tyrosine phosphorylation, PI3K and downstream genes involved in insulin signalling which would then lead to insulin resistance (Samuel, 2011; Erion and Shulman, 2010). Further work is required to elucidate the role of PPAP2C in the pathogenesis of NASH.

CHAPTER 5

Primary Human Hepatic stellate cells culture

5.1. Introduction

Hepatic stellate cells (HSCs) are cells that regulate retinoid acid metabolism by storing vitamin A and are usually located in the perisinusoidal space of disse (Moreira, 2007). Other than that, HSCs are also involved in the regulation hepatic blood flow, portal venous pressure (Friedman et al., 1992) and also maintaining the level of basement membrane matrix secretion of type IV and VI collagen in hepatic sinusoids (Geerts, 2001; Ikeda et al., 2004). Thus, stellate cells play an important role in regulation of hepatic function and morphogenesis.

In quiescent stellate cells, PPAR γ, SREBP1C, LXRα, CEBPα and β are adipogenic genes that are highly expressed (She et al, 2005) (Figure 5.1). These transcription factors will in turn regulate a large number of metabolic and other genes. The expression of these adipogenic genes declines rapidly in stellate cells when exposed to TNFα, TGF-α, β and PDGF or other pro-inflammatory stimuli, leading to transformation into myofibroblasts (MF) (Friedman, 2000; She et al., 2005, Figure 5.1).

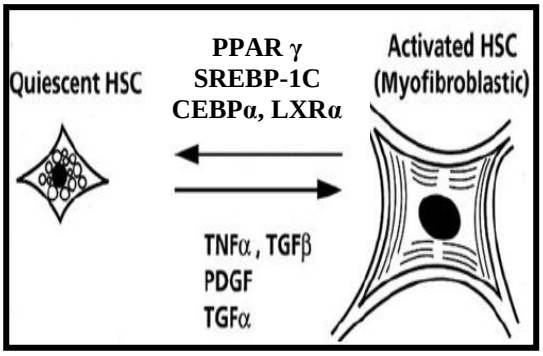

Figure 5.1: Adipogenic transcriptional factors involved in regulating the quiescent phenotype of the hepatic stellate cells. (Adapted from She et al., 2005)

Drug induced liver injury, viral induced hepatitis, metabolic syndrome and obesity can all induce NAFLD / NASH (Iredale, 2007). In the case of injury induced by one or more of the factors mentioned above, liver cells such as hepatocytes and kupffer cells produce reactive oxygen intermediates and inflammatory mediators that will activate HSCs to produce type I and IV collagen and increase HSC proliferation (Friedman, 2000; Maher, 1999).

Injured sinusoidal endothelial cells then release both fibronectin and plasmin that activate stellate cells and transform the inactive form of TGFβ1 to the active, pro-fibrogenic form further promoting fibrogenesis (Friedman, 2000; 1999). Activated HSCs rapidly lose their adipogenic phenotype, followed by an increase in Kruppel-like factor 6 (KLF-6) expressions (Mann & Smart, 2002). KLF-6 activates type 1 collagen production which causes extracellular matrix accumulation (Mann & Smart, 2002). This phase is known as the initiation phase of stellate cell activation (Friedman, 2000).

The next phase of stellate cell activation is perpetuation, where there is an increase in cytokine secretion and activation of the cognate receptor tyrosine kinases (RTKs) as shown as in Figure 5.2. This in turn leads to accelerated extracellular matrix (ECM) remodelling that will worsen liver injury. This process is known as fibrosis. As the degree of liver injury worsens, it will eventually lead to cirrhosis. Fibrosis is thought to be reversible if injurious stimuli are removed or treated (Iimuro & Brenner, 2007) whereas cirrhosis is described as an irreversible process (Friedman, 2000). However a recent study has reported that cirrhosis in HCV patients treated with a combination of α-interferon and Ribavirin may now be reversible (Poynard et al., 2002).

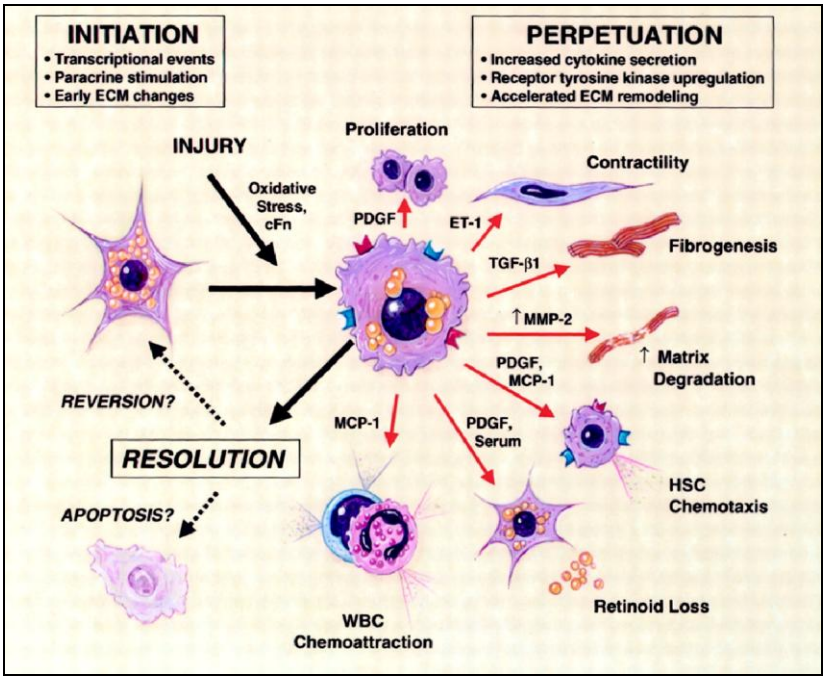

Figure 5.2: Initiation and perpetuation phases of stellate cell activation. (Adapted from Friedman, 2000)

.

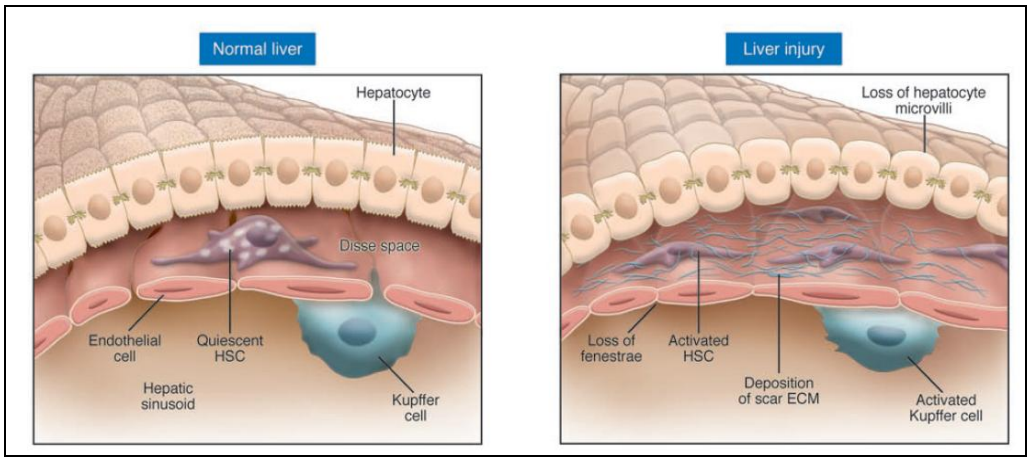

Figure 5.3: Sinusoidal events in the development of liver fibrosis. Injury to hepatocytes results in the recruitment and stimulation of inflammatory cells, as well as the stimulation of resident inflammatory cells (including Kupffer cells). Factors released by these inflammatory cells lead to transformation of HSCs into a myofibroblast-like phenotype. HSC activation leads to accumulation of scar (fibrillar) ECM. The presence of a fibrillar ECM in the Disse space has consequences for hepatocyte function, leading to the loss of microvilli and endothelial fenestrae. Therefore, the loss of normal tissue architecture contributes to impairment of organ function. (Adapted from Iredale, 2007)

Sinusoidal events in liver injury during fibrogenesis are as shown in Figure 5.3. In NAFLD and NASH, stellate cells become activated and proliferate as described in Chapter 3. Activation of these HSCs occurs primarily via increased levels of TNFα, PDGF-BB, TGFβ, TGFα as well as other proinflammatory cytokines (She et al., 2005). PDGF-BB is thought to be the most potent cytokine that causes activated HSCs to proliferate (Paik et al., 2009). Inhibition / reversal of activation of stellate cells and decreased proliferation should reduce fibrosis, associated liver injury, and is therefore an attractive target for therapeutic intervention in NAFLD and NASH.

In vitro cell culture of primary rat (Da Sliva Morais et al., 2007) and human HSCs (Galli et al., 2000) indicate that activation of the adipogenic repertoire of genes by PPAR γ ligands may decrease stellate cell activation (Da Silva Morais et al., 2007) and reduce cell proliferation (Galli et al., 2000). Furthermore, in carbon tetrachloride (CCl_4) induced liver injury in rats, treatment with Pioglitazone (PGZ) reduced αSMA and type 1 collagen production, suggesting that activation of stellate cells and subsequent fibrosis may be reduced by PPAR γ agonists (Kon et al., 2002).

Interestingly, another PPAR isotype, PPAR β has been implicated in stellate cell activation and proliferation (Hellemans et al., 2003) despite evidence of an anti-inflammatory role for this nuclear receptor being described in both Crohn's Disease and ulcerative colitis (Peters et al., 2008; Rival et al., 2002). The role of PPAR β in HSCs is still unclear and requires further study.

A variety of other nuclear receptors including LXRα (She et al., 2005) and PXR (Wright, 2006) are known to be expressed in quiescent HSCs. These are also potential targets for treatment of NAFLD and NASH as their activation has been shown to decrease inflammation and immune cell activation (Wallace et al., 2010; Scholz et al., 2009). Data from existing HSC culture experiments are complicated by the range of culture conditions and number of passages of HSC after initial isolation. This can make inter-experimental comparisons difficult and extrapolation to the phenotype of HSCs *in vivo* highly speculative.

In this chapter, the aims were to examine the effects of culture conditions and length of time in culture upon HSC activation and proliferation rates. Once this was achieved, the effects of nuclear receptor ligands upon stellate cell gene expression and proliferation at various stages at cell culture and activation were studied.

Results:

5.2. Human Hepatic stellate cells cultured on different surfaces

Freshly isolated human hepatic stellate cells (HSCs) were plated either on plastic, collagen type 1 or matrigel coated plates for 1 week. The depth of matrigel cast in the well is about 0.4mm thick. Images were taken and both gene and protein expression were studied as shown overleaf.

Human HSC on plastic surface (Day 1) freshly isolated

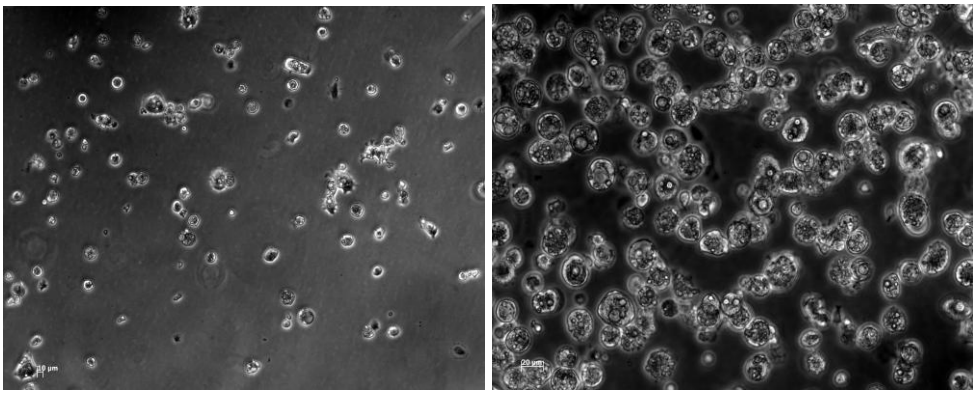

Human HSC on Collagen type 1 surface (Day 1) freshly isolated

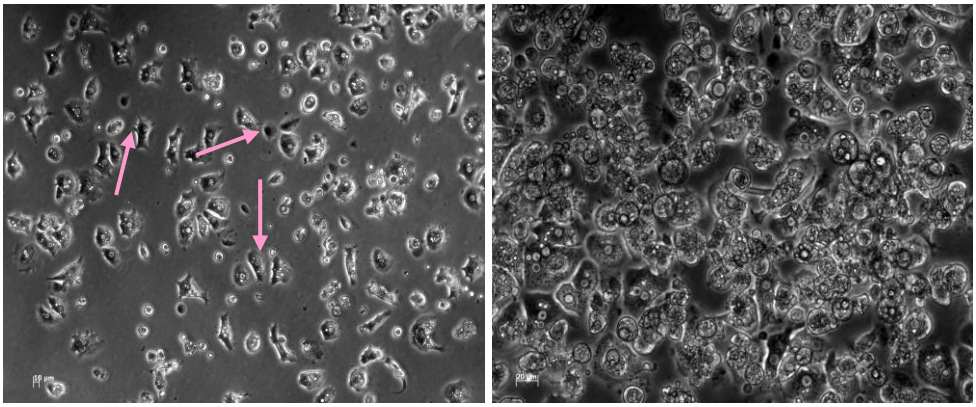

Human HSC on Matrigel surface (Day 1) freshly isolated

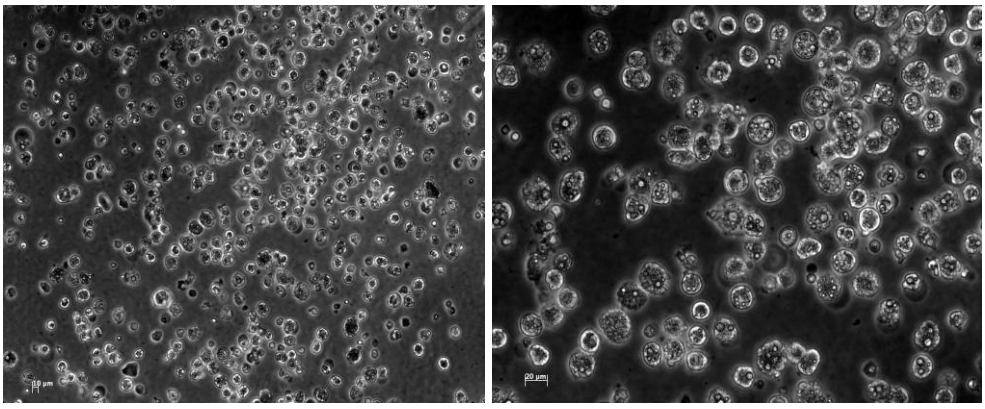

(10X magnification) (20X magnification)

Figure 5.4: Day 1 of human hepatic stellate cells plated on different surfaces. The stellate cells remained round and contain retinol droplets on plastic and matrigel surfaces. HSCs grown on type 1 collagen show some star shaped cell morphology (as shown by pink arrows) indicating the initiation of activation.

Human HSC on plastic surface (Day 4)

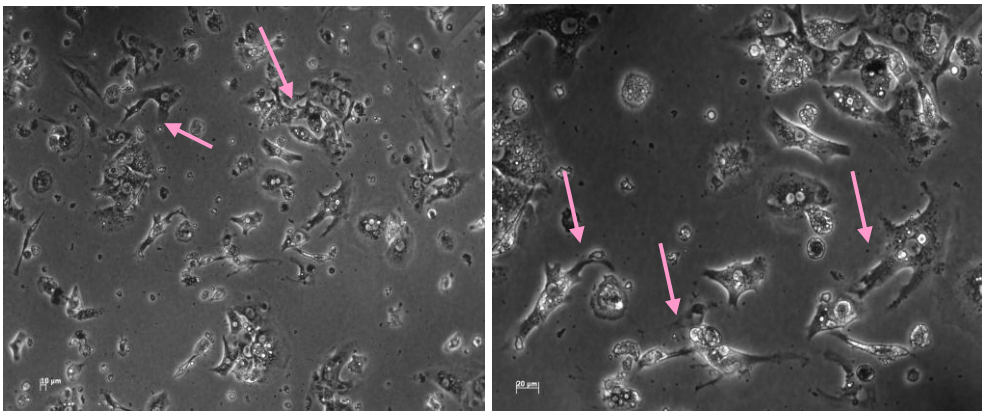

Human HSC on Collagen type 1 surface (Day 4)

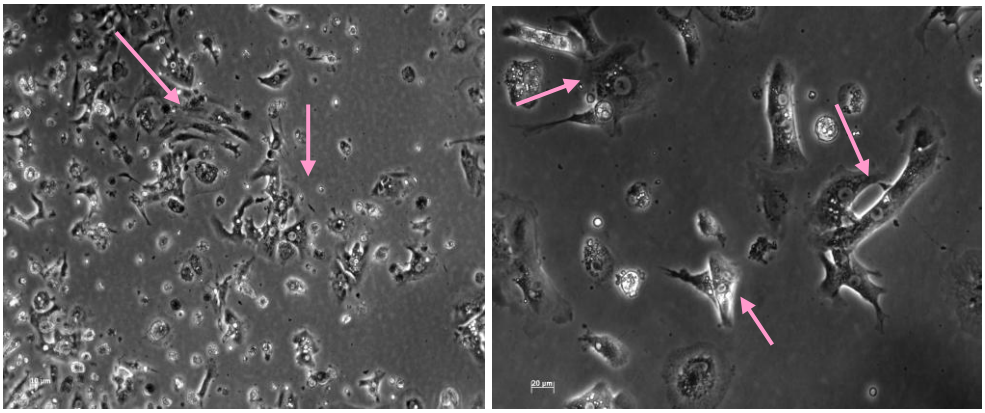

Human HSC on Matrigel surface (Day 4)

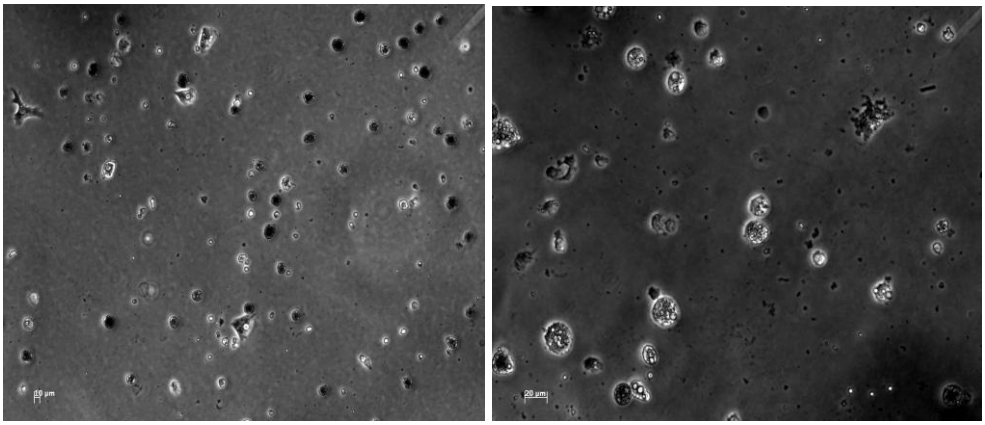

(10X magnification) (20X magnification)

Figure 5.5: Day 4 of human hepatic stellate cells plated on different surfaces. The stellate cells remain round and contain retinol droplets on matrigel. HSCs plated on plastic and collagen now show star shaped cell morphology and are increased in size (as shown by pink arrows).

Human HSC on plastic surface (Day 7)

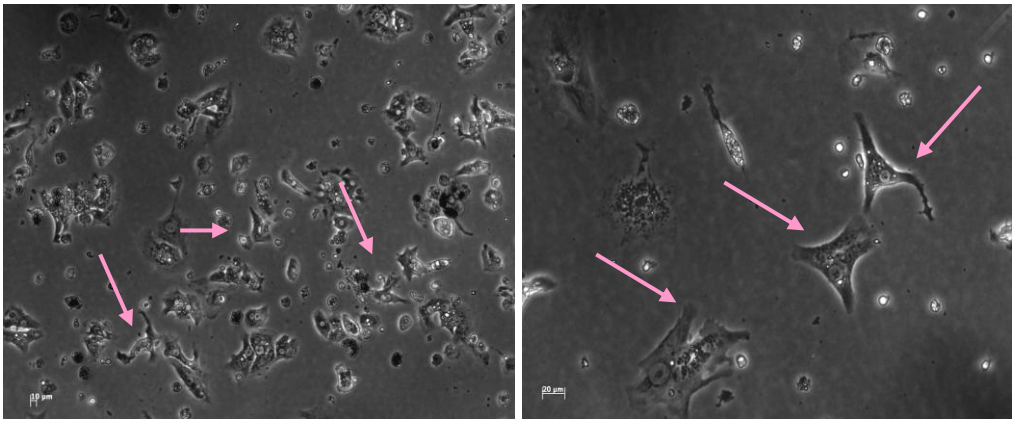

Human HSC on Collagen type 1 surface (Day 7)

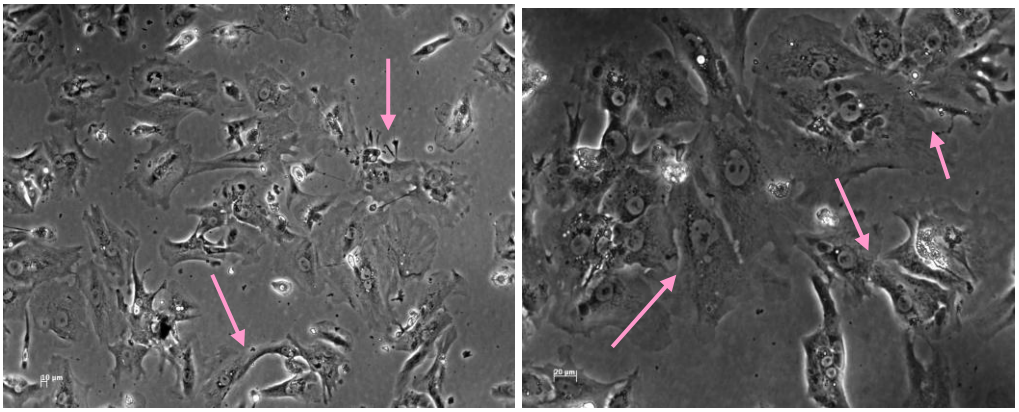

Human HSC on Matrigel surface (Day 7)

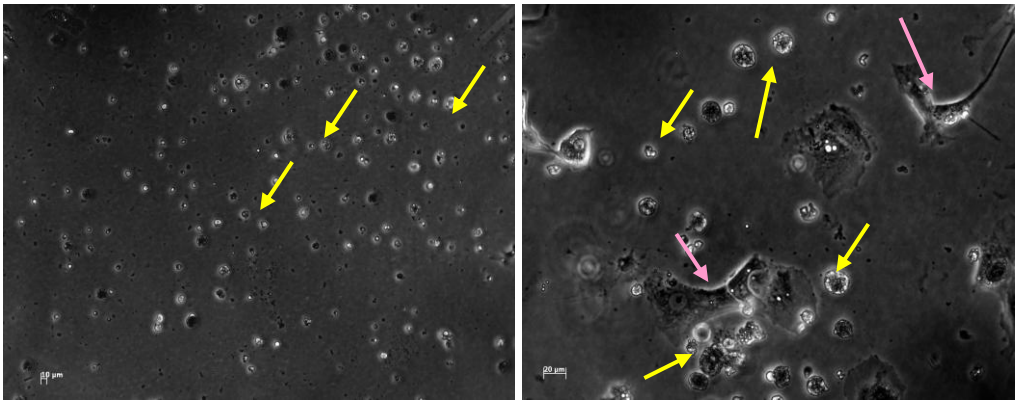

(10X magnification) (20X magnification)

Figure 5.6: Day 7 of human hepatic stellate cells plated on different surfaces. The stellate cells plated on matrigel remain round and contain retinol (as shown by yellow arrows), but some HSCs were activated, possibly due to thinning of the matrigel layer over time (as shown by pink arrows). Cells plated on collagen and plastic have now taken on the classic activated stellate cell star shape (as shown by pink arrows).

5.3. Human Hepatic stellate cells (HSCs) (Day 14) before sub-culturing

HSCs become activated when plated on plastic surfaces as previously reported by Bachem et al. (1992). In a subsequent experiment, freshly isolated human hepatic stellate cells were plated on plastic and cultured for 14 days. The cells were then sub-cultured and plated them on different surfaces (plastic, collagen type 1 and matrigel) for a further 7 days. The aim of this experiment was to observe potential changes in cell morphology; in particular would plating on matrigel reverse cell activation.

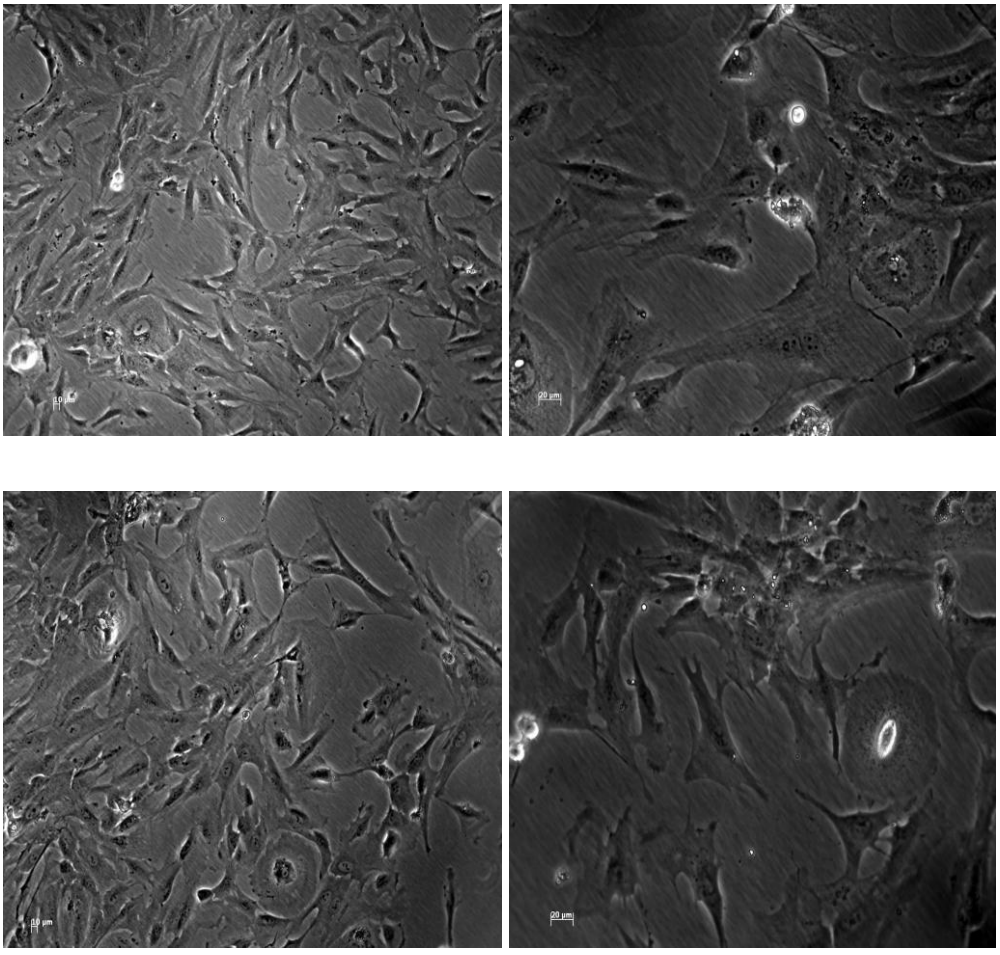

(10X magnification) (20X magnification)

Figure 5.7: Human Hepatic stellate cells (HSCs) (Day 14) before sub-culturing.

Human HSC sub-culture plated on plastic surface (Day 1)

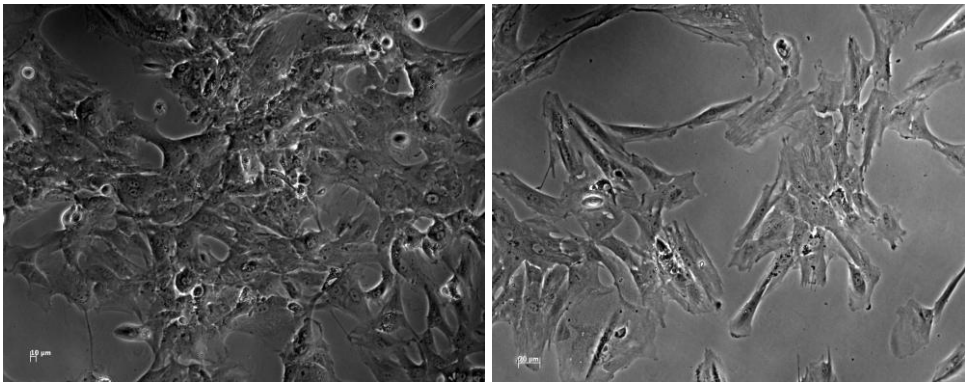

Human HSC sub-culture plated on collagen type 1 surface (Day 1)

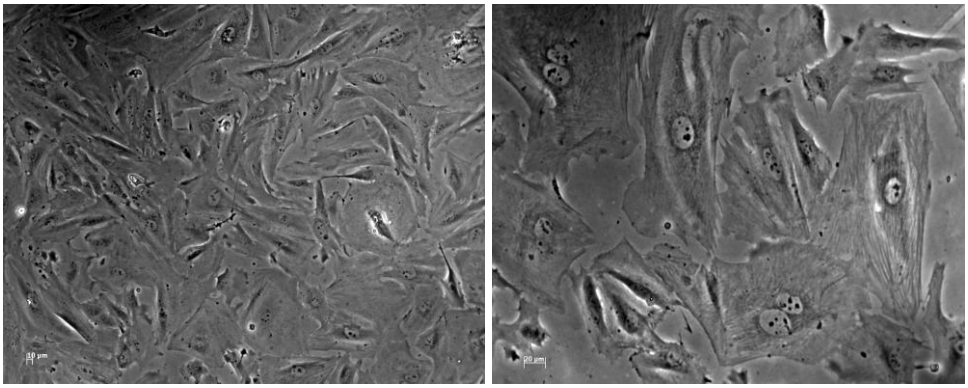

Human HSC sub-culture plated on matrigel surface (Day 1)

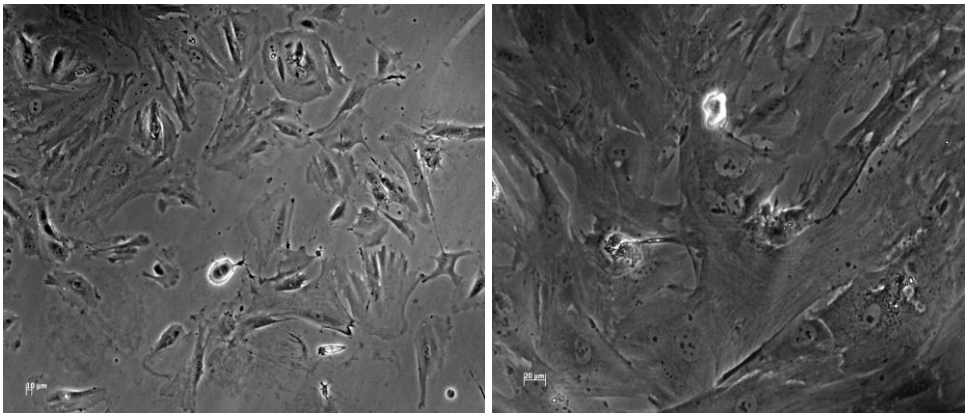

(10X magnification) (20X magnification)

Figure 5.8: Human hepatic stellate plated on different surfaces following sub-culture and day 1 of the culture on new surfaces.

Human HSC sub-culture plated on plastic surface (Day 4)

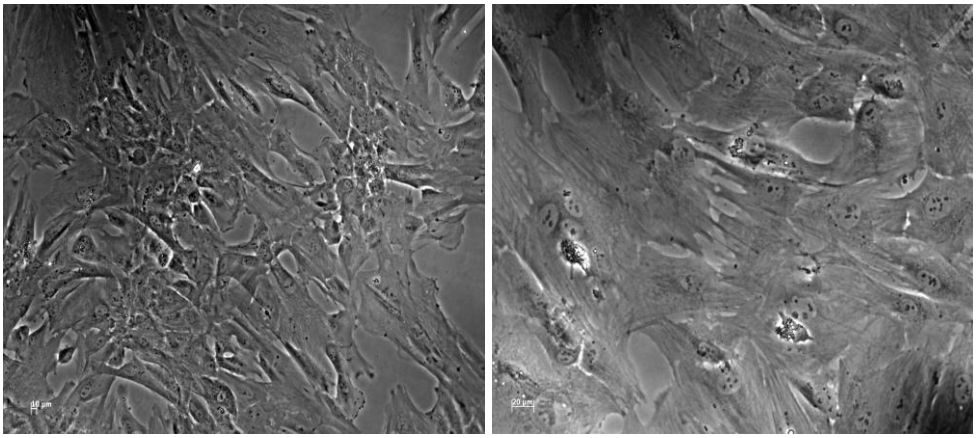

Human HSC sub-culture plated on collagen type 1 surface (Day 4)

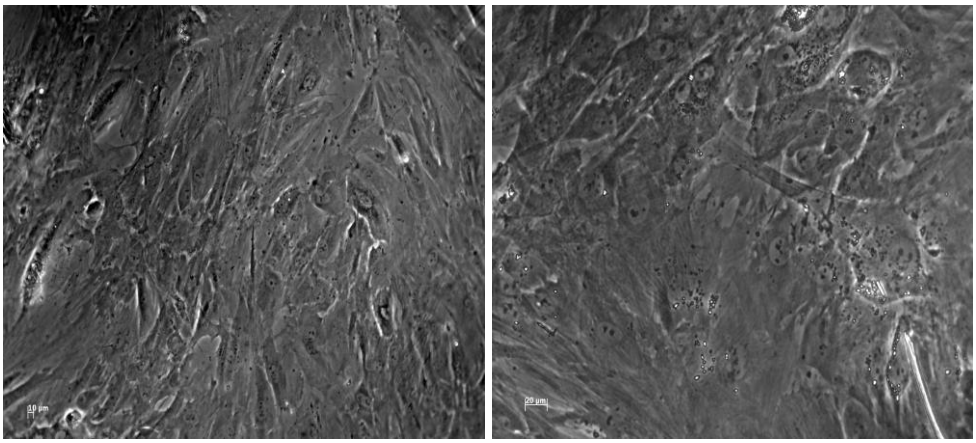

Human HSC sub-culture plated on matrigel surface (Day 4)

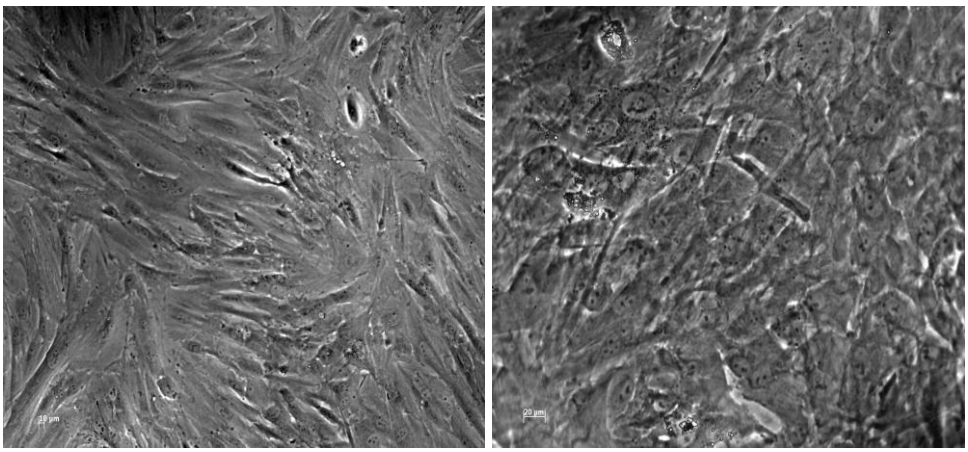

(10X magnification) (20X magnification)

Figure 5.9: Human hepatic stellate plated on different surfaces following sub-culture and day 4 of the culture on new surfaces.

Human HSC sub-culture plated on plastic surface (Day 7)

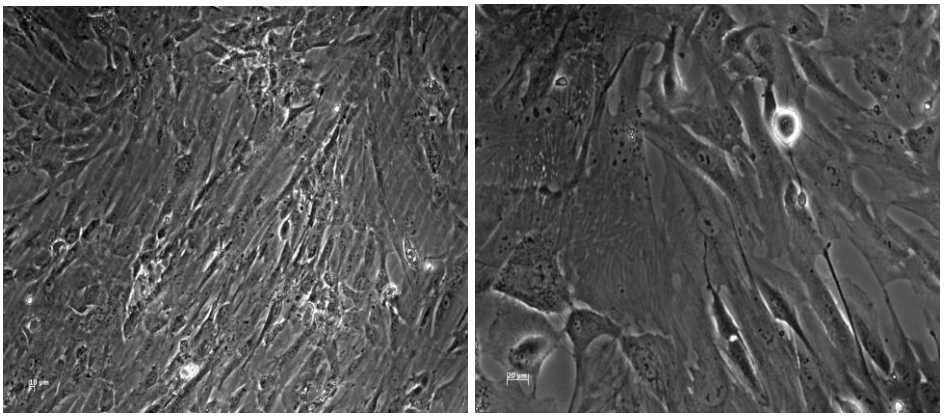

Human HSC sub-culture plated on collagen type 1 surface (Day 7)

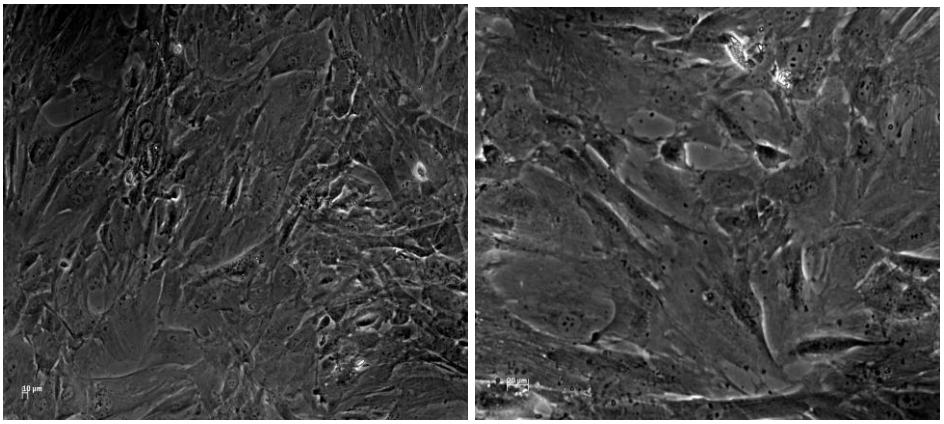

Human HSC sub-culture plated on matrigel surface (Day 7)

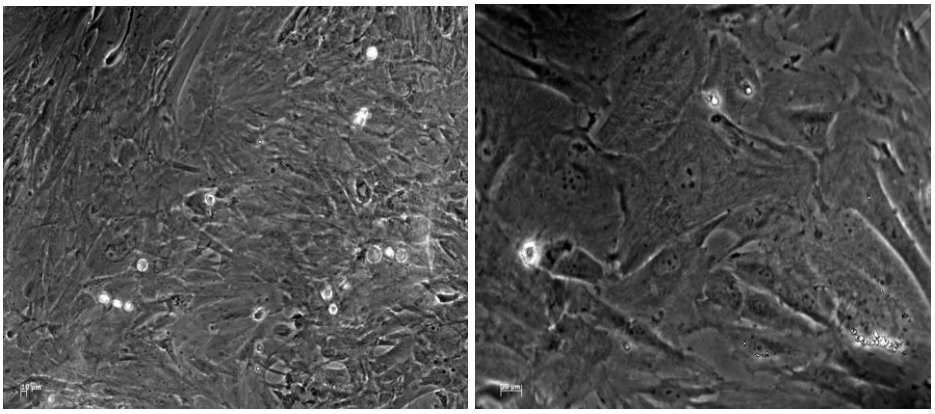

(10X magnification) (20X magnification)Figure 4.10:

Figure 5.10: Human hepatic stellate cells plated on different surfaces following sub-culture and day 7 of the culture on new surfaces. No change in morphology was observed. Therefore, HSC activation is irreversible and does not appear to alter when they are plated on surfaces such as matrigel, which can maintain quiescence in freshly isolated cells.

Subsequent studies focussed on the changes in gene expression associated with changes in HSC phenotype as shown in Table 5.1.

Table 5.1: List of genes included for mRNA expression analysis in this study.

Gene	Abbreviation
Adipogenic Genes	
PPAR γ	Peroxisome proliferator activated receptor γ
SREBP1C	Sterol regulatory element binding protein -1C
CEBPα	CCAT enhancer binding protein α
CEBPβ	CCAT enhancer binding protein β
LXRα	Liver-X-receptor
Fatty Acid Transporters	
CD36	Fatty acid tranlocase
FABP4	Fatty acid binding protein 4
Nuclear Receptors	
PPAR β	Peroxisome proliferator activated receptor β
LXRβ	Liver-X-receptor
PXR	Pregnane-X-receptor
FXR	Farnesoid-X-receptor
HSC Markers	
αSMA	α-smooth muscle actin
CRBP1	Cellular retinol binding protein 1
GFAP	Glial fibrillary acidic protein
CSRP2	Cysteine and glycine-rich protein 2
TGFβ1	Transforming growth factor β1

All the human hepatic stellate cell cDNA samples were preamplified before Taqman RT-PCR run, as described in Chapter 2 (section 2.5). Both Adipsin and Cyclooxygenase 2 (COX-2) were studied but no expression was observed, regardless of cellular activation state.

5.4. Gene expression in isolated stellate cells cultured on different surfaces for 7 days

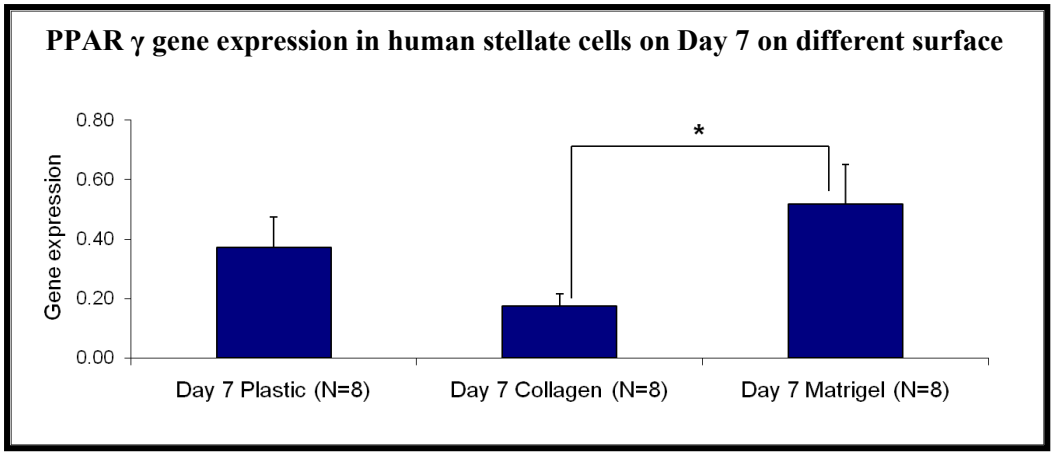

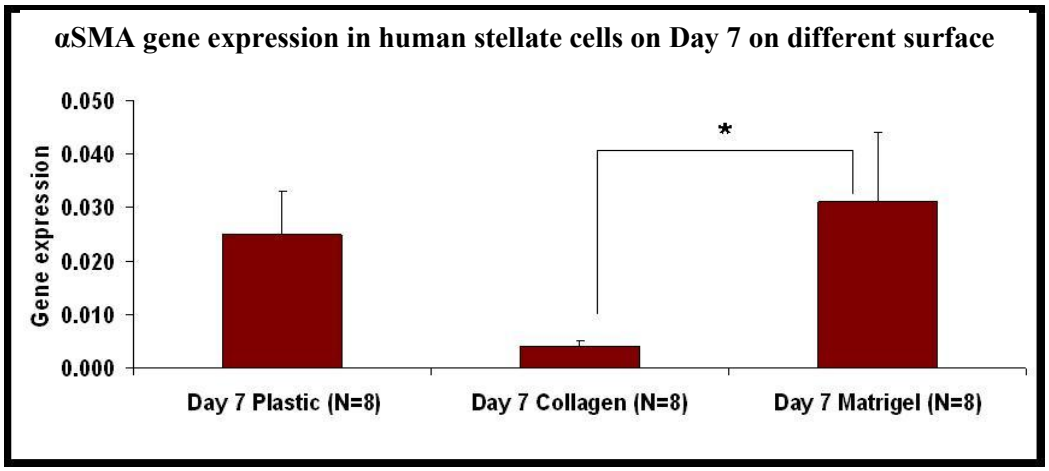

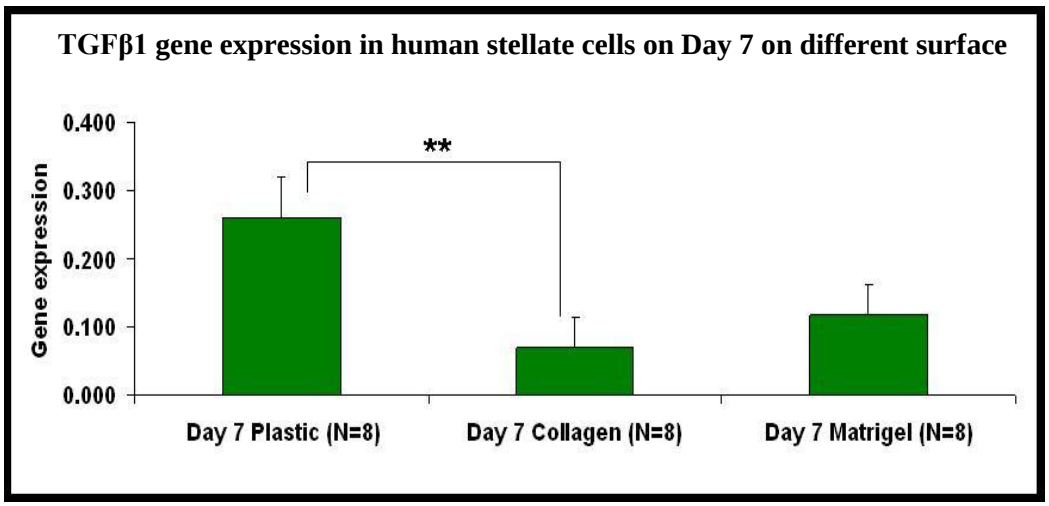

Figure 5.11: PPAR γ, αSMA and TGFβ1 gene expression in human stellate cells plated on different surfaces on Day 7 of culture. mRNA level measured using Taqman Real-time PCR, values shown relative to β-actin, n = 8 for each group. Data is presented as mean ± S.E.M. (*: $p<0.05$; **: $p<0.01$; ***: $p<0.000$).

Table 5.2: Gene expression levels in human hepatic stellate cells cultured on 3 different surfaces for 7 days

Adipogenic Genes	**DAY 7 PLASTIC**	**DAY 7 COLLAGEN**	**DAY 7 MATRIGEL**	**P VALUE**
SREBP-1C	0.038 ± 0.010	0.022 ± 0.004	0.046 ± 0.016	NS
CEBP α	0.544 ± 0.138	0.523 ± 0.078	0.505 ± 0.153	NS
CEBPβ	**0.747 ± 0.270[a]**	**0.184 ± 0.047[a]**	0.217 ± 0.071	**0.030[a]**
LXR α	**1.769 ± 0.524[a,b]**	**0.520 ± 0.112[a]**	**0.500 ± 0.177[b]**	**0.014[a]; 0.016[b]**
Fatty acid Transporter	**DAY 7 PLASTIC**	**DAY 7 COLLAGEN**	**DAY 7 MATRIGEL**	**P VALUE**
CD36	**0.650 ± 0.101[a,b]**	**0.197 ± 0.033[a]**	**0.041 ± 0.017[b]**	**0.000[a,b]**
FABP4	**3.637 ± 1.159[b]**	3.625 ± 0.817	**0.801 ± 0.458[b]**	**0.049[b]**
Nuclear receptor	**DAY 7 PLASTIC**	**DAY 7 COLLAGEN**	**DAY 7 MATRIGEL**	**P VALUE**
PPAR β	0.455 ± 0.057	0.301 ± 0.066	0.340 ± 0.068	NS
LXR β	0.527 ± 0.135	0.226 ± 0.043	0.403 ± 0.137	NS
PXR	0.372 ± 0.102	**0.176 ± 0.040[c]**	**0.519 ± 0.133[c]**	**0.021[c]**
FXR	**0.060 ± 0.021[b]**	**0.051 ± 0.011[c]**	**0.334 ± 0.143[b,c]**	**0.018[b]; 0.012[c]**
HSC Marker	**DAY 7 PLASTIC**	**DAY 7 COLLAGEN**	**DAY 7 MATRIGEL**	**P VALUE**
CRBP1	**1.141 ± 0.415[a]**	**0.070 ± 0.010[a]**	1.115 ± 0.513	**0.048[a]**
GFAP	**1.289 ± 0.372[b]**	3.952 ± 1.302	**5.936 ± 2.145[b]**	**0.026[b]**
CSRP2	0.018 ± 0.001	**0.051 ± 0.016[c]**	**0.005 ± 0.004[c]**	**0.019[c]**

mRNA level measured using Taqman Real-time PCR, values shown relative to β-actin, n = 8 for each group. Data is presented as mean ± S.E.M.

(a: Day 7 plastic vs Day 7 collagen; b: Day 7 plastic vs Day 7 matrigel; c: Day 7 collagen vs Day7 matrigel; NS- Not significant)

Day 7 plastic plated HSCs, showed an increase in CEBPβ, LXRα, CD36, FABP4, and TGFβ1 expression and a reduction in GFAP expression significantly compared to other groups. This indicated that HSCs on plastic surface were activated and in the early initiation phase, however some of the adipogenic genes thought to be associated with quiescence were still expressed at similar levels to those cells plated on matrigel. Interstingly, α-SMA expression was similar on plastic and matrigel surfaces after 7 days in culture suggesting that clear differences in terms of activation state of the HSCs was not apparent.

Day 7 collagen plated cells expressed lower levels of CRBP1, TGFβ1, and αSMA accompanied by an elevation in CSRP2. The cell morphology indicated that stellate cells plated on collagen were transdifferentiated.

Day 7 matrigel plated HSCs had higher levels of PPAR γ, PXR, FXR and GFAP expression and surprisingly, reduced FABP4 expression.

5.5. Gene expression in activated HSCs culture on different surfaces

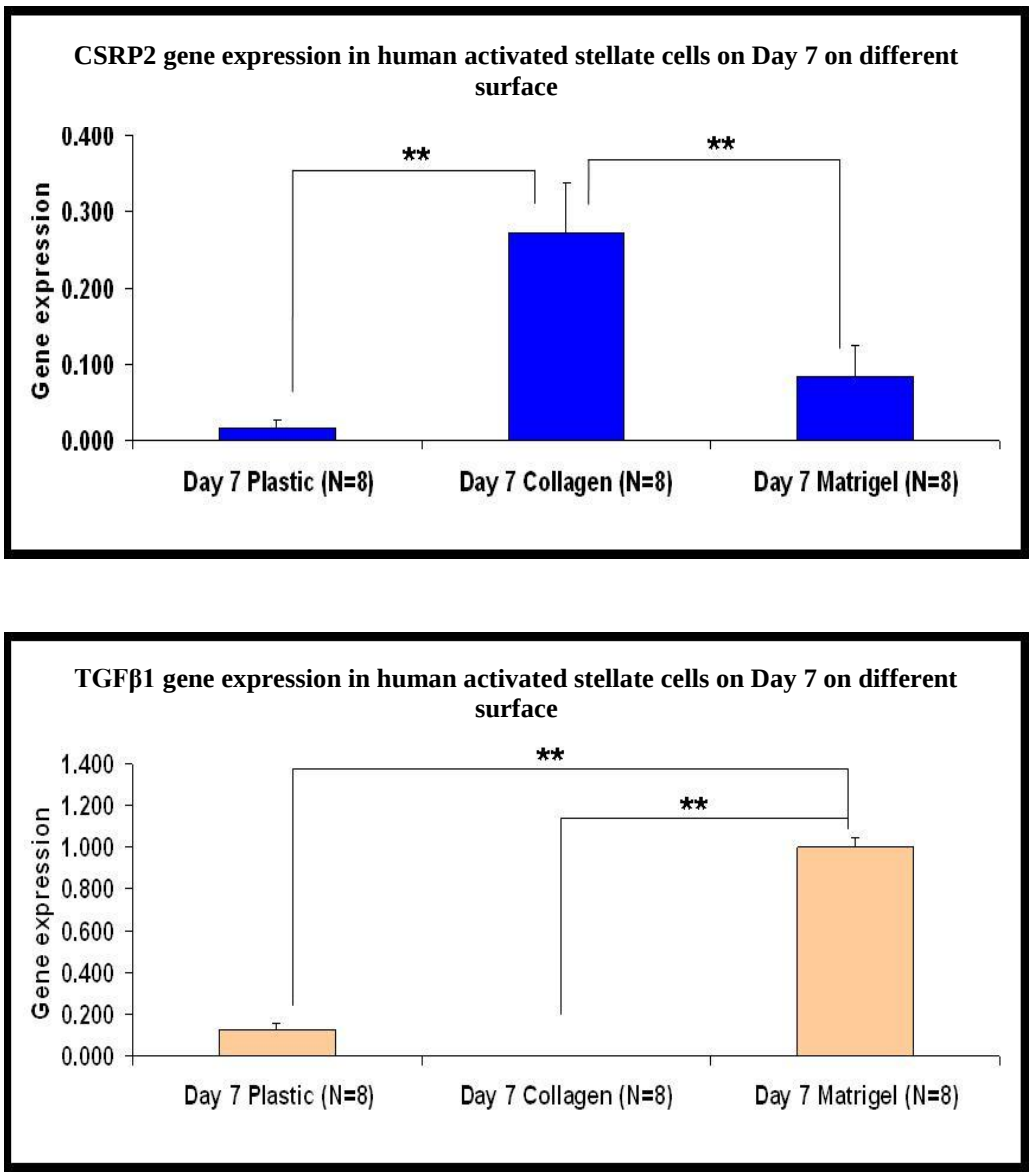

Figure 5.12: CSRP2 and TGFβ1 gene expression in human activated stellate cells plated on different surfaces for 7 days. mRNA level measured using Taqman Real-time PCR, values shown relative to β-actin, n = 8 for each group. Data is presented as mean ± S.E.M. (*: $p<0.05$; **: $p<0.01$; ***: $p<0.000$).

Activated stellate cells plated on collagen surfaces increased in CSRP2 expression and decreased in TGFβ1 expression compared to other groups.

5.5. Gene expression in activated HSCs culture on different surfaces

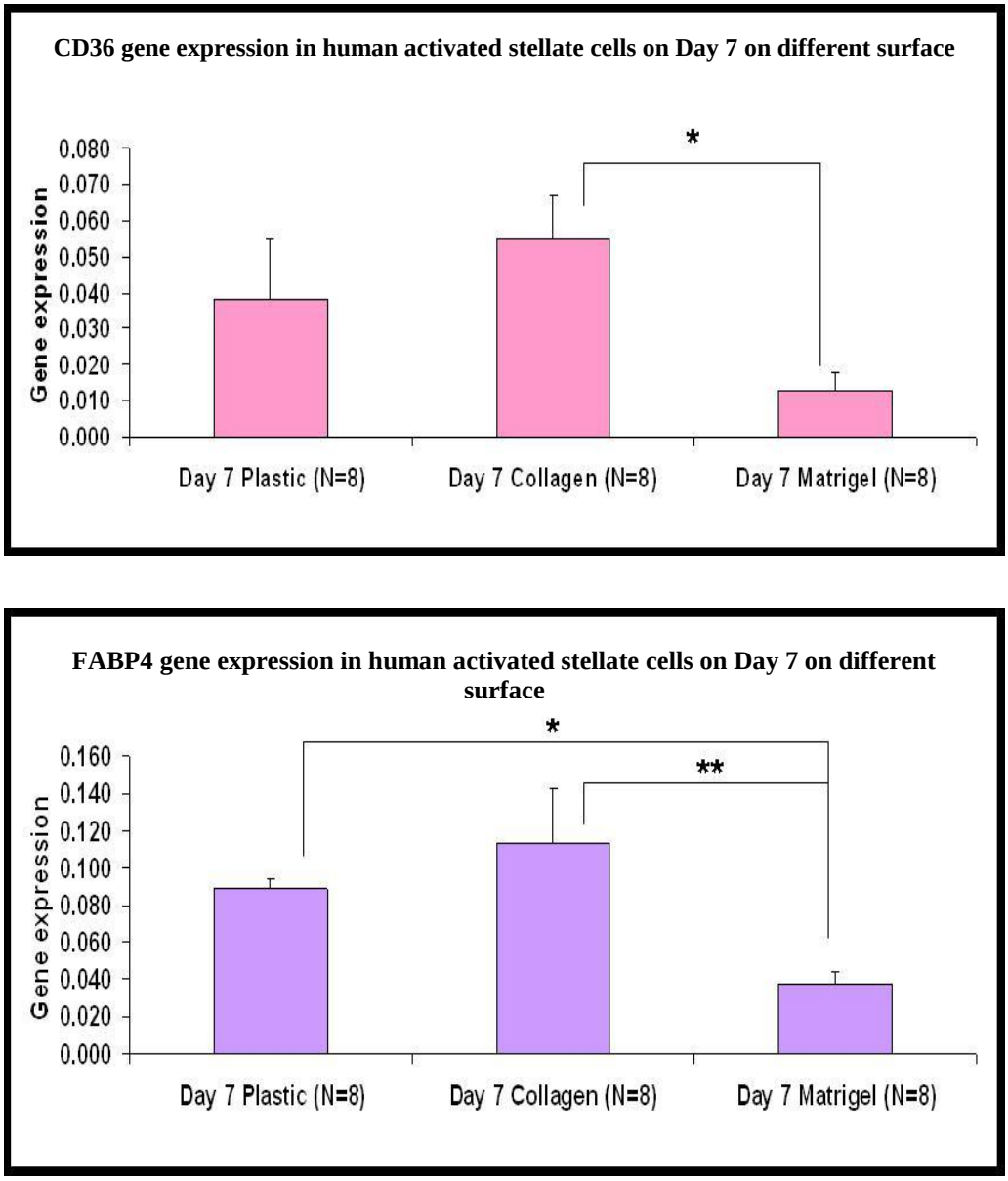

Figure 5.13: CD36 and FABP4 gene expression in human activated stellate cells plated on different surfaces for 7 days. mRNA level measured using Taqman Real-time PCR, values shown relative to β-actin, n = 8 for each group. Data is presented as mean ± S.E.M. (*: $p<0.05$; **: $p<0.01$; ***: $p<0.000$).

Both CD36 and FABP4 expression increased significantly in collagen plated activated stellate cells in culture compared to other group.

Table 5.3: Gene expression levels of HSCs grown for 14 days on plastic followed by 7 days culture on new tissue culture surfaces.

Adipogenic genes	**DAY 7 on PLASTIC**	**DAY 7 on COLLAGEN**	**DAY 7 on MATRIGEL**	**P VALUE**
PPAR γ	0.111 ± 0.044	0.004 ± 0.001	0.071 ± 0.035	NS
SREBP-1C	0.053 ± 0.017	0.062 ± 0.014	0.070 ± 0.016	NS
CEBP α	0.010 ± 0.003	0.022 ± 0.004	0.021 ± 0.006	NS
CEBPβ	0.150 ± 0.054	0.101 ± 0.017	0.174 ± 0.044	NS
LXR α	0.033 ± 0.011	0.022 ± 0.004	0.035 ± 0.009	NS
Nuclear receptor	**DAY 7 on PLASTIC**	**DAY 7 on COLLAGEN**	**DAY 7 on MATRIGEL**	**P VALUE**
PPAR β	0.588 ± 0.139	1.029 ± 0.315	0.784 ± 0.061	NS
LXR β	0.173 ± 0.054	0.276 ± 0.059	0.271 ± 0.034	NS
PXR	0.023 ± 0.011	0.005 ± 0.001	0.024 ± 0.005	NS
FXR	0.268 ± 0.117	0.197 ± 0.032	0.206 ± 0.062	NS
HSC marker	**DAY 7 on PLASTIC**	**DAY 7 on COLLAGEN**	**DAY 7 on MATRIGEL**	**P VALUE**
αSMA	0.688 ± 0.279	0.296 ± 0.039	0.927 ± 0.274	NS
CRBP1	0.160 ± 0.062	0.050 ± 0.004	0.260 ± 0.111	NS
GFAP	0.014 ± 0.005	0.091 ± 0.058	0.052 ± 0.040	NS

mRNA level measured using Taqman Real-time PCR, values shown relative to β-actin, n = 8 for each group. Data is presented as mean ± S.E.M. (a: Day 7 on plastic vs Day 7 on collagen; b: Day 7 on plastic vs Day 7 on matrigel; c: Day 7 on collagen vs Day 7 on matrigel; NS: Not significant).

No clear pattern of changes in gene expression on different surfaces or at different time points was observed in terms of cells either maintaining their adipogenic phenotype or becoming activated. Overall, levels of expression of many of the gens studied, particularly after 21 days in culture were low. It was possible that the HSCs had effectively become de-differentiated to a certain degree.

5.6. Investigation of changes in human HSCs phenotype over time in culture

Human HSCs phenotypic changes and changes in underlying gene expression levels are not described clearly in the literature. Thus, the aim of this section of the study was to describe the changes in stellate cells activation over time.

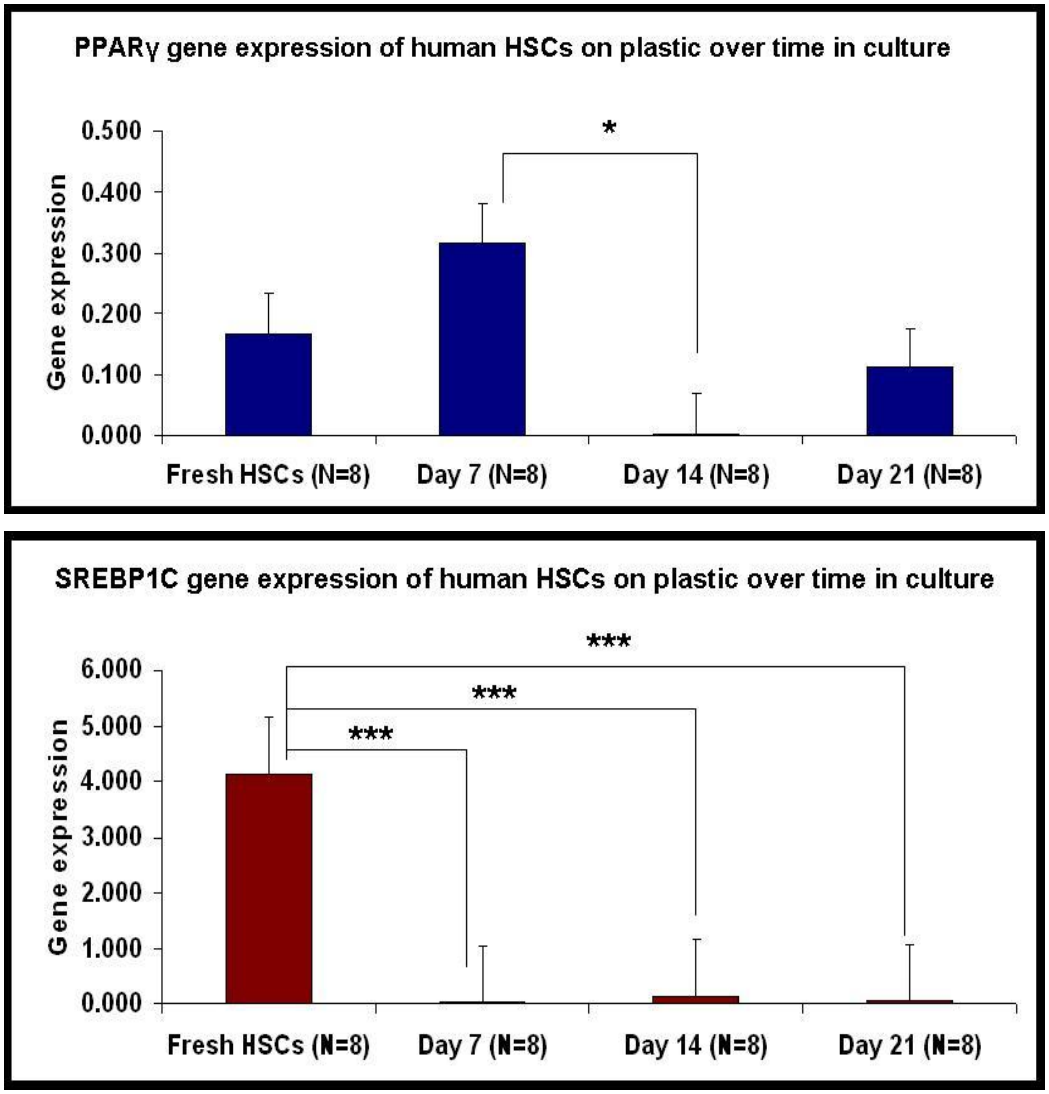

Figure 5.14: PPAR γ and SREBP1C gene expression in human hepatic stellate cells plated on plastic over time in culture. mRNA level measured using Taqman Real-time PCR, values shown relative to β-actin, n = 8 for each group. Data is presented as mean ± S.E.M. (*: $p<0.05$; **: $p<0.01$; ***: $p<0.000$).

PPAR γ expression decreased significantly on day 14 compared to day 7. SREBP1C expression was at the highest in fresh stellate cells group compared to other group.

5.6. Investigation of changes in Human HSCs phenotype over time in culture

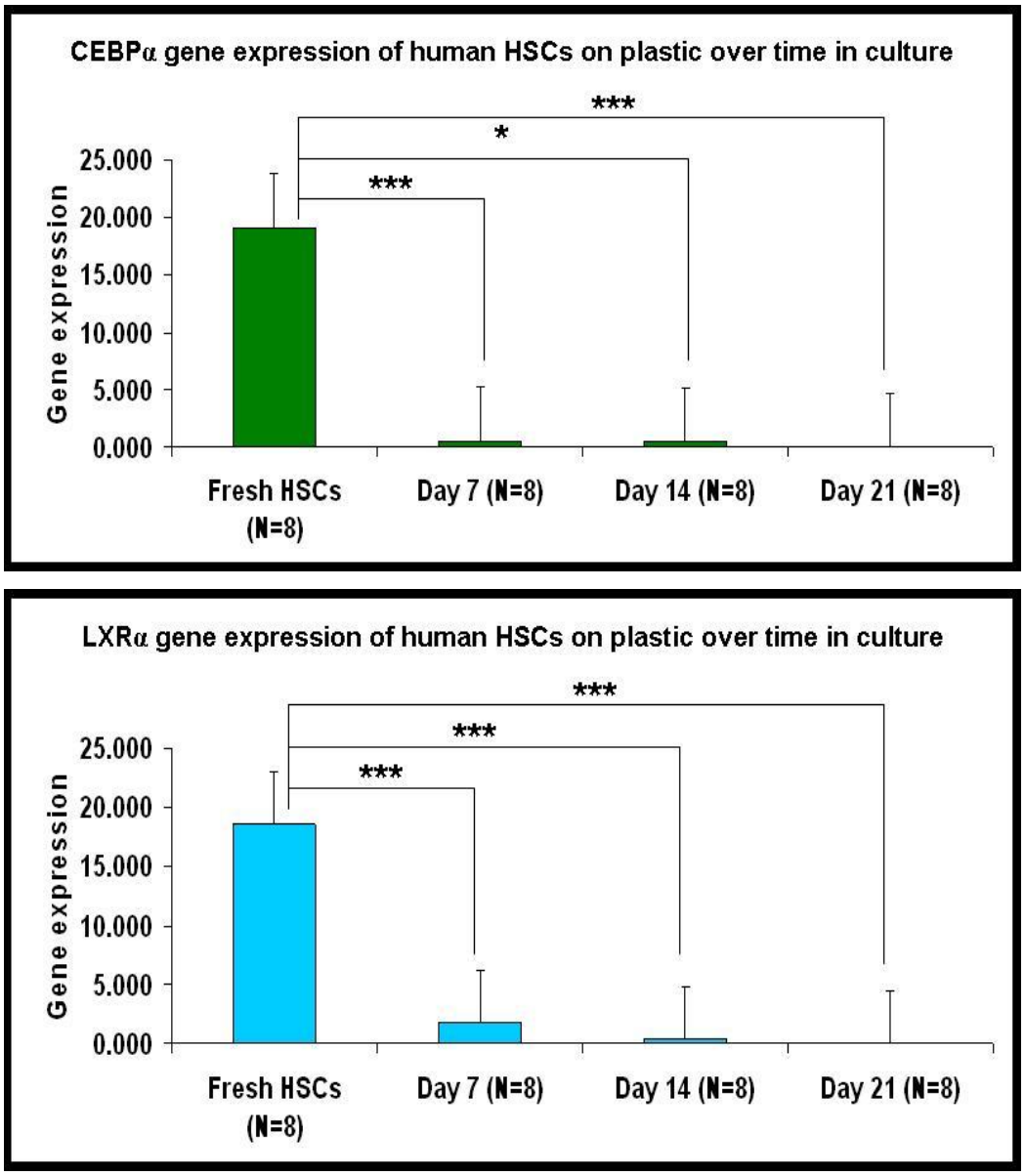

Figure 5.15: CEBPα and LXRα gene expression in human hepatic stellate cells plated on plastic over time in culture. mRNA level measured using Taqman Real-time PCR, values shown relative to β-actin, n = 8 for each group. Data is presented as mean ± S.E.M. (*: $p<0.05$; **: $p<0.01$; ***: $p<0.000$).

Both CEBPα and LXRα were highly expressed in fresh stellate cells group compared to other group.

5.6. Investigation of changes in Human HSCs phenotype over time in culture

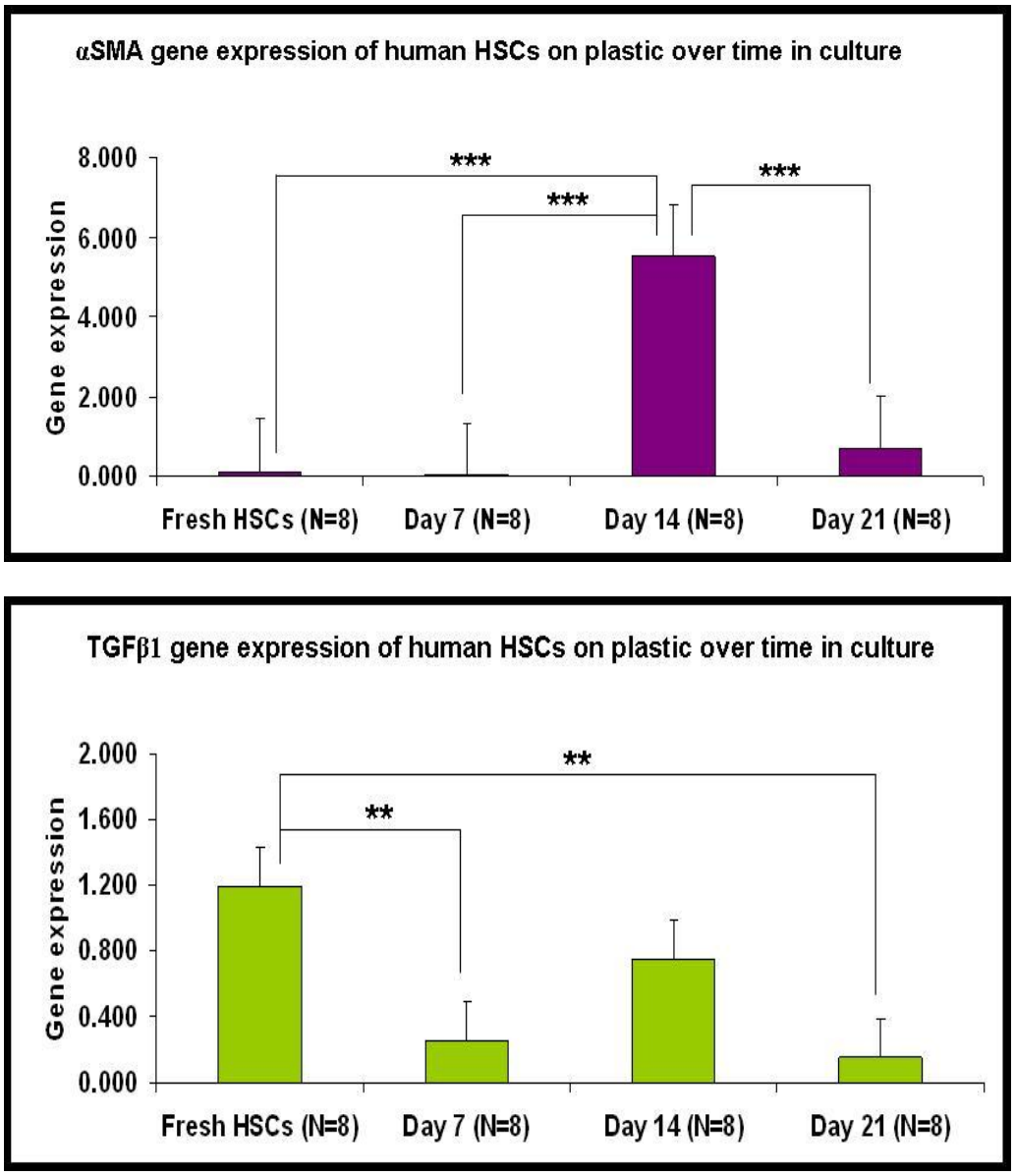

Figure 5.16: αSMA and TGFβ1 gene expression in human hepatic stellate cells plated on plastic over time in culture. mRNA level measured using Taqman Real-time PCR, values shown relative to β-actin, n = 8 for each group. Data is presented as mean ± S.E.M. (*: $p<0.05$; **: $p<0.01$; ***: $p<0.000$).

αSMA expression was increased significantly on day 14 compared to other group. TGFβ1 was at the highest in fresh stellate cells group compared to day 7 and day 21.

5.6. Investigation of changes in Human HSCs phenotype over time in culture

Table 5.4: Gene expression in human hepatic stellate cells plated on plastic over time in culture.

Adipogenic genes	**Fresh HSCs**	**DAY 7**	**DAY 14**	**DAY 21**	**P VALUE**
CEBPβ	**7.469 ± 2.417[a,b,c]**	**0.747 ± 0.270[a]**	**0.945 ± 0.079[b]**	**0.150 ± 0.054[c]**	**0.005[a]; 0.032[b]; 0.003[c]**
Fatty acid transporter	**Fresh HSCs**	**DAY 7**	**DAY 14**	**DAY 21**	**P VALUE**
CD36	**3.715 ± 0.913[a,b,c]**	**0.650 ± 0.101[a]**	**0.551 ± 0.060[b]**	**0.038 ± 0.017[c]**	**0.000[a,b,c]**
FABP4	0.747 ± 0.413	**3.637 ± 1.159[d,e]**	**0.195 ± 0.048[d]**	**0.089 ± 0.005[e]**	**0.037[d]; 0.030[e]**
Nuclear receptor	**Fresh HSCs**	**DAY 7**	**DAY 14**	**DAY 21**	**P VALUE**
PPAR β	1.389 ± 0.571	0.455 ± 0.057	0.830 ± 0.682	0.588 ± 0.139	NS
LXR β	**2.151 ± 0.576[a,c]**	**0.527 ± 0.135[a]**	0.843 ± 0.108	**0.173 ± 0.054[c]**	**0.006[a]; 0.001[c]**
PXR	**3.687 ± 0.867[a,b,c]**	**0.372 ± 0.102[a]**	**0.150 ± 0.002[b]**	**0.023 ± 0.011[c]**	**0.000[a,c]; 0.001[b]**
FXR	**24.691 ± 4.903[a,b,c]**	**0.060 ± 0.021[a]**	**2.292 ± 0.392[b]**	**0.268 ± 0.117[c]**	**0.000[a,b,c]**
HSC Marker	**Fresh HSCs**	**DAY 7**	**DAY 14**	**DAY 21**	**P VALUE**
CRBP1	1.206 ± 0.271	1.141 ± 0.415	1.390 ± 0.435	0.160 ± 0.062	NS
GFAP	0.965 ± 0.468	1.289 ± 0.372	**2.436 ± 0.107[f]**	**0.014 ± 0.005[f]**	**0.003[f]**
CSRP2	**1.734 ± 0.313[a,c]**	**0.018 ± 0.001[a,d]**	**1.118 ± 0.235[d,f]**	**0.016 ± 0.001[c,f]**	**0.000[a,c];0.004[d]; 0.007[f]**

mRNA levels were measured using Taqman Real-time PCR, values are shown relative to β-actin, n = 8 for each group. (a: Fresh HSC vs. Day 7 HSC; b: Fresh HSC vs. Day 14; c: Fresh HSC vs. Day 21; d: Day 7 vs. Day 14; e: Day 7 vs. Day 21; f: Day 14 vs. Day 21)

Stellate cell gene expression was studied from Day 0 to Day 21 in cells plated on plastic. SREBP1C, CEBPα, CEBPβ, LXRα, LXRβ, CD36, PXR, FXR and TGFβ1 expression were all highest in freshly isolated HSCs, and the mRNA levels of these genes decreased significantly by day 7 and continued to fall at day 21. Surprisingly, given their role in the adipogenic phenotype of HSCs, PPAR γ and FABP4 expression increased at day 7 relative to freshly isolated cells and then gradually decreased.

αSMA expression was only significantly elevated at day 14 and CSRP2 levels were also highest at this time point. This suggests that HSCs may only become fully activated after 14 days in culture. GFAP expression were increased gradually day 0 to day 14, but decreased significantly at the end of the culture. On day 21, gene expression in general was at the lowest levels.

5.7. Human HSC proliferation rate assessment using PCNA expression levels

Human HSC proliferation rates were assessed initially by determining the level of proliferating cell nuclear antigen using western blotting.

5.7.1. Day 7 HSCs on Matrigel coated surface

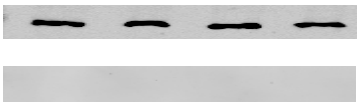

5.7.2. Day 7 HSCs on collagen coated surface

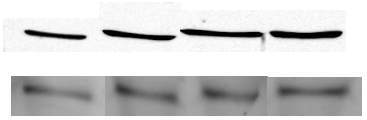

5.7.3. Day 7 on Matrigel coated surface after subculturing

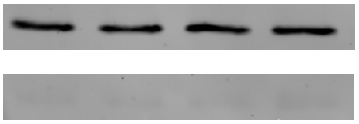

5.7.4. Day 7 on collagen coated surface after subculturing

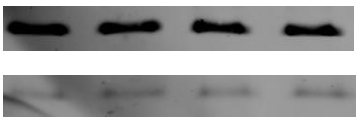

5.7.5.PCNA protien levels in Human HSCs over time when plated on plastic

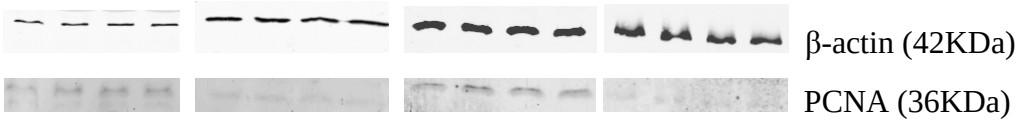

HSCs plated on matrigel did not show any PCNA expression whereas collagen plated HSCs show clear PCNA expression, suggesting higher level of mitosis. Day 14 HSCs show higher PCNA expression compared to freshly isolated HSCs. Both day 7 and 21 HSCs in culture did not show PCNA expression.

5.8. Effects of PDGF-BB on HSCs proliferation and gene expression

PDGF-BB is a potent mitogenic factor that activates and causes the proliferation of stellate cells (Paik et al., 2009). PDGF is released during liver injury by kupffer cells. This section of the study aimed to determine the effects of PDGF-BB (Sigma, UK) upon stellate cell proliferation and activation to determine whether treatment with potentially anti-inflammatory and anti-proliferative nuclear receptor ligands **[(Pioglitazone: Molekula, Dorset); (GW0742 & GSK0660: Tocrisolve, UK); (GW3965: Sigma, UK)]** could inhibit the effects of PDGF-BB. (As shown over leaf)

5.8.1. Effects of Pioglitazone (PGZ) in PDGF-BB treated freshly isolated HSCs

Freshly isolated HSCs were incubated with vehicle (0.004% DMSO), PGZ (5μM) for 72hours consecutively. After 24 hours of drug treatment, PDGF-BB (15ng/ml) was added for 48hours consecutively, followed by RNA extraction for gene expression analysis.

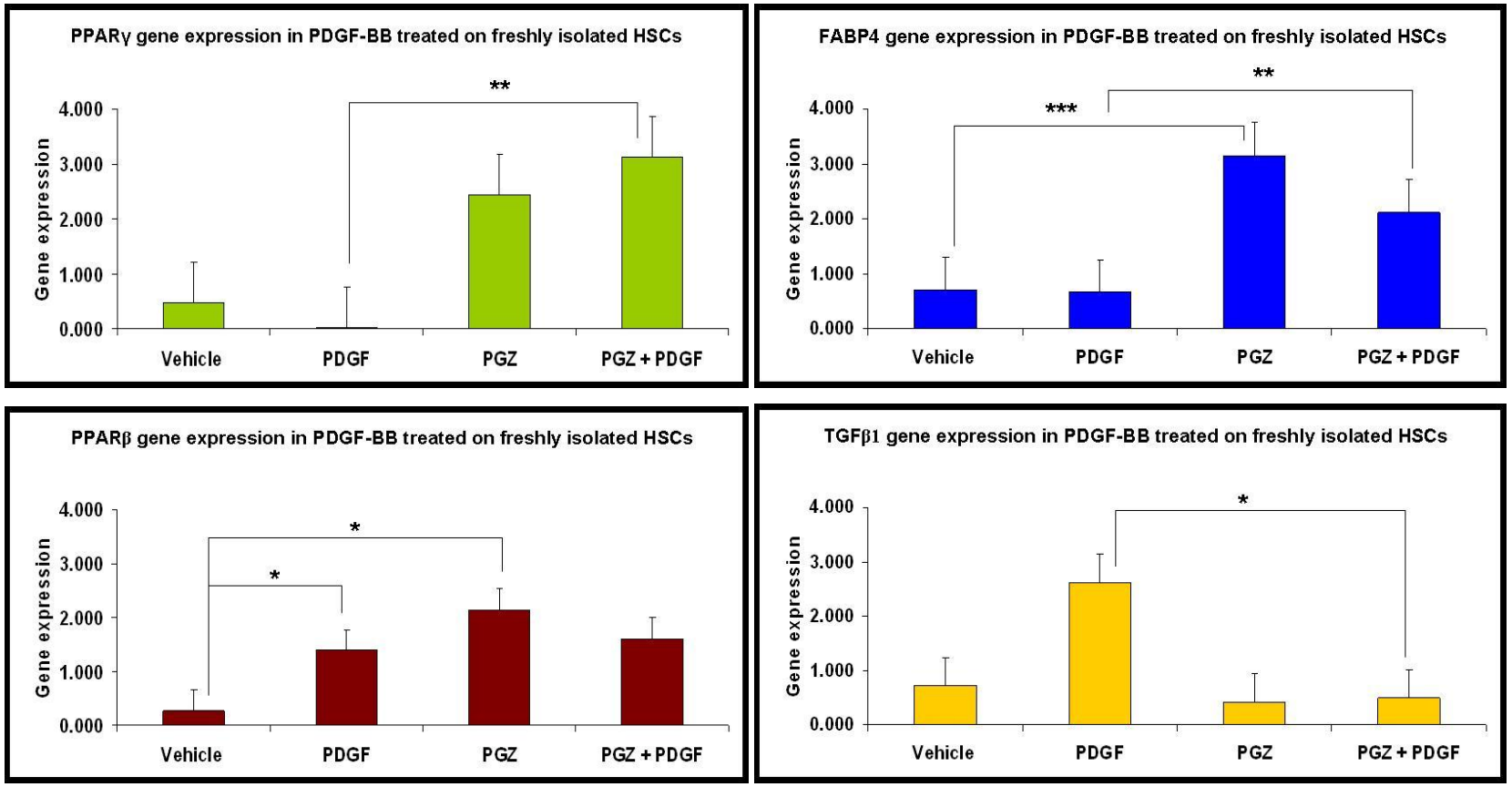

Figure 5.17: Effect of PDGF-BB incubation on freshly isolated HSCs for 48hours followed by treatment with Pioglitazone (PGZ). mRNA level measured using Taqman Real-time PCR, values shown relative to β-actin, n = 8 for each group. Data is presented as mean ± S.E.M. (*: $p<0.05$; **: $p<0.01$; ***: $p<0.000$).

Table 5.5: Effects of PDGF-BB incubation on freshly isolated HSCs for 48 hours followed by treatment with Pioglitazone on gene expressions.

Adipogenic genes	**Vehicle**	**PDGF (15ng/ml)**	**PGZ (5μM)**	**PGZ (5μM) + PDGF(15ng/ml)**	**P VALUE**
SREBP1C	**0.605 ± 0.196[a]**	**0.000 ± 0.000[a,c]**	2.529 ± 0.952	**3.820 ± 1.226[c]**	**0.000[a]; 0.005[c]**
CEBPα	**1.429 ± 0.227[a]**	**0.553 ± 0.168[a]**	0.614 ± 0.218	1.353 ± 0.417	**0.043[a]**
CEBPβ	1.305 ± 0.159	0.633 ± 0.087	1.026 ± 0.265	0.612 ± 0.273	NS
LXRα	**1.118 ± 0.059[a,b]**	**0.417 ± 0.169[a]**	**0.505 ± 0.190[b]**	0.866 ± 0.146	**0.006[a]; 0.013[b]**
Fatty acid transporter	**Vehicle**	**PDGF (15ng/ml)**	**PGZ (5μM)**	**PGZ (5μM) + PDGF(15ng/ml)**	**P VALUE**
CD36	0.915 ± 0.118	1.304 ± 0.896	0.870 ± 0.210	2.391 ± 0.924	NS
Nuclear receptor	**Vehicle**	**PDGF (15ng/ml)**	**PGZ (5μM)**	**PGZ (5μM) + PDGF(15ng/ml)**	**P VALUE**
LXRβ	0.886 ± 0.299	0.410 ± 0.131	0.803 ± 0.282	0.844 ± 0.431	NS
PXR	0.324 ± 0.114	0.462 ± 0.277	1.113 ± 0.276	3.003 ± 1.451	NS
FXR	**1.503 ± 0.330[a]**	**0.318 ± 0.269[a]**	1.353 ± 0.838	2.680 ± 1.656	**0.003[a]**
HSC marker	**Vehicle**	**PDGF (15ng/ml)**	**PGZ (5μM)**	**PGZ (5μM) + PDGF(15ng/ml)**	**P VALUE**
CRBP1	**1.098 ± 0.280[a]**	**0.084 ± 0.051[a,c]**	0.589 ± 0.223	**1.431 ± 0.367[c]**	**0.016[a]; 0.003[c]**
αSMA	0.714 ± 0.151	1.381 ± 0.888	0.462 ± 0.127	0.198 ± 0.192	NS
GFAP	**0.913 ± 0.276[a]**	**0.096 ± 0.059[a]**	0.822 ± 0.345	0.665 ± 0.211	**0.037[a]**
CSRP2	**0.922 ± 0.133[a]**	**5.167 ± 3.656[a]**	0.703 ± 0.132	1.295 ± 0.311	**0.029[a]**

(a: Vehicle vs. PDGF; b: Vehicle vs. PGZ ; c:PDGF vs. (PGZ + PDGF); NS: not significant). mRNA levels measured using Taqman Real-time PCR, values shown relative to β-actin, n = 8 for each group. Data is presented as mean ± S.E.M.

PDGF-BB decreased SREBP1C, CEBPα, LXRα, FXR, CRBP1 and GFAP followed by an increased PPAR β and CSRP2 expression in freshly isolated HSCs. Meanwhile, PGZ increased SREBP1C, PPAR γ, FABP4, CRBP1 and decreased TGFβ1 expression in PDGF-BB treated HSCs. PGZ also increased PPAR β expression compared to vehicle.

5.8.2. Effects of LXR Agonist GW3965 in PDGF-BB treated freshly isolated HSCs

Freshly isolated HSCs were incubated with vehicle (0.004% DMSO), GW3965 (2μM) for 72hours consecutively. After 24 hours of drug treatment, PDGF-BB (15ng/ml) was added for 48hours consecutively, followed by RNA extraction for gene expression analysis.

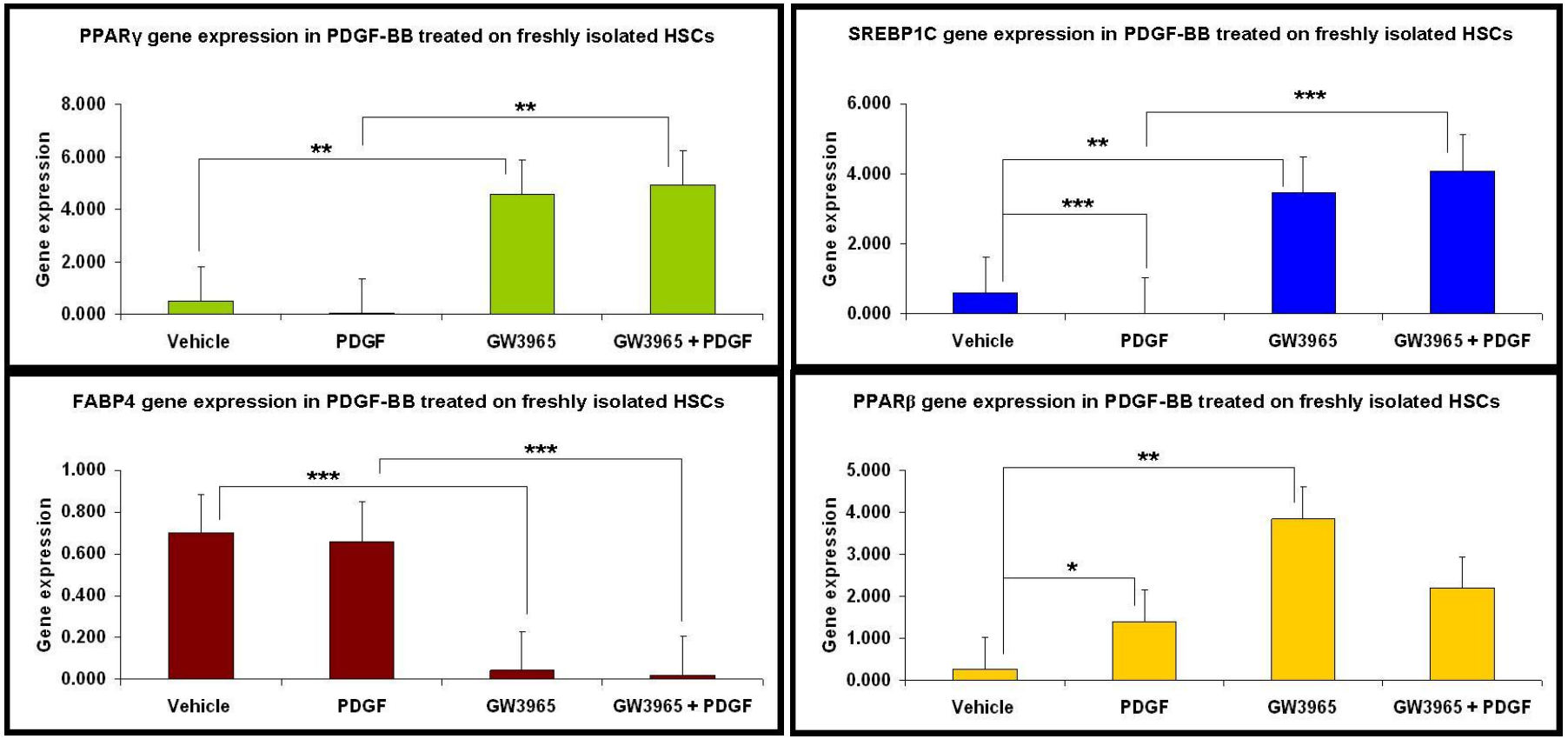

Figure 5.18: Effect of PDGF-BB incubation on freshly isolated HSCs for 48hours followed by treatment with GW3965. mRNA level measured using Taqman Real-time PCR, values shown relative to β-actin, n = 8 for each group. Data is presented as mean ± S.E.M. (*: $p<0.05$; **: $p<0.01$; ***: $p<0.000$).

5.8.2. Effects of LXR Agonist GW3965 in PDGF-BB treated freshly isolated HSCs

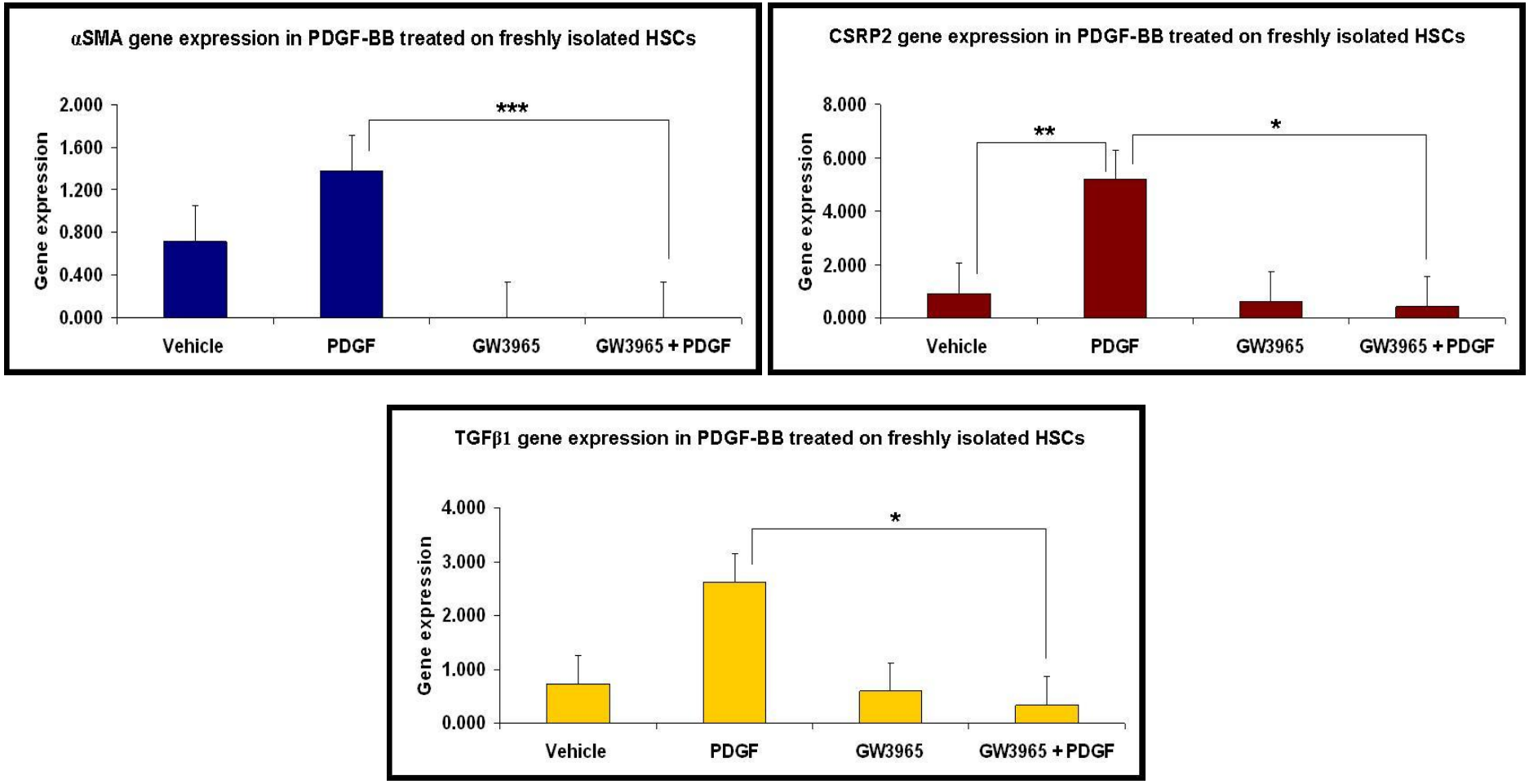

Figure 5.19: Effect of PDGF-BB incubation on freshly isolated HSCs for 48hours followed by treatment with GW3965. mRNA level measured using Taqman Real-time PCR, values shown relative to β-actin, n = 8 for each group. Data is presented as mean ± S.E.M. (*: $p<0.05$; **: $p<0.01$; ***: $p<0.000$).

Table 5.6: Effects of PDGF-BB incubation on freshly isolated HSCs for 48 hours followed by treatment with GW3965 on gene expressions.

Adipogenic genes	**Vehicle**	**PDGF (15ng/ml)**	**GW3965 (2μM)**	**GW3965 (2μM) + PDGF(15ng/ml)**	**P VALUE**
CEBPα	**1.429 ± 0.227[a]**	**0.553 ± 0.168[a]**	0.841 ± 0.325	0.343 ± 0.210	**0.043[a]**
CEBPβ	**1.305 ± 0.159[b]**	0.633 ± 0.087	**0.521 ± 0.159[b]**	0.805 ± 0.378	**0.036[b]**
LXRα	**1.118 ± 0.059[a]**	**0.417 ± 0.169[a]**	0.537 ± 0.188	0.693 ± 0.279	**0.006[a]**
Fatty acid transporter	**Vehicle**	**PDGF (15ng/ml)**	**GW3965 (2μM)**	**GW3965 (2μM) + PDGF(15ng/ml)**	**P VALUE**
CD36	0.915 ± 0.118	1.304 ± 0.896	0.969 ± 0.507	0.563 ± 0.335	NS
Nuclear receptor	**Vehicle**	**PDGF (15ng/ml)**	**GW3965 (2μM)**	**GW3965 (2μM) + PDGF(15ng/ml)**	**P VALUE**
LXRβ	0.886 ± 0.299	0.410 ± 0.131	0.867 ± 0.195	0.788 ± 0.350	NS
PXR	**0.324 ± 0.114[b]**	0.462 ± 0.277	**6.105 ± 1.590[b]**	1.385 ± 0.346	**0.001[b]**
FXR	**1.503 ± 0.330[a,b]**	**0.318 ± 0.269[a]**	**0.004 ± 0.001[b]**	0.006 ± 0.001	**0.003[a]** **0.001[b]**
HSC marker	**Vehicle**	**PDGF (15ng/ml)**	**GW3965 (2μM)**	**GW3965 (2μM) + PDGF(15ng/ml)**	**P VALUE**
CRBP1	**1.098 ± 0.280[a]**	**0.084 ± 0.051[a]**	0.741 ± 0.489	0.548 ± 0.286	**0.016[a]**
GFAP	**0.913 ± 0.276[a]**	**0.096 ± 0.059[a]**	0.709 ± 0.225	0.550 ± 0.258	**0.037[a]**

(a: Vehicle vs. PDGF; b:Vehicle vs. GW3965; c: PDGF vs. (GW3965 + PDGF); NS: Not significant). mRNA levels measured using Taqman Real-time PCR, values shown relative to β-actin, n = 8 for each group. Data is presented as mean ± S.E.M.

GW3965 increased SREBP1C and PPAR γ and reduced FABP4, αSMA, CSRP2 and TGFβ1 in PDGF-BB treated cells. GW3965 alone increased SREBP1C, PPAR γ, PPAR β, PXR and reduced CEBPβ and FXR expression compared to vehicle.

5.8.3. Effects of PPAR β Agonist (GW0742) in PDGF-BB treated freshly isolated HSCs

Freshly isolated HSCs were incubated with vehicle (0.004% DMSO), GW0742 (100nM) for 72hours consecutively. After 24 hours of drug treatment, PDGF-BB (15ng/ml) was added for 48hours consecutively, followed by RNA extraction for gene expression analysis.

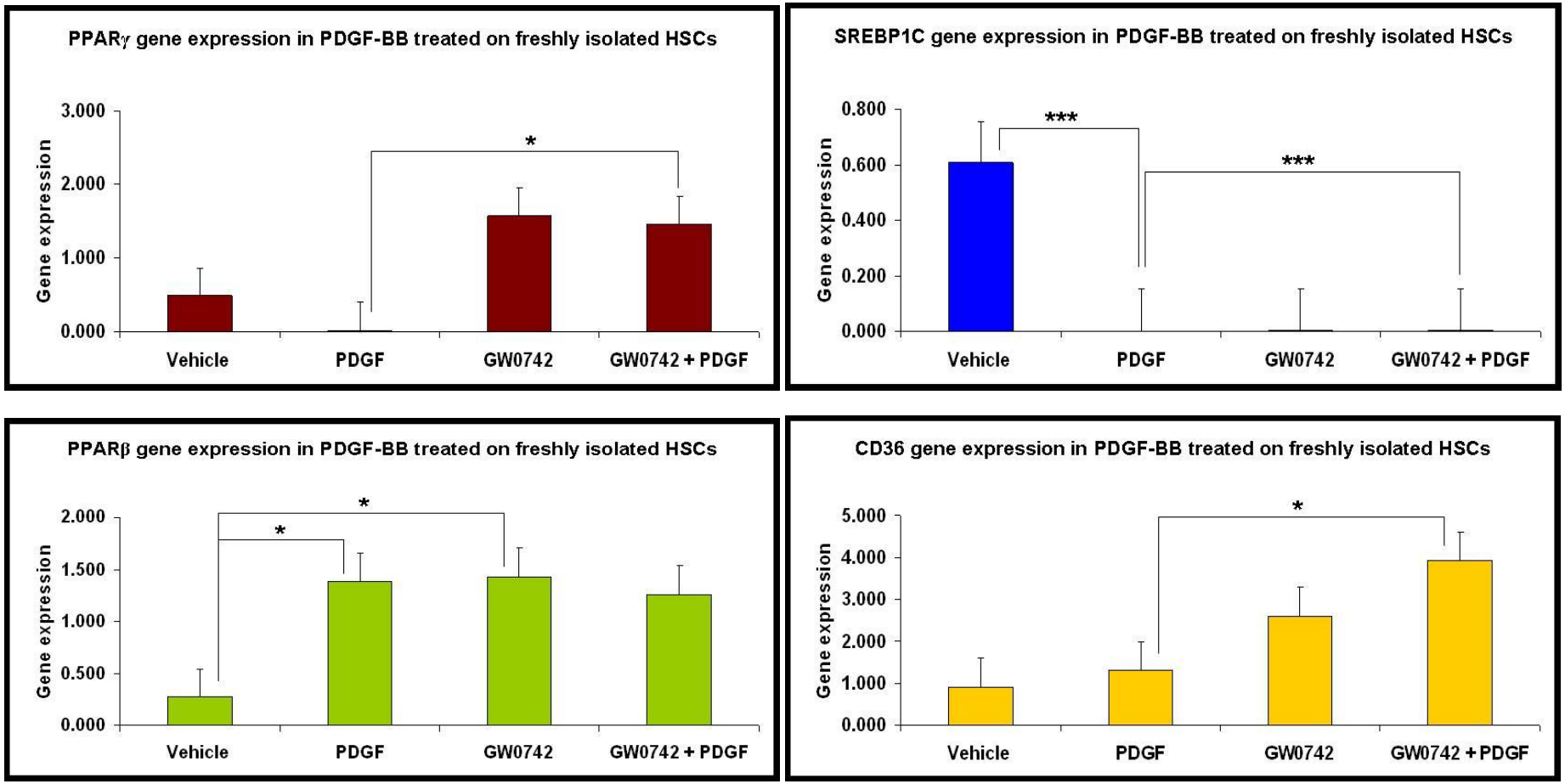

Figure 5.20: Effect of PDGF-BB incubation on freshly isolated HSCs for 48hours followed by treatment with GW0742. mRNA level measured using Taqman Real-time PCR, values shown relative to β-actin, n = 8 for each group. Data is presented as mean ± S.E.M. (*: $p<0.05$; **: $p<0.01$; ***: $p<0.000$).

5.8.3. Effects of PPAR β Agonist (GW0742) in PDGF-BB treated freshly isolated HSCs

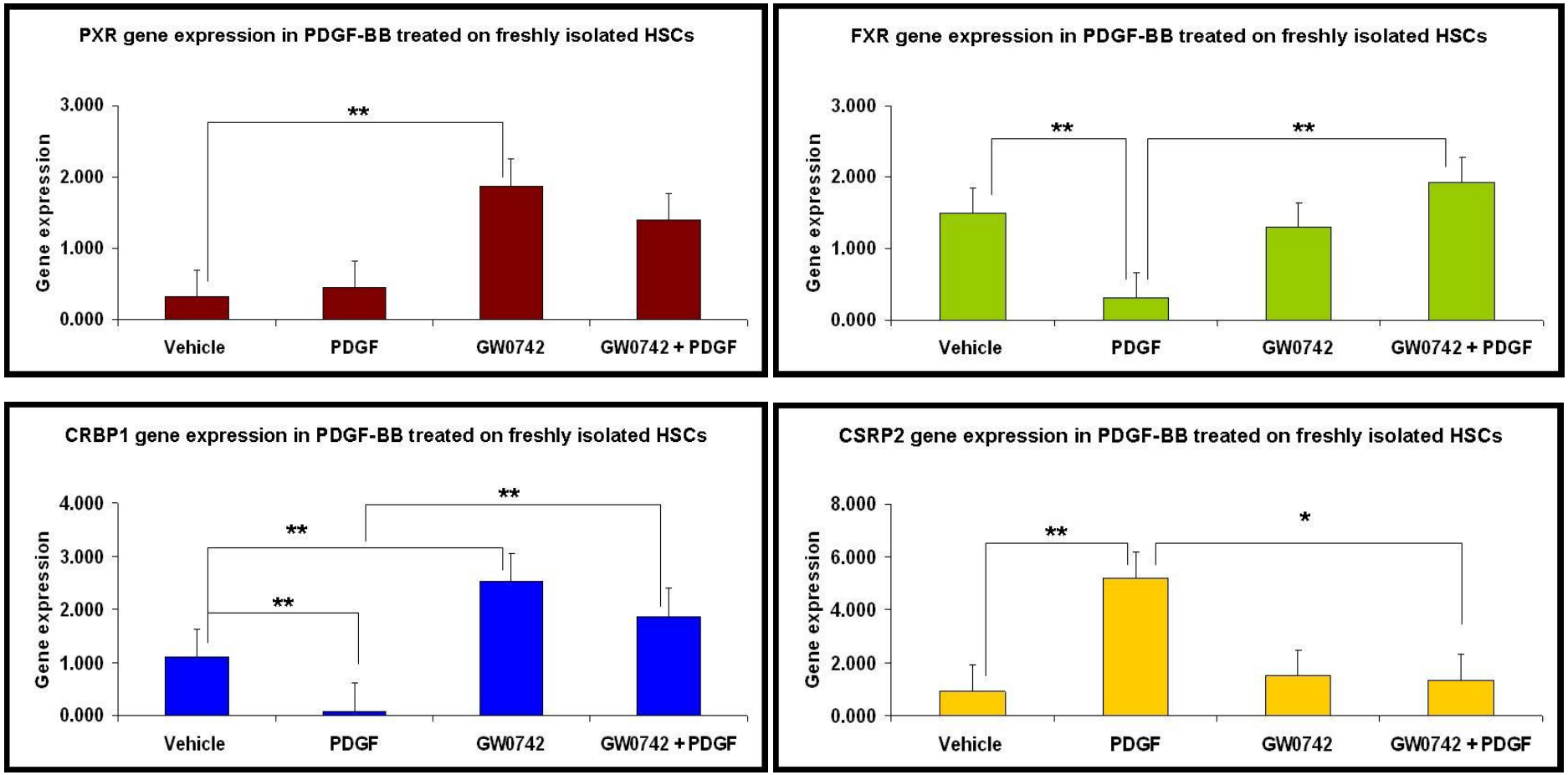

Figure 5.21: Effect of PDGF-BB incubation on freshly isolated HSCs for 48hours followed by treatment with GW0742. mRNA level measured using Taqman Real-time PCR, values shown relative to β-actin, n = 8 for each group. Data is presented as mean ± S.E.M. (*: $p<0.05$; **: $p<0.01$; ***: $p<0.000$).

Table 5.7: Effects of PDGF-BB incubation on freshly isolated HSCs for 48 hours followed by treatment with GW0742 on gene expressions.

Adipogenic genes	**Vehicle**	**PDGF (15ng/ml)**	**GW0742 (100nM)**	**GW0742(100nM) + PDGF(15ng/ml)**	**P VALUE**
CEBPα	**1.429 ± 0.227[a]**	**0.553 ± 0.168[a]**	1.792 ± 0.332	1.480 ± 0.636	**0.043[a]**
CEBPβ	1.305 ± 0.159	0.633 ± 0.087	2.930 ± 0.899	3.130 ± 0.888	NS
LXRα	**1.118 ± 0.059[a]**	**0.417 ± 0.169[a]**	1.371 ± 0.618	1.771 ± 0.506	**0.006[a]**
Fatty acid transporter	**Vehicle**	**PDGF (15ng/ml)**	**GW0742 (100nM)**	**GW0742(100nM) + PDGF(15ng/ml)**	**P VALUE**
FABP4	0.698 ± 0.140	0.659 ± 0.025	0.147 ± 0.100	0.137 ± 0.085	NS
Nuclear receptor	**Vehicle**	**PDGF (15ng/ml)**	**GW0742 (100nM)**	**GW0742(100nM) + PDGF(15ng/ml)**	**P VALUE**
LXRβ	0.886 ± 0.299	0.410 ± 0.131	2.561 ± 1.452	1.182 ± 0.351	NS
HSC marker	**Vehicle**	**PDGF (15ng/ml)**	**GW0742 (100nM)**	**GW0742(100nM) + PDGF(15ng/ml)**	**P VALUE**
αSMA	0.714 ± 0.151	1.381 ± 0.888	0.338 ± 0.129	0.188 ± 0.073	NS
GFAP	**0.913 ± 0.276[a]**	**0.096 ± 0.059[a]**	11.055 ± 8.072	5.664 ± 2.704	**0.037[a]**
TGFβ1	0.726 ± 0.095	2.616 ± 1.506	2.929 ± 0.164	3.001 ± 0.621	NS

(a: Vehicle vs. PDGF; b: Vehicle vs. GW0742; c: PDGF vs. (GW0742 + PDGF); NS: Not significant). mRNA levels measured using Taqman Real-time PCR, values shown relative to β-actin, n = 8 for each group. Data is presented as mean ± S.E.M.

GW0742 increased PPAR γ, CD36, FXR, CRBP1 and reduced CSRP2 expression in PDGF-BB treated freshly isolated HSCs.GW0742 increased PPAR β, PXR and CRBP1 but reduced SREBP1C expression compared to vehicle.

5.8.4. Effects of PPAR β Antagonist (GSK0660) in PDGF-BB treated freshly isolated HSCs

Freshly isolated HSCs were incubated with vehicle (0.004% DMSO), GSK0660 (1μM) for 72hours consecutively. After 24 hours of drug treatment, PDGF-BB (15ng/ml) was added for 48hours consecutively, followed by RNA extraction for gene expression analysis.

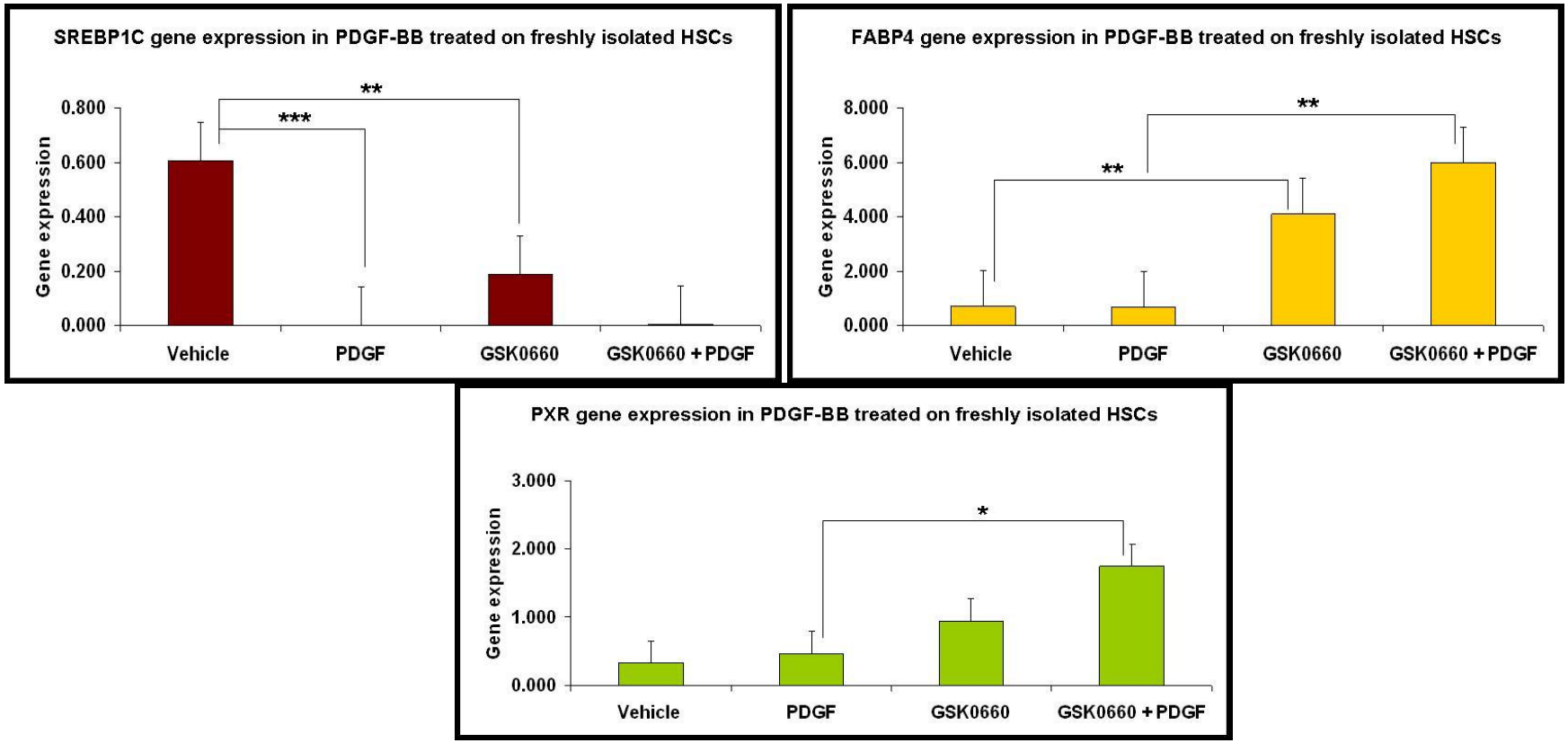

Figure 5.22: Effect of PDGF-BB incubation on freshly isolated HSCs for 48hours followed by treatment with GSK0660. mRNA level measured using Taqman Real-time PCR, values shown relative to β-actin, n = 8 for each group. Data is presented as mean ± S.E.M. (*: $p<0.05$; **: $p<0.01$; ***: $p<0.000$). GSK0660 increased FABP4 and PXR expression in PDGF-BB treated freshly isolated HSCs. GSK0660 increased SREBP1C and FABP4 expression compared to vehicle group.

Table 5.8: Effects of PDGF-BB incubation on freshly isolated HSCs for 48 hours followed by treatment with GSK0660 on gene expressions.

Adipogenic genes	**Vehicle**	**PDGF (15ng/ml)**	**GSK0660 (1µM)**	**GSK0660 (1µM) + PDGF(15ng/ml)**	**P VALUE**
PPAR γ	0.479 ± 0.097	0.021 ± 0.016	0.688 ± 0.387	1.174 ± 0.499	NS
CEBPα	**1.429 ± 0.227[a]**	**0.553 ± 0.168[a]**	1.221 ± 0.516	0.831 ± 0.469	**0.043[a]**
CEBPβ	1.305 ± 0.159	0.633 ± 0.087	4.437 ± 2.166	3.842 ± 1.493	NS
LXRα	**1.118 ± 0.059[a]**	**0.417 ± 0.169[a]**	1.296 ± 0.354	1.529 ± 0.769	**0.006[a]**
Fatty acid transporter	**Vehicle**	**PDGF (15ng/ml)**	**GSK0660 (1µM)**	**GSK0660 (1µM) + PDGF(15ng/ml)**	**P VALUE**
CD36	0.915 ± 0.118	1.304 ± 0.896	1.867 ± 0.249	2.074 ± 0.517	NS
Nuclear receptor	**Vehicle**	**PDGF (15ng/ml)**	**GSK0660 (1µM)**	**GSK0660 (1µM) + PDGF(15ng/ml)**	**P VALUE**
PPAR β	**0.272 ± 0.054[a]**	**1.382 ± 0.341[a]**	1.094 ± 0.335	1.595 ± 0.562	**0.044[a]**
LXRβ	0.886 ± 0.299	0.410 ± 0.131	1.000 ± 0.128	0.962 ± 0.376	NS
FXR	**1.503 ± 0.330[a]**	**0.318 ± 0.269[a]**	1.031 ± 0.427	0.405 ± 0.307	**0.003[a]**
HSC marker	**Vehicle**	**PDGF (15ng/ml)**	**GSK0660 (1µM)**	**GSK0660 (1µM) + PDGF(15ng/ml)**	**P VALUE**
CRBP1	**1.098 ± 0.280[a]**	**0.084 ± 0.051[a]**	1.044 ± 0.160	1.208 ± 0.163	**0.016[a]**
αSMA	0.714 ± 0.151	1.381 ± 0.888	0.602 ± 0.399	0.233 ± 0.156	NS
GFAP	**0.913 ± 0.276[a]**	**0.096 ± 0.059[a]**	2.886 ± 1.366	3.946 ± 1.551	**0.037[a]**
CSRP2	**0.922 ± 0.133[a]**	**5.167 ± 3.656[a]**	1.089 ± 0.242	1.752 ± 0.549	**0.029[a]**
TGFβ1	0.726 ± 0.095	2.616 ± 1.506	2.794 ± 0.325	1.808 ± 0.659	NS

(a: Vehicle vs. PDGF; b: Vehicle vs. GSK0660; c: PDGF vs. (GSK0660 + PDGF); NS: not significant). mRNA levels measured using Taqman Real-time PCR, values shown relative to β-actin, n = 8 for each group. Data is presented as mean ± S.E.M.

5.8.5. Effects of PDGF-BB incubation on freshly isolated HSCs for 48hours followed by treatment with Pioglitazone (PGZ) & LXR Agonist (GW3965), PPAR β Agonist and PPAR β Antagonist (GSK0660) on cell proliferation assay

Freshly isolated HSCs were incubated on vehicle (0.004% DMSO), PGZ (5µM), GW3965 (2µM), GW0742 (100nM) & GSK0660 (1µM) for 72hours consecutively. After 24hours of drug treatment, PDGF-BB (15ng/ml) was added for 48hours consecutively, followed by MTT assay for cell proliferation analysis

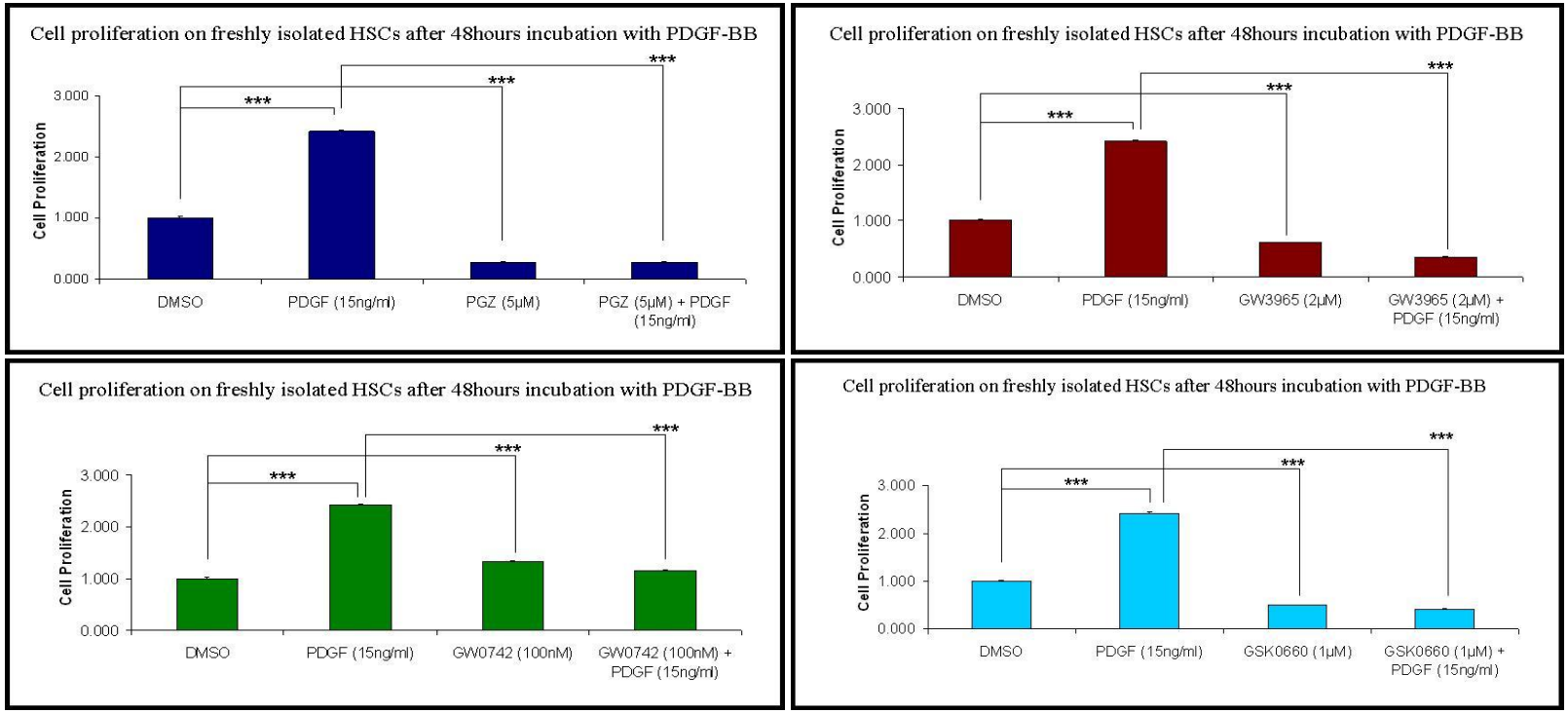

Figure 5.23: Effect of PDGF-BB incubation on freshly isolated HSCs for 48hours followed by treatment with Pioglitazone (PGZ) & LXR Agonist (GW3965), PPARβ Agonist and PPARβ Antagonist (GSK0660) on cell proliferation assay (**: $p<0.05$; ***: $p<0.005$).
PGZ, GW3965, GW0742 and GSK0660 reduced PDGF-BB induced cell proliferation in freshly isolated HSCs.

5.8.6. Effects of Pioglitazone (PGZ) in PDGF-BB treated Day 7 HSCs

Day 7 HSCs were incubated on vehicle (0.004% DMSO) and PGZ (5μM) for 72hours consecutively. On day 8, PDGF-BB (15ng/ml) was added for 48hours consecutively, followed by RNA extraction for gene expression analysis.

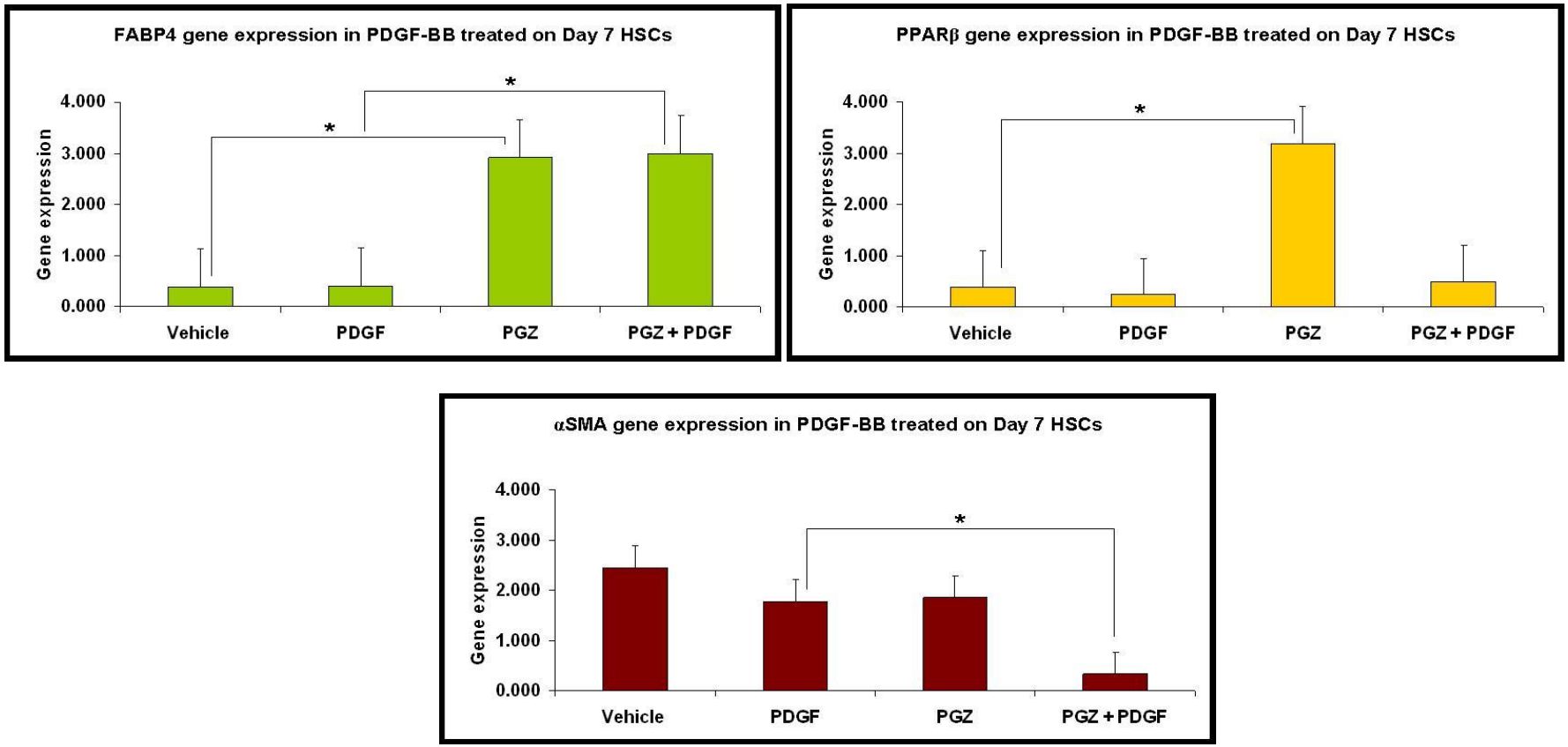

Figure 5.24: Effect of PDGF-BB incubation on day 7 HSCs for 48hours followed by treatment with PGZ. mRNA level measured using Taqman Real-time PCR, values shown relative to β-actin, n = 8 for each group. Data is presented as mean ± S.E.M. (*: $p<0.05$; **: $p<0.01$; ***: $p<0.000$).

Table 5.9: Effects of PDGF-BB incubation on Day 7 HSCs for 48 hours followed by Pioglitazone treatment on gene expressions.

Adipogenic genes	**Vehicle**	**PDGF (15ng/ml)**	**PGZ (5µM)**	**PGZ (5µM) + PDGF(15ng/ml)**	**P VALUE**
PPAR γ	1.412 ± 0.451	0.842 ± 0.250	0.606 ± 0.031	0.591 ± 0.357	NS
SREBP1C	0.002 ± 0.000	0.001 ± 0.000	0.003 ± 0.001	0.003 ± 0.001	NS
CEBPα	0.251 ± 0.112	0.106 ± 0.006	0.314 ± 0.097	0.363 ± 0.225	NS
CEBPβ	0.594 ± 0.209	1.399 ± 0.936	0.525 ± 0.285	0.647 ± 0.374	NS
LXRα	0.395 ± 0.145	0.370 ± 0.092	0.256 ± 0.069	0.267 ± 0.088	NS
Fatty acid transporter	**Vehicle**	**PDGF (15ng/ml)**	**PGZ (5µM)**	**PGZ (5µM) + PDGF(15ng/ml)**	**P VALUE**
CD36	0.409 ± 0.179	0.293 ± 0.100	0.068 ± 0.057	0.466 ± 0.406	NS
Nuclear receptor	**Vehicle**	**PDGF (15ng/ml)**	**PGZ (5µM)**	**PGZ (5µM) + PDGF(15ng/ml)**	**P VALUE**
LXRβ	0.636 ± 0.257	0.610 ± 0.139	0.570 ± 0.069	0.629 ± 0.357	NS
PXR	1.080 ± 0.197	0.639 ± 0.024	2.647 ± 0.651	2.500 ± 0.931	NS
FXR	0.001 ± 0.000	0.001 ± 0.000	0.002 ± 0.000	0.002 ± 0.001	NS
HSC marker	**Vehicle**	**PDGF (15ng/ml)**	**PGZ (5µM)**	**PGZ (5µM) + PDGF(15ng/ml)**	**P VALUE**
CRBP1	0.330 ± 0.125	0.432 ± 0.112	0.572 ± 0.042	0.391 ± 0.092	NS
GFAP	0.674 ± 0.253	0.852 ± 0.360	1.463 ± 0.495	1.663 ± 0.883	NS
CSRP2	0.503 ± 0.068	0.627 ± 0.160	0.381 ± 0.044	0.282 ± 0.095	NS
TGFβ1	0.859 ± 0.178	0.983 ± 0.348	0.848 ± 0.013	0.650 ± 0.262	NS

[NS: not significant]. mRNA levels measured using Taqman Real-time PCR, values shown relative to β-actin, n = 8 for each group. Data is presented as mean ± S.E.M.

PDGF-BB has much less effect upon gene expression in cells cultured for 7 days as compared to freshly isolated cells. No significant different between vehicle and PDGF-BB treated HSCs on day 7. PGZ increased FABP4 expression and decreased αSMA levels in PDGF-BB treated Day 7 HSCs. PGZ increased both PPARβ and FABP4 expression compared to vehicle.

5.8.7. Effects of LXR Agonist (GW3965) in PDGF-BB treated Day 7 HSCs

Day 7 HSCs were incubated on vehicle (0.004% DMSO) and GW3965 (2μM) for 72hours consecutively. On day 8, PDGF-BB (15ng/ml) was added for 48hours consecutively, followed by RNA extraction for gene expression analysis.

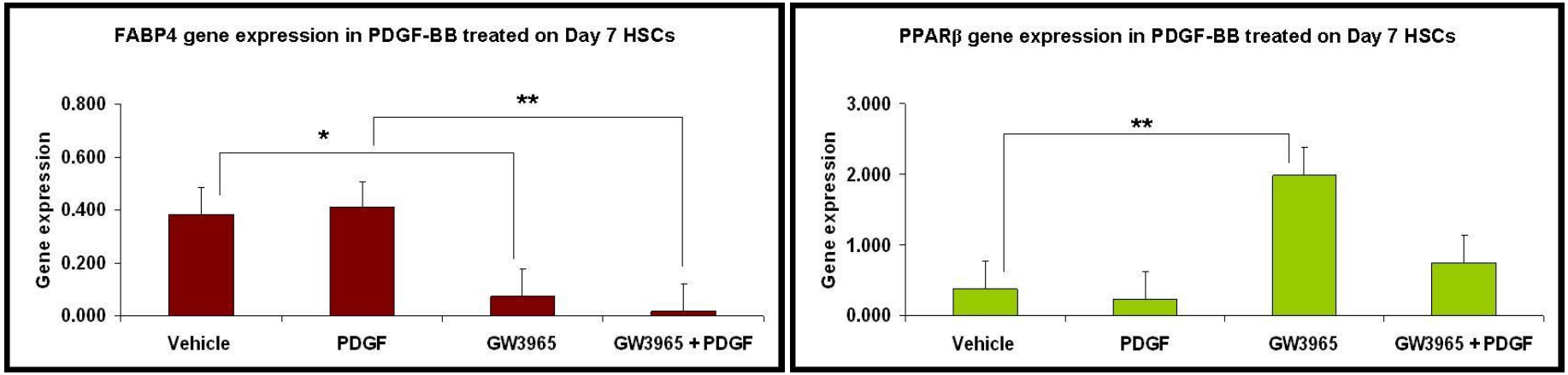

Figure 5.25: Effect of PDGF-BB incubation on day 7 HSCs for 48hours followed by treatment with GW3965. mRNA level measured using Taqman Real-time PCR, values shown relative to β-actin, n = 8 for each group. Data is presented as mean ± S.E.M. (*: $p<0.05$; **: $p<0.01$; ***: $p<0.000$).

GW3965 reduced FABP4 expression in PDGF treated Day 7 HSCs. Meanwhile, GW3965 alone increased PPAR β expression but reduced FABP4 expression. All the other genes show no significant difference as shown in Table 5.7.1. over leaf.

Table 5.10: Effects of PDGF-BB incubation on Day 7 HSCs for 48 hours followed by GW3965 treatment on gene expressions.

Adipogenic genes	**Vehicle**	**PDGF (15ng/ml)**	**GW3965 (2μM)**	**GW3965 (2μM) + PDGF(15ng/ml)**	**P VALUE**
PPAR γ	1.412 ± 0.451	0.842 ± 0.250	0.972 ± 0.427	1.390 ± 0.665	NS
SREBP1C	0.002 ± 0.000	0.001 ± 0.000	1.465 ± 1.140	0.971 ± 0.691	NS
CEBPα	0.251 ± 0.112	0.106 ± 0.006	0.394 ± 0.209	0.571 ± 0.182	NS
CEBPβ	0.594 ± 0.209	1.399 ± 0.936	2.617 ± 1.282	0.667 ± 0.273	NS
LXRα	0.395 ± 0.145	0.370 ± 0.092	1.289 ± 0.255	1.466 ± 0.570	NS
Fatty acid transporter	**Vehicle**	**PDGF (15ng/ml)**	**GW3965 (2μM)**	**GW3965 (2μM) + PDGF(15ng/ml)**	**P VALUE**
CD36	0.409 ± 0.179	0.293 ± 0.100	0.665 ± 0.427	1.599 ± 1.061	NS
Nuclear receptor	**Vehicle**	**PDGF (15ng/ml)**	**GW3965 (2μM)**	**GW3965 (2μM) + PDGF(15ng/ml)**	**P VALUE**
LXRβ	0.636 ± 0.257	0.610 ± 0.139	1.263 ± 0.557	0.428 ± 0.147	NS
PXR	1.080 ± 0.197	0.639 ± 0.024	4.943 ± 1.795	4.835 ± 2.053	NS
FXR	0.001 ± 0.000	0.001 ± 0.000	0.006 ± 0.001	0.005 ± 0.002	NS
HSC marker	**Vehicle**	**PDGF (15ng/ml)**	**GW3965 (2μM)**	**GW3965 (2μM) + PDGF(15ng/ml)**	**P VALUE**
CRBP1	0.330 ± 0.125	0.432 ± 0.112	0.768 ± 0.111	1.406 ± 1.133	NS
αSMA	2.429 ± 1.006	1.764 ± 0.656	1.413 ± 0.861	0.556 ± 0.277	NS
GFAP	0.674 ± 0.253	0.852 ± 0.360	1.247 ± 0.259	0.416 ± 0.182	NS
CSRP2	0.503 ± 0.068	0.627 ± 0.160	0.558 ± 0.166	0.425 ± 0.184	NS
TGFβ1	0.859 ± 0.178	0.983 ± 0.348	1.436 ± 0.302	0.770 ± 0.383	NS

[NS: Not significant]. mRNA levels measured using Taqman Real-time PCR, values shown relative to β-actin, n = 8 for each group. Data is presented as mean ± S.E.M.

5.8.8. Effect of PPAR β Agonist (GW0742) in PDGF-BB treated on Day 7 HSCs

Day 7 HSCs were incubated on vehicle (0.004% DMSO), GW0742 (100nM) for 72hours consecutively. On day 8, PDGF-BB (15ng/ml) was added for 48hours consecutively, followed by RNA extraction for gene expression analysis.

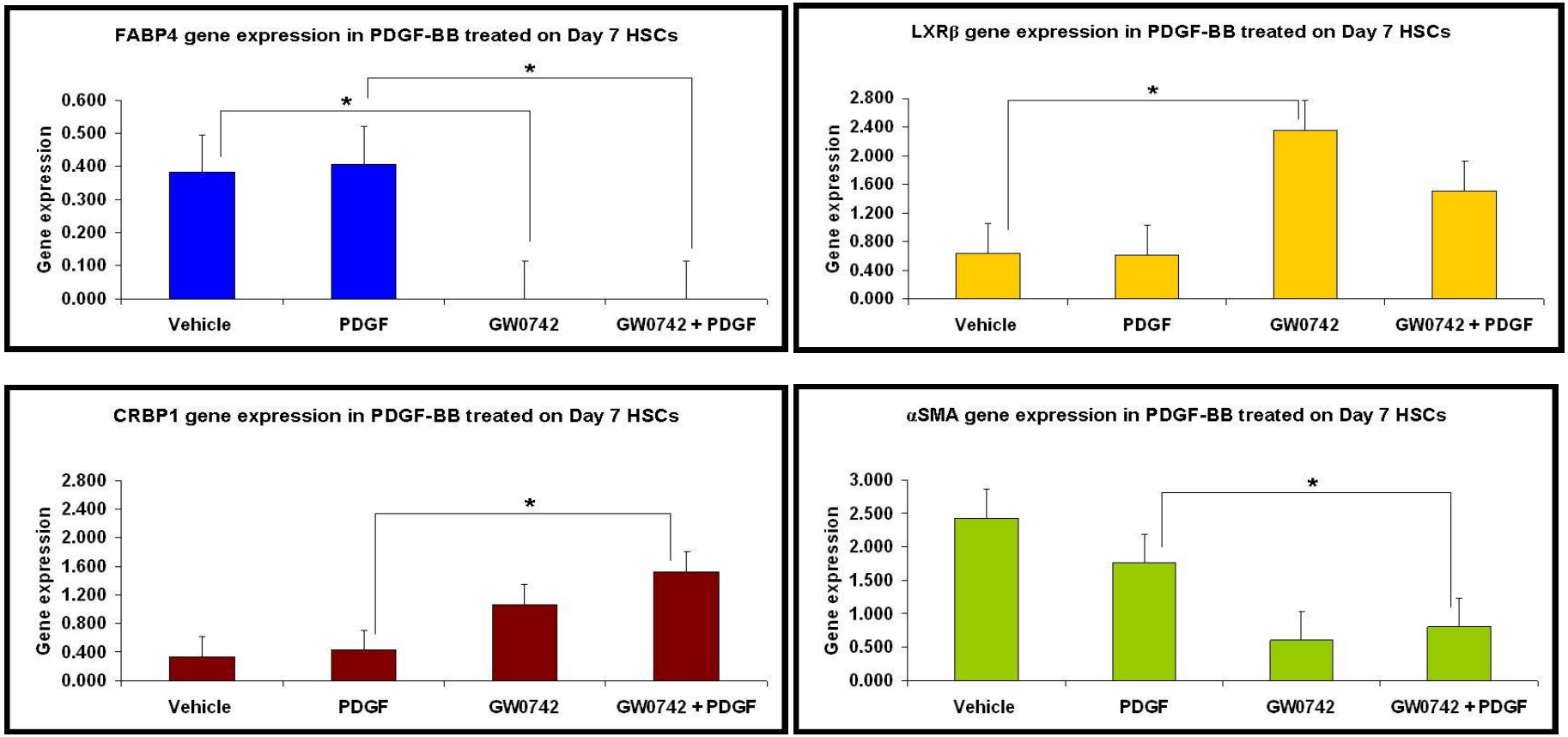

Figure 5.26: Effect of PDGF-BB incubation on day 7 HSCs for 48hours followed by treatment with GW0742. mRNA level measured using Taqman Real-time PCR, values shown relative to β-actin, n = 8 for each group. Data is presented as mean ± S.E.M. (*: $p<0.05$; **: $p<0.01$; ***: $p<0.000$).

Table 5.11: Effects of PDGF-BB incubation on Day 7 HSCs for 48 hours followed by GW0742 treatment on gene expressions.

.

Adipogenic genes	**Vehicle**	**PDGF (15ng/ml)**	**GW0742 (100nM)**	**GW0742(100nM) + PDGF(15ng/ml)**	**P VALUE**
PPAR γ	1.412 ± 0.451	0.842 ± 0.250	5.340 ± 2.307	3.975 ± 1.425	NS
SREBP1C	0.002 ± 0.000	0.001 ± 0.00	0.005 ± 0.002	0.008 ± 0.003	NS
CEBPα	0.251 ± 0.112	0.106 ± 0.006	1.194 ± 0.489	2.327 ± 1.430	NS
CEBPβ	0.594 ± 0.209	1.399 ± 0.936	2.788 ± 1.496	2.901 ± 1.994	NS
LXRα	0.395 ± 0.145	0.370 ± 0.092	1.187 ± 0.497	0.645 ± 0.374	NS
Fatty acid transporter	**Vehicle**	**PDGF (15ng/ml)**	**GW0742 (100nM)**	**GW0742(100nM) + PDGF(15ng/ml)**	**P VALUE**
CD36	0.409 ± 0.179	0.293 ± 0.100	0.023 ± 0.016	0.586 ± 0.430	NS
Nuclear receptor	**Vehicle**	**PDGF (15ng/ml)**	**GW0742 (100nM)**	**GW0742(100nM) + PDGF(15ng/ml)**	**P VALUE**
PPAR β	0.375 ± 0.121	0.229 ± 0.047	12.638 ± 8.692	1.952 ± 0.837	NS
PXR	1.080 ± 0.197	0.639 ± 0.024	15.305 ± 11.899	6.050 ± 1.208	NS
FXR	0.001 ± 0.000	0.001 ± 0.000	0.013 ± 0.010	0.009 ± 0.004	NS
HSC marker	**Vehicle**	**PDGF (15ng/ml)**	**GW0742 (100nM)**	**GW0742(100nM) + PDGF(15ng/ml)**	**P VALUE**
GFAP	0.674 ± 0.253	0.852 ± 0.360	4.364 ± 3.159	2.326 ± 0.954	NS
CSRP2	0.503 ± 0.068	0.627 ± 0.160	1.067 ± 0.403	0.616 ± 0.307	NS
TGFβ1	0.859 ± 0.178	0.983 ± 0.348	0.627 ± 0.621	0.710 ± 0.434	NS

(NS: Not significant). mRNA levels measured using Taqman Real-time PCR, values shown relative to β-actin, n = 8 for each group. Data is presented as mean ± S.E.M.

PDGF-BB has much less effect upon gene expression in cells cultured for 7 days as compared to freshly isolated cells. No significant different between vehicle and PDGF-BB treated HSCs on day 7.GW0742 reduced both FABP4 and αSMA levels and increased CRBP1 levels in PDGF-BB treated Day 7 HSCs.GW0742 increased LXRβ and reduced FABP4 expression compared to vehicle.

5.8.9. Effect of PPAR β Antagonist (GSK0660) in PDGF-BB treated on Day 7 HSCs

Day 7 HSCs were incubated on vehicle (0.004% DMSO) and GSK0660 (1μM) for 72hours consecutively. On day 8, PDGF-BB (15ng/ml) was added for 48hours consecutively, followed by RNA extraction for gene expression analysis.

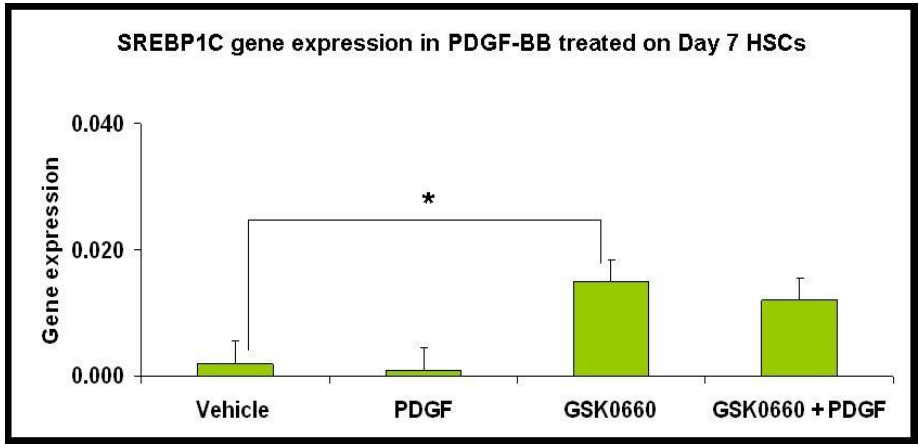

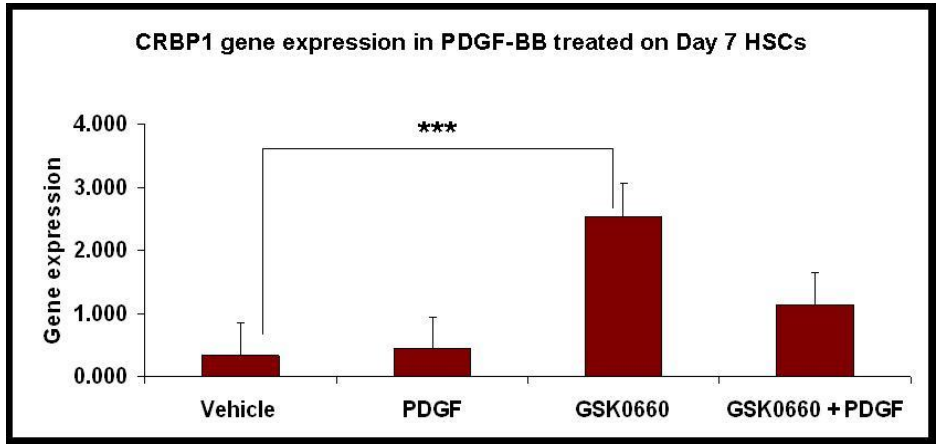

Figure 5.27: Effect of PDGF-BB incubation on day 7 HSCs for 48hours followed by treatment with GSK0660. mRNA level measured using Taqman Real-time PCR, values shown relative to β-actin, n = 8 for each group. Data is presented as mean ± S.E.M. (*: $p<0.05$; **: $p<0.01$; ***: $p<0.000$).

GSK0660 increased both SREBP1C and CRBP1 level compared to vehicle. No other gene expressions showed any significant difference (as shown in Table 5.8.1. over leaf).

Table 5.12: Effects of PDGF-BB incubation on Day 7 HSCs for 48 hours followed by GSK0660 treatment on gene expressions.

Adipogenic genes	**Vehicle**	**PDGF (15ng/ml)**	**GSK0660 (1μM)**	**GSK0660 (1μM) + PDGF(15ng/ml)**	**P VALUE**
PPAR γ	1.412 ± 0.451	0.842 ± 0.250	3.831 ± 1.502	3.092 ± 1.212	NS
CEBPα	0.251 ± 0.112	0.106 ± 0.006	0.491 ± 0.149	0.435 ± 0.334	NS
CEBPβ	0.594 ± 0.209	1.399 ± 0.936	1.949 ± 0.669	0.119 ± 0.075	NS
LXRα	0.395 ± 0.145	0.370 ± 0.092	0.460 ± 0.270	0.308 ± 0.179	NS
Fatty acid transporter	**Vehicle**	**PDGF (15ng/ml)**	**GSK0660 (1μM)**	**GSK0660 (1μM) + PDGF(15ng/ml)**	**P VALUE**
CD36	0.409 ± 0.179	0.293 ± 0.100	1.076 ± 1.073	0.003 ± 0.001	NS
FABP4	0.382 ± 0.092	0.406 ± 0.127	0.099 ± 0.099	0.246 ± 0.245	NS
Nuclear receptor	**Vehicle**	**PDGF (15ng/ml)**	**GSK0660 (1μM)**	**GSK0660 (1μM) + PDGF(15ng/ml)**	**P VALUE**
PPAR β	0.375 ± 0.121	0.229 ± 0.047	6.806 ± 5.692	2.381 ± 1.135	NS
LXRβ	0.636 ± 0.257	0.610 ± 0.139	1.519 ± 0.761	0.759 ± 0.496	NS
PXR	1.080 ± 0.197	0.639 ± 0.024	9.645 ± 3.411	4.140 ± 1.994	NS
FXR	0.001 ± 0.000	0.001 ± 0.000	0.009 ± 0.003	0.008 ± 0.003	NS
HSC marker	**Vehicle**	**PDGF (15ng/ml)**	**GSK0660 (1μM)**	**GSK0660 (1μM) + PDGF(15ng/ml)**	**P VALUE**
αSMA	2.429 ± 1.006	1.764 ± 0.656	0.202 ± 0.197	1.804 ± 1.266	NS
GFAP	0.674 ± 0.253	0.852 ± 0.360	4.231 ± 3.212	2.010 ± 1.204	NS
CSRP2	0.503 ± 0.068	0.627 ± 0.160	1.130 ± 0.450	0.802 ± 0.142	NS
TGFβ1	0.859 ± 0.178	0.983 ± 0.348	2.245 ± 1.011	1.125 ± 0.733	NS

[NS: Not significant]. mRNA levels measured using Taqman Real-time PCR, values shown relative to β-actin, n = 8 for each group. Data is presented as mean ± S.E.M.

5.8.10. Effect of Pioglitazone (PGZ) & LXR Agonist (GW3965), and PPAR β Agonist (GW0742) in PDGF-BB treated Day 7 HSCs on cell proliferation assay

Day 7 HSCs were incubated with vehicle (0.004%), PGZ or GW3965 for 72hours consecutively. On day 8, PDGF-BB was added for 48hours consecutively, followed by MTT assay for cell proliferation analysis.

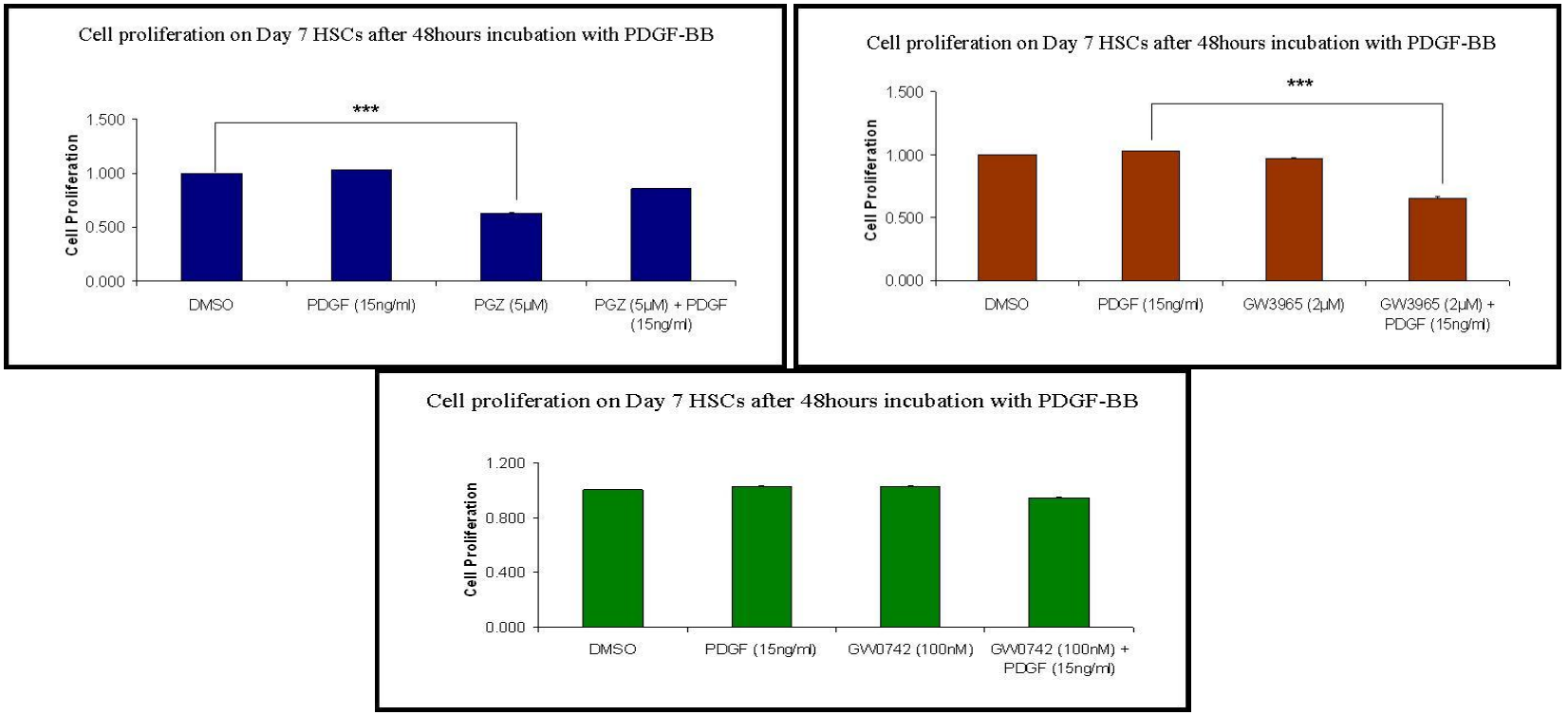

Figure 5.28: Effect of Pioglitazone (PGZ) & LXR Agonist (GW3965) and PPAR β Agonist (GW0742)in PDGF-BB treated Day 7 HSCs on cell proliferation assay (**: $p<0.05$; ***: $p<0.005$).

PGZ reduced cell proliferation compared to vehicle group, whereas GW3965 reduced PDGF-BB induced cell proliferation in day 7 HSCs. There are no significant effects of GW0742 treatment.

5.9. Discussion

In this chapter, the primary objective was to produce an *in vitro* cell culture model that is representative of human HSC *in vivo* and to model both quiescent and activated myofibroblastic phenotypes. The second objective was to determine the effect of potentially therapeutic nuclear receptor agonists and antagonists upon quiescent and activated stellate cell proliferation and gene expression.

Culturing the human stellate cells for different lengths of time and on different culture surfaces was assessed for the ability to generate quiescent and myofibroblastic HSCs. Day 7 HSC plated on plastic expressed a number of adipogenic genes at comparable levels to cells plated on matrigel suggesting that they had not become fully transdifferentiated into myofibroblast. CEBPβ expression was highest in HSC grown on plastic as compared to other surfaces. Ribosomal S-6 kinase (RSK) activation and phosphorylation of Thr217 of CEBPβ has been shown to promote liver fibrosis both in humans and in animal models (Buck & Chojkier, 2007). Therefore, the elevation of CEBPβ in HSCs plated on plastic may be indicative of an activated phenotype. The lower levels of GFAP expression observed in the HSCs plated on plastic could occur as a result of the increased TGFβ1 expression (Carrotti et al., 2008; Gressner & Weiskirchen, 2006). Interestingly, the results of PCNA expression protein analysis indicated that HSCs plated on plastic were not proliferating at a rapid rate. TGFβ has been reported to regulate proliferation and activation of stellate cells (Gressner & Weiskirchen, 2006; Robert & Sporn, 1993; Robert, 1998). It is possible that elevated TGFβ1 expression may inhibit mitosis (Robert & Sporn, 1993; Robert, 1998).

CSRP2 is involved in stellate cell transdifferentiation, is a marker of myofibroblastic activation and is not expressed in hepatocytes, kupffer cells or sinusoidal endothelial cells (Weiskirchen et al., 2001). HSCs plated on collagen had the highest levels of CSRP2 and showed the clearest morphological signs of transdifferentiation.

Matrigel plated cells had the highest levels of PPAR γ and PXR expression both of which are reported to inhibit stellate cell transdifferentiation (Haughton et al., 2006; She et al., 2005; Miyahara et al., 2000). FXR expression was also high in matrigel plated HSCs, and may be responsible for inhibition of α(1) collagen production (Fiorucci et al., 2004b). Also, the HSCs plated on matrigel had low levels of proliferation in agreement with Gaca et al. (2003).

Overall, cells plated on plastic, collagen and matrigel behaved in a similar way to that previously described in the literature. HSCs grown on matrigel showed the lowest level of expression of activated HSC marker genes and had the lowest proliferation rates as assessed by PCNA protein content.

HSCs become activated when plated on plastic surfaces as previously reported by Bachem et al. (1992). Therefore in this study, stellate cells were activated and then plated on different surfaces to determine whether activation can be reversed by plating them on matrigel surface. No change in HSCs morphology was observed nor was adipogenic and nuclear receptor gene expression altered when HSCs were sub-cultured on matrigel after previously being cultured on plastic.

Previous studies have reported that, PPAR γ, SREBP-1C liver-X-receptor (LXR)-α, CCAAT/ enhanced binding protein family (C/EBP)-α and β which are adipogenic transcriptional factors, are highly expressed in HSCs which help to maintain quiescent phenotype (Hazra et al., 2004; She et al., 2005). In liver injury, HSC are activated and expression of the adipogenic transcriptional factors are reduced resulting in HSC transdifferentiation into activated myofibroblasts (Miyahara et al., 2000; Hazra et al., 2004; She et al., 2005). Figure 5.29 shows the genes that are expressed in quiescent and activated stellate cells, and it indicates the roles of various growth factors and transcription factors in the two phases of stellate cell activation.

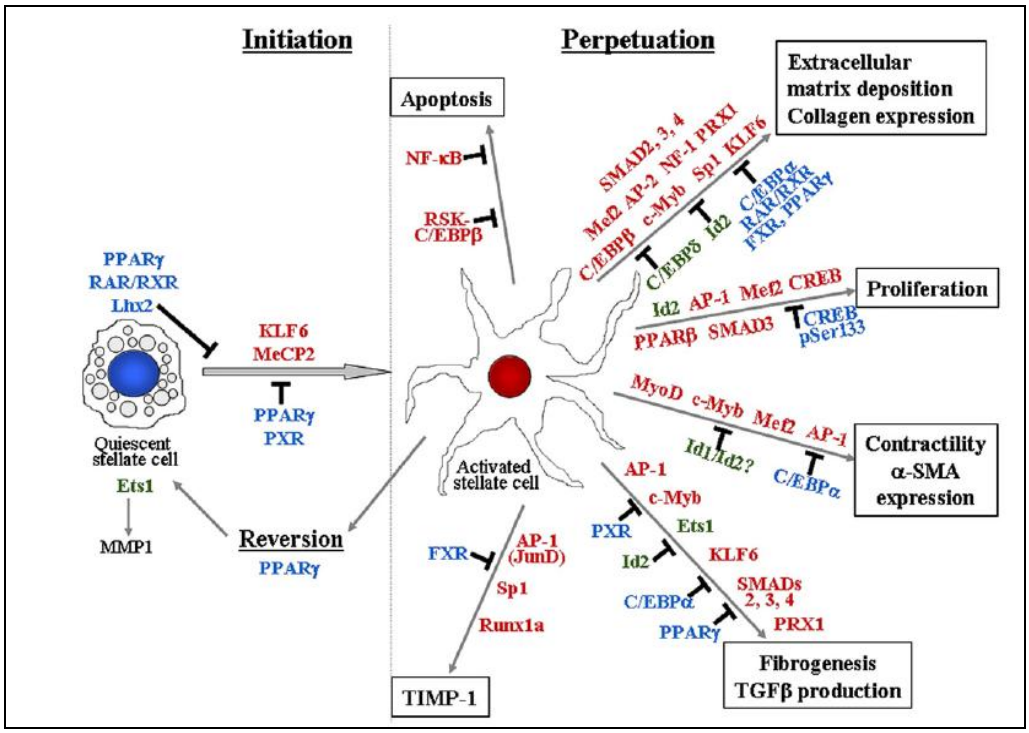

Figure 5.29: Quiescent and activated stellate cells gene expression. Quiescent stellate cells express a number of transcription factors which regulate the quiescent phenotype (names in blue). Once appropriate stimuli are received by the HSC, they undergo an initiation phase of activation, followed by perpetuation. Activated HSCs acquire expression of a number of transcription factors that quiescent cells did not have (names in red). Transcription factors shown in green are either equivalently expressed in both quiescent and activated HSCs (Ets) or their function remains poorly defined (Id1/2). (Adapted from Mann & Mann, 2009).

(RAR: retinoid acid receptor; RXR: retinoid X-receptor; Lhx2: LIM Homoebox 2; MeCP2: methyl CpG binding protein 2; CREB: cyclic AMP response element binding protein; AP: activator protein; NF1: Nuclear factor 1; PRX: paired type Homoebox; KLF6: Kruppel like factor 6; MyoD: Myogenic D; c-Myb: Myb family protein; Id: Inhibitor of DNA binding; Ets1:E26 transformation-specific 1; Sp1:specificity protein 1; SMAD: SMAD, mothers against decapentaplegic ; Mef2: Monocyte enhancer factor 2; Runx1a: runt-related transcription factor ; RSK: ribosomal S-6 kinase; TIMP1: Tissue inhibitor metaloporteinase 1; C/EBP: CCAT enhancer binding protein; PXR: Preganane X-receptor; FXR: Farnesoid X-receptor; PPAR: peroxisome proliferator activator receptor; NFkB: nuclear factor kappa beta).

PPAR γ, PXR, FXR, CEBPα have all been reported as being expressed at high levels in quiescent stellate cells whereas CEBPβ is expressed in activated stellate cells as shown in Figure 5.29 above (Mann & Mann, 2009). The data in this study indicates that in freshly isolated HSCs SREBP1C, CEBPα, LXRα, LXRβ, PXR, FXR and CD36 are all expressed at relatively high levels and expression declines over time in culture. Conversely, CEBPβ, CSRP2 and TGFβ1 were highest in freshly isolated HSC as compared to cells grown for 7, 14 or 21 days. This may indicate an overall de-differentiation of HSCs over time rather than transdifferentiation into myofibroblasts. However it is noteworthy that as β-actin expression increased 6 times during stellate cells activation in a rat model (Derek Mann, personal communication university of Nottingham 2011), and that in these studies β-actin was used as a reference gene, this may have potential confound effect, if the same is true in the current model. Indeed many previous studies have used HSC that are passaged up to 5 times in their experiments (Handy et al., 2010; Jameel et al., 2009). It may well be that when left in culture HSC in fact become partially dormant and have an intermediate phenotype that is neither activated nor quiescent; however, a comparison of gene expression profiles with HSC passaged several times and the normalisation using other reference gene [Glyceraldehyde-3-phosphate dehydrogenase (GAPDH)] will be required to substantiate this.

If the observed reduction in nuclear receptor and adipogenic gene expression over time is indicative of an activated phenotype, as indicated in part by the data from this study and from previous work, they may not be expressed at sufficient level in activated stellate cells to be a functional therapeutic target. This may indicate that .the therapeutic effects of nuclear receptor ligands.

PDGF-BB released by kupffer cells *in vivo* will bind to the PDGFB receptor (PDGFBR) on HSCs. This will in turn, lead to stellate cell activation and proliferation (Bonner, 2004; Pinzani et al., 1996). The next phase of this study was to determine the effects of nuclear receptor ligands upon blocking PDGF-BB mediated activation and proliferation of freshly isolated HSCs and

HSCs cultured for 7 days in an attempt to model the effects of nuclear receptor ligands upon quiescent and activated stellate cells respectively.

PDGF-BB treatment of freshly isolated HSCs reduced both adipogenic gene and CRBP1 expression, but increased PPAR β and CSRP2 expression and cell proliferation. PPARβ has been described as being a promoter of stellate cell activation and proliferation (Hellemans et al., 2003). CSRP2 is a marker for stellate cell transdifferentiation as reported in a previous study (Weiskirchen et al., 2001). Current findings suggest that, PDGF-BB induced stellate cells transdifferentiation into activated phenotype.

Davis et al. (1990) has reported that, retinoic acid incubation in rat stellate cells, inhibit cell proliferation, interstitial collagen production as well as TGFβ expression. Thus, reduction in CRBP1 by PDGF-BB, leads to increased cell proliferation in this study.

Pioglitazone (PGZ) is a PPAR γ ligand reported to exert anti-inflammatory and anti-fibrotic effects as described in Chapter 3 & 4. Pioglitazone treatment of PDGF-BB activated stellate cells restored both the adipogenic gene expression and nuclear receptor expression. PGZ also abolished PDGF-BB induced stellate cell proliferation and induction of activation markers such as α-SMA. PGZ also increased FABP4 and PPAR β expression in stellate cells. FABP4 is a fatty acid transporter which has been shown to play a role in maintaining the adipogenic phenotype of the stellate cells (Larter et al., 2008).

GW3965 is an LXR agonist that can exert anti-inflammatory effects (Park et al., 2010). GW3965 significantly increased SREBP1C and PPAR γ expression in PDGF treated HSCs, whereas FABP4 expression was reduced as were activational markers. These data suggest that LXR activation can block stellate cell activation and proliferation induced by PDGF-BB, but the mechanism of action in terms of signal transduction. GW3965 reduced CEBPβ expression and that of PPAR β as compared to vehicle treated cells.

PDGF-BB, Pioglitazone and GW3965 all increased PPAR β expression, which indicates that signals that both promote and repress stellate cell activation can increase PPAR β expression. PPAR β is thought to play a role in regulating retinol ester (RE) levels in rat stellate cells (Hellemans et al., 2003) and has also been implicated in stellate cell activation and proliferation (Hellemans et al., 2003). Shan et al. (2008) demonstrated that PPAR β null mice treated with CCl_4 had increased hepatic ALT, TNFα and αSMA expression levels, which they attributed to increased NFKß activation as compared to wild type mice. Thus, in the absence of PPAR β, hepatoxicity and liver fibrosis are exacerbated in response to chemically induced liver injury (Shan et al., 2008). PXR and PPAR β activation have been demonstrated to block NFkB-mediated transcriptional activation of inflammatory genes in the liver (Wahli, 2008). In contrast, PPAR β has also been shown to increase cell proliferation in skin during wound healing (Michalik & Wahli, 2006) and potentiate colon poly formation in colon carcinogenesis animal model (Harman et al., 2004). Thus, the role of PPAR β in stellate cells and indeed in all cellular systems is undetermined in terms of whether activation is pro-proliferative and pro-inflammatory or the reverse.

This study showed that, treatment with the PPAR β agonist GW0742 increased PPAR γ, CD36, PXR, and CRBP1 expression, and decreased CSRP2 expression and cell proliferation induced by PDGF-BB in freshly isolated HSCs. These effects indicate that activation of PPAR β in freshly isolated HSCs does not promote stellate cell activation and proliferation as has been previously described (Hellemans et al., 2003). GW0742 also increased PPAR β, PXR and CRBP1 and reduced SREBP1C expression compared to vehicle, indicating that in quiescent HSCs, activation of PPAR β may promote expression of genes primarily involved in maintenance of stellate cell quiescence. GSK0660 is a PPAR β antagonist that in this study was shown to increase FABP4 and PXR expression and reduce cell proliferation induced by PDGF-BB in freshly isolated HSCs. GSK0660 also elevated FABP4 expression when compared to vehicle in contrast to PPAR β agonist treatment (GW0742). Thus the effects of both PPAR β agonists and antagonists promote changes in gene expression that are hard to reconcile with both the received

wisdom in terms of the changes in gene expression observed when stellate cells become activated and also previous studies by Hellemans et al. (2003) examining the role of PPAR β in HSC.

The effects of PDGF-BB were also studied in stellate cells cultured for 7 days .The response of these cells to PDGF was minimal when compared to freshly isolated HSCs. This perhaps could be viewed as further evidence to suggest that when HSCs are cultured for any given length of time without sub-culturing, they de-differentiate rather than trans-differentiate.

In summary, the nuclear receptor ligands used in this study can clearly inhibit both proliferation and activation of quiescent stellate cells when challenged with PDGF-BB. The role of PPAR β however is unclear as both agonist and antagonist seemed to promote the expression of genes associated with a quiescent HSC phenotype and the PPAR β antagonist GSK0660 decreased PDGF-BB induced HSC proliferation.

CHAPTER 6
General Discussion

Pioglitazone is a Thiazolidinediones (TZD) peroxisome proliferator activated receptor (PPAR) γ agonist. It exerts its effect by activating both PPAR γ1 and PPAR γ2 isoforms as reported in CV-1 cells (Lehmann et al., 1995) and also promotes cell differentiation in adipose tissue (Spiegelman & Flier, 1996). However, the effects of PPAR γ activation after TZD treatment have not been reported in detail in human liver. PGZ treatment in non-diabetic NASH patients did not appear to induce PPAR γ expression at the mRNA level in whole liver, but an increase in expression was seen in human hepatic stellate cells in culture as seen in Chapter 5. This finding indicates that PGZ mediates at least some of its effects by acting directly upon PPAR γ in human hepatic stellate cells rather than acting upon whole body lipid metabolism. However the effects of PGZ upon PPAR γ expression in kupffer cells was not observed in this study, but it has been reported that kupffer cell expressed both PPAR α and PPAR γ (Everett et al., 2000). Given the importance of Kupffer cells in hepatic inflammation, it is likely that PGZ may also exert some of its effects upon tissue resident immune cells in the liver.

PPAR β expression was induced after PGZ treatment both in vivo and in stellate cells in culture and these findings appear to be novel. PPAR β has been reported to promote cell proliferation in stellate cells (Hellemans et al., 2003) and also implicated in regulating proinflammatory genes in mice treated with CCl_4 (Shan et al., 2008). Based on current findings, the increase in PPAR β expression observed in NASH patients may be primarily in hepatocytes rather than stellate cells as PPAR β-positive stellate cells as observed by immunohistochemistry were reduced in PGZ-treated individuals. This increase in hepatocytes PPAR β could potentially elevate mitochondrial β-oxidation in non-diabetic NASH patients treated with PGZ.

In freshly isolated stellate cells in culture, PPAR β expression was increased after incubation with PDGF, PGZ, LXR agonist (GW3965) and PPAR β agonist (GW0742). Both PDGF and GW0742 treatment increased cell

proliferation. But in PGZ, GW3965 and (GW0742 + PDGF) treated inhibit both cell proliferation and the expression of stellate cell activation markers such as α-SMA. The fact that GW0742 alone caused up regulation of PPAR γ, CRBP1 and GFAP expression, all 3 genes associated with the quiescent, adipogenic stellate cell phenotype, suggests that the relationship between PPAR β induction and stellate cell phenotype may not be as simple as previously described. Further studies are required understand the role of PPAR β activation in activated stellate cells as compared to freshly isolated cells. In much of the current literature, stellate cells passaged 4 or 5 times are used as a model of myofibroblastic cells and it will be interesting to see how these cells respond to PPAR β ligands.

FABP4 is a fatty acid binding protein that is highly expressed in adipocytes and macrophages and the expression and activation of FABP4 has been reported to contribute to the pathogenesis of obesity, metabolic syndrome and associated inflammation (Makowski & Hotamisligil, 2004). FABP4 expression was elevated in NAFLD liver compared to normal liver and NASH in this study. PGZ treatment did not increase FABP4 expression in human non-diabetic NASH liver but increases were observed in human hepatic stellate cells in culture. This suggests that in stellate cells, FABP4 may play a different role to that observed in adipocytes and immune cells. It may also be true that FABP4 expression is associated with the quiescent state, FABP4 ligands may induce inflammatory signalling as has been observed in immune cells. Future studies should examine the role of FABP4 in both stellate cells and in kupffer cells to observe the effects of FABP4 ligands and PGZ, upon cellular activation and inflammation in the liver.

Farnesoid X receptor (FXR) expression was studied both in human liver and stellate cells. In human liver biopsies, there was no observed difference in FXR expression between any of the groups studied. But in human hepatic stellate cells FXR expression was shown to be higher in freshly isolated stellate cells, as compared to cells cultured for longer periods of time. Furthermore, FXR expression was reduced by PDGF treatment and this reduction could be reversed by PGZ. The FXR ligand (GW4064) has been reported to induce

PPARγ and decrease α(1) collagen, αSMA and TIMP1 expression in rat stellate cells in culture (Fiorucci et al., 2005). Thus, PGZ may exert anti-fibrotic effects at least in part by increasing stellate cell FXR expression in vivo. A future study should examine the effects of the specific FXR ligand (GW4064) and the FXR antagonist Guggulsterone upon PDGF-BB incubated HSCs.

PGZ treatment increased PXR expression both in human liver and stellate cells. PXR is thought to exert anti-inflammatory effects by inhibiting NFkB transcriptional activity. Both PGZ and the PPAR β agonist (GW0742) increased PXR expression in stellate cells. The PXR agonist Rifampicin has been reported to play a role in inhibiting stellate cell proliferation, and represses TGFβ and αSMA expression. The effects of PXR agonist (2μM SR12813) and PXR antagonist (50μM of Ketoconazole) inhibit stellate cell proliferation (was observed but not reported in this study). However, due to time constraints the effects of these ligands was not examined in PDGF-BB treated HSC.

Cell proliferation was an important measurement in this study. Both PCNA and Ki67 expression were used as surrogate markers of cell proliferation. PCNA has been reported to be expressed in G_1 and S phase followed by a decline in expression during G_2 and M phase of the cell cycle (Foley et al. 1993). Ki67 is a more specific marker to of cell proliferation rate, and is used in cancer diagnosis and prognosis e (Scholzen & Gerdes, 2000). Ki67 is not expressed during G_0 phase of the cell cycle and thus it only is detected in the nucleus of dividing cells.

There are several limitations in this study, where in human hepatic stellate cells culture; β-actin was used as the reference gene for Taqman RT-PCR. During the viva voce examination, Prof Derek Mann advised that GAPDH should be used as the reference gene in the future for stellate cells gene expression. β-actin expression increased 6 times during stellate cells activation (Derek Mann personal communication, University of Nottingham 2011). The usage of β-actin as the reference gene for stellate cells culture over

time period may explain the lower expression of αSMA and TGFβ1 expression on day 7 and day 21.

Furthermore verification of αSMA expression in human hepatic stellate cells culture was not performed (immunocytochemistry staining), but the markers for stellate cell activation (αSMA & TGFβ1) were measured using Taqman RT-PCR. For liver immunohistochemistry, the αSMA antibody dilution should be increased either 1:100 or 1:200 due to slightly weak immunohistochemistry staining was observed in some samples.

This thesis only examined liver biopsy and human hepatic stellate cell samples. There are other cell types that require individual study in order to understand the pathogenesis of NAFLD and NASH (see Figure 6.1). Kupffer cells, sinusoidal endothelial cells, billiary epithelial cells, platelets and T cells are all sources of proinflammatory signals that would activate stellate cells (see Figure 6.1). The data in this thesis indicate that PGZ treatment and PPAR γ activation in general prevents stellate cell activation and proliferation. Future studies could examine the role of PPAR γ and other nuclear receptors in other non-parenchymal cells types such as kupffer cells and sinusoidal endothelial cells.

Table 6.1: Mechanism pathway of hepatic fibrosis and stellate cell activation symbol and abbreviation

Symbol	Abbreviation
CCL21	Chemokine (C-C motif) ligand 21
CD40	CD40 molecule, TNF receptor superfamily member 5
COL	Collagen
EGF	Epidermal growth factor
IFNγ	Interferon gamma
IGF	Insulin like growth factor
IL6	Interleukin 6
KLF6	Kruppel-like factor 6
LHX2	LIM homeobox protein 2
MMP	Matrix metaloproteinase
NS3	Nonstructural viral protein 3
NS5	Nonstructural viral protein 5
PDGF	Platelet derived growth factor
SPARC	secreted protein, acidic, cysteine-rich (osteonectin)
TGFβ1	Transforming growth factor
TIMP	Tissue inhibitor metalloproteinase
TNFα	tumor necrosis factor alpha
VEGF	vascular endothelial growth factor

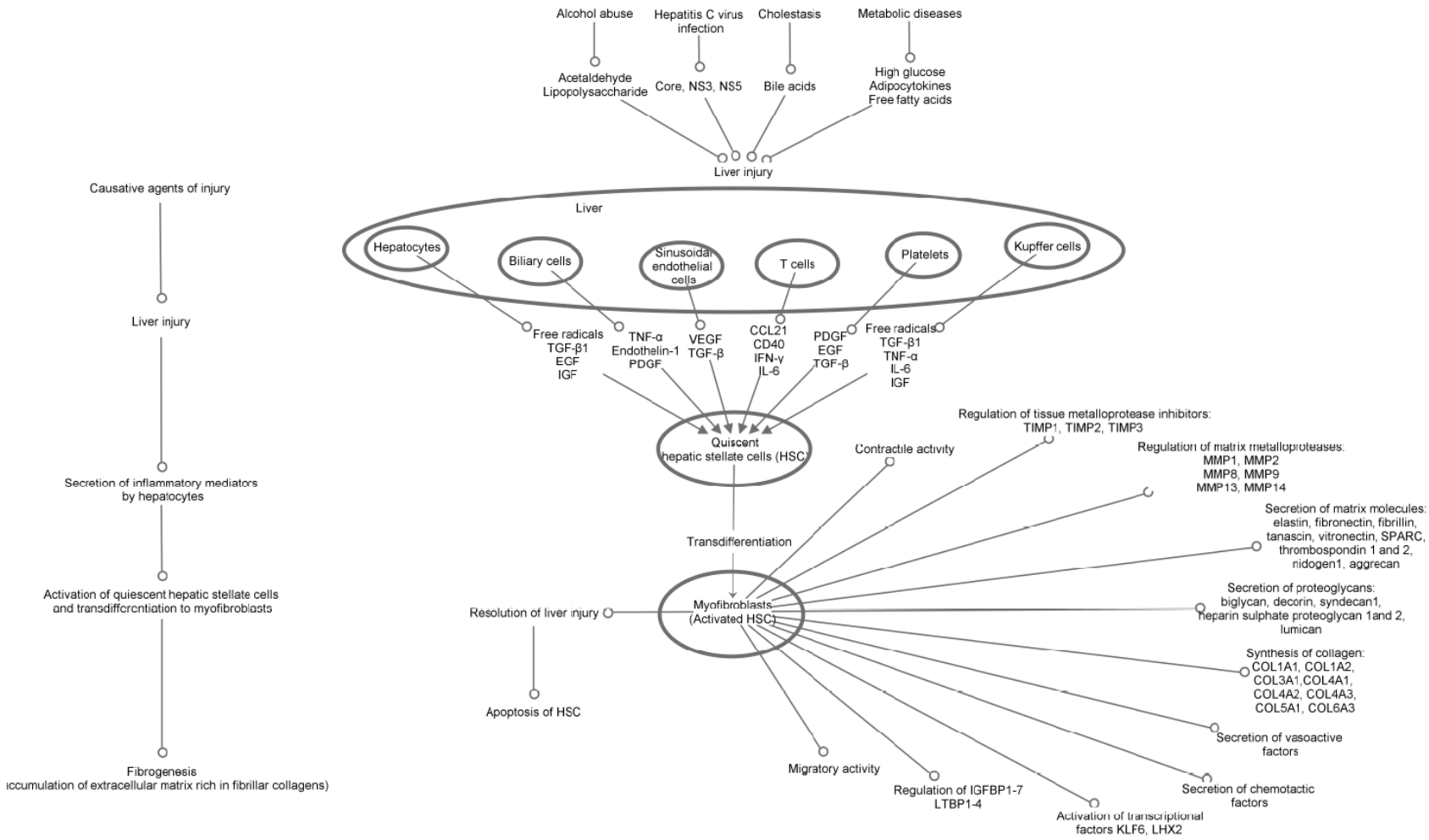

Figure 6.1: Mechanism pathway of hepatic fibrosis and stellate cell activation

REFERENCE

Adams LA, Feldstein A, Lindor KD, Angulo P. Nonalcoholic fatty liver disease among patients with hypothalamic and pituitary dysfunction. Hepatology 2004; 39: 909–14.

Aithal GP, Thomas JA, Kaye PV, Lawson A, Ryder SD, Spendlove I, Austin AS, Freeman JG, Morgan L, Webber J. Randomized, placebo-controlled trial of pioglitazone in nondiabetic subjects with nonalcoholic steatohepatitis. Gastroenterology. 2008;135 (4):1176-84

Andersen T, et al. Hepatic effects of dietary weight loss in morbidly obese subjects. J Hepatol 1991; 12: 224–9.

Angulo P, Lindor KD. Insulin resistance and mitochondrial abnormalities in NASH: a cool look into a burning issue. Gastroenterology 2001;120(5):1281– 5.

Angulo P. Nonalcoholic fatty liver disease. N Engl J Med 2002; 346(16):1221 – 31.

Apte, M.V., Haber, P.S., Applegate, T.L et al. Periacinar stellate shapes cells in rat pancreas: identification, isolation and culture. Gut 1998; 43 (128-133).

Arner, P. Not all fat is alike. Lancet 1998; 351:1301-1302.

Auger A, Truong TQ, Rhainds D, Lapointe J, Letarte F, Brissette L. Low and high density lipoprotein metabolism in primary cultures of hepatic cells from normal and apolipoprotein E knockout mice. Eur J Biochem. 2001 Apr;268(8):2322-30.

Bachem MG, Meyer D, Melchior R, Sell KM, Gressner AM. Activation of rat liver perisinusoidal lipocytes by transforming growth factors derived from myofibroblastlike cells. A potential mechanism of self perpetuation in liver fibrogenesis. *J Clin Invest* 89: 19–27, 1992.

Bacon B, et al. Nonalcoholic steatohepatitis: an expanded clinical entity. Gastroenterology 1994; 107:1103–1109.

Bajaj M, et al. Plasma resistin concentration, hepatic fat content, and hepaticand peripheral insulin resistance in pioglitazone-treated type-2 diabetic patients. Int J Obes Relat Metab Disord 2004; 28: 783-789.

Bajaj M, Suraamornkul S, Pratipanawatr T, Hardies LJ, Pratipanawatr W, Glass L, Cersosimo E, Miyazaki Y, DeFronzo RA. Pioglitazone reduces hepatic fat content and augments splanchnic glucose uptake in patients with type 2 diabetes. Diabetes. 2003 Jun;52(6):1364-70.

Baldwin AS Jr. The NF-kB and IkB proteins: new discoveries and insights. Annu Rev Immunol 1996;14:649-83.

Banerjee RR, Rangwala SM, Shapiro JS, Rich AS, Rhhoades B, Qi Y, et al. Regulation of fasted blood glucose by resistin. Science 2004;303:1195–8.

Barnes PJ, Karin M. Nuclear factor-kappaB: a pivotal transcription factor in chronic inflammatory diseases. N Engl J Med. 1997 Apr 10;336(15):1066-71.

Barnouin K, Dubuisson ML, Child ES, Fernandez de Mattos S, Glassford J, Medema RH, Mann DJ, et al. H2O2 induces a transient multi-phase cell cycle arrest in mouse fibroblasts through modulating cyclin D and p21Cip1 expression. J Biol Chem 2002;277:13761–13770

Belfort, R., et al. A placebo-controlled trial of Pioglitazone in subjects with non-alcoholic steatohepatitis. N Eng J Med 2006;355:2297-2307.

Ben-Ari Z, Tambur AR, Pappo O, Sulkes J, Pravica V, Hutchinson I, Klein T, Tur-Kaspa R, Mor E. Platelet-derived growth factor gene polymorphism in recurrent hepatitis C infection after liver transplantation. Transplantation. 2006 Feb 15;81(3):392-7.

Benzie IF. Lipid peroxidation: a review of causes, consequences, measurement and dietary influences. Int J Food Sci Nutr 1996; 47(3):233–61.

Blomhoff R, Wake K. Perisinusoidal stellate cells of the liver : important roles in retinol metabolism and fibrosis. FASEB J 1991;5:271-277.

Blomhoff R, Rasmussen M, Nilsson A, Norum KR, Berg T, Blaner WS, Kato M, Mertz JR, Goodman DS, Eriksson U, Peterson PA. Hepatic retinol metabolism. Distribution of retinoids, enzymes, and binding proteins in isolated rat liver cells. J Biol Chem 1985; 260:13560–13565

Boden, G. Role of fatty acids in the pathogenesis of insulin resistance and NIDDM. Diabetes 1997; 46, 3–10.

Bonner, J.C. Regulation of PDGF and its receptors in fibrotic diseasesCytokine & Growth Factor Reviews 15 (2004) 255–273.

Buck M, Chojkier M. A ribosomal S-6 kinase-mediated signal to C/EBP-beta is critical for the development of liver fibrosis. PLoS One. 2007 Dec 26;2(12):e1372.

Buniatian G, Gebhardt R, Schrenk D, HamprechtBravo AA, Sheth SG, Chopra S. Currents concepts: liver biopsy. N Engl J Med 2001;344:495–500.

Brown, M.S. & Goldstein, J.L. The SREBP pathway, regulation of cholesterol metabolism by proteolysis of a membrane-bound transcription factor. Cell 1997;89:846-854.

Brown, S.B., Maloney, M., Kinlaw, W.B., 1997. "Spot 14" protein functions at the pretranslational level in the regulation of hepatic metabolism by thyroid hormone and glucose. J. Biol. Chem. 272, 2163–2166

Browning, J.D., et al. Ethnic differences in the prevalence of crytogenic cirrhosis. Am. J. Gastroenterol. 2004 :99:292-298.

Browning. J.D., Horton, J.D. Molecular mediator of hepatic steatosis and liver injury. J Clin. Inves. 2004 114 (2): 147-52.

Brunt EM, Tiniakos DG. Histopathology of nonalcoholic fatty liver disease. World J Gastroenterol. 2010 Nov 14;16(42):5286-96

Brunt, E.M., Yeh, M.M. Pathology of non-alcoholic fatty liver disease. Am J. Clin. Pathol 2005;128:837-847.

Brunt E.M, et al. Nonalcoholic steatohepatitis: a proposal for grading and staging the histological lesions. Am J Gastroenterol 1999; 94: 2467–2474.

Buniatian, G., Traub, P., Albinus, M., et al. The immunoreactivity of Glial fibrillary acidic protein in mesangial cells and podocytes of the glomeruli of rat kidney in vivo and in culture.Biol cell 1998; 90, 53-61.

Buniatian, G., Gebhardt, R., Schrenk D., et al. Colocalization of 3 types of intermediate filament proteins in perisinusoidal stellate cells: Glial fibrillary acidic protein as a new cellular marker.Eur J cell boil 1996;70-2332.

Bullwinkel J, Baron-Lühr B, Lüdemann A, Wohlenberg C, Gerdes J, Scholzen T. Ki-67 protein is associated with ribosomal RNA transcription in quiescent and proliferating cells". J. Cell. Physiol. 2006: 206 (3): 624–35.

Cai, D. et al., Local and systemic insulin resistance resulting from hepatic activation of IKK-β and NF-κB, Nat. Med. 11 (2005), pp. 183–190.

Caldwell, S.H., et al., A pilot study of a thiazolidinedione, troglitazone, in non-alcoholic steatohepatitis. Am J. Gastroenterol 2001;96:519-525.

Carotti S, Morini S, Corradini G.S., Burza A.M et al. Glial fibrillary acidic acidic protein as an early marker of hepatic stellate cell activation in chronic and posttransplant recurrent hepatitis C. Liver Transplantation 2008 ; 14:806-814.

Caulin, C. et al. (1997) Caspase Cleavage of Keratin 18 and Reorganization of Intermediate Filaments during Epithelial Cell Apoptosis. J. Cell Biol. 138, 1379-1394.

Celis JE, Madsen P, Celis A. Cylin (PCNA, auxiliary protein of DNA polymerase delta) is a central component of the pathways leading to DNA replication and cell division. FEBS Let 1987; 220: 1 - 7.

Cha, J.Y. & Repa, J.J. The Liver X receptor (LXR) and hepatic lipogenesis:the carbohydrate-response element-binding protein is a target gene of LXR. J. Biol. Chem 2007;282:743–751.

Charlton, M., Sreekumar, R., Rasmussen, D., Lindor, K. and Nair, K.S. Apolipoprotein synthesis in nonalcoholic steatohepatitis. Hepatology 2002 35: 898-904.

Chen, G., et al. Central role for liver X receptor in insulin-mediated activation of Srebp-1c transcription and stimulation of fatty acid synthesis in liver. Proc. Natl. Acad. Sci. USA 2004; 101:11245–11250

Chen ZJ, Parent L, Maniatis T. Site-specific phosphorylation of IkBa by a novel ubiquitination-dependent protein kinase activity. Cell 1996;84:853-62.

Chew V, Tow C, Teo M, Wong HL, Chan J, Gehring A, Loh M, Bolze A, Quek R, Lee VK, Lee KH, Abastado JP, Toh HC, Nardin A. Inflammatory tumour microenvironment is associated with superior survival in hepatocellular carcinoma patients. J Hepatol. 2010 Mar;52(3):370-9

Chiang DJ, Pritchard MT, Nagy LE. Obesity, diabetes mellitus and liver fibrosis. Am J Physiol Gastrointest Liver Physiol. 2011 Feb 24.

Chitturi S, et al. NASH and insulin resistance: insulin hypersecretion and specific association with the insulin resistance syndrome. Hepatology 2002; 35(2):373– 9.

Clark JM, et al. The prevalence and etiology of elevated aminotransferase levels in the united states. Am J Gastroenterol 2003; 98:960–7.

Clark JM, et al. Nonalcoholic fatty liver disease. Gastroenterology 2002;122(6):1649–57.

Coletta DK, Sriwijitkamol A, Wajcberg E, Tantiwong P, Li M, Prentki M, Madiraju M, Jenkinson CP, Cersosimo E, Musi N, Defronzo RA. Pioglitazone stimulates AMP-activated protein kinase signalling and increases the expression of genes involved in adiponectin signalling, mitochondrial function and fat oxidation in human skeletal muscle in vivo: a randomised trial. Diabetologia. 2009 Apr;52(4):723-32.

Corpechot C, Barbu V, Wendum D, Kinnman N et al. Hypoxia-induced VEGF and collagen I expressions are associated with angiogenesis and fibrogenesis in experimental cirrhosis. Hepatology 2002; 35:1010-1021.

Cortez-Pinto, H., et al. Non-alcoholic fatty liver: another feature of the metabolic syndrome? Clin Nutr 1999; 18:353-358.

Davis BH, Kramer RT, Davidson NO. Retinoic acid modulates rat Ito cell proliferation, collagen, transforming growth factor beta production. J Clin Invest 1990; 86: 2062–2070.

Day C, James O. Steatohepatitis: a tale of two "hits"? (editorial). Gastroenterology 1998;114:842–845.

Day CP. Pathogenesis of steatohepatitis. Best practice and research Clin Gastroenterol 2002;16(5):663–78.

Day, C.P. The potential role of genes in non-alcoholic fatty liver disease. Clin Liver Dis 2004; 8: 673-91.

DeFronzo RA. Insulin resistance: a multifaceted syndrome responsible for NIDDM, obesity, hypertension, dyslipidaemia and atherosclerosis. Neth J Med 1997;50(5):191– 7.

DiDonato J, Mercurio F, Rosette C, et al. Mapping of the inducible IkB phosphorylation sites that signal its ubiquitination and degradation. Mol Cell Biol 1996;16:1295-304.

De Knegt RJ. Non-alcoholic steatohepatitis: clinical significance and pathogenesis. Scand J Gastroenterol 2001;234:88– 92 [Suppl.].

Da Silva Morais A, Abarca-Quinones J, Horsmans Y, Stärkel P, Leclercq IA. Peroxisome proliferated-activated receptor gamma ligand, Pioglitazone, does not prevent hepatic fibrosis in mice. Int J Mol Med. 2007 Jan;19(1):105-12.

Dentin R, Benhamed F, Hainault I, Fauveau V, Foufelle F, Dyck JR, Girard J, Postic C. Liver-specific inhibition of ChREBP improves hepatic steatosis and insulin resistance in ob/ob mice. Diabetes. 2006 Aug;55(8):2159-70.

Dentin R, Pégorier JP, Benhamed F, Foufelle F, Ferré P, Fauveau V, Magnuson MA, Girard J, Postic C: Hepatic glucokinase is required for the synergistic action of ChREBP and SREBP-1c on glycolytic and lipogenic gene expression. J Biol Chem279 2004 : 20314 –20326.

Delerive P, Wu Y, Burris TP, Chin WW, Suen CS. PGC-1 functions as a transcriptional coactivator for the retinoid X receptors. J Biol Chem 2002 Feb 8;277(6):3913-7.

Demeter LM, Stoler MH, Broker TR, Chow LT. Induction of proliferating cell nuclear antigen in differentiated keratinocytes of human papillomavirus-infected lesions. Human Pathol 1994; 25:343 - 348.

De Minicis S, Seki E, Uchinami H, Kluwe J, Zhang Y, Brenner DA, Schwabe RF. Gene expression profiles during hepatic stellate cell activation in culture and in vivo. . Gastroenterology. 2007 May;132(5):1937-46.

Da Silva Morais, .A., et al. Adiponectin-dependent activation of AMPK, but not PPARA, is implicated in the preventive effect of PGZ on steatohepatitis. J of Hepatology 2008;2(48):S40.

Denechaud, P.D., et al., Role of ChREBP in hepatic steatosis & insulin resistance. FEBS Letters 2008; 582:68-73.

Diez, J.J.,Iglesias, P. The role of the novel adipocytes-derived hormone adiponectin in human disease. Eur J Endocrinol 2003;285:E1182-95.

Dixon JB, et al. Nonalcoholic fatty liver disease: Improvement in liver histological analysis with weight loss. Hepatology 2004; 39: 1647–54.

Dooley S, Hamzavi J, Breitkopf K, Wiercinska E, Said HM, Lorenzen J, Ten Dijke P, Gressner AM. Smad7 prevents activation of hepatic stellate cells and liver fibrosis in rats. Gastroenterology. 2003 Jul;125(1):178-91

Dorn C, Riener MO, Kirovski G, Saugspier M, Steib K, Weiss TS, Gäbele E, Kristiansen G, Hartmann A, Hellerbrand C. Expression of fatty acid synthase in nonalcoholic fatty liver disease. Int J Clin Exp Pathol. 2010 Mar 25;3(5):505-14

Dowman JK, Tomlinson JW, Newsome PN. Systematic review: the diagnosis and staging of non-alcoholic fatty liver disease and non-alcoholic steatohepatitis.Aliment Pharmacol Ther. 2011 Mar; 33(5):525-40.

Erion DM, Shulman GI. Diacylglycerol-mediated insulin resistance. Nat Med. 2010 Apr;16(4):400-2.

Estep, J.M., Baranova, A., Hossain, N., Elariny, H., Ankrah, K., Afendy, A. et al. Expression of cytokine signaling genes in morbidly obese patients with non-alcoholic steatohepatitis and hepatic fibrosis. Obes Surg 2009; 19: 617-624.

Espinoza DO, Boros LG, Crunkhorn S, Gami H, Patti ME. Dual modulation of both lipid oxidation and synthesis by peroxisome proliferator-activated receptor-{gamma} coactivator-1{alpha} and -1{beta} in cultured myotubes. FASEB J 2010 Apr 01;24(4):1003-14.

Essers J, Theil AF, Baldeyron C, van Cappellen WA, Houtsmuller AB, Kanaar R, Vermeulen W. Nuclear dynamics of PCNA in DNA replication and repair. Mol. Cell. Biol. 2005; 25 (21): 9350–9.

Everett L, Galli A, Crabb D. The role of hepatic peroxisome proliferator-activated receptors (PPARs) in health and disease. Liver. 2000 Jun;20(3):191-9.

Feldstein AE, Wieckowska A, Lopez AR, Liu YC, Zein NN, McCullough AJ. Cytokeratin-18 fragment levels as noninvasive biomarkers for nonalcoholic steatohepatitis: a multicenter validation study. Hepatology 2009; 50: 1072-1078

Feldstein AE, Gores GJ. Apoptosis in alcoholic and nonalcoholic steatohepatitis. Front Biosci 2005;10:3093–3099.

Feldstein E.A., Canbay A., Angula P., et al. Hepatocytes Apoptosis and Fas expression are prominent features of human nonalcoholic steatohepatitis. Gastroenterology 2003; 125:437-443.

Fiorucci S, Rizzo G, Antonelli E, Renga B, Mencarelli A, Riccardi L, Morelli A, Pruzanski M, Pellicciari R. Cross-talk between farnesoid-X-receptor (FXR) and peroxisome proliferator-activated receptor gamma contributes to the antifibrotic activity of FXR ligands in rodent models of liver cirrhosis. J Pharmacol Exp Ther. 2005 Oct;315(1):58-68.

Fiorucci S, Antonelli E, Rizzo G, Renga B, Mencarelli A, Riccardi L, Orlandi S, Pellicciari R, and Morelli A. The nuclear receptor SHP mediates inhibition of hepatic stellate cells by FXR and protects against liver fibrosis. Gastroenterology 2004b;14:1444–1456.

Finkel T, Holbrook NJ. Oxidants, oxidative stress and the biology of ageing. Nature 2000;408:239 –247

Fleury C, Neverova M, Collins S, Raimbault S, Champigny O, Levi- Meyrueis C, Bouillaud F, et al. Uncoupling protein-2: a novel gene linked to obesity and hyperinsulinemia. Nat Genet 1997;15:269 –272.

Foley J, Ton T, Maranpot R, Butterworth B, Goldsworthy TL. Comparison of proliferating cell nuclear antigen to tritiated thymidine as a marker of proliferating hepatocytes in rats. Environ Health Perspect 1993; 101(suppl 5):199–206

Foretz M, Guichard C, Ferré P, Foufelle F.Sterol regulatory element binding protein-1c is a major mediator of insulin action on the hepatic expression of glucokinase and lipogenesis-related genes.Proc Natl Acad Sci U S A. 1999 Oct 26; 96(22):12737-42

Forman, B.M., et al. Hypolipidemic drugs, PUFAs, eicosanoids are ligands for PPAR alpha & delta. Proc. Natl. Acad. Sci. USA 1997; 94:4312-4317.

Friedman SL. Molecular regulation of hepatic fibrosis, an integrated cellular response to tissue injury [review]. J Biol Chem 2000;275:2247-2250.

Friedman SL. The cellular basis of hepatic fibrosis. Mechanisms and treatment strategies. N Engl J Med 1993;328:1828-1835.

Friedman SL, Rockey DC, McGuire RF, Maher JJ, Boyles JK, Yamasaki GIsolated hepatic lipocytes and Kupffer cells from normal human liver: morphological and functional characteristics in primary culture. Hepatology. 1992 Feb;15(2):234-43.

Fruhbeck G, et al. The adipocyte: a model for integration of endocrine and metabolic signalling in energy metabolism regulation. Am J Physiol Endocrinol Metab. 2001 Jun; 280(6):E827-47.

Gaça MD, Zhou X, Issa R, Kiriella K, Iredale JP, Benyon RC. Basement membrane-like matrix inhibits proliferation and collagen synthesis by activated rat hepatic stellate cells: evidence for matrix-dependent deactivation of stellate cells.Matrix Biology 2003; Volume 22, Issue 3, Pages 229-239

Galli, A., et al. Antidiabetic thiazolidinediones inhibit collagen synthesis and hepatic stellate cell activation in vivo and in vitro. Gastroenterology 2002; 122(7):1924– 40.

Galli A, Crabb D, Price D, Ceni E, Salzano R, Surrenti C, Casini A. Peroxisome proliferator-activated receptor γ transcriptional regulation is involved in platelet derived growth factor-induced proliferation of human hepatic stellate cells. Hepatology 2000: 31, 101–108.

Gard AL, White FP, Dutton GR. Extra-neural glial fibrillary acidic protein (GFAP) immunoreactivity in perisinusoidal stellate cells of rat liver. J Neuroimmunol 1985; 8:359–375

Gastaldelli A, Ferrannini E, Miyazaki Y, Matsuda M, Mari A, DeFronzo RA. Thiazolidinediones improve beta-cell function in type 2 diabetic patients. Am J Physiol Endocrinol Metab. 2007 Mar;292(3):E871-83.

Geerts A., Eliasson C., Niki T., et al. Formation of normal desmin intermediate filament in mouse hepatic stellate cells requires vimentin. Hepatology (2001); 33:177-188.

Gerdes J, Li L, Schlueter C, et al. Immunobiochemical and molecular biologic characterization of the cell proliferation associated nuclear antigen that is defined by monoclonal antibody Ki-67. Am J Pathol 1991; 138: 867 - 873.

Gizard F, Amant C, Barbier O, Bellosta S, Robillard R, Percevault F, Sevestre H, Krimpenfort P, Corsini A, Rochette J, Glineur C, Fruchart JC, Torpier G, Staels B. PPAR alpha inhibits vascular smooth muscle cell proliferation underlying intimal hyperplasia by inducing the tumor suppressor p16INK4a. J Clin Invest. 2005 Nov;115(11):3228-38.

Gressner AM, Weiskirchen R. Modern pathogenetic concepts of liver fibrosis suggest stellate cells and TGF-beta as major players and therapeutic targets. J Cell Mol Med. 2006 Jan-Mar;10(1):76-99

Grimaldi P.A. Regulatory role of peroxisome proliferator-activated receptor delta (PPAR delta) in muscle metabolism. A new target for metabolic syndrome treatment? Biochemie 2005; 87:5-8.

Han S, Zheng Y, Roman J. Rosiglitazone, an Agonist of PPARgamma, Inhibits Non-Small Cell Carcinoma Cell Proliferation In Part through Activation of Tumor Sclerosis Complex-2. PPAR Res. 2007;2007:29632.

Handy JA, Saxena NK, Fu P, Lin S, Mells JE, Gupta NA, Anania FA. Adiponectin activation of AMPK disrupts leptin-mediated hepatic fibrosis via suppressors of cytokine signaling (SOCS-3). J Cell Biochem. 2010 Aug 1;110(5):1195-207

Harman FS, Nicol CJ, Marin HE, Ward JM, Gonzalez FJ, Peters JM. Peroxisome proliferator-activated receptor-delta attenuates colon carcinogenesis. Nat Med. 2004 May;10(5):481-3.

Hashimoto E, Tokushige K. Prevalence, gender, ethnic variations, and prognosis of NASH. J Gastroenterol. 2011 Jan;46 Suppl 1:63-9.

Haughton EL, Tucker SJ, Marek CJ, Durward E, Leel V, Bascal Z, Monaghan T, Koruth M, Collie-Duguid E, Mann DA, Trim JE, Wright MC. Pregnane X receptor activators inhibit human hepatic stellate cell transdifferentiation in vitro. Gastroenterology. 2006 Jul;131(1):194-209.

Hazra S, Xiong S, Wang J, Rippe RA, Krishna V, Chatterjee K, Tsukamoto H. Peroxisome proliferator-activated receptor gamma induces a phenotypic switch from activated to quiescent hepatic stellate cells. J Biol Chem. 2004 Mar 19;279(12):11392-401.

Hellemans K, Michalik L, Dittie A, Knorr A, Rombouts K, De Jong J, Heirman C, Quartier E, Schuit F, Wahli W, Geerts A. Peroxisome proliferator-activated receptor-beta signaling contributes to enhanced proliferation of hepatic stellate cells. Gastroenterology. 2003 Jan;124(1):184-201.

Hellemans K, Rombouts K, Quartier E, Dittié AS, Knorr A, Michalik L, Rogiers V, Schuit F, Wahli W, Geerts A.PPARbeta regulates vitamin A metabolism-related gene expression in hepatic stellate cells undergoing activation. J Lipid Res. 2003 Feb; 44(2):280-95.

Hernandez R, et al. Rosiglitazone ameliorates insulin resistance in brown adipocytes of Wistar rats by impairing TNF-alpha induction of p38 and p42/p44 mitogen-activated protein kinases. Diabetologia 2004; 47: 1615–24.

Hertz R, Magenheim J, Berman I, Bar-Tana J. Fatty acyl-CoA thioesters are ligands of hepatic nuclear factor-4a. Nature 1998; 392: 2.

Hillgartner, F.B., Charron, T., Chesnut, K.A. Triiodothyronine stimulates and glucagon inhibits transcription of the acetyl-CoA carboxylase gene in chick embryo hepatocytes: glucose and insulin amplify the effect of triiodothyronine. Arch. Biochem. Biophys. 1997; 337, 159–168.

Hirosumi, J. et al., A central role for JNK in obesity and insulin resistance, Nature 420 (2002), pp. 333–336.

Hoffler U, Hobbie K, Wilson R, Bai R, Rahman A, Malarkey D, Travlos G, Ghanayem BI. Diet-induced obesity is associated with hyperleptinemia, hyperinsulinemia, hepatic steatosis, and glomerulopathy in C57Bl/6J mice. Endocrine. 2009 Oct; 36(2):311-25.

Horton JD, Goldstein JL, Brown MS. SREBPs: activators of the complete program of cholesterol and fatty acid synthesis in the liver. J Clin Invest. 2002 May;109(9):1125-31

Hotamisligil GS, Arner P, Caro JF, Atkinson RL, and Spiegelman BM. Increased adipose tissue expression of tumor necrosis factor-a in human obesity and insulin resistance. J Clin Invest 1995; 95: 2409–2415.

Hube F, Birgel M, Lee YM, and Hauner H. Expression pattern of tumour necrosis factor receptors in subcutaneous and omental human adipose tissue: role of obesity and noninsulin-dependent diabetes mellitus. Eur J Clin Invest 1999; 29: 672–678.

Hughes, S., Moody A. PCR, The Method Express Series. 2007.

Huang SS, Huang JS. TGF-beta control of cell proliferation. J Cell Biochem. 2005 Oct 15;96(3):447-62.

Jump DB, Clarke SD, MacDougald O, Thelen A. Polyunsaturated fatty acids inhibit S14 gene transcription in rat liver and cultured hepatocytes. Proc Natl Acad Sci USA 1993; 90:8454–8458

Ichikawa S, Sakiyama H, Suzuki G, Hidari KI, Hirabayashi Y. Expression cloning of a cDNA for human ceramide glucosyltransferase that catalyzes the first glycosylation step of glycosphingolipid synthesis. Proc Natl Acad Sci USA1996; 93: 4638–4643.

Iimuro Y, Brenner DA.. Matrix metalloproteinase gene delivery for liver fibrosis. Pharm Res. 2008 Feb;25(2):249-58.

Iizuka K, Horikawa Y. ChREBP: a glucose-activated transcription factor involved in the development of metabolic syndrome. Endocr J. 2008 Aug;55(4):617-24

Ikeda H, Nagashima K, Yanase M, Tomiya T, Arai M, Inoue Y, Tejima K, Nishikawa T, Watanabe N, Omata M, Fujiwara K. Sphingosine 1-phosphate enhances portal pressure in isolated perfused liver via S1P2 with Rho activation. Biochem Biophys Res Commun. 2004 Jul 30;320(3):754-9

Ikejima, Y.T., et al. Leptin receptor-mediated signalling regulates hepatic fibrogenesis and remodeling of extracellular matrix in the rat. Gastroenterology 2002; 122: 1399 - 1410.

Iredale JP. Models of liver fibrosis: exploring the dynamic nature of inflammation and repair in a solid organ. J Clin Invest. 2007 Mar; 117(3):539-48.

Iwata M, et al. Pioglitazone ameliorates tumor necrosis factor-alpha-induced insulin resistance by a mechanism independent of adipogenic activity of peroxisome proliferator-activated receptor-gamma. Diabetes 2001; 50: 1083–92.

Jameel NM, Thirunavukkarasu C, Wu T, Watkins SC, Friedman SL, Gandhi CR. p38-MAPK- and caspase-3-mediated superoxide-induced apoptosis of rat hepatic stellate cells: reversal by retinoic acid. J Cell Physiol. 2009 Jan;218(1):157-66

Jung HS, et al. The effects of rosiglitazone and metformin on the plasma concentrations of resistin in patients with type 2 diabetes mellitus. Metabolism 2005; 54: 314–20.

Kahn, R.C., et al. Unravelling mechanism of action of Thiazolidinediones. J Clin Invest. 2000; 106(11):1305-1307.

Kadowaki, T. 2000. Insights into insulin resistance and type 2 diabetes from knockout mouse models. J. Clin. Invest. 106:459-465.

Kawaguchi, T., et al. Mechanism for fatty acid 'sparing' effect on glucose-induced transcription. Regulation of ChREBP by AMP-activated protein kinase. J. Biol Chem 2002; 277:3829-3835.

Keller, H., et al. Fatty acids and retinoids control lipid metabolism through activation of peroxisome proliferator-activated receptor-retinoid X receptor heterodynes, PNAS 1993;90:2160-2164.

Kim SY, Kim HI, Kim TH, Im SS, Park SK, Lee IK, Kim KS, Ahn YH.SREBP-1c mediates the insulin-dependent hepatic glucokinase expression. J Biol Chem. 2004 Jul 16;279(29):30823-9.

Kleiner, D.E., et al. Design and validation of a histological scoring system for nonalcoholic fatty liver disease. Hepatology 2005;41:1313-1321.

Kliewer, S.A., et al. Convergence of 9-sis retinoic acid and peroxisome proliferator signaling pathways through heterodimer formation of their receptors, Nature 1992; 358: 771-774.

Kon K, Ikejima K, Hirose M, Yoshikawa M, Enomoto N, Kitamura T, Takei Y, Sato N. Pioglitazone prevents early-phase hepatic fibrogenesis caused by carbon tetrachloride. Biochem Biophys Res Commun. 2002 Feb 15;291(1):55-61.

Kopp EB, Ghosh S. NF-k B and rel proteins in innate immunity. Adv Immunol 1995;58:1-27.

Kuipers, F., J. M. van Ree, M. H. Hofker, H. Wolters, G. In't Veld, R. Havinga, R. J. Vonk, H. H. G. Princen, and L. M. Havekes. Altered lipid metabolism in apolipoprotein E-deficient mice does not affect cholesterol balance across the liver. Hepatology 1996;. 24: 241–247.

LaFave LT, Augustin LB, Mariash CN. S14: insights from knockout mice. Endocrinology. 2006 Sep;147(9):4044-7.

Lam, B. and Younossi, Z.B. Treatment options for nonalcoholic fatty liver disease. Ther Adv Gastroenterol 2010: 3(2) 121-137.

Larrouy D, Laharrague P, Carrera G, Viguerie-Bascands N, Levi-Meyrueis C, Fleury C, Pecqueur C, et al. Kupffer cells are a dominant site of uncoupling protein 2 expression in rat liver. Biochem Biophys Res Commun 1998;235:760 –764.

Larter CZ, Yeh MM, Williams J, Bell-Anderson KS, Farrell GC MCD-induced steatohepatitis is associated with hepatic adiponectin resistance and adipogenic transformation of hepatocytes. Hepatol. 2008 Sep;49(3):407-16.

Lee AH, Scapa EF, Cohen DE, Glimcher LH. Regulation of hepatic lipogenesis by the transcription factor XBP1. Science. 2008 Jun 13;320(5882):1492-6.

Lee C.H., Olson P., et al. PPAR delta regulates glucose metabolism and insulin sensitivity. Proc Natl Acad Sci USA 2006 ;103 :3444-3449.

Lee R. Nonalcoholic steatohepatitis: a study of 49 patients. Hum Pathol 1989;20: 594–598.

Lehmann JM, Moore LB, Smith-Oliver TA, Wilkison WO, Willson TM, Kliewer SA: An antidiabetic thiazolidinedione is a high affinity ligand for peroxisome proliferator - activated
receptor gamma. J Biol Chem (1995); 270: 12953–12956.

Leibowitz M.D., Fievet C., Hennuyer N. et al. Activation of PPAR delta alter lipid metabolism in db/db mice. FEBS Lett 2000; 473:333-336.

Lim MC, Maubach G, Zhuo L. Glial fibrillary acidic protein splice variants in hepatic stellate cells--expression and regulation. Mol Cells. 2007 May 31;25(3):376-84

Lin, H.Z., et al. Metfromin reverses fatty liver disease in obese, leptin deficient mice. Nat. Med. 2000;6:998-1003.

Listenberger, L.L., et al. 2003. Triglyceride accumulation protects against fatty acid-induced lipotoxicity. Proc. Natl. Acad. Sci. U. S. A. 100:3077-3082.

Loguercio C, et al. Non-alcoholic fatty liver disease in an area of southern Italy: main clinical, histological, and pathophysiological aspects. J Hepatol 2001;35(5):568– 74.

Loria P, Carulli L, Bertolotti M, Lonardo A. Endocrine and liver interaction: the role of endocrine pathways in NASH. Nat Rev Gastroenterol Hepatol 2009; 6: 236–47.

Ludwig J, et al. Nonalcoholic steatohepatitis. Mayo clinic experiences with a hitherto unnamed disease.Mayo Clin Proc 1980;55:434–438.

Lutchman, G., et al. The effects of discontinuing Pioglitazone in patients with non-alcoholic steatohepatitis. Hepatology 2007;46(2):424-429.

Maeda K, Okubo K, Shimomura I, Funahashi T, Matsuzawa Y, Matsubara K. cDNA cloning and expression of a novel adipose specifi c collagen-like factor, apM1 (AdiPose Most abundant Gene transcript 1). Biochem Biophys Res Commun 1996;221: 286–9.

Magee T R, Cai Y, El-Houseini M E, Locker J. J Biol Chem 1998; 273(45): 30024-32.

Magnuson, M.A., et al. Rat glucokinase gene: structure & regulation by insulin. Proc Natl Acad Sci USA 1989; 86:4838-4842.

Maher JJ. Leukocytes as modulators of stellate cell activation. Alcohol Clin Exp Res. 1999 May;23(5):917-21.

Mahley, R. W., and Y. Huang. Apolipoprotein E: from atherosclerosis to Alzheimer's disease and beyond. Curr. Opin. Lipidol.1999; 10: 207–217.

Makowski L, Hotamisligil GS. Fatty acid binding proteins - the evolutionary crossroads of inflammatory and metabolic responses. J Nutr 2004; 134: 2464S–2468S.

Malhi, H. and Gores, G.J. Molecular mechanisms of lipotoxicity in nonalcoholic fatty liver disease. Semin Liver Dis 2008: 28: 360-369.

Mangelsdorf, D.J. et al. The nuclear receptor superfamily: the second decade. Cell 1995;83:835–839.

Mann J, Mann DA. Transcriptional regulation of hepatic stellate cells. Adv Drug Deliv Rev. 2009 Jul 2;61(7-8):497-512.

Mann DA, Smart DE..Transcriptional regulation of hepatic stellate cell activation. Gut. 2002 Jun;50(6):891-6.

Marchesini G, et al. Metformin in non-alcoholic steatohepatitis. Lancet 2001;358(9285):893-4.

Marchesini, G., et al. Association of non-alcoholic fatty liver disease to insulin resistance. Am J Med 1999: 107: 450-455.

Marra, F., et al. Molecular basis and mechanism of progression of non-alcoholic steatohepatitis. Trends in Molecular Medicine 2008;14:72-81.

Marra F. Leptin and liver fibrosis: A matter of fat. Gastroenterology 2002;122:1529 – 1532.

Marciniak, S.J. and Ron, D. Endoplasmic reticulum stress signaling in disease, Physiol. Rev. 2006; 86 (2006), pp. 1133–1149.

Matchinsky, F.M. & Magnuson, M.A. Molecular Pathogenesis of MODYs. Frontier in Daibetes 2000:15;99-165.

Marx N, et al. Antidiabetic PPAR gamma-activator Rosiglitazone reduces MMP-9 serum levels in type 2 diabetic patients with coronary artery disease. Arterioscler Thromb Vasc Biol 2003;23:283-8.

Matsushima-Nishiu M, Unoki M, Ono K, Tsunoda T, Minaguchi T, Kuramoto H, Nishida M, Satoh T, Tanaka T, Nakamura Y. Growth and gene expression profile analyses of endometrial cancer cells expressing exogenous PTEN. Cancer Res. 2001 May 1;61(9):3741-9

Maugeais C, Tietge UJ, Tsukamoto K, Glick JM, Rader DJ. Hepatic apolipoprotein E expression promotes very low density lipoprotein-apolipoprotein B production in vivo in mice. J Lipid Res. 2000 Oct;41(10):1673-9

Maxwell KN, Soccio RE, Duncan EM, Sehayek E, Breslow JL. Novel putative SREBP and LXR target genes identified by microarray analysis in liver of cholesterol-fed mice. J Lipid Res. 2003 Nov;44(11):2109-19

Mayhew, T.M. How to count synapses unbiasedly and efficiently at the ultrastructural level: proposal for a standard sampling and counting protocol. J Neurocytol. 1996 Dec; 25(12):793-804

McClain, C.J., et al. Good fat and bad fat. Hepatology 2007;45:1343-1346.

McCullough AJ. The epidemiology and risk factors of NASH. In: Farrell GC, George J, Hall P, Mc McCullough AJ, eds. Fatty Liver Disease: NASH and Related Disorders. Oxford: Blackwell Publishing, 2005: 23–37.

McGarry, J.D., et al. A possible role for malonyl-CoA in the regulation of hepatic fatty acid oxidation & ketogenesis. J. Clin. Invest. 1977; 60:265-70.

McHutchison JG, Manns M, Patel K, Poynard T, Lindsay KL, Trepo C, Dienstag J, Lee WM, Mak C, Garaud JJ, Albrecht JK. Adherence to combination therapy enhances sustained response in genotype-1-infected patients with chronic hepatitis C. Gastroenterology. 2002 Oct;123(4):1061-9

Mencarelli A, Migliorati M, Barbanti M, Cipriani S, Palladino G, Distrutti E, Renga B, Fiorucci S. Pregnane-X-receptor mediates the anti-inflammatory activities of rifaximin on detoxification pathways in intestinal epithelial cells. Biochem Pharmacol 2010;80 (11)1700-1707

Michalik L, Wahli W. Involvement of PPAR nuclear receptors in tissue injury and wound repair. J Clin Invest. 2006 Mar;116(3):598-606

Miele, L., Grieco, A., Armuzzi, A., Candelli, M., Forgione, A., Gasbarrini, A. et al. Hepatic mitochondrial-beta-oxidation in patients with non-alcoholic steatohepatitis assessed by 13C-octanoate breath test. Am J Gastroenterol (2003) 98: 2335-2336.

Migita K, Maeda Y, Abiru S, Komori A, Yokoyama T, Takii Y, Nakamura M, Yatsuhashi H, Eguchi K, Ishibashi H. Peroxynitrite-mediated matrix metalloproteinase-2 activation in human hepatic stellate cells. FEBS Lett. 2005 Jun 6;579(14):3119-25

Mitro, N., et al. The nuclear receptor LXR is a glucose sensor. Nature 2007;445: 219–223.

Miura S, Kai Y, Kamei Y, Ezaki O. Isoform-Specific Increases in Murine Skeletal Muscle Peroxisome Proliferator-Activated Receptor-{gamma} Coactivator-1{alpha} (PGC-1{alpha}) mRNA in Response to {beta}2-Adrenergic Receptor Activation and Exercise. Endocrinology 2008 Sep 01;149(9):4527-33.

Miyahara T, Schrum L, Rippe R, Xiong S, Yee HF Jr, Motomura K, Anania FA, Willson TM, Tsukamoto H. Peroxisome proliferator-activated receptors and hepatic stellate cell activation. J Biol Chem. 2000 Nov 17;275(46):35715-22

Miyazaki Y, et al. Effect of pioglitazone on abdominal fat distribution and insulin sensitivity in type 2 diabetic patients. J Clin Endocrinol Metab 2002;87:2784-91.

Miyazaki Y, et al. Improved glycemic control and enhanced insulin sensitivity in type 2 diabetic subjects treated with pioglitazone. Diabetes Care 2001;24:710-9.

Mofrad P, et al. Clinical and histologic spectrum of nonalcoholic fatty liver disease associated with normal ALT values. Hepatology 2003; 37(6):1286-92.

Mohamed-Ali V, Pinkney JH, and Coppack SW. Adipose tissue as an endocrine and paracrine organ. Int J Obes 1998; 22:1145–1158.
Moreira RK. Hepatic stellate cells and liver fibrosis. Arch Pathol Lab Med. 2007 Nov;131(11):1728-34.

Morral, N., et al. Effects of glucose metabolism on the regulation of genes of fatty acid synthesis & triglyceride secretion in the liver. J Lipid Research 2007; 48:1499-1510.

Musso, G., et al. Dietary habits and their relations to insulin resistance and postprandial lipemia in nonalcoholic steatohepatitis. Hepatology 2003;37(4):909– 16.

Mutel E, Abdul-Wahed A, Ramamonjisoa N, Stefanutti A, Houberdon I, Cavassila S, Pilleul F, Beuf O, Gautier-Stein A, Penhoat A, Mithieux G, Rajas F. Targeted deletion of liver glucose-6 phosphatase mimics glycogen storage disease type 1a including development of multiple adenomas. J Hepatol. 2011 Mar; 54(3):529-37

Myers M P, Stolarov J P, Eng C, Li J, Wang S I, Wigler M H, Parsons R, Tonks N K. P-TEN, the tumor suppressor from human chromosome 10q23, is a dual-specificity phosphatase. Proc Natl Acad Sci U S A. 1997 Aug 19;94(17):9052-7

Nair, S., et al. Metformin in the treatment of non-alcoholic steatohepatitis: a pilot open label trial. Aliment Pharmacol Ther 2004; 20: 23–8.

Negre-Salvayre A, Hirtz C, Carrera G, Cazenave R, Troly M, Salvayre R, Penicaud L, et al. A role for uncoupling protein-2 as a regulator of mitochondrial hydrogen peroxide generation. FASEB J 1999;11:809–815.

Neuchwander-Tetri, B.A., Caldwell, S.H. Nonalcoholic steatohepatitis: summary of an AASLD Single Topic Conference. Hepatology 2003; 37:1202-1219.

Neuschwander Tetri BA, et al. Interim results of a pilot study demonstrating the early effects of the PPAR-gamma ligand rosiglitazone on insulin sensitivity, aminotransferases, hepatic steatosis and body weight in patients with non-alcoholic steatohepatitis. J Hepatol 2003; 38(4):434– 40.

Niki T, de Bleser PJ, Xu G, Van Den BK, Wisse E, Geerts A. Comparison of Glial fibrillary acidic protein and desmin staining in normal and CCl4-induced Wbrotic rat livers. Hepatology 1996; 23:1538–1545

Nijtmans LG, de Jong L, Artal Sanz M, Coates PJ, Berden JA, Back JW, Muijsers AO, van der Spek H, Grivell LA. Prohibitins act as a membrane-bound chaperone for the stabilization of mitochondrial proteins. EMBO J. 2000 Jun 1;19(11):2444-51

Oliver W.R., Shenk Jr., Snaith M.R et al. A selective peroxisome proliferator-activated receptor delta agonist promotes reverse cholesterol transport. Proc Natl Acad Sci USA 2001; 98:5306-5311.

Orfila C, Lepert JC, Alric L, Carrera G, Béraud M, Pipy B. Immunohistochemical distribution of activated nuclear factor kappaB and peroxisome proliferator-activated receptors in carbon tetrachloride-induced chronic liver injury in rats. Histochem Cell Biol. 2005 Jun;123(6):585-93

Ota T, Gayet C, Ginsberg HN. Inhibition of apolipoprotein B100 secretion by lipid-induced hepatic endoplasmic reticulum stress in rodents. J Clin Invest. 2008 Jan;118(1):316-32.

Paik YH, Kim JK, Lee JI, Kang SH, Kim DY, An SH, Lee SJ, Lee DK, Han KH, Chon CY, Lee SI, Lee KS, Brenner DA. Celecoxib induces hepatic stellate cell apoptosis through inhibition of Akt activation and suppresses hepatic fibrosis in rats. Gut. 2009 Nov;58(11):1517-27.

Paradis V, et al. High glucose and hyperinsulinemia stimulate connective tissue growth factor expression: a potential mechanism involved in progression to fibrosis in nonalcoholic steatohepatitis. Hepatology 2001;34(4 Pt. 1):738– 44.

Patsouris D, Mandard S, Voshol PJ, Escher P, Tan NS, Havekes LM, Koenig W, März W, Tafuri S, Wahli W, Müller M, Kersten S. PPARalpha governs glycerol metabolism. J Clin Invest. 2004 Jul;114(1):94-103.

Peraldi P, Hotamisligil GS, Buurman WA, White MF, Spiegelman BM.Tumor necrosis factor (TNF)-alpha inhibits insulin signaling through stimulation of the p55 TNF receptor and activation of sphingomyelinase. J Biol Chem. 1996 May 31;271(22):13018-22.

Perez-Castillo A, Schwartz HL, Oppenheimer JH. Rat hepatic mRNA-S14 and lipogenic enzymes during weaning: role of S14 in lipogenesis. Am J Physiol 1987 253:E536–E542

Peters JM, Hollingshead HE, Gonzalez FJ. Role of peroxisome-proliferator-activated receptor beta/delta (PPARbeta/delta) in gastrointestinal tract function and disease. Clin Sci (Lond). 2008 Aug;115(4):107-27

Peters JM, Cheung C, Gonzalez FJ. Peroxisome proliferator-activated receptor-alpha and liver cancer: where do we stand? Mol Med. 2005 Oct;83(10):774-85.

Pinzani M, Milani S, Herbst H, DeFranco R, Grappone C, Gentilini A, et al. Expression of platelet-derived growth factor and its receptors in normal human liver and during active hepatic fibrogenesis. Am J Pathol 1996;148:785–800.

Postic C, Dentin R, Denechaud PD, Girard J. ChREBP, a transcriptional regulator of glucose and lipid metabolism. Annu Rev Nutr. 2007;27:179-92.

Powell E, et al. The natural history of nonalcoholic steatohepatitis: a follow-up study of forty-two patients for up to 21 years. Hepatology 1990; 11:74–80.

Poynard T, McHutchison J, Manns M, Trepo C, Lindsay K, Goodman Z, Ling MH, Albrecht J. Impact of pegylated interferon alfa-2b and ribavirin on liver fibrosis in patients with chronic hepatitis C. Gastroenterology. 2002 May;122(5):1303-13

Préaux AM, Mallat A, Nhieu JT, D'Ortho MP, Hembry RM, Mavier P. Matrix metalloproteinase-2 activation in human hepatic fibrosis regulation by cell-matrix interactions. Hepatology. 1999 Oct;30(4):944-50

Preiss D, Sattar N. Non-alcoholic fatty liver disease: an overview of prevalence, diagnosis, pathogenesis and treatment considerations. Clin Sci (Lond) 2008;115:141–50.

Pyper SR, Viswakarma N, Yu S, Reddy JK. PPARalpha: energy combustion, hypolipidemia, inflammation and cancer. Nucl Recept Signal. 2010 Apr 16;8:e002

Ravikumar B, Gerrard J, Dalla Man C, Firbank MJ, Lane A, English PT, Cobelli C, Taylor R. Pioglitazone decreases fasting and postprandial endogenous glucose production in proportion to decrease in hepatic triglyceride content. Diabetes. 2008 Sep;57(9):2288-95.

Reid A.E. Nonalcoholic steatohepatitis. Gastroenterology 2001; 121(3):710– 23.

Rival Y, Beneteau N, Taillandier T, et al. PPARα and PPARδ activators inhibit cytokine-induced nuclear translocation of NF-κB and expression of VCAM-1 in EAhy926 endothelial cells. Eur J Pharmacol. 2002;435:143–151.

Roberts AB. 1998. Molecular and cell biology of TGF-β. Miner. Electrolyte Metab 24: 111–119.

Roberts AB, Sporn MB. 1993. Physiological actions and clinical applications of transforming growth factor-β (TGF-β). Growth Factors 8: 1–9.

Rockey, D. The cellular pathogenesis of portal hypertension : stellate cell contractility, endothelin, and nitric oxide. Hepatology 1997; 15-2-5.

Rutkowski, D.T., J. Wu, S.H. Back, M.U. Callaghan, S.P. Ferris, J. Iqbal, R. Clark, H. Miao, J.R. Hassler, J. Fornek, et al. UPR pathways combine to prevent hepatic steatosis caused by ER stress-mediated suppression of transcriptional master regulators. Dev. Cell. (2008) 15:829–840.

Rust C, Gores GJ. Apoptosis and liver disease. Am J Med. 2000 May;108(7):567-74.

Safadi, R. and Friedman, S.L. Hepatic fibrosis—role of hepatic stellate cell activation, MedGenMed 4 (2002), p. 27

Saha, A.K., et al. Pioglitazone treatment activates AMP-activated protein kinase in rat liver & adipose tissue in vivo. Biochem Biophys Res Commun 2004; 314:580-585.

Sakamoto J, Kimura H, Moriyama S, Odaka H, Momose Y, Sugiyama Y, Sawada H. Activation of human peroxisome proliferator-activated receptor (PPAR) subtypes by pioglitazone. Biochem Biophys Res Commun. 2000: 30;278(3):704-11

Samuel VT. Fructose induced lipogenesis: from sugar to fat to insulin resistance.Trends Endocrinol Metab. 2011 Feb;22(2):60-5.

Sanchez I, Hughes RT, Mayer BJ, Yee K, Woodgett JR, Avruch J, Kyriakis JM, Zon LI. Role of SAPK/ERK kinase-1 in the stress-activated pathway regulating transcription factor c-Jun. Nature 1994;372: 794–798.

Sato K, Kobayashi K, Inoguchi T, Sonoda N, Imamura M, Sekiguchi N, et al. Adenovirus-mediated high expression of resistin causes dyslipidemia in mice. Endocrinology 2005;146:273–9.

Scholz H, Lund T, Dahle MK, Collins JL, Korsgren O, Wang JE, Foss A. The synthetic liver X receptor agonist GW3965 reduces tissue factor production and inflammatory responses in human islets in vitro. Diabetologia. 2009 Jul;52(7):1352-62.

Scholzen T, Gerdes J. The Ki-67 protein: from the known and the unknown.. J. Cell. Physiol. 2000; 182 (3): 311–22.

Schmierer B, Hill CS. TGFbeta-SMAD signal transduction: molecular specificity and functional flexibility. Nat Rev Mol Cell Biol. 2007 Dec;8(12):970-82

Schmitt-Graff A, Kruger S, Bochard F, Gabbiani G, Denk H. Modulation of alpha smooth muscle actin and desmin expression in perisinusoidal cells of normal and diseased human livers. Am J Pathol 1991; 138:1233–1242

Schwabe, R.F. and Brenner, D.A. Nuclear factor-κB in the liver: friend or foe?, Gastroenterology 132 (2007), pp. 2601–2604.

Serviddio G, Bellanti F, Tamborra R, Rollo T, Capitanio N, Romano AD, Sastre J, Vendemiale G, Altomare E. Uncoupling protein-2 (UCP2) induces mitochondrial proton leak and increases susceptibility of non-alcoholic steatohepatitis (NASH) liver to ischaemia-reperfusion injury. Gut. 2008 Jul;57(7):957-65.

Setji TL, Holland ND, Sanders LL, Pereira KC, Diehl AM, Brown AJ. Nonalcoholic steatohepatitis and non-alcoholic Fatty liver disease in young women with polycystic ovary syndrome. J Clin Endocrinol Metab 2006; 91: 1741–7.

Sethi, J. K. & Hotamisligil, G. S. The role of TNF alpha in adipocyte metabolism. Semin. Cell. Dev. Biol. (1999) ;10:19–29.

Shan W, Palkar PS, Murray IA, McDevitt EI, Kennett MJ, Kang BH, Isom HC, Perdew GH, Gonzalez FJ, Peters JM. Ligand activation of peroxisome proliferator-activated receptor beta/delta (PPARbeta/delta) attenuates carbon tetrachloride hepatotoxicity by downregulating proinflammatory gene expression. Toxicol Sci. 2008 Oct;105(2):418-28.

She H, Xiong S, Hazra S, Tsukamoto H. Adipogenic transcriptional regulation of hepatic stellate cells. J Biol Chem. 2005 Feb 11;280(6):4959-67

Shklyaev S, Aslanidi G, Tennant M, Prima V, Kohlbrenner E, Kroutov V, et al. Sustained peripheral expression of transgene adiponectin offsets the development of diet-induced obesity in rats. Proc Natl Acad Sci USA 2003;100:14217–22.

Siebenlist U, Franzoso G, Brown K. Structure, regulation and function of NF-k B. Annu Rev Cell Biol 1994;10:405-55.

Shimano H, Yahagi N, Amemiya-Kudo M, Hasty AH, Osuga J, Tamura Y, Shionoiri F, Iizuka Y, Ohashi K, Harada K, Gotoda T, Ishibashi S, Yamada N. Sterol regulatory element-binding protein-1 as a key transcription factor for nutritional induction of lipogenic enzyme genes. J Biol Chem. 1999 Dec 10;274(50):35832-9.

Shimano,H., et al. Isoforms 1c of SREBP is less active than isoforms 1a in livers of transgenic mice & cultured cells. J Clin Invest 1997;99:846-854.

Shimomura, I., et al. Insulin selectively increases SREBP-1c mRNA in the livers of rats with streptozotocin-induced diabetes. Proc. Natl. Acad. Sci. 1999;96:13656-61.

Shulman GI. Cellular mechanisms of insulin resistance. J Clin Invest 2000; 106(2):171– 6.

Shin HW, Park SY, Lee KB, Shin E, Nam SW, Lee JY, Jang JJ. Transcriptional profiling and Wnt signaling activation in proliferation of human hepatic stellate cells induced by PDGF-BB. Korean J Hepatol. 2009 Dec;15(4):486-95

Sonsuz A, et al. Relationship between aminotransferase levels and histopathological findings in patients with non-alcoholic steatohepatitis. Am J Gastroenterol 2000;95(5):1370– 1.

Spiegelman BM, Flier JS. Adipogenesis and obesity: rounding out the big picture. Cell 1996 Nov 1;87(3):377-89.

Stapleton, S.R., Mitchell, D.A., Salati, L.M., Goodridge, A.G., 1990.Triiodothyronine stimulates transcription of the fatty acid synthase gene inchick embryo hepatocytes in culture. Insulin and insulin-like growth factor amplify that effect. J. Biol. Chem. 265, 18442–18446.

Stefan N, Kantartzis K, Haring HU. Causes and metabolic consequences of fatty liver. Endocr Rev 2008; 29: 939–60.

Steppan, C.M., et al. Resistin and obesity-associated insulin resistance. Trends Endocrin Metab. 2001;13(1):18-23.

Takano S, Kubota T, Nishibori H, Hasegawa H, Ishii Y, Nitori N, Ochiai H, Okabayashi K, Kitagawa Y, Watanabe M, Kitajima M.Pioglitazone, a ligand for peroxisome proliferator-activated receptor-gamma acts as an inhibitor of colon cancer liver metastasis. Anticancer Res. 2008 Nov-Dec;28(6A):3593-9.

Taniguchi CM, Kondo T, Sajan M, Luo J, Bronson R, Asano T, Farese R, Cantley LC, Kahn
CR. Divergent regulation of hepatic glucose and lipid metabolism by phosphoinositide 3-kinase via Akt and PKClambda/zeta. Cell Metab. 2006 May;3(5):343-53.

Tilg H, Kaser A, Moschen AR How to modulate inflammatory cytokines in liver diseases. Liver Int. 2006 Nov;26(9):1029-39

Tontonoz, P., Hu, E. and Spiegelman, B. M. Stimulation of adipogenesis in fibroblasts by PPAR γ 2, a lipid-activated transcription factor. Cell 1994; 79, 1147-56.

Uchimura K, Nakamuta M, Enjoji M, Irie T, Sugimoto R, Muta T, Iwamoto H, Nawata H. Activation of retinoic X receptor and peroxisome proliferator-activated receptor-gamma inhibits nitric oxide and tumor necrosis factor-alpha production in rat Kupffer cells. Hepatology. 2001 Jan; 33(1):91-9

Ulven, S.M., et al. LXR is crucial in lipid metabolism. Prostaglandins Leukot. Essent. Fatty Acids 2005;73:59–63.

Van Raalte D., Li M., Prithchard H.P., Wasan M.K. Peroxisome proliferator-activated receptor (PPARα): A pharmalogical target with a promising future. Pharmaceutical Research 2004; 21:9.

Van Rossen E, Vander Borght S, van Grunsven LA, Reynaert H, Bruggeman V, Blomhoff R, Roskams T, Geerts AVinculin and cellular retinol-binding protein-1 are markers for quiescent and activated hepatic stellate cells in formalin-fixed paraffin embedded human liver. Histochem Cell Biol. 2009 Mar;131(3):313-25

Verheij M, Bose R, Lin XH, Yao B, Jarvis WD, Grant S, Birrer MJ, Szabo E, Zon LI, Kyriakis JM, Haimovitz-Friedman A, Fuks Z, Kolesnick RN. Requirement for ceramide-initiated SAPK/JNK signalling in stress-induced apoptosis. Nature 1996; 380: 75–79.

Wahli W. A gut feeling of the PXR, PPAR and NF-kappaB connection. J Intern Med. 2008 Jun;263(6):613-9

Wallace K, Cowie DE, Konstantinou DK, Hill SJ, Tjelle TE, Axon A, Koruth M, White SA, Carlsen H, Mann DA, Wright MC. The PXR is a drug target for chronic inflammatory liver disease.J Steroid Biochem Mol Biol. 2010 May 31;120(2-3):137-48.

Wang HY, Cheng ML.Effects of Dan-shao-hua-xian on expression of PPAR-gamma and NF-kappa B in rat liver fibrosis. Hepatobiliary Pancreat Dis Int. 2008 Apr;7(2):179-84

Wang Y, Lam KS, Chan L, Chan KW, Lam JB, Lam MC, et al. Post-translational modifi cations of the four conserved lysine residues within the collagenous domain of adiponectin are required for the formation of its high molecular weight oligomeric complex. J Biol Chem 2006;281:16391–400.

Wanless, I.R., Lentz, J.S. Fatty liver hepatitis and obesity: an autopsy study with analysis of risk factors. Hepatology 1990;12:1106-1110.

Watkins PB, et al. Hepatic dysfunction associated with troglitazone. N Engl J Med 1998; 338: 916–7.

Weiskirchen R, Moser M, Weiskirchen S, Erdel M, Dahmen S, Buettner R, Gressner AM. LIM-domain protein cysteine- and glycine-rich protein 2 (CRP2) is a novel marker of hepatic stellate cells and binding partner of the protein inhibitor of activated STAT1. Biochem J. 2001 Nov 1;359(Pt 3):485-96.

Wellen KE, Hotamisligil GS. Inflammation, stress, and diabetes. J Clin Invest. 2005 May;115(5):1111-9.

Wieckowska A, Zein NN, Yerian LM, Lopez AR, McCullough AJ, Feldstein AE..In vivo assessment of liver cell apoptosis as a novel biomarker of disease severity in nonalcoholic fatty liver disease. Hepatology. 2006 Jul;44(1):27-33.

Wright MC. The impact of pregnane X receptor activation on liver fibrosis. Biochem Soc Trans. 2006 Dec;34(Pt 6):1119-23.

Wynn TA, Barron L. Macrophages: master regulators of inflammation and fibrosis. Semin Liver Dis. 2010 Aug;30(3):245-57

Xu A, Wang Y, Keshaw H, Xu LY, Lam KSL, Cooper GJS. The fat-derived hormone adiponectin alleviates alcoholic and nonalcoholic fatty liver disease in mice. J Clin Invest 2003;112: 91–100.

Yahagi, N., et al. Absence of sterol regulatory element binding protein-1 (SREBP-1) ameliorates fatty livers but not obesity or insulin resistance in Lepob/Lepob mice. J Biol Chem 2002; 277; 19353-19357.

Yamaguchi, K., et al. Inhibiting triglyceride synthesis improves hepatic steatosis but exacerbates liver damage and fibrosis in obese mice with nonalcoholic steatohepatitis. Hepatology. 2007; 45:1366-1374.

Yamamoto Y, Ono T, Dhar DK, Yamanoi A, Tachibana M, Tanaka T, Nagasue N. Role of peroxisome proliferator-activated receptor-gamma (PPARgamma) during liver regeneration in rats. J Gastroenterol Hepatol. 2008 Jun;23(6):930-7

Yin L, Wang Y, Dridi S, Vinson C, Hillgartner FB. Role of CCAAT/enhancer binding protein, histone acetylation, and coactivator recruitment in the regulation of malic enzyme transcription by thyroid hormone. Mol Cell Endocrinol 2005 12 21;245 (1-2):43-52.

Yki-Jarvinen H. Thiazolidinediones. N Engl J Med 2004; 351: 1106–18.

Younossi ZM, Gorreta F, Ong JP, Schlauch K, Del Giacco L, Elariny H, Van Meter A, Younoszai A, Goodman Z, Baranova A, Christensen A, Grant G, Chandhoke V. Hepatic gene expression in patients with obesity-related non-alcoholic steatohepatitis. Liver Int. 2005 Aug;25(4):760-71

Zelcer, N. & Tontonoz, P. Liver X receptors as integrators of metabolic and inflammatory signaling. J. Clin. Invest. 2006;116:607–614.

Zhang N, Sundberg JP, Gridley T. Mice mutant for Ppap2c, a homolog of the germ cell migration regulator wunen, are viable and fertile. Genesis. 2000 Aug;27(4):137-40

Zhou X, Jamil A, Nash A, Chan J, Trim N, Iredale JP, Benyon RC. Impaired proteolysis of collagen I inhibits proliferation of hepatic stellate cells: implications for regulation of liver fibrosis. J Biol Chem. 2006 Dec 29;281(52):39757-65

Znoyko I, Trojanowska M, Reuben A. Collagen binding alpha2beta1 and alpha1beta1 integrins play contrasting roles in regulation of Ets-1 expression in human liver myofibroblasts. Mol Cell Biochem. 2006 Jan;282(1-2):89-99

Appendix 1: Human Primers and Probes used in this study

β actin Forward Primer
5'- CCTGGCACCCAGCACAAT- 3'
β actin Reverse Primer
5' –GCCGATCCACACGGAGTACT- 3'
β actin Probe
5'ATCAAGATCATTGCTCCTCCTGAGCGC-3'

HMBS Forward Primer
5'-ACCTGGTTGTTCACTCCTTGAAG-3'
HMBS Reverse Primer
5'-GGTTTTCCCGCTTGCAGAT-3'
HMBS Probe
5'-ACCTGCCCACTGTGCTTCCTCCTG-3'

SREBP1C Forward Primer
5'-GGAGGGGTAGGGCCAAC-3'
SREBP1C Reverse Primer
5'-GTCAAATAGGCCAGGGAAGTC-3'
SREBP1C Probe
5'-CGCGGAGCCATGGATTGCAC-3'

ChREBP Forward Primer
5'-AGTATCGACCCCACACTCACAC-3'
ChREBP Reverse Primer
5'-TTATTCAGGCGGATCTTGTCT-3'
ChREBP Probe
5'-GCCTGGCCTACAGTGGCAAGCTG-3'

GCK Forward Primer
5'-GCTGGAATCAATTTCCCAGA-3'
GCK Reverse Primer
5'-CTCCCCACACAGGATGAGTT-3'
GCK Probe
5'-AGGGAGTTGCTCACTCAGGA-3'

PK2 Forward Primer
5'-CACTAAAGGACCTGAGATCCGAACT-3'
PK2 Reverse Primer
5'-TGTTCTCGTCACACTTTTCCATGT-3'
PK2 Probe
5'-TCATCAAGGGCAGCGGCACTGCA-3'

PDK4 Forward Primer
5'-CAAGGATGCTCTGTGATCAGTATTATTT-3'
PDK4 Reverse Primer
5'-TGTGAATTGGTTGGTCTGGAAA-3'
PDK Probe
5'-CATCTCCAGAATTAAAGCTTACACAAGTGAATGGA-3'

PPAR β Forward primer
5'-TGCGGCCATCATTCTGTGT-3'
PPAR β Reverse primer
5'-CAGGATGGTGTCCTGGATAGC-3'
PPAR β Probe
5'-ACC GGC CAG GCC TCA TGA ACG-3'

Appendix 1: Human Primers and Probes used in this study

PPAR γ Forward Primer
5’-GAT TCT CCT ATT GAC CCA GAA AGC-3’
PPAR γ Reverse Primer
5’-GCA TCT CTG TGT CAA CCA TGG T-3’
PPAR γ Probe
5’-ATTCCTTCACTGATACACTGTCTGCAAACATAT-3’

FABP4 Forward Primer
5’-CATAAAGAGAAAACGAGAGGATGATAAAC-3’
FABP4 Reverse Primer
5’-CCCTTGGCTTATGCTCTCTCA-3’
FABP4 Probe
5’-TGCGTCATGAAAGGCGTCACTTCC-3’

CEBPα Forward Primer
5’-CAAATATTTTGCTTTATCAGCCGATA-3’
CEBPα Reverse Primer
5’-CGCACATTCACATTGCACAA-3’
CEBPα Probe
5’-AACACTTGTATCTGGCCTCTGTGCCCC-3’

CEBPβ Forward Primer
5’-GAAGAAACGTCTATGTGTACAGATGAATG-3’
CEBPβ Reverse Primer
5’-CCGATTGCATCAACTTCGAA-3’
CEBPβ Probe
5’-TAAACTCTCTGCTTCTCCCTCTGCCCCTC-3’

LXRα Forward Primer
5’-GAGGAGTGTGTCCTGCTAGAAGAA-3’
LXRα Reverse Primer
5’-CCTCCTCTTGCCGCTTCA-3’
LXRα Probe
TCCGCCTGAAGAAA

LXRβ Forward Primer
5’-AGCAGTGCGTCCTTTCTGAAG-3’
LXRβ Reverse Primer
5’-CCACAGGTGACTGCGACTGT-3’
LXRβ Probe
AAGAAGAAGATTCGGAAA

PXR Forward Primer
5’-GCCCAGTGTCAACGCAGAT-3’
PXR Reverse Primer
5’-AGTGGCCTTGTCCCCACATA-3’
PXR Probe
5’-TCGGAGGTCCCCAAATCTGCCG-3’

FXR Forward Primer
5’-TCCTCCCAGGGCCTTGA-3’
FXR Reverse Primer
5’-CTTTCACTCCTTCTACGATGTCTTCTAC-3’
FXR Probe
5’-AGTCCATCTCTGACCCAAAACAATCCAAGG-3’

Appendix 1: Human Primers and Probes used in this study

αSMA Forward Primer
5'-GCAAGTGATCACCATCGGAAA-3'
αSMA Reverse Primer
5'-GACTCCATCCCGATGAAGGA -3'
αSMA Probe
5'-AACGTTTCCGCTGCCCAGAGACC-3'

CRBP1 Forward Primer
5'-GTGGCCTTGCGCAAAATC-3'
CRBP1 Reverse Primer
5'-CCGTCCTGCACGATCTCTTT-3'
CRBP1 Probe
5'-CAACTTGCTGAAGCCAGA-3'

GFAP Forward Primer
5'-GAGATCCGCACGCAGTATGA -3'
GFAP Reverse Primer
5'-ACTTGGAGCGGTACCACTCTTC-3'
GFAP Probe
5'-CAATGGCGTCCAGCAACATGCATG-3'

CSRP2 Forward Primer
5'-ACCGTGTACCACGCAGAAGAG-3'
CSRP2 Reverse Primer
5'-AAAGCAGCAGCGGTGGAA-3'
CSRP2 Probe
5'-TGCAGTGTGATGGCAG-3'

TGFβ1 Forward Primer
5'-CGCGCATCCTAGACCCTTT-3'
TGFβ1 Reverse Primer
5'-CTGTGGCAGGTCGGAGAGA-3'
TGFβ1 Probe
5'-TCCTCCAGGAGACGGA-3'

Adipisin Forward Primer
5'-GGTCACCCAAGCAACAAAGTC-3'
Adipsin Reverse Primer
5'-TCAATAAAGACCAACCAGATGCA-3'
Adipsin Probe
5'-AGCAATGAAGTCATCC-3'

COX2 Forward Primer
5'-GAATCATTCACCAGGCAAATTG-3'
COX2 Reverse Primer
5'-CTTTCTGTACTGCGGGTGGAA-3'
COX2 Probe
5'-TGCTGGTGGTAGGAAT-3'

CD36 Forward Primer
5'-CTGGAGTCTGGAATTCAGAACGT -3'
CD36 Reverse Primer
5'-GAAGTGAGGATGGGAGAGAAACA -3'
CD36 Probe
5′-CCTGCAGGTTCAGTGCCCCC-3′

Appendix 2: Low density Taqman Arrays Pathway

Pathway Description:

Decrease activation/ expression 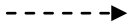

Increase activation/expression 

Enzyme 

Transcription regulator 

Ligand dependent nuclear receptor 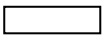

Transmembrane receptor 

Kinase 

Transporter 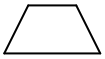

Peptidase 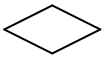

Phosphate 

Chemical endogenous 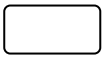

Growth factor 

Cytokine 

G-protein coupled receptor 

microRNA 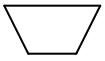

Unknown (family)  or 

Protein- protein interaction 

(Dark red box show higher expression and light pink box show lower expression in this study. Transparent box show the gene that is not determined in this study.)

NAFLD compared to Normal liver pathway analysis

Pathway 1: Lipid metabolism, molecular transport, small molecular biochemistry

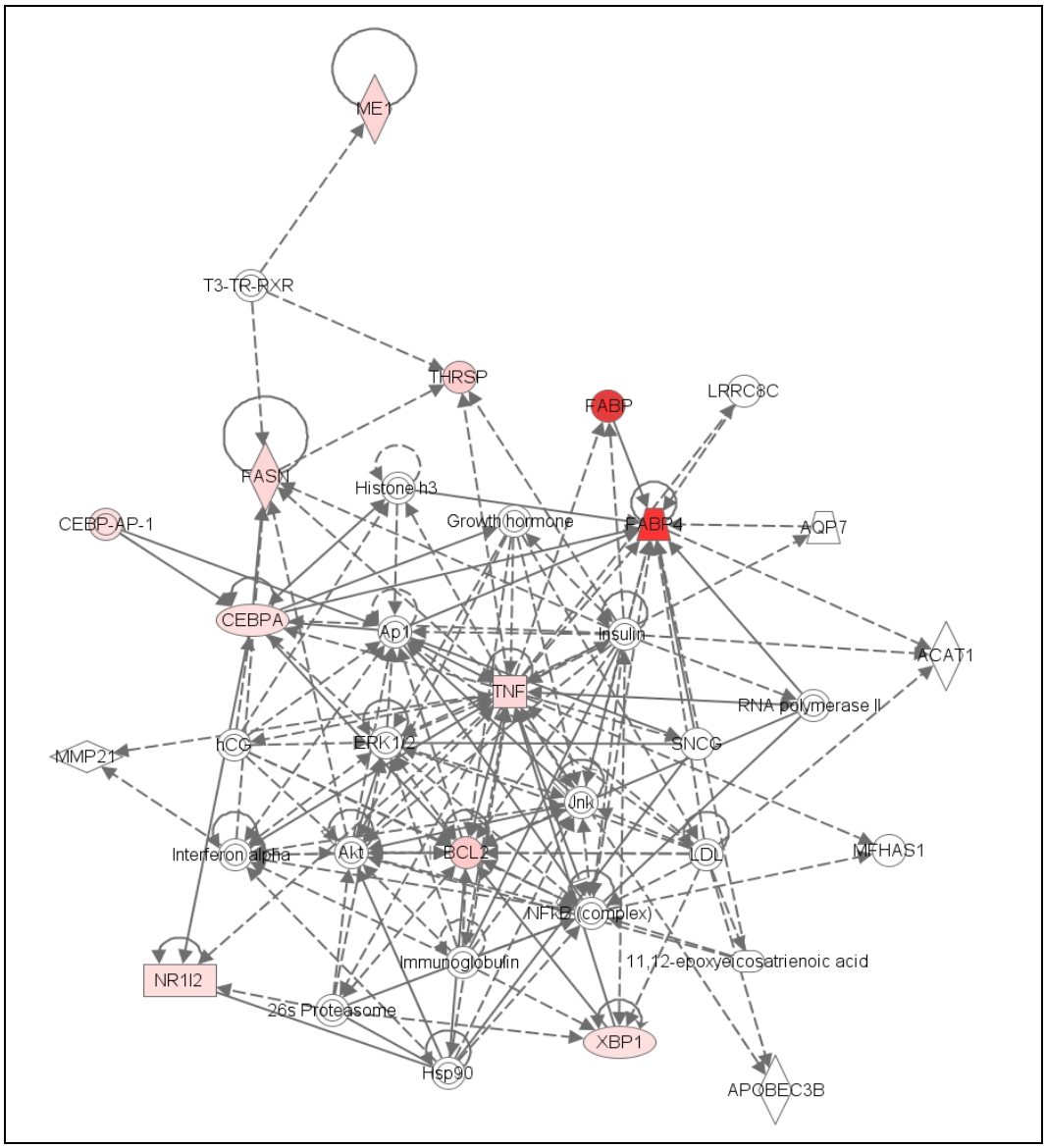

(ME1:malic enzyme; T3-TR-RXR: T3-TR-RXR Interaction network; THRSP: thyroid hormone responsive; FASN: fatty acid synthase, FABP: fatty acid binding protein; LRRC8C: leucine rich repeat containing 8 family, member C; AQP7: aquaporin 7; CEBP-AP1: CEBP-API nucleus complex; CEBPA: CCAT-enhancer binding protein alpha; TNF: tumor necrosis factor; ACAT1:acetyl-CoA acetyltransferase 1; SCCG: synuclein gamma; MMP21: matrix metallopeptidase 21; Hcg: Chorionic gonadotrophin; ERK1/2: p42/44 mapk; Akt: Protein kinase B; Jnk: JUN Kinase; BCL2: lymphoma 2; LDL: low density lipoprotein; MFHAS1:malignant fibrous histiocytoma amplified sequence 1; NR1I2: preganane X-receptor; XBP1: X-box binding protein; APOBEC3B: apolipoprotein B mRNA editing enzyme)

NAFLD compared to Normal liver pathway analysis

Pathway 2: Cancer, cellular movement, Gene expression

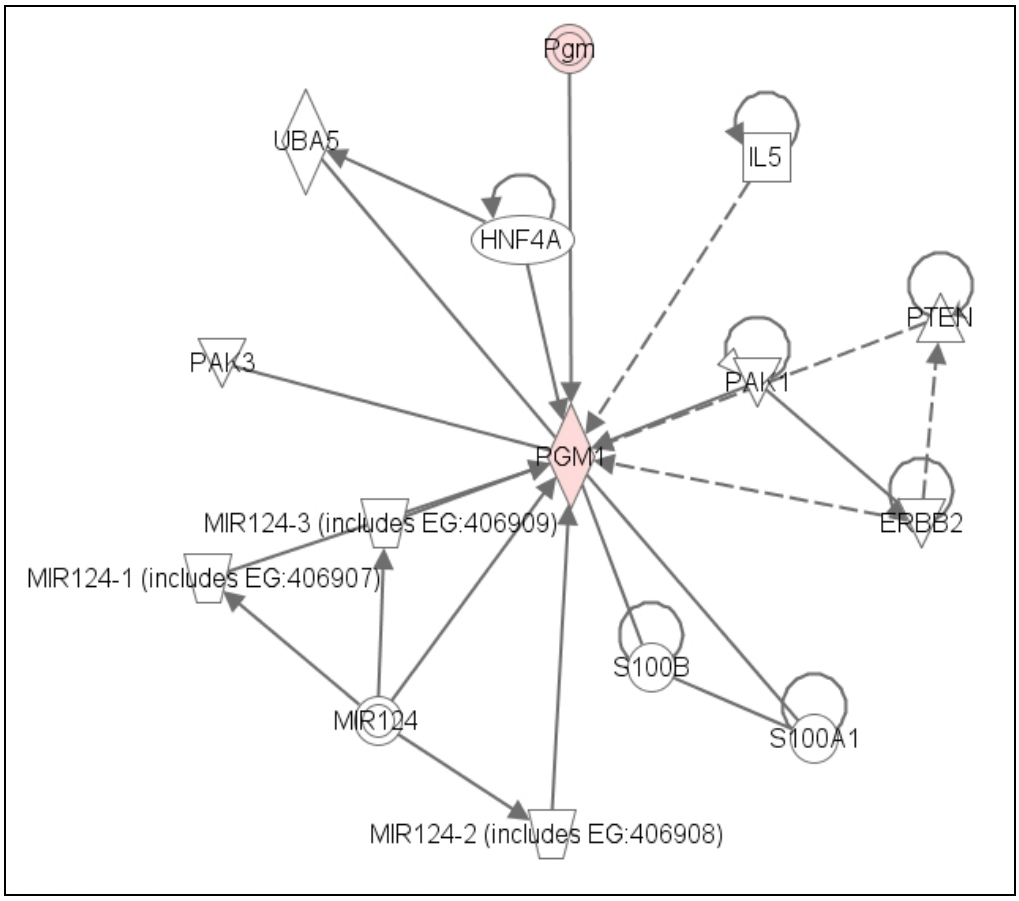

(UBA5: ubiquitin like modifier activating enzyme 5; HNF4A: HNF4 dimer; IL5: Interleukin 15; Pgm: phosphoglucomutase; PAK1: p21 activated kinase 1; PAK3: p21-activated kinase 3; PTEN: phospahtase and tensin homolog; ERBB2: v-erb-b2 erythroblastic leukaemia viral oncogene homolog 2; S100A1: S100 calcium binding protein A1; S100B: S100 calcium binding protein)

NASH compared to Normal liver pathway analysis

Pathway 1: Infection Mechanism, Infection Disease, Lipid Metabolism

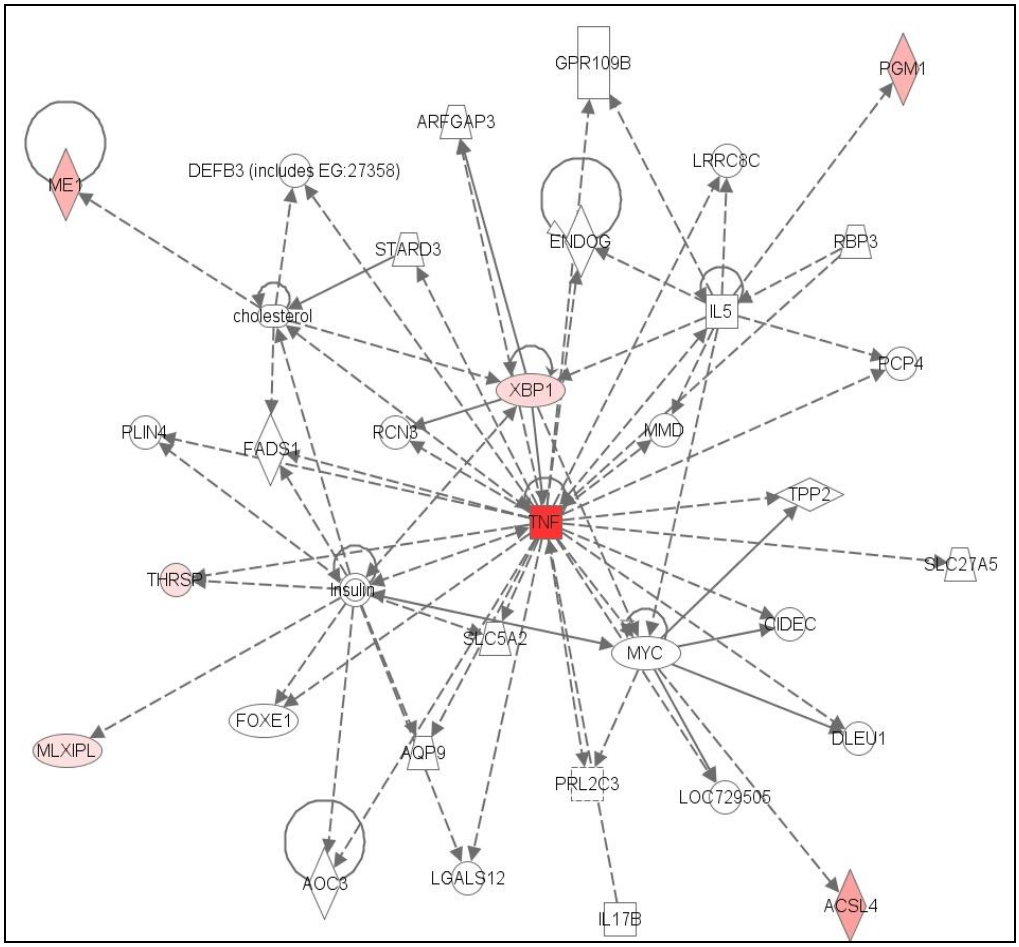

(ME1:malic enzyme; DEFB3:defensin beta 3; ARFGAP3: ADP ribosylation factor GTPase activating protein 3; GPR109B: G-protein coupled receptor 109B ; STARD3: StAR-related lipid transfer domain containing 3; ENDOG: endonuclease G; LRRC8C: leucine rich repeat containing 8 family, member C; PGM1: phosphoglucomutase 1; IL5: Interleukin 15; RBP3: retinol biding protein 3; PLIN4: perilipin 4; FADS1: fatty acid desaturase 1; RCN3: reticulocalbin 3; XBP1- X-box binding protein 1; MMD: Monocyte to macrophage differentiation associated; PCP4: purkinje cell protein 4; THRSP: thyroid hormone responsive; TNF: tumor necrosis factor; TPP2: tripeptidyl peptidase 2; SLC5A2: solute carrier family 5; MYC: v-myc myelocytomasis viral oncogene homolog; CIDEC: cell death inducing DFFA-like effector c; SLC27A5: solute carrier 27, family 5; MLXIPL: MLX interacting protein-like; FOXE1:Foxhead box E1; AQP9: aquaporin 9; AOC3: amine oxidase 3; LGALS12: lectin, galactoside-binding soluble, 12; PRL2C3:prolactin family 2, subfamily C member 3; IL17B: Interleukin 17B; LOC729506: high mobility group nucleosomal biding domain 2 pseudogene; ACSL4: acyl-CoA synthetase long chain family 4)

NAFLD compared to NASH pathway analysis

Pathway 1: Lipid Metabolism, small molecular biochemistry, carbohydrate metabolism

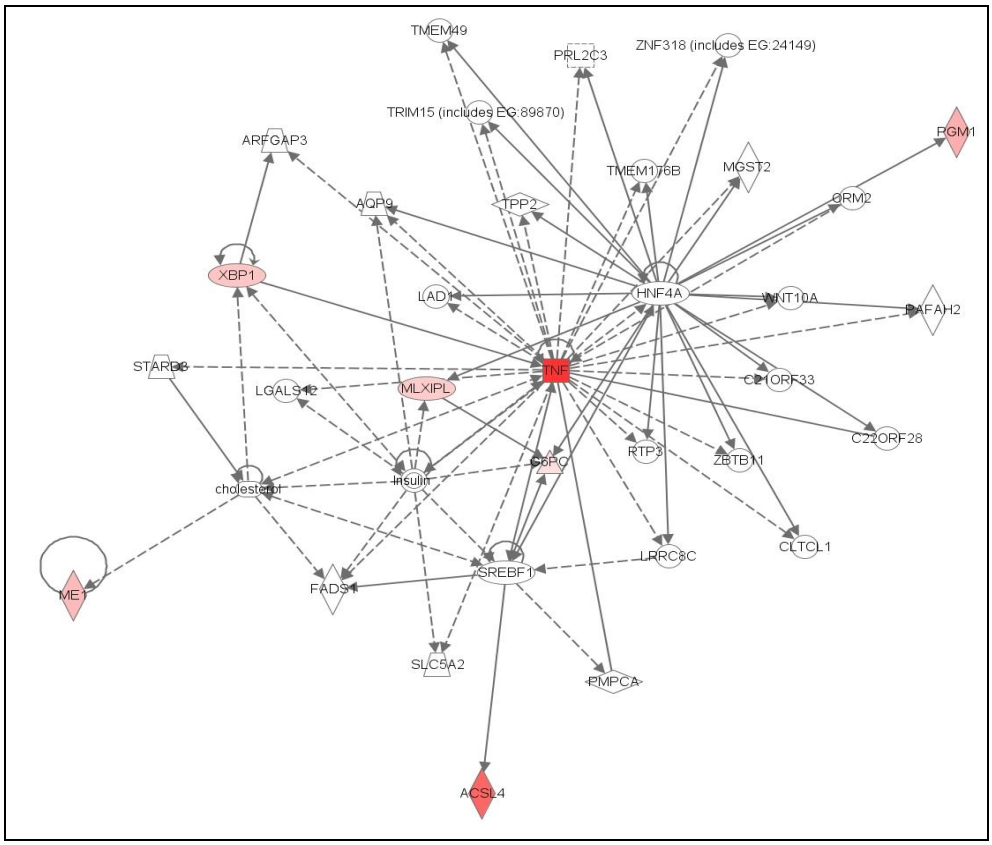

[ME1:malic enzyme; ARFGAP3: ADP ribosylation factor GTPase activating protein 3; STARD3: StAR-related lipid transfer domain containing 3; LRRC8C: leucine rich repeat containing 8 family, member C; PGM1: phosphoglucomutase 1; FADS1: fatty acid desaturase 1; RCN3: reticulocalbin 3; XBP1- X-box binding protein 1; TNF: tumor necrosis factor; TPP2: tripeptidyl peptidase 2; SLC5A2: solute carrier family 5; MLXIPL: MLX interacting protein-like; AQP9: aquaporin 9; LGALS12: lectin galactoside-binding soluble, 12; PRL2C3:prolactin family 2, subfamily C member 3; ACSL4: acyl-CoA synthetase long chain family 4; TMEM49: transmembrane protein 49; ZNF318: zink finger protein 318; TRIM15: tripartite motif containing 15; MGST2: microsomal glutathione S-transferase 2; ORM2:orosomucoid 2; LAD1:ladinin 1; HNF4A:hepatocyte nuclear factor 4 alpha; WNT10A:wingless type MMTV integration site family, member 10A; PAFAH2:platelet activating factor acetylhyrodrolase 2; LGALS42:lectin galactoside-binding soluble 42; G6PC:glucose 6 phosphatase; RTP3:receptor transporter protein 3; ZBTB1:zink finger BTB domain containing 11; C21ORF33:chromosome 21 open reading frame 33; C22ORF28: chromosome 22 open reading frame 28; CLTCL1:clathrin, heavy chain like 1; PMPCA: peptidase (mitochondrial processing) alpha; SREBF1: sterol regulatory element binding protein factor 1]

Pioglitazone compared to Pre-trial pathway analysis

Pathway 1: Lipid Metabolism, Molecular transport, Small molecule biochemistry

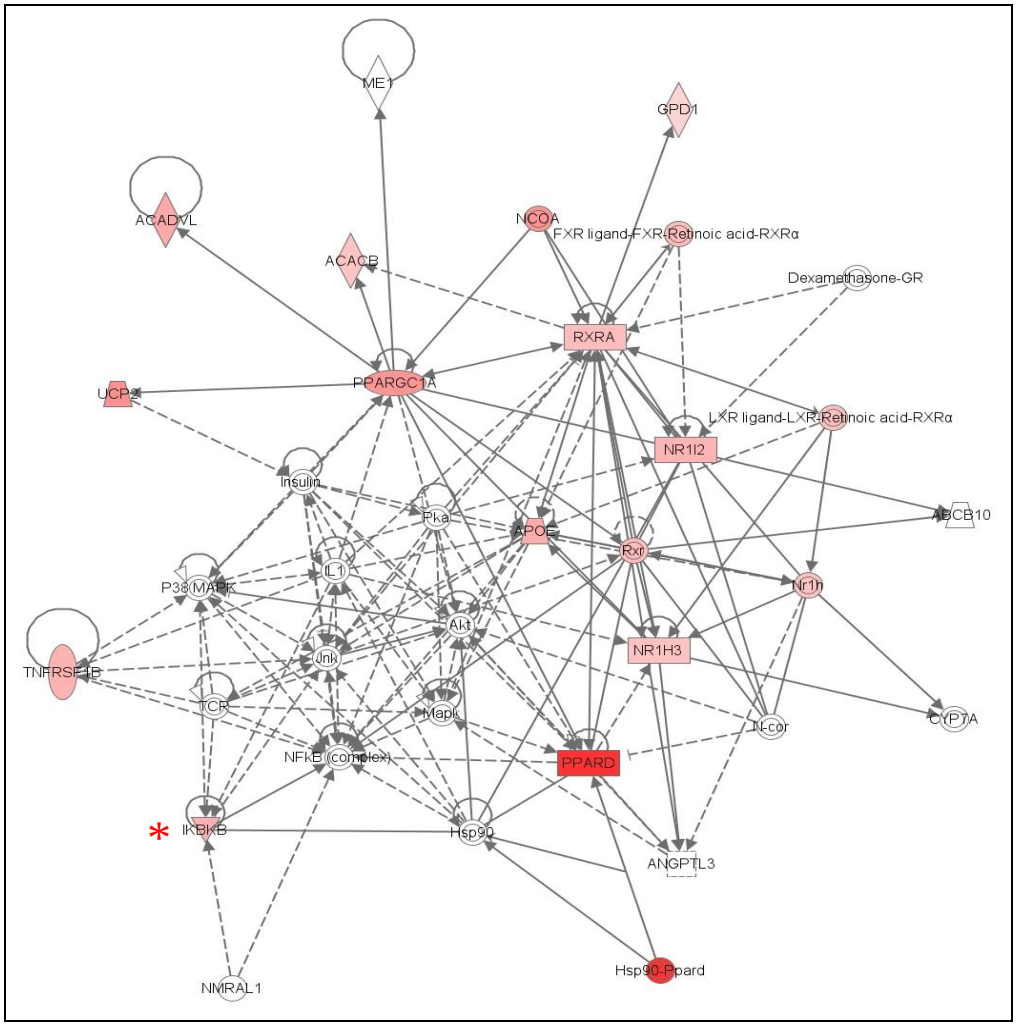

(ME1:malic enzyme 1; ACADVL:acyl-CoA dehydrogenase very long chain; ACACB:acetyl CoA carboxylase beta; NCOA: interaction network; GPD1: glycerol-3-phosphate dehydrogenase 1; UCP2: uncoupling protein 2; PPARGC1A: peroxisome proliferator receptor gamma, coactivator alpha; RXRA: retinoid-X-receptor alpha; NR1I2: Pregnane-X-receptor; TNFRSF1B: tumor necrosis factor receptor superfamily 1B; **IKBKB: inhibitor kappa light polypeptide gene enhancer in beta cells**; Jnk: JUN KINASE; Pka: protein kinase A; APOE: Apolipoprotein E; Rxr: retinoid receptor; IL1: Interleukin 1; P38MAPK:P38 MITOGEN ACTIVATED PROTEIN KINASE ; Akt: Protein kinase B; Mapk: MAP Kinase; TCR: T-cell receptor; NR1H3: liver-X-receptor alpha; NR1h: LXR; ANGPTL3: angiopoietin-like 3; PPAR D: peroxisome proliferator activated receptor delta/beta; NMRAL1:NmrA-like family domain containing 1; ABCB10: ATP-binding cassette super family B member 10; NFkB: nuclear factor kappa beta)

* Please note that it is actually **IkBα (nuclear factor of kappa light polypeptide gene enhancer in B-cells inhibitor, alpha)** and not IKBKB (inhibitor kappa light polypeptide gene enhancer in beta cells).

Pioglitazone compared to Pretrial pathway analysis

Pathway 2: Cancer, cellular movement, Gene expression

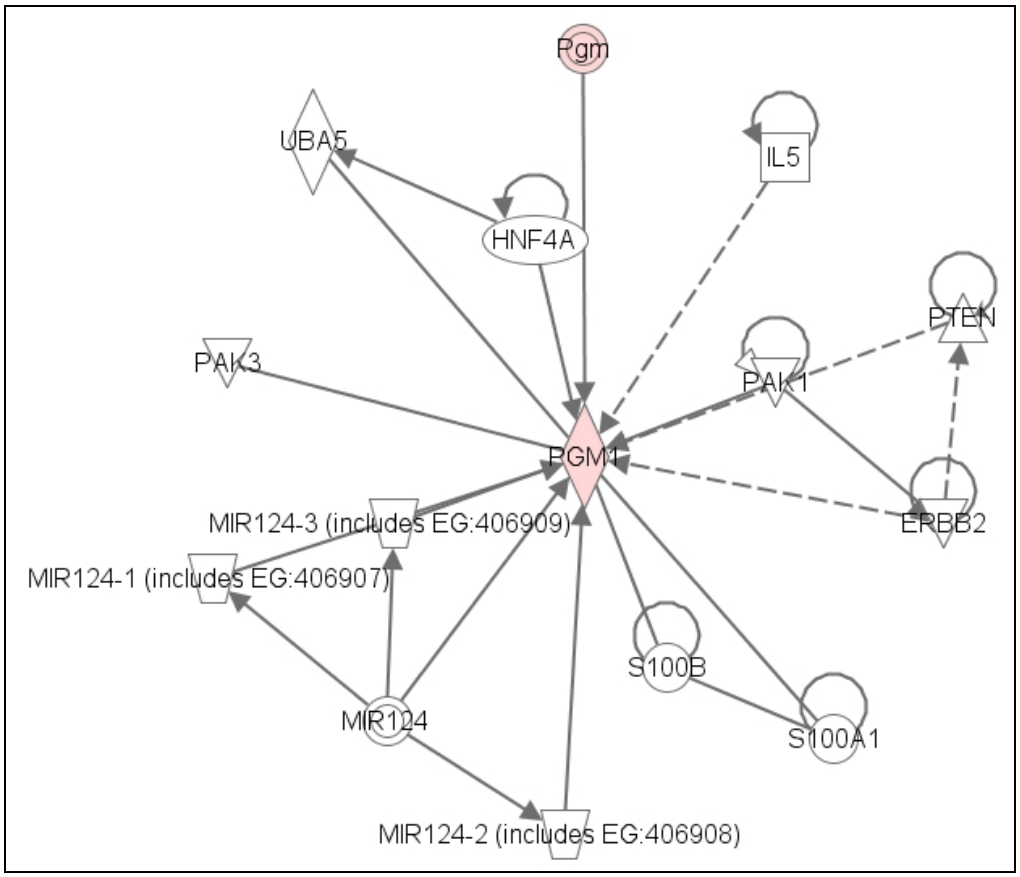

(UBA5: ubiquitin like modifier activating enzyme 5; HNF4A: HNF4 dimer; IL5: Interleukin 15; Pgm: phosphoglucomutase; PAK1: p21 activated kinase 1; PAK3: p21 activated kinase 3; PTEN: phospahtase and tensin homolog; ERBB2: v-erb-b2 erythroblastic leukaemia viral oncogene homolog 2; S100A1: S100 calcium binding protein A1; S100B: S100 calcium binding protein)

Placebo compared to Pretrial pathway analysis

Pathway 1: Cellular assembly & organization, development disorder, neurological disease

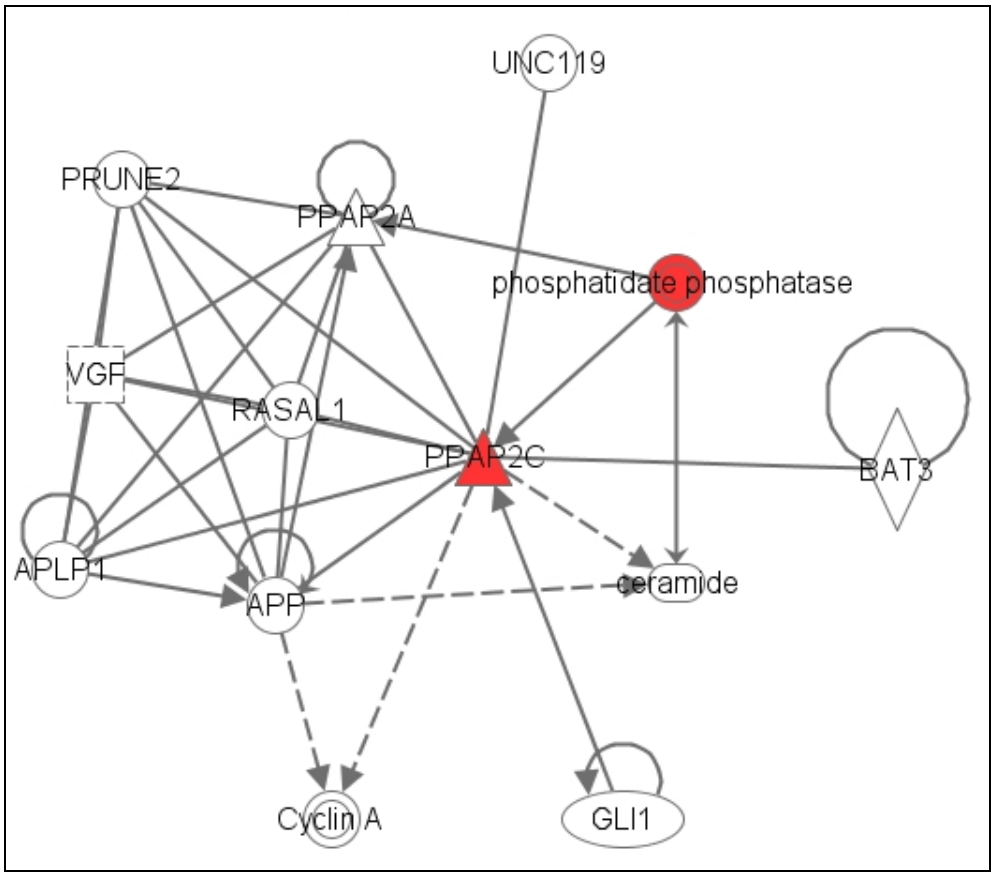

(PRUNE2: PRUNE HOMOLOG 2; PPAP2A: PHOSPHATIDIC ACID PHOSPAHTASE TYPE 2A; UNC119: unc-119 homolog; VGF: VFG nerve growth factor inducible; RASAL1: RAS protein activator like 1; PPAP2C: phosphatidic acid phosphatase type 2C; BAT3: HLA-B associated transcript 3; APLP1: ameloid beta (A4) precursor like protein 1; APP: ameloid beta (A4) precursor; GLI1: GLI family zinc finger 1)